

Chemistry of Antiviral Metallomacrocycles

A Thesis Submitted for the Degree of

Doctor of Philosophy

by

Tina M. Hunter, MChem.



School of Chemistry

Faculty of Science and Engineering

University of Edinburgh

September 2005



Abstract

Certain bicyclams are highly potent and selective HIV inhibitors, which bind to the CXCR4 co-receptor. The lead bicyclam compound, AMD3100 (1,1'-(1,4-phenylenebismethylene)-bis-1,4,8,11-tetraazacyclotetradecane, referred to as xylyl-bicyclam) has been in clinical trials as an anti-HIV drug, and is also used clinically for the mobilization of stem cells. Studies have shown that the Zn(II) complex of xylyl-bicyclam is more active than the free ligand. However, all other transition metal complexes of xylyl-bicyclam are less active. Zn(II) is a biologically essential metal ion and may play a key role in the anti-HIV activity of bicyclams. Recently, a new bis-macrocyclic was discovered with even greater activity, AMD3329, which incorporates a pyridine ring into the macrocyclic framework.

In order to elucidate the mechanism of action of AMD3100, the synthesis of several metal-cyclam complexes, metal complexes of xylyl-bicyclam, AMD3329 and its component macrocycle, and their metal complexes was carried out.

1D and 2D ^1H , ^{13}C and ^{15}N NMR spectroscopy revealed that Pd(II)-cyclam complexes exist as one configuration in aqueous solution, the *trans*-III configuration. Ni(II)-cyclam was found to be in the *trans*-III configuration in the solid state, and in a mixture of *trans* square-planar (diamagnetic) and octahedral (paramagnetic) configurations in solution. The configuration of Cu(II)-cyclam in the solid state was also *trans*-III. Co(III)-cyclam was shown to be in three *trans* configurations by 1D and

2D ^1H , ^{13}C and ^{15}N studies and UV-vis spectroscopy. In the solid state, the cobalt cyclam was also found to be in the *trans*-III configuration.

Xylyl-bicyclam was synthesised, and complexed with palladium, nickel, copper and cobalt. 1D and 2D ^1H , ^{13}C and ^{15}N NMR studies revealed that $[\text{Pd}_2(\text{xylyl-bicyclam})](\text{OAc})_4$ exists as one major configuration in aqueous solution, the *trans*-III configuration. The addition of acetate to this solution did not induce any configurational change. NMR studies on $[\text{Ni}_2(\text{xylyl-bicyclam})](\text{OAc})_4$ showed it to be a mixture of paramagnetic and diamagnetic species in solution. UV-vis spectroscopy showed the main configuration to be square-planar. Two *trans* configurations of $[\text{Co}_2(\text{xylyl-bicyclam})\text{Cl}_4]\text{Cl}_2$ were identified using 1D and 2D ^1H , ^{13}C and ^{15}N NMR spectroscopy. Upon addition of acetate to this complex, configurational changes occur, eventually to give one *trans* configuration. Mass spectrometry on this product showed it to be $[\text{Co}_2(\text{xylyl-bicyclam})(\text{OAc})_4](\text{OAc})_2$.

AMD 3329 (a bis-macrocycle of pyridyl isocyclam with a phenyl linker) and its component macrocycle were synthesised, and complexed with Cd(II), using NMR-active enriched ^{111}Cd . Using 1D and 2D ^1H , ^{13}C , ^{15}N and ^{111}Cd NMR spectroscopy, these novel metallomacrocycles were fully characterised, and two configurations were found in solution for both the ^{111}Cd -macrocycle and the analogous AMD 3329 complex. The monomer was also complexed with Zn(II), and NMR studies showed it to exist also in two configurations in solution. Addition of excess acetate to the Zn(II) complex did not induce any configurational change in the macrocyclic framework.

The interaction between Cu(II)-cyclam, Ni(II)-cyclam and Cu(II)-xylyl-bicyclam and lysozyme was studied. NMR spectroscopy revealed binding sites in lysozyme

involving tryptophan residues. Solid-state x-ray crystallographic studies on the copper complexes showed the presence of two distinct binding sites. Polar and non-polar interactions were established in the protein recognition of the metallomacrocycles, including H-bonding between the cyclam ring and protein carboxylate groups, and hydrophobic stacking interactions. These studies provide the first direct demonstration of the mode of interaction between metal cyclams and proteins and the relevance to binding to the CXCR4 protein is discussed.

Declaration

I hereby declare that except where specific reference is made to other sources, the work contained in this thesis is the original work of the author. It has been composed by myself and has not been submitted, in whole or in part of, for any other degree, diploma, or other qualification.

Acknowledgements

I would like to thank Professor Peter J. Sadler for his supervision, advice and encouragement throughout the course of my study. I am very grateful for everything he has taught me during my project.

I am eternally grateful to Dr. Xiangyang Liang, who worked on this project before me, for teaching me many things about this project. It is thanks to his excellent work that the project was continued. I am extremely grateful to Dr. Claudia Blindauer for all her help, especially regarding NMR techniques. Also, I would like to thank Juraj Bella and Dr. Dusan Uhrin for their assistance with NMR experiments. My thanks go to Dr. Stephen Paisey, Dr. Hye-seo Park and Dr. Abraha Habtemariam for their help and advice with all matters, in particular synthetic chemistry. Many thanks to Alison Smith, who carried out some initial work on nickel cyclam as part of her MChem Honours project. I would like to express tremendous gratitude to Dr Iain McNae for solving the X-ray crystal structures with lysozyme in Chapter 6. His exceptional work was greatly appreciated.

I would also like to thank Dr. Simon Parsons and his group members for the determination of X-ray crystal structures for me.

I also thank the BBRSC for financial support during this project, and the University of Edinburgh Development Trust for giving me the opportunity to present work at a conference in Australia.

I would like to thank all the members of the PJS group, both past and present, for their friendship, help and support. Particular thanks to Dr. Geraldine McGowan, Fiona Mackay and Dr. Ana Pizarro for their friendship and support over the years, they have made my time doing this project very enjoyable.

Special thanks all my friends who have supported me throughout this work, particularly during the writing up stage, for making me see there was light at the end of the tunnel.

My sincerest thanks go to David Benstead, who was a constant source of help and encouragement during this work. His insightful discussions were of a great help to me when writing up this work, and I am extremely grateful for everything he has done for me.

Finally I would like to thank my mother, for support, understanding, patience and encouragement during the time I have spent on this project.

Contents

Abstract	i
Declaration	iv
Acknowledgements	v
Contents	vii
Abbreviations	xv

Chapter 1 Introduction

1.1	Metallo drugs	1
1.2	HIV and AIDS	4
1.2.1	The Discovery of HIV and AIDS	4
1.2.2	HIV Life Cycle	4
1.3	Current Treatments for HIV	6
1.3.1	Nucleoside Reverse Transcriptase Inhibitors	7
1.3.2	Non-Nucleoside Reverse Transcriptase Inhibitors	7
1.3.3	Protease Inhibitors	8
1.3.4	Entry Inhibitors	9
1.4	CXCR4 Coreceptor	10
1.4.1	CXCR4 Coreceptor Function and Structure	10
1.4.2	Side-effects	12
1.5	Optimising the Structure of the Bicyclams	13

1.5.1	Varying the size of the ring	13
1.5.2	Varying the Linker	16
1.5.3	Heteroaromatic Linkers	16
1.5.4	Changing the Amine Groups	18
1.5.5	Incorporation of Pyridine Rings Into the Macrocyclic Framework	19
1.5.6	Metals and Bicyclam	22
1.5.7	Zn ₂ (Xylyl-Bicyclam) Binding to CXCR4 Coreceptor	24
1.6	Cyclam	25
1.6.1	Cyclam Background	25
1.6.2	Configurational Isomers	29
1.6.3	Metal Cyclams	29
1.7	Recent Developments Involving Cyclam Derivatives	33
1.8	Aims of This Thesis	34
1.9	References	35
Chapter 2 Materials and Methods		
2.1	Chemicals and Instruments	42
2.1.1	Chemicals	42
2.1.2	IR Spectroscopy	42
2.1.3	NMR Spectroscopy	43
2.1.4	X-ray Crystallography	43
2.1.5	CHN Analysis	43
2.1.6	Electrospray Ionisation-Mass Spectrometry (ESI-MS)	43

2.1.7	Ultraviolet and Visible Spectroscopy (UV-Vis)	44
2.1.8	pH Measurements	44
2.2	NMR Spectroscopy	44
2.2.1	Nuclear Spin	45
2.2.2	Chemical Shift	46
2.2.3	Spin-Spin Coupling	47
2.2.4	¹⁵ N NMR Spectroscopy	48
2.2.5	Quadrupolar Relaxation	49
2.2.6	1D NMR Spectroscopy	49
2.2.7	2D NMR Spectroscopy	50
2.2.8	COrrrelation SpectroscopY (COSY)	51
2.2.9	Nuclear Overhauser Effect SpectroscopY (NOESY)	52
2.2.10	TOtal Correlation SpectroscopY (TOCSY)	52
2.2.11	Heteronuclear Single-Quantum Correlation (HSQC)	54
2.3	IR Spectroscopy	55
2.4	Electrospray Ionisation Mass Spectrometry (ESI-MS)	56
2.5	CHN Analysis	58
2.6	References	60
 Chapter 3 Synthesis and Characterisation of Metallocyclam Complexes		
3.1	Introduction	62
3.2	Experimental	64
3.2.1	Synthesis of Palladium(II) Cyclam Complexes	65

3.2.2	Synthesis of Nickel(II) Cyclam Complexes	66
3.2.3	Synthesis of a Cobalt(III) Cyclam Complex	68
3.2.4	Synthesis of a Copper(II) Cyclam Complex	69
3.2.5	NMR Studies of [Ni(cyclam)](OAc) ₂	70
3.2.6	UV-Vis Spectroscopy	70
3.3	Results	70
3.3.1	NMR Studies of Pd(II) Cyclam Complexes	70
3.3.2	NMR Studies of Ni(II) Cyclam Complexes	74
3.3.3	NMR Studies of Co(III) Cyclam Complex	78
3.3.4	NMR Studies of Cu(II) Cyclam Complex	82
3.3.5	X-Ray Crystallography	84
3.3.6	UV-Vis Spectroscopy	93
3.4	Discussion	94
3.4.1	Comparison of Metal-Cyclam Complexes in the Solid State	94
3.4.2	NMR Studies	96
3.4.3	UV-Vis Spectroscopy	102
3.5	Conclusions	103
3.6	References	106
Chapter 4 Synthesis and Reactions of Xylyl-Bicyclam and its Metal Complexes		
4.1	Introduction	109
4.1.1	Discovery of AMD 3100	109
4.1.2	Metal Complexation	112

4.1.3	Zinc Histidine	112
4.2	Synthesis	113
4.2.1	Synthesis of Xylyl-Bicyclam, Route 1	113
4.2.2	Synthesis of Xylyl-Bicyclam, Route 2	114
4.2.3	Synthesis of Metal-Xylyl-Bicyclam Complexes	117
4.2.4	UV-Vis Spectroscopy	120
4.2.5	Zinc Uptake of Xylyl-Bicyclam at 37 °C	120
4.2.6	Reaction of Zn(histidine) ₂ with Xylyl-Bicyclam at 37°C	120
4.2.7	Addition of Acetate to [Pd ₂ (Xylyl-Bicyclam)](OAc) ₄	121
4.2.8	Addition of Acetate to [Co ₂ (Xylyl-Bicyclam)Cl ₄]Cl ₂	122
4.3	Results	122
4.3.1	Synthesis of Xylyl-Bicyclam	122
4.3.2	[Ni ₂ (Xylyl-Bicyclam)](OAc) ₄	123
4.3.3	[Cu ₂ (Xylyl-Bicyclam)](OAc) ₄	126
4.3.4	[Pd ₂ (Xylyl-Bicyclam)](OAc) ₄	128
4.3.5	[Co ₂ (Xylyl-Bicyclam)Cl ₄]Cl ₂	133
4.3.6	UV-Vis Spectroscopy	140
4.3.7	Zinc Uptake of Xylyl-Bicyclam at 37 °C	141
4.3.8	Reaction of Xylyl-Bicyclam With Zinc Histidine	143
4.3.9	Addition of Acetate to Pd ₂ (Xylyl-Bicyclam)](OAc) ₄	146
4.3.10	Addition of Acetate to Co ₂ (Xylyl-Bicyclam)Cl ₄]Cl ₂	146
4.4	Discussion	151
4.4.1	Reactions of Xylyl-Bicyclam With Zinc Complexes	151

4.4.2	Configurations of Metal-Xylyl-Bicyclam Complexes in Solution	152
4.4.3	Addition of Acetate to $[\text{Co}_2(\text{Xylyl-bicyclamCl}_4)]\text{Cl}_2$	155
4.5	Conclusions	156
4.6	References	158

Chapter 5 Synthesis and Solution Studies of Pyridyl Isocyclam and its Metal Complexes

5.1	Introduction	160
5.1.1	Anti-HIV Macrocycles	160
5.1.2	Cadmium Chemistry	162
5.2	Experimental	163
5.2.1	Synthesis of 14	163
5.2.2	Synthesis of 15	170
5.2.3	Preparation of ^{111}Cd Acetate Complex, 16	172
5.2.4	Preparation of Zn Acetate Complex, 17	173
5.2.5	Preparation of ^{111}Cd Acetate Complex, 18	174
5.2.6	Addition of Acetate to Zn(II) Acetate Complex, 17	175
5.2.7	pH Titration of 14	175
5.3	Results	175
5.3.1	Synthesis of 14	175
5.3.2	Synthesis of 15	178
5.3.3	Synthesis and NMR Spectroscopy of $^{111}\text{Cd(II)}$ Complex, 16	180
5.3.4	Synthesis and NMR Spectroscopy of Zn(II) Complex, 17	189

5.3.5	Synthesis and NMR Spectroscopy of 18	193
5.3.6	Addition of Acetate to Zn(II) Complex, 17	202
5.3.7	pH Titration of Ligand 14	203
5.4	Discussion	204
5.4.1	Pyridyl Isocyclams	204
5.4.2	¹¹¹ Cd NMR Studies	206
5.4.3	NMR Studies of Zn(II)-Pyridyl Isocyclam	208
5.5	Conclusions	209
5.6	References	211

Chapter 6 Interaction of Metal Cyclams with Lysozyme

6.1	Introduction	213
6.2	Experimental	214
6.2.1	Crystallization of Lysozyme with [Cu ₂ (xylyl-bicyclam)](OAc) ₄	214
6.2.2	Crystallization of Lysozyme at pH=4.5	215
6.2.3	Soaking of Lysozyme Crystals With [Cu(cyclam)(H ₂ O) ₂](OAc) ₂	215
6.2.4	Soaking of Lysozyme Crystals With [Cu ₂ (xylyl-bicyclam)](OAc) ₄	216
6.2.5	NMR Studies of Lysozyme with [Cu(cyclam)(H ₂ O) ₂](OAc) ₂	216
6.2.6	NMR Studies of Lysozyme with [Cu ₂ (xylyl-bicyclam)](OAc) ₄	216
6.2.7	NMR Studies of Lysozyme with [Ni(cyclam)(OAc) ₂]-H ₂ O	217
6.3	Results	217
6.3.1	NMR Studies with Lysozyme and Metal Cyclams	217
6.3.2	Crystallization of Lysozyme	223

6.4	Discussion	226
6.4.1	Copper-Macrocycle-Lysozyme Interactions in Solution	226
6.4.2	Nickel-Macrocycle-Lysozyme Interactions in Solution	228
6.4.3	Copper-Macrocycle Binding Sites in Crystalline Lysozyme	229
6.4.4	Metal Coordination, H-bonding and Hydrophobic Interactions	231
6.4.5	CXCR4 binding sites	236
6.5	Conclusions	237
6.6	References	239
Chapter 7 Conclusions and Future Work		
7.1	Conformations of Metalloclamams	241
7.2	Future Work	245
7.3	References	247
Courses Attended		249
Conferences Attended		249
Publications		250

Abbreviations

AIDS	Acquired immune deficiency syndrome
Ala	Alanine
Asn	Asparagine
Asp	Aspartic acid
AZT	Zidovudine
CC ₅₀	50 % cytotoxic concentration
COSY	Correlation Spectroscopy
Cys	Cysteine
DNA	Deoxyribonucleic acid
DQF	Double-quantum filtered
EC ₅₀	50 % effective concentration
en	Ethylenediamine
ESI	Electrospray ionisation
ES-MS	Electrospray mass spectrometry
FID	Free induction decay
Glu	Glutamic acid
Gly	Glycine
gp	Glycoprotein
HEWL	Hen egg white lysozyme
HIV	Human immunodeficiency virus

HPLC	High pressure liquid chromatography
HSQC	Heteronuclear single quantum correlation
mRNA	Messenger ribonucleic acid
NOESY	Nuclear overhauser effect spectroscopy
NRTI	Nucleoside reverse transcriptase inhibitor
NtRTI	Non-nucleoside reverse transcriptase inhibitor
RF	Radio frequency
RNA	Ribonucleic acid
SDF-1	Stromal-cell derived factor 1
TM	Trans-membrane
TOCSY	Total correlation spectroscopy
Trp	Tryptophan

Chapter 1 Introduction

1.1 Metallodrugs

Since the discovery of the anticancer drug cisplatin (*cis*-[Pt(NH₃)₂Cl₂]) in the 1960's,¹ the field of bioinorganic chemistry has expanded rapidly. Inorganic elements are known to play a vital role in many biological processes, and many organic compounds used in medicine are activated by metal ions including metalloenzymes.² Inorganic elements are used in many fields ranging from therapeutic agents, radiopharmaceuticals and enzyme inhibitors to essential elements mineral supplements.²

Diam(m)ino Pt(II) complexes are now well established in the clinic as anticancer drugs.³ Cisplatin is one of the most widely used anticancer drugs, as is the second generation drug carboplatin. Four injectable Pt(II) complexes have been approved for clinical trials, and many other *cis*-diam(m)ine complexes are in clinical trials.² It was initially thought that *trans* Pt(II) drugs were inactive, as *trans*-platin is inactive. However, recent discoveries have shown that the cytotoxic activity of *trans*-diam(m)inedichloroplatinum(II) complexes can be comparable to, or even greater than, that of cisplatin, and as such, *trans* complexes are being studied in increasing numbers.⁴⁻⁸ With the large variety of amine ligands available, it is possible to vary the rates of hydrolysis of the platinum drugs, and in some cases, the mode of binding of Pt to DNA has been changed, resulting in drugs that can be used in cisplatin resistant cells.⁹

Another group of inorganic compounds found to have anticancer activity is metallocenes. The first of these complexes to have its anticancer activity recognized

was titanocene dichloride (Cp_2TiCl_2) in 1979.¹⁰ Since then, the activities of vanadium, niobium, molybdenum, iron, germanium and tin metallocenes have also been reported.¹¹ These complexes were initially tested as possible analogues of cisplatin, however, the activity of Cp_2TiCl_2 in platinum resistant cell lines suggests a different mechanism of action.¹²⁻¹⁴

More recently, ruthenium complexes have been shown to have anticancer activity.^{3, 15} Ruthenium(II) arene complexes $[(\eta^6\text{-arene})\text{Ru}(\text{en})\text{Cl}][\text{PF}_6]$ (en = ethylenediamine) have been shown to be cytotoxic to cancer cells including cisplatin-resistant cancer cells.^{16, 17} DNA is a potential target for this class of anticancer complexes, which exhibit a high selectivity for binding to N7 of guanine bases and in contrast to cisplatin, these ruthenium(II) arene complexes show little interaction with adenine.¹⁸⁻²⁰

Several injectable gold drugs are used in the clinic for the treatment of rheumatoid arthritis.²¹ These include Au(I) thiolate complexes which have a high affinity for sulfur ligands, yet bind only weakly to N and O ligands. As such, the targets for Au(I) drugs are proteins which contain cysteine thiolate groups. Throughout Au(I) therapy, Au levels in the blood can reach 20 μM , and gold is primarily bound to albumin, which implies a protein-mediated transport of gold during therapy. It is known that Au(I) complexes can be oxidised to Au(III) after administration, and it is thought that this could be responsible for some of the toxic side effects of Au(I) drugs.²²

Radioactive metal ions can be used in diagnosis and therapy.^{23, 24} High intensity γ -ray emitters, such as $^{99\text{m}}\text{Tc}$ and ^{67}Ga are used for diagnostic imaging, and β emitters, such as ^{89}Sr and ^{153}Sm are used for therapy. More than 20 $^{99\text{m}}\text{Tc}$

complexes are currently in clinical use. Technetium has an extensive redox chemistry, with oxidation states ranging from -1 to +7, and can be tailored to target different areas of the body. ^{99m}Tc also has a half life of 6 hours, ideal for use in radioimaging, long enough to synthesise, purify, inject into the patient and observe, while short enough to minimise the radiation dose to the patient.

Magnetic resonance imaging is now a common used powerful diagnostic tool used in medicine. Contrast agents, containing for example Gd(III) complexes, are used to detect differences between normal and abnormal tissues, observable by differences in the ^1H NMR resonances of H_2O .²⁵ Four Gd(III) complexes are widely used in the clinic, and can be used to detect many problems in the body, for example abnormalities at the blood-brain barrier. There is also a Mn(II) complex used in the clinic for similar purposes. Most contrasting agents consist of ions which have a large number of unpaired electrons, for example Gd(III) has 7, and long electron relaxation spin times.

Bismuth compounds have long been used as a treatment for intestinal disorders.²⁶ Bi(III) complexes, such as the nitrate and salicylate salts, are used to treat ulcers, although little is known about their structure and exact mode of action. Bi(III) citrates are used as antiulcer drugs, as they have antimicrobial activity against *Helicobacter pylori*, a bacterium which prevents ulcers from healing.

Lithium is used in the treatment of bipolar affective disorders such as manic depression.³ It is taken in tablet form, as Li_2CO_3 . Li^+ is a very small ion, which binds weakly to ligands, and becomes strongly hydrated in water. After administration, lithium is widely distributed throughout the body, with blood plasma concentrations reaching up to 0.8 mM. However, lithium has a narrow

therapeutic/toxic ratio, and as such, blood plasma concentrations must be monitored closely.

1.2 HIV and AIDS

1.2.1 The Discovery of HIV and AIDS

In 1981, health care workers in the USA became aware of an increased frequency of Kaposi's sarcoma, a cancer of the skin and blood vessels, and of *Pneumocystis pneumonia*, a respiratory infection.²⁷ Both of these diseases are extremely rare in the general population, but occur more frequently in immunosuppressed individuals. This led to the recognition of an immune system disorder that was named acquired immunodeficiency virus (AIDS). By 1983, the precursor was identified, and called human immunodeficiency virus (HIV). It is thought that the virus arose by evolution from another virus in central Africa and may have been an unrecognised cause of death for many years. The virus has been identified in preserved blood samples from as early as 1959.²⁷ As HIV causes T helper cells to become depleted, the immune system becomes extremely compromised as more and more T helper cells are destroyed, until a point when opportunistic diseases, such as Kaposi's sarcoma, can become established in the body without the body's normal defence mechanisms to fight off these diseases.

1.2.2 HIV Life Cycle

HIV enters the cell by first binding to the CD4 cellular receptor, which causes a conformational change in gp120, a viral envelope protein.²⁸ It then binds to a

second receptor, which exposes part of the gp41 viral protein, which allows fusion to the host cell membrane and the viral protein gp41 anchors to the cell membrane. This allows the contents of the virus to be emptied into the cell, and then replication of the viral RNA can occur. The second receptor was found to be the CXC-chemokine receptor CXCR4. Its natural ligand is stromal-cell derived factor 1 (SDF-1). Chemokines are small secreted proteins that control the recruitment of many cell types to sites of infection or injury, and guide immature cells to their sites for maturation and activation.

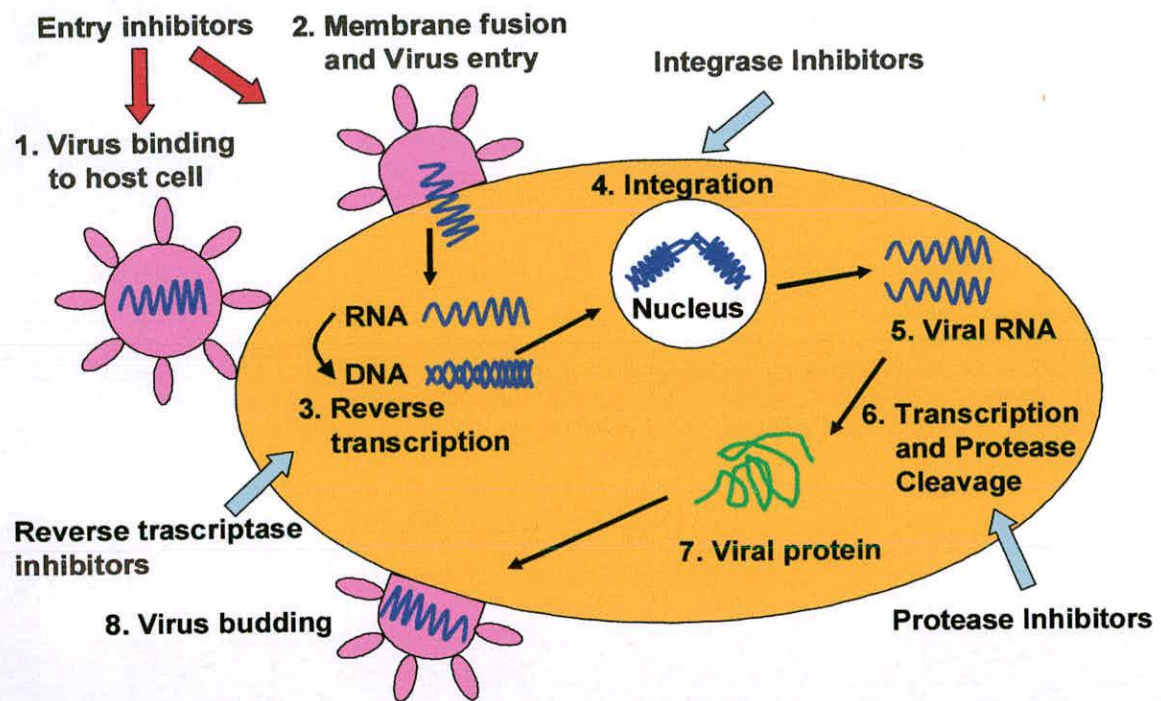


Figure 1.1 HIV replication cycle in a T helper cell, showing the eight steps involved in viral replication. Key targets for anti-HIV drugs shown. A T helper cell is a type of white blood cell.

Once the virus has released its contents into the cell, reverse transcriptase catalyses the synthesis of a DNA strand complementary to the viral RNA (Figure 1.1). The new DNA strand then acts as a template for the synthesis of its complementary DNA strand and the double stranded DNA is then incorporated as a provirus into the host cell's genome. Proviral genes are then transcribed into messenger RNA molecules that are translated in the cytoplasm into HIV proteins. The RNA transcribed from the provirus also provides genomes for the next generation of viruses. The assembly of capsids around the genomes is followed by the budding of the new viruses from the host cell. The infected cells may then produce more viruses for some time or may be killed quickly by the virus itself or by the immune system. This process occurs in T helper cells, which defend against intracellular pathogens. The T helper cell binds to antigens on the surface of a pathogen, and this triggers a response in the body that causes the destruction of the pathogen. CD4 is a protein on the surface of T helper cells that greatly enhances the binding of T helper cells to the pathogen.²⁷

1.3 Current Treatments for HIV

There are three main types of drugs currently used in the treatment of HIV infections. The classes are (i) nucleoside reverse transcriptase inhibitors (NRTIs), (ii) non-nucleoside reverse transcriptase inhibitors (NtRTIs) and (iii) protease inhibitors. However these only target two parts of the HIV life cycle, so new targets are being considered, mainly (i) viral adsorption, through binding to the viral envelope glycoprotein gp120, (ii) viral entry, through blocking the viral coreceptors CXCR4 and CCR5, (iii) virus-cell fusion, through binding to the viral envelope protein gp41,

(iv) viral assembly and disassembly, (v) proviral DNA integration, through integrase inhibitors and (iv) viral mRNA transcription, through inhibitors of the transcription process. Combination therapy, consisting of at least three different anti-HIV drugs has become the standard method of treatment for HIV-infected patients.

1.3.1 Nucleoside Reverse Transcriptase Inhibitors

This category consists of zidovudine, **1**, didanosine, **2**, and abacavir, **3**, shown in Figure 1.2, which act by inhibiting the replication of HIV by blocking the synthesis of proviral DNA.²⁷ They are first activated in the cell after phosphorylation steps by cell enzymes and then act as chain terminators and/or inhibitors at the substrate binding site of the reverse transcriptase, hence inhibiting viral DNA replication. Zidovudine is commonly known as AZT.

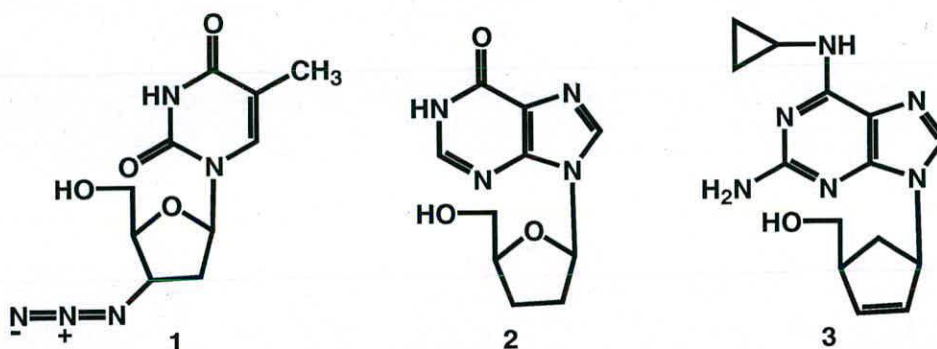


Figure 1.2 Zidovudine, **1**, didanosine, **2**, and abacavir, **3**

1.3.2 Non-Nucleoside Reverse Transcriptase Inhibitors

Non-nucleoside reverse transcriptase inhibitors are not DNA chain-terminators. These interact with the reverse transcriptase enzyme at a non-substrate

binding site, which changes the conformation of the binding site, preventing virus replication.²⁷ However, resistant mutated viruses quickly arise and as such, these drugs are best used in combination with other anti-HIV drugs. This category includes the drugs nevirapine, **4**, efavirenz, **5**, and delavirdine **6**, shown in Figure 1.3.

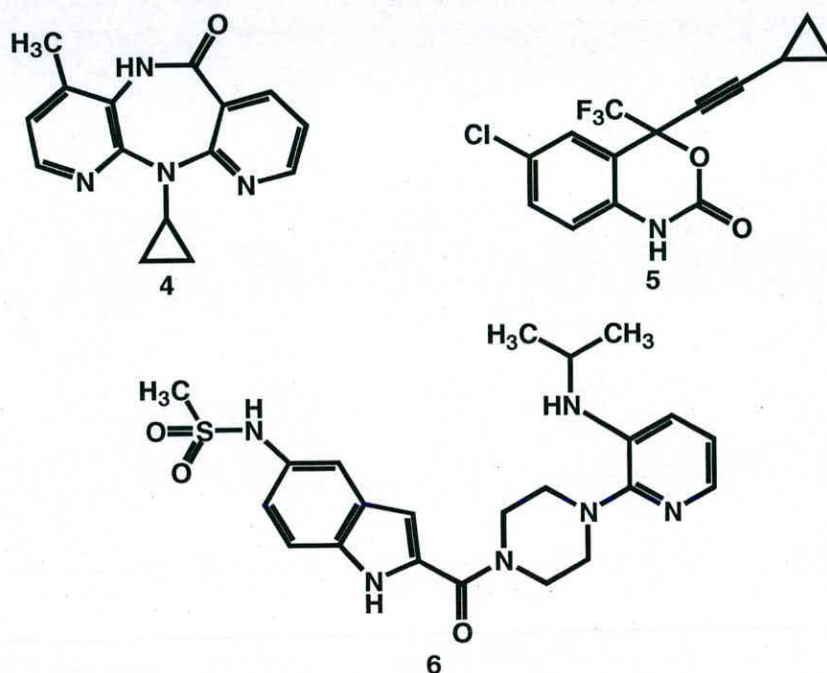


Figure 1.3 Nevirapine, **4**, efavirenz, **5**, and delavirdine **6**

1.3.3 Protease Inhibitors

Protease inhibitors specifically inhibit the virus-associated protease, and drugs such as saquinavir, **7**, and indinavir, **8**, shown in Figure 1.4, fall into this category. Saquinavir was the first drug of this type to be approved for the treatment of HIV, and it was designed by computer modelling as a molecule that would fit into the active site of the HIV protease enzyme.²⁷ This protease cleaves the viral structural proteins to form the mature virion core and activate the reverse

transcriptase needed for the next round of infection. Protease inhibitors produce non-infectious viral particles.

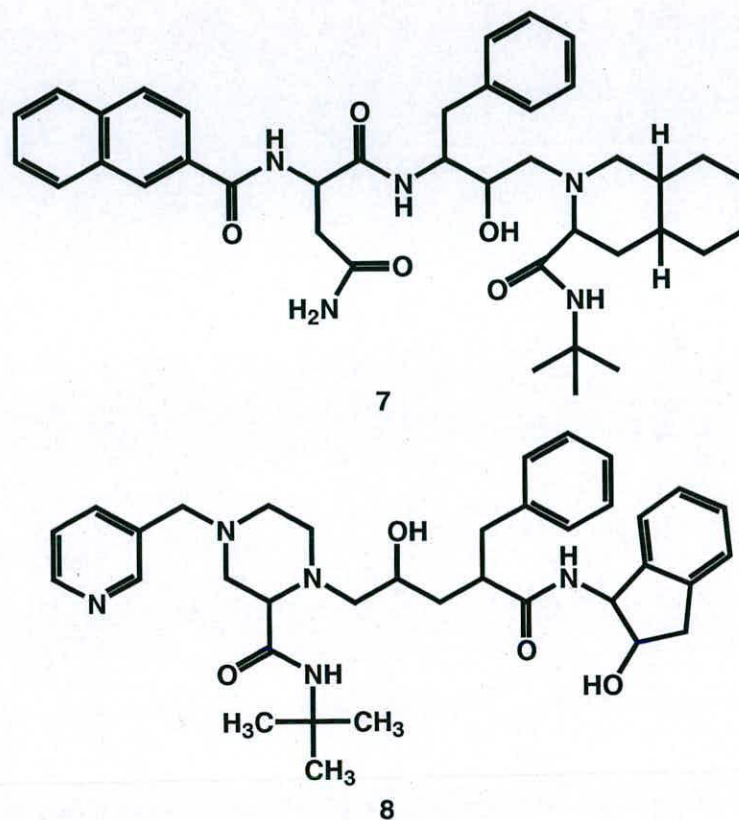


Figure 1.4 Saquinavir, 7, and indinavir, 8

1.3.4 Entry Inhibitors

Entry inhibitors are potential new anti-HIV drugs.²⁹ An example of an entry inhibitor is a CXCR4 antagonist. CXCR4 antagonists work by blocking the replication of X4 HIV-1 strains through selective antagonism of CXCR4. A series of bicyclams have been found to be the most potent CXCR4 antagonists to date.³⁰ The most active of these is xyllyl-bicyclam, **9**, shown in Figure 1.5, (also known as AMD 3100, which is the octahydrochloride salt) which inhibits the replication of X4 HIV-1

strains within the nanomolar concentration range. It is not toxic to the host cells at concentrations up to 500 μM , as such its ratio of 50 % cytotoxic concentration (CC_{50}) to 50 % antivirally effective concentration (EC_{50}) can be estimated at > 100,000.³¹

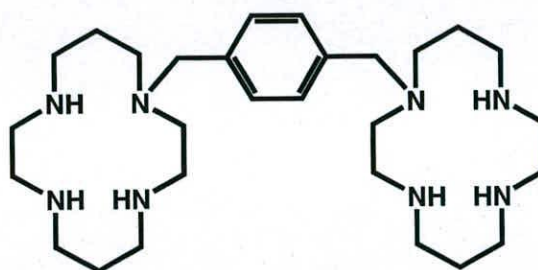


Figure 1.5 Xylyl-bicyclam, **9**

1.4 CXCR4 Coreceptor

1.4.1 CXCR4 Coreceptor Function and Structure

The CXCR4 chemokine receptor is expressed on a wide variety of cells, not only leukocytes, but also cells outside the immune system.²⁷ The receptor and its ligand SDF are involved in the control of migration and tissue targeting.

The CXCR4 receptor is a G-protein-coupled, seven-helix transmembrane protein (Figure 1.6). G-protein-coupled receptors are involved in the regulation of nearly all physiological conditions.

The CXCR4 receptor does not have any free extracellular cysteines, the main interaction points with xylyl-bicyclam has been shown to be two aspartates.³² Several histidine residues are located in the TM-III, TM-V and TM-VII helices pointing toward the main ligand binding crevice. As such, metal ion coordination

could improve the binding mode of xylyl-bicyclam by interacting with one or both of the aspartates (Asp171 and Asp262), or histidine residues could interact with the metal ions in bicyclam.³³

CCR5 is also a chemokine receptor located on the surface of T helper cells, and HIV also uses this receptor to enter the cells. It has been shown that different phenotypes of the virus, R5 and X4, use the different receptors, CCR5 and CXCR4 respectively. The X4 virus has been associated with a faster decline in T cell counts and faster progression to AIDS.³⁴

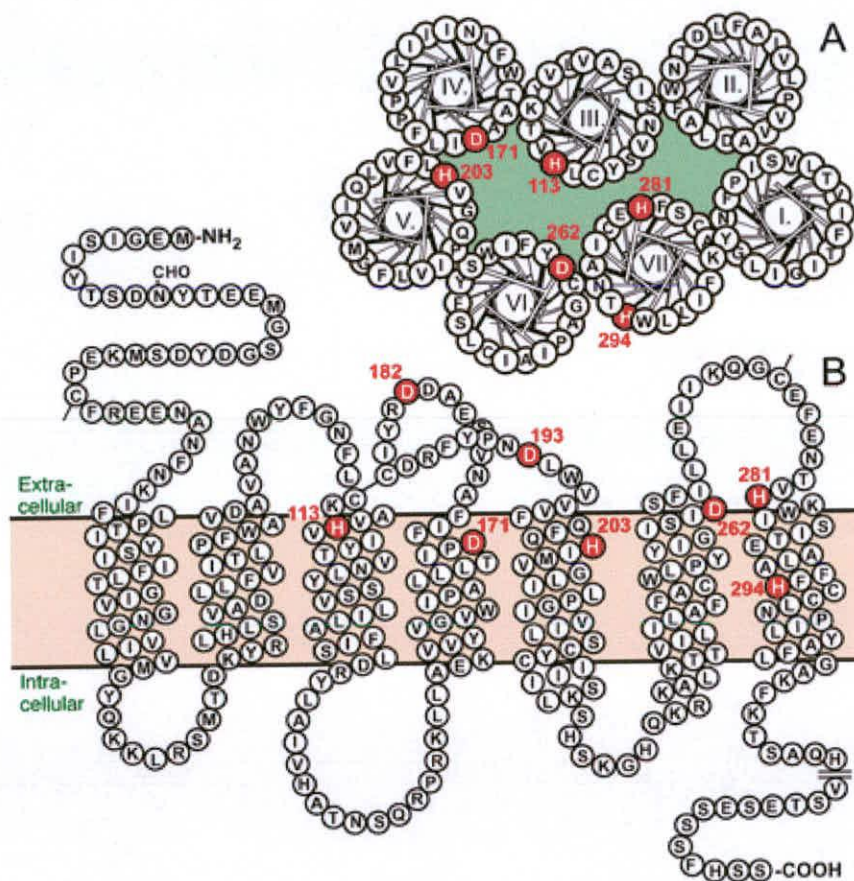


Figure 1.6 Helical wheel (A) and serpentine diagram (B) of the CXCR4 receptor. White letters in red circles represent residues that could interact with xylyl-bicyclam.³³

Xylyl-bicyclam does not interfere with the replication of the R5 HIV strains, which use the CCR5 receptor to enter host cells. The natural ligand for the CXCR4 receptor, SDF-1, was found to inhibit HIV replication for X4 HIV strains. When exposed to a mixture of X4 and R5 HIV-1 strains, xylyl-bicyclam specifically impeded the replication of X4 strains, although it allowed the growth of the R5 strains. These findings suggest that the selective blockade of the CXCR4 receptor by xylyl-bicyclam would prevent the switch from the less pathogenic R5 HIV strains to the more pathogenic X4 HIV strains. When this process occurs *in vivo*, it leads to the onset of AIDS.³⁰

1.4.2 Side-effects

By blocking the CXCR4 receptor, xylyl-bicyclam mobilises CD34⁺ stem cells from the bone marrow. Stem cells are normally retained in the bone marrow by the agonistic action of SDF-1.³⁰ (Agonist – triggers a response, antagonist – blocks a response). By blocking this agonist interaction, xylyl-bicyclam causes stem cells to be released into the bloodstream. This has been observed in mice and in humans. Mice that are genetically modified so as not to have CXCR4 receptors die in utero, and are lacking in vascular development. However, this is related to development, and it is questioned whether or not CXCR4 and its ligand SDF-1 are essential and functional in post development.³⁰ Moreover, as opposed to being a side effect, the mobilization of stem cells has been utilized as an important action of AMD 3100, and it is now in clinical trials, as the drug Mozobil. Stem cell mobilization therapy is used to restore the immune system of cancer patients who have had treatments that previously destroyed their immune cells.

1.5 Optimising the Structure of the Bicyclams

1.5.1 Varying the size of the ring

In order to maximise the anti-HIV activity of the newly discovered bicyclams, many derivatives were synthesised and tested.³⁵ Firstly, the size of the cyclam ring was varied, from 12 membered to 16 membered, compounds **10-19** in Figure 1.7, with both *meta* and *para* substituted aromatic bridges. It was found that by increasing the size of the ring from 12 to 14 membered generally increased the activity in both *meta* and *para* substituted bicyclams. However, upon increasing the size of the ring further, activity began to decline again.

In varying the substitution of the phenyl linker, it was found that *meta* substituted compounds had a greater activity than *para* compounds at a ring size of 12 and 13, however, a ring size of 14 or above was found to result in the *para* variants having greater activity. The activities for these are summarised in Table 1.1. *Ortho*, *meta* and *para* xylyl-bicyclam have all been tested for their anti-HIV activity, *para* having the greatest, *meta* slightly less, and *ortho* being significantly less active than both.

One of the cyclam rings has been replaced with an acyclical polyamine equivalent, compound **20**, shown in Figure 1.7. This resulted in an 89-fold reduction in activity, suggesting that a more rigid array was necessary for optimum activity. Adding ethyl groups to each of the nitrogen groups (**21**) reduced the activity by 2 orders of magnitude, as did changing the position of the linker from the nitrogens to 6, 6' carbons (**22**).

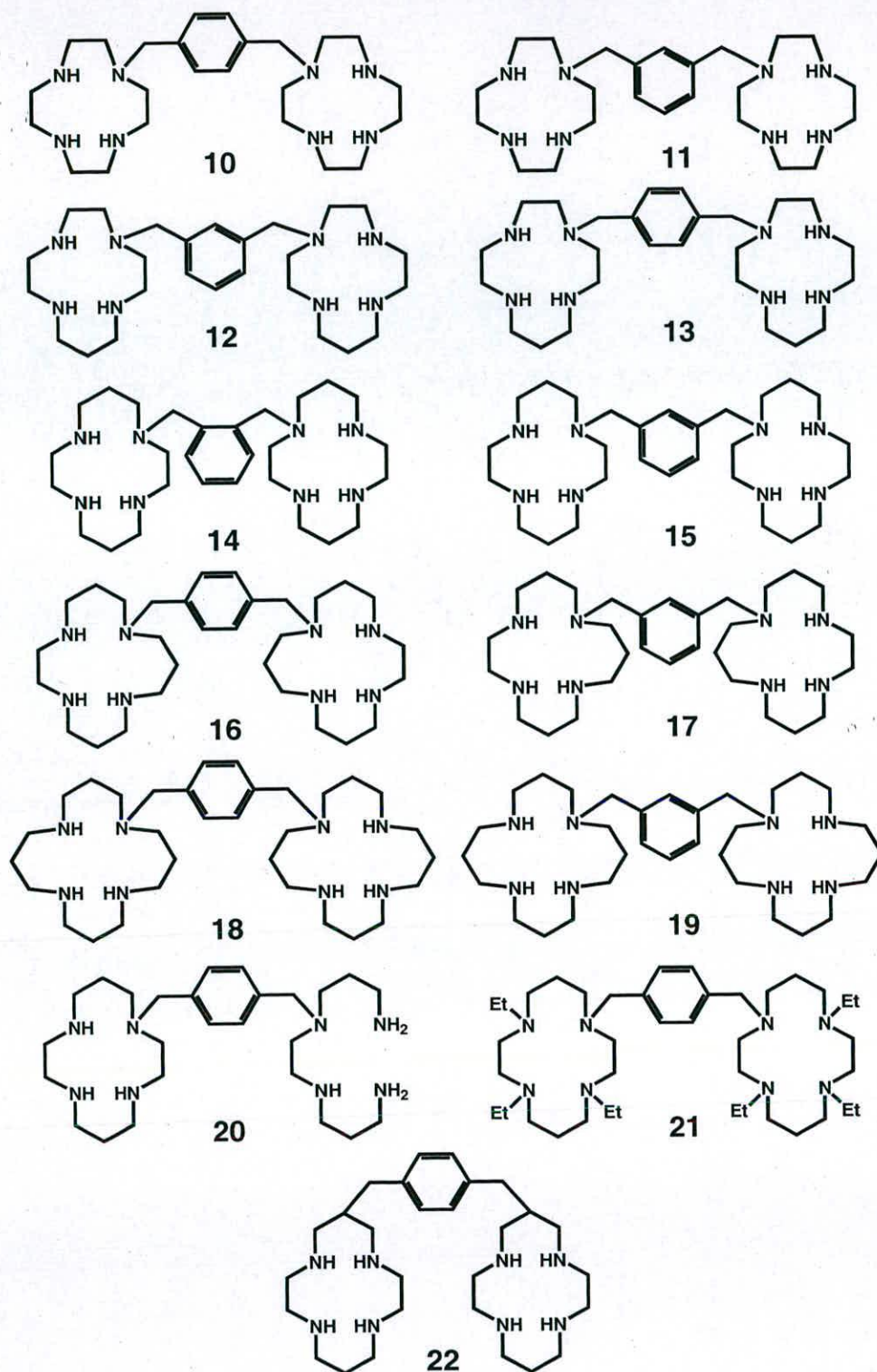


Figure 1.7 Various bicyclams that have been tested for their anti-HIV activity, with varying macrocyclic ring size^{35, 36}

Table 1.1 EC₅₀^a and CC₅₀^b values for bicyclam derivatives of differing ring size³⁵

Compound Number	EC ₅₀ (μM)	EC ₅₀ (μM)	CC ₅₀ (μM)
	HIV-1 (III _B)	HIV-2 (ROD)	
9	0.0042	0.0059	>421
10	0.3218	2.3600	>55
11	0.0751	0.5364	>20
12	0.1668	0.2341	>216
13	0.0408	0.0618	>191
14	1.3574	3.1279	>168
15	0.0337	0.0422	>421
16	1.6714	2.0072	171
17	2.7247	11.715	>190
18	9.1301	13.695	48
19	16.739	71.519	193
20	0.3730	0.7110	>444
21	7.7947	14.564	>341
22	0.5059	0.6745	406

^a EC₅₀ = The 50 % antiviral effective concentration; the molar concentration of an agonist which produces 50% of the maximum possible response for that agonist.

^b CC₅₀ = The 50 % cytotoxic concentration; the concentration of an agonist which reduces viral viability in infected cells by 50%.

Where greater than is used, this was the highest concentration tested.

1.5.2 Varying the Linker

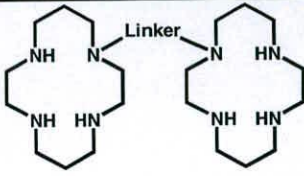
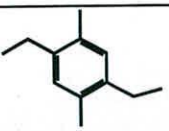
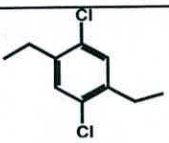
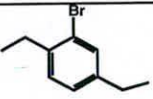
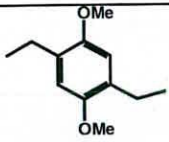
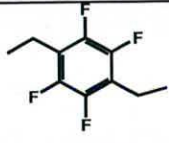
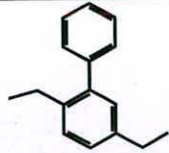
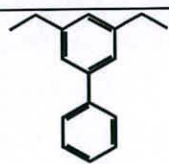


The effect of adding substituents, of varying electron-withdrawing and donating strength, to the phenyl linker has also been investigated.³⁵ The results showed that by adding dimethyl, dichloro, bromo, dimethoxy and tetrafluoro to the phenyl linker did not significantly alter the activity compared to xylyl-bicyclam alone (Table 1.2). However, the introduction of multiple halogen substituents did significantly increase the cytotoxicity of the compounds. It was found that the addition of bulky substituents to the phenyl linker, for example, another phenyl ring, greatly reduced the activity. It is thought that this reduction in activity was brought about by a restriction in the ability of the cyclam rings to rotate around the linker. This was proved by showing that the *para*-substituted phenyl linker with another phenyl group attached in the 2 position has a much lower activity than that of the *meta* substituted analogue, where the substituent is in a nonrestricting position (position 5) and the activity is not as reduced.

In a further series of tests, the length of the linker was increased, to an ethylene or a propylene chain, to study how the activity changed. The results of this were surprising. Although both had reduced activity compared to xylyl-bicyclam, the compound with the propylene linker was found to have a high selectivity against HIV-1 over HIV-2, with its EC₅₀ value against HIV-1 being 36-fold lower than its EC₅₀ value against HIV-2. However, it is clear that the optimum activity is achieved by having a methylene group between the cyclam ring and the phenyl group.

1.5.3 Heteroaromatic Linkers

Bicyclam analogues with pyridine and pyrazine linkers in place of the phenyl

Table 1.2 Structure of linkers (each one replacing the phenyl linker in xylylbicyclam, 9) and EC₅₀ and CC₅₀ values

		EC ₅₀ (μM) HIV-1 (III _B)	EC ₅₀ (μM) HIV-2 (ROD)	CC ₅₀ (μM)
2,5-dimethyl		0.0064	0.0011	>208
2,5-dichloro		0.0107	0.0025	58
2-bromo		0.0061	0.0035	>203
2,5-dimethoxy		0.0058	0.0066	>206
2,3,5,6-tetrafluoro		0.0079	0.0079	47
2-phenyl		0.1062	0.0800	>198
5-phenyl		0.2060	0.0246	>198
		14.852	69.713	>201
		0.4025	14.489	283

linker have been synthesised and their anti-HIV properties determined.³⁶ It was found that the position of the substituents on the heteroaromatic linker greatly influenced the anti-HIV activity. The 2,6- and the 3,5-pyridine-linked bicyclams showed good anti-HIV activity, but the 2,5- and the 2,4- versions had substantially reduced activity and a higher level of cytotoxicity. Replacing the pyridine linker with pyrazine, which is a weaker base, gave similar results, in that the 2,6- analogue had better anti-HIV activity than the 2,5- analogue. It was suggested that when the pyridine is linked via the 2,4- or the 2,5- positions pendant interactions to occur between the macrocycle cavity and the pyridine N, which would prevent favourable interactions occurring with the anti-HIV target.

Replacing the pyridine linker with an aniline linker, with aniline having a relatively similar pK_a as pyridine, had little effect on the overall activity of the compound. Adding a carboxylate to the phenyl linker greatly reduced the activity of bicyclam, possibly because the carboxylate on the linker may have a repulsive interaction with the target for bicyclam activity, the CXCR4 receptor. This is supported by the activity of the methyl ester derivative, which has good activity (EC_{50} values of 0.6825 and 0.5904 μM against HIV-1 and HIV-2). This shows that it is not a steric effect that is causing the reduction in activity when the CO_2H group is added.

1.5.4 Changing the Amine Groups

Replacing two of the NH groups in each cyclam ring with either sulfur (**23**, Figure 1.8) or oxygen (**24**) resulted in a significant decrease in activity.³⁷ In addition to this, the introduction of sulfur to the macrocycle greatly increased the cytotoxicity

of the compound.

A macrocycle similar to cyclam, but with the CH₂ chain lengths having the sequence 2,2,3,3 (compound **25**, *meta* version and **26**, *para* version, Figure 1.8) instead of 3,2,3,2 as in cyclam, has been prepared and analogues of it tested.³⁸ Replacing one of the NH groups with either oxygen (**27**) or a methyl (**28**) resulted in a loss of activity, compared to the 4 amine version, showing that all 4 amine groups are necessary for the anti-HIV activity. This isocyclam had slightly less activity than the original xylyl-bicyclam.

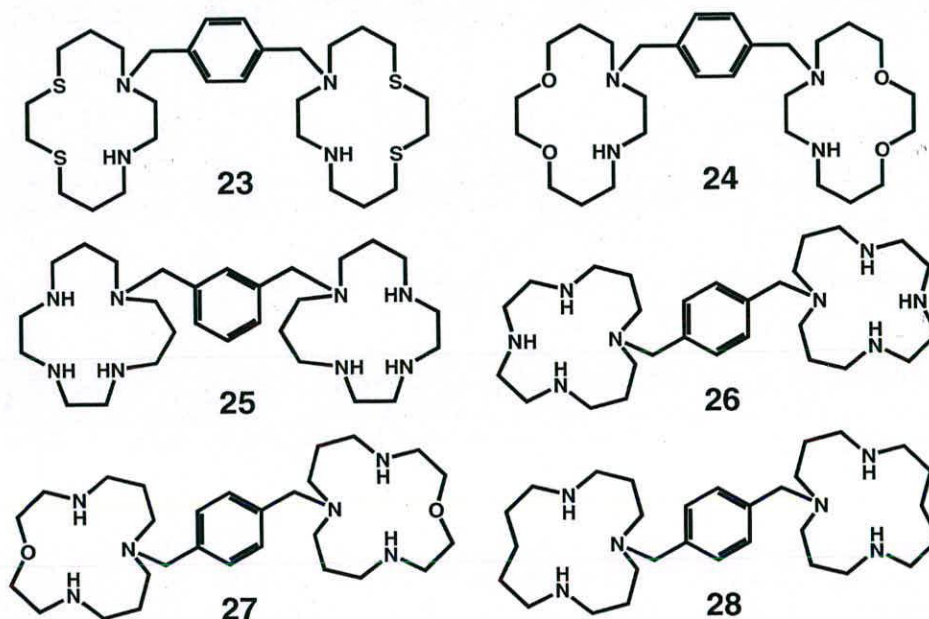


Figure 1.8 Bis-macrocycles that have been tested for their anti-HIV activity

1.5.5 Incorporation of Pyridine Rings Into the Macrocyclic Framework

Several analogues were also prepared with a pyridine ring incorporated into the macrocyclic framework (Figure 1.9).³⁸ The first reported compound with a pyridine

more basic, for example electron-donating methoxy (**32**) or phenyl (**33**) groups, resulted in a loss of anti-HIV activity. Exchanging the pyridine ring for a pyrazine ring (**34**), which is significantly less basic than pyridine, resulted in an unexpected loss of activity.

The ring size of the macrocycle with a pyridine ring incorporated into it was also varied to optimise the anti-HIV activity. The ring size was varied from 12 (**35**) to 16 (**36**), with little difference being found in the activity between the different ring sizes, unlike in the analogous bicyclam study. Finally, an isomer of the most potent pyridine macrocycle was synthesised (**37**), and it was found to have the best EC₅₀ values of any of the bicyclams synthesised, including xylyl-bicyclam. This new compound, AMD3329, had EC₅₀ values of 0.8 nM against HIV-1 and 1.6 nM against HIV-2, with the CC₅₀ value being 199 μM.

Table 1.3 EC₅₀ and CC₅₀ Values against HIV for Bis-Macrocycles with Aromatic Rings Incorporated into the Framework³⁷

Compound Number	EC ₅₀ (μM) HIV-1 (III _B)	EC ₅₀ (μM) HIV-2 (ROD)	CC ₅₀ (μM)
29	0.5342	Not tested	199
30	7.9605	Not tested	133
31	0.7509	0.7593	17.8
32	3.0979	8.4605	216
33	1.7547	Not tested	19.3
34	30.942	20.741	209
35	0.5238	0.1273	8.5
36	0.4213	1.2068	142
37	0.0008	0.0016	199

1.5.6 Metals and Bicyclam

The activity of M^{2+} transition metal complexes of xylyl-bicyclam has been investigated.^{35, 39} It was found that the addition of zinc gave a similar result to bicyclam against HIV-1, and a 2-fold increase in activity against HIV-2 (Table 1.4). The copper complex was found to be slightly less active, and the palladium derivative was inactive. It was suggested that perhaps xylyl-bicyclam forms complexes with zinc in the blood, and as such should be considered a prodrug, rather than a drug.

Table 1.4 EC_{50} and CC_{50} values against HIV for metal-xylyl-bicyclam complexes

Complexing metal	$EC_{50}/\mu M$		$CC_{50}/\mu M$
	HIV-1 (III _B)	HIV-2 (ROD)	
Zn^{2+}	0.0077	0/0009	>250
Ni^{2+}	0.0078	0.0157	>250
Cu^{2+}	0.0436	0.1818	>250
Co^{3+}	0.7697	0.5200	>250
Pd^{2+}	57.881	10.544	>250

Zn^{2+} is located in the centre of the cyclam ring, bonded to the 4 nitrogen groups. Zn^{2+} can be 4-, 5- or 6-coordinate, and this can leave one or two vacant coordination sites which could interact with histidine or cysteine residues on the protein, or with acidic residues such as aspartates.

The affinity of xylyl-bicyclam for to the CXCR4 chemokine receptor is enhanced 7, 36, and 50-fold respectively, by incorporation of Cu^{2+} , Zn^{2+} or Ni^{2+} into the cyclam rings of the compound.³³ Studies of xylyl-bicyclam with only one metal ion complexed (either Cu^{2+} or Ni^{2+}) showed that the increased binding affinity of the metal ion substituted xylyl-bicyclam is achieved through an enhanced interaction of just one of the ring systems. Mutational analysis showed that the binding of the xylyl-bicyclam is dependent on both Asp171 and Asp262.³³ The enhancing effect of the metal ion was selectively eliminated by substitution of Asp262 located at the extracellular end of TM-VI. It was concluded that the increased binding affinity of the metal ion substituted xylyl-bicyclam is obtained through enhanced interaction of one of the cyclam ring systems with the carboxylate group of Asp262. It was suggested that this occurs through a strong interaction of one of the oxygen atoms directly with the metal ion and the other oxygen with one of the nitrogens of the cyclam ring through a hydrogen bond.

The only crystal structure of a metal-xylyl-bicyclam is zinc(II) xylyl-bicyclam, as the acetate complex $[\text{Zn}_2(\text{xylyl-bicyclam})(\text{OAc})_2](\text{OAc})_2$.⁴⁰ It was shown that both cyclam rings crystallised in the same configuration, the folded *cis*-V configuration (see Figure 1.10 for configurations of metal cyclams). The zinc is in a distorted octahedral geometry. The acetate ligand is chelating, and on the other face of the ring, the acetate forms a double hydrogen bond to two of the NH protons. However, NMR studies showed that in solution, over a period of approximately 20 minutes, equilibrium was reached and the configuration of the macrocycle altered. The end composition of the solution was 58 % *cis*-V, 35 % *trans*-I and 7 % *trans*-III. It was shown that the predominant species was *cis*-V/*trans*-I (44 %) with *cis*-V/*cis*-V

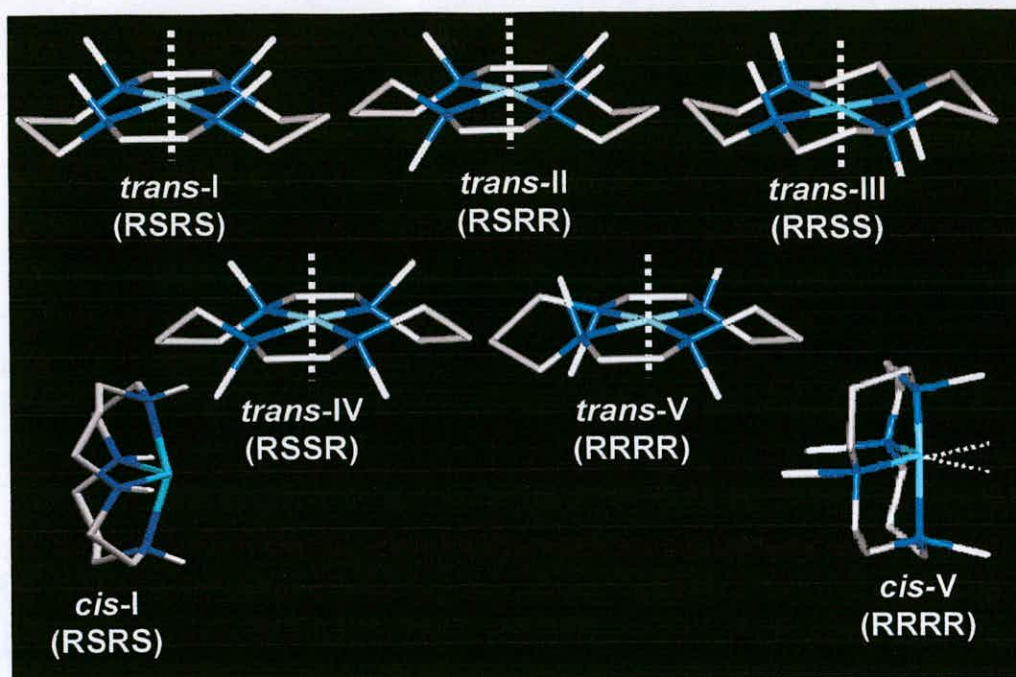


Figure 1.10 Configurational isomers of cyclam

making up 29 % of the total solution. The solution structure for $Zn_2(\text{xylyl-bicyclam})(\text{ClO}_4)_4$ has also been determined. This solution took longer to reach equilibrium (6 hours) and was found to be 45 % *trans-I*, 34 % *trans-III* and 21 % *cis-V*. The *cis-V/trans-I* was again found to be the major configuration in the solution (26 %). Addition of acetate (4 molar equivalents) to this solution was found to induce a configurational change, with the *cis-V* configuration becoming the most predominant. The *cis-V/cis-V* configuration increased from 0 % to 19 %, and the *cis-V/trans-I* configuration increased to 38 %.

1.5.7 $Zn_2(\text{Xylyl-Bicyclam})$ Binding to CXCR4 Coreceptor

An homology model of the CXCR4 coreceptor, based on the 7 helical transmembrane structure of bovine rhodospin has been prepared,⁴¹ and this model

was used to model the binding of Zn₂-xylyl-bicyclam to the receptor.⁴⁰ The *cis-V/trans-I* model was used as this is the most predominant configuration in solution. The *cis-V* cyclam ring was coordinated to Asp262, with the Zn(II)-carboxylate bond length of 2.27 Å, which was similar to the equivalent bond length in the [Zn₂(xylyl-bicyclam)(OAc)₂](OAc)₂ crystal structure. The opposite face of the *cis-V* cyclam ring forms a double hydrogen bond from the two NH groups to the oxygens of the Glu288, with the hydrogen bonds being 2.01 Å in length. The *trans-I* cyclam ring is bound to the oxygens of Asp171, with the bond length being 2.28 Å.

Asp171 and Asp262 are found in the *trans*-membrane helices IV and VI, respectively, and these were identified as key binding sites for xylyl-bicyclam by mutagenesis studies.³² The phenyl linker is known to be important for the high anti-HIV activity of the bicyclams,³⁷ and in the homology model of the CXCR4 coreceptor there is a high population of aromatic amino acid side chains in the extracellular loop which could form aromatic π - π stacking interactions with the phenyl linker. This could stabilize intermediate binding steps along the pathway through the extracellular loops.

1.6 Cyclam

1.6.1 Cyclam Background

Macrocyclic ligands are prominent in naturally occurring ligands in biology, such as the 16-membered inner ring in the porphyrin ligand of heme proteins and the 15-membered ring in the corrin ligand of vitamin B12. The man-made ligand cyclam (1,4,8,11-tetraazacyclotetradecane, **38**, Figure 1.11), was first synthesized in

1937⁴², and is a 14-membered heterocycle. Cyclam, along with its derivatives, is of interest in diverse fields, such as catalysis, selective metal recovery, and therapy and diagnosis.⁴³⁻⁴⁸

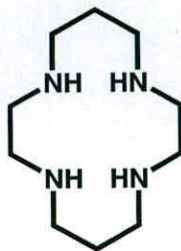


Figure 1.11 Cyclam, **38**

Macrocyclic polyamines are highly protonated and bind transition metal ions strongly via coordination.⁴⁹ As macrocyclic polyamines have a restricted geometry, the nitrogen lone pairs may overlap to bring about high electron density within the cavity. Cyclam has a high affinity for protons, the first two pK_a values being 11.5 and 10.3 (See Table 1.5). However, once these two protons are incorporated, steric and electrostatic repulsions come into effect (shown in Figure 1.12) and the last two proton affinities are weak, with pK_a values for cyclam of 1.6 and 0.9.⁵⁰ For the linear tetraamine, the third and fourth pK_a values for it are 7.3 and 6.0.

Several values for the pK_a values for cyclam have been published. Most are in close agreement for the first three, but the values of the last pK_a differ from 0.9 to 2.4. These are shown in Table 1.5.

Table 1.5 Protonation Values for Cyclam

pKa ₁	pKa ₂	pKa ₃	pKa ₄	Conditions	Reference
11.49	10.24	1.64	0.86	Unknown	50
11.585	10.62	1.61	2.41*	0.5 M KNO ₃ , 25 °C	51
11.3	10.23	1.43	2.27*	0.1 M NaNO ₃ , 25 °C.	52
11.29	10.19	1.61	1.91*	0.1 M KCl, 25 °C	53

* No explanation is given for the value of pKa₄ being higher than that of pKa₃.

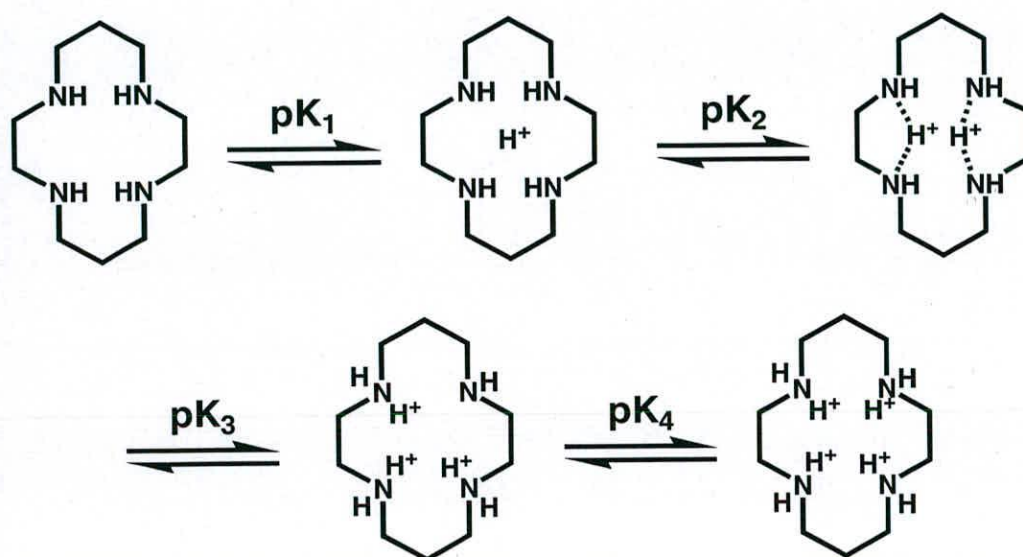


Figure 1.12 Protonation steps for cyclam.

Macrocycles are also extremely favourable for metal complexation. In terms of the entropy factor, this can be seen as an extension of the “chelate effect” that is a major contribution to an increase in complex stability as the number of chelate rings increases. The size of the metal ion and the cavity size greatly influences the stability of a metal-macrocycle complex. For example Cu(II)-cyclam is more stable ($\log K = 30.5$) than the equivalent 15-membered macrocycle complex ($\log K =$

24.4).⁴⁹

Macrocyclic amines form stable complexes with nearly all transition metal ions.⁴⁹ The stability of the macrocyclic complexes depends on the size of the metal ion and the configuration of the cyclam. The values for log K for Cu(II), Ni(II), Co(II), Zn(II) and Cd(II) cyclam complexes have been determined and are shown in Table 1.6, and this shows the stability depends on the size of the metal ion.

Table 1.6 Stability constants for cyclam complexes and ionic radii

M ²⁺	r (Å)	log K Cyclam	Reference
Cu ²⁺	0.72	27.2	54
Ni ²⁺	0.69	22.2	50
Zn ²⁺	0.74	15.0 or 15.5	55,56
Co ²⁺	0.75	12.7	57
Cd ²⁺	0.97	11.7	58

Work has been done on the uptake of zinc by cyclam under physiological conditions. It is possible that bicyclam picks up zinc from the blood so this was investigated. It was shown that at 37 °C and pH = 7.4, cyclam can complex zinc, and that the initial reaction rate is $7.2 \times 10^{-9} \text{ M s}^{-1}$, with equilibrium being reached in approximately 2 hours, at which point 66 % of the zinc was bound to the cyclam.⁵⁹ In the same study, competitive binding between zinc and copper was monitored, as copper is also present in the blood. It was found that zinc bound in preference to copper under these conditions, despite Cu(II) being the more thermodynamically

favoured metal ion.

1.6.2 Configurational Isomers

There are five configurational *trans* isomers of metal cyclam adducts, which differ in the chirality of the N atoms.^{60, 61} These are usually designated as *trans*-I (RSRS,++++), *trans*-II (RSRR,+--+), *trans*-III (RRSS,+--+), *trans*-IV (RSSR,+--+), and *trans*-V (RRRR,+--+), shown in Figure 1.10. The configurations that are symmetrical about the diagonal can fold to form *cis* isomers, e.g., the *trans*-V isomer can fold to give the *cis*-V structure. Semi-quantitative analysis of the relative strain energies of the five isomers indicates that the *trans*-III form is the most stable.^{61, 62} However, it has been noted that *trans*-I is more favoured for square-planar complexes, while octahedral complexes prefer *trans*-III.⁶³

In contrast to oxygen-donor and sulfur-donor macrocyclic ligands, macrocyclic polyamines are much more basic and are also subject to deprotonation.⁶⁴ Much work had been carried out on the kinetics of the formation of Ni(II) cyclam in aqueous solution.⁶⁵ It was found that the monoprotonated and diprotonated species exhibit formation rate constants 3×10^4 times slower than the equivalent open chain species.

1.6.3 Metal Cyclams

A search of the Cambridge Crystallographic Structural Database was carried out for configurations of nickel, cobalt, copper, zinc and palladium cyclam complexes. The results are shown in Table 1.7. For Ni(II) and Zn(II), the reported

trans-III structures all contain 6-coordinate, octahedral metal ions, while the *cis*-V complexes all contain bridging or chelating ligands. However, there is one exception to this. Barefield *et al.*⁶⁶ reported a *cis*-V complex with two water molecules bound to a Ni (II)-cyclam. In this case, the complex was prepared via the acidification of *cis*-V [Ni(cyclam)(en)]²⁺. The ethylenediamine ligand can coordinate only in the *cis* positions, which forces the cyclam to fold. Their findings indicate that configurational interconversion of *cis*-V to *trans*-III Ni(II)-cyclam is slow, in contrast to Zn(II)-cyclam.⁴⁰ There is an interesting example of a Ni(II) complex that crystallises with two different cyclam configurations within the unit cell.⁶⁷ The complex [Ni₂(cyclam)₂(SH)₂](ClO₄)₂·[Ni(cyclam)(SH)₂] features two *cis*-V Ni(II)-cyclam units bridged by two SH⁻ groups, and a separate Ni(II)-cyclam in the *trans*-III configuration, with two SH ligands bound in the axial positions to octahedral Ni(II). The only *trans*-V complex found in the database is [Ni(cyclam)](ZnCl₄), which contains four co-ordinate Ni(II).⁶⁶

Table 1.7 Number of Entries and Configurations of Metal-Cyclam Complexes in the CSD

Metal	<i>trans</i> -I, II, IV	<i>trans</i> -III	<i>trans</i> -V	<i>cis</i> -V	<i>trans</i> -III + <i>cis</i> -V
Nickel	0	53	1	6	1
Cobalt	0	17	0	5	0
Copper	0	34	0	0	0
Zinc	0	11	0	0	0
Palladium	0	8	0	0	0

In the X-ray crystal structures of $[\text{Zn}(\text{cyclam})(\text{H}_2\text{O})_2](\text{OAc})_2$ the macrocycle adopts the *trans*-III configuration and the axial Zn–OH₂ bonds are long (2.27 Å).⁶⁸ Similarly the phthalate bridged complex $[\text{Zn}(\text{cyclam})(\text{phthalate})]_n(\text{CH}_3\text{OH})^{2n}$ is also *trans*-III. In aqueous solution these carboxylato Zn(II) cyclam complexes exist as mixtures of *trans*-I, *trans*-III and *cis*-V configurations.

Liang *et al.* carried out NMR solution studies on $\text{Cd}(\text{cyclam})(\text{ClO}_4)_2$, $\text{Cd}(\text{cyclam})\text{Cl}_2$ and $[\text{Cd}_3(\text{cyclam})_3(\text{CO}_3)](\text{ClO}_4)_4 \cdot 3\text{H}_2\text{O}$ and used these to identify key markers for various configurations adopted by these complexes.⁶⁹ Cadmium was used for this study because its isotopes (¹¹¹Cd and ¹¹³Cd, $I = 1/2$) are favourable for NMR studies, unlike those of zinc. A variety of solution conditions were analysed using 1D and 2D ¹H, ¹³C, ¹⁵N and ¹¹¹Cd NMR spectroscopy, including Karplus-type analyses of ¹H, ¹H and ¹H, ¹¹¹Cd coupling constants. Only the *trans*-I and *trans*-III configurations have six non-equivalent protons and hence give rise to six proton resonances, while the *trans*-IV, *trans*-V and *cis*-V configurations have five non-equivalent protons and give rise to five proton resonances. The X-ray crystal structure of $[\text{Cd}_3(\text{cyclam})_3(\text{CO}_3)](\text{ClO}_4)_4 \cdot 3\text{H}_2\text{O}$ showed it to be in the uncommon folded *cis*-I configuration with all of the N–H bonds oriented upwards, while the NMR studies suggested that it adopts the *trans*-I configuration in solution.

Co(III)-cyclam chloride and Mn(II)-cyclam chloride complexes have been co-crystallised by Chen *et al.*⁷⁰ In both of these units, the cyclam rings are in the *trans*-III configuration. Both metals are octahedral with two *trans* chloride ligands. All the reported Co(III)-cyclam complexes contain octahedral cobalt. There are three reported Co(III)-cyclam complexes that have chelating ligands, $[\text{Co}(\text{cyclam})(\text{acetylacetonate})](\text{BF}_4)$,⁷¹ $[\text{Co}(\text{cyclam})(\text{ethylenediamine})]\text{Cl}_3 \cdot 3\text{H}_2\text{O}$ ⁷²

and [Co-(cyclam)(oxalato-*O,O'*)](NO₃).⁷³ These complexes are in the *cis*-V configuration, which is expected as a chelating ligand would not accommodate the more common *trans*-III configuration. The reported *trans*-III Co(II) structures are all six coordinate, except for the complex [Co(cyclam)](ClO₄), reported by Endicott *et al.*, which is four-coordinate, with a perchlorate counterion.⁷⁴ There are only two reported *cis*-V cobalt complexes that contain bridging ligands, [{Co(II)(cyclam)(μ₂-HS)}₂]-2(HS) and [{Co(III)(cyclam)(μ₂-S)}₂]-2(ClO₄)-2(C₂H₃N);⁶⁷ both are dimers, with SH and S as bridging ligands.

The Cu(II)-cyclam complexes are again mostly six coordinate, but five four-coordinate complexes have been reported. These are [Cu(cyclam)](BH₄)₂,⁷⁵ [Cu(cyclam)](CuBr₃),⁷⁶ [Cu(cyclam)](CuCl₄),⁷⁷ the catena complex [Cu(cyclam)(μ₂-Cl)]_n, *n*(CdCl₃·2H₂O)⁷⁸ and the tri-cyclam complex 3[Cu(cyclam)]·2(Cl₂-Cu₂O₆S₆),2(H₃O)(H₂O).⁷⁹

The reported Pd(II)-cyclam complexes are all *trans*-III and are four-coordinate. Yamashita *et al.* reported the unusual mixed valence complex [Pd(II)(cyclam)][Pd(IV)(cyclam)Cl₂](ClO₄)₄.⁸⁰ The four-coordinate Pd(II) and six-coordinate Pd(IV) units are stacked alternately in the direction of the *c* axis, which forms linear chains of Cl-Pd(IV)-Cl-Pd(II), with successive cyclam units rotated 180° about the chain axis. Neighbouring Pd(II) and Pd(IV) units are held together by two hydrogen bonds, NH-O-NH. These hydrogen bonds are thought to play a vital role in the formation of the mixed-valence complex. They also made the six-coordinate Pd(IV) complex, [Pd(cyclam)Cl₂](NO₃)₂·H₂O·HNO₃. The Pd(IV)-Cl bond lengths in the mixed-valence complex are slightly longer than in that of the Pd(IV) complex. This was attributed to electronic interactions along the chain. A

further six coordinate Pd(IV) complex, $[\text{Pd(II)(cyclam)}][\text{Pd(IV)(cyclam)Cl}_2](\text{PF}_6)_4$, has been reported by Toriumi *et al.*⁸¹ In both mixed-valence complexes, the Cl bridging ligands are statistically disordered and all the Pd sites comprise $1/2\text{Pd(II)} + 1/2\text{Pd(IV)}$.

1.7 Recent Developments Involving Cyclam Derivatives

Interest in cyclam and its derivatives remains strong, and new uses for it are still being identified. Lipophilic derivatives of cyclam, have been shown to inhibit tumour cell growth.⁸² It is thought the lipophilicity of the new analogues facilitates the transport of the macrocycles into the cell, where the macrocycle can then carry out its function. Cyclam was found to have no effect on the tumour cell growth, while the two derivatives had IC_{50} values of 6.2 and 8.7 μM . Xylyl-bicyclam has also been suggested as a possible treatment for tumours, such as breast cancer, which are partially dependent on signalling through the CXCR4 receptor.⁸³

A series of covalently-coupled cyclam and bicyclam conjugates with AZT have been synthesised. AZT was the first drug to be approved by the US Food and Drug Administration as an anti-HIV drug and has been extensively studied. One variant was shown to be particularly effective, and it seems to target the CXCR4 on the cell surface and selectively delivers AZT into the cell, thus increasing the efficiency of action.

Xylyl-bicyclam is currently in Phase 2 clinical trials as a stem cell mobiliser, marketed as Mozobil.^{84, 85} By blocking CXCR4, a specific cellular receptor, xylyl-bicyclam triggers the rapid movement of stem cells out of the bone marrow and into circulating blood. Once in the circulating blood, the stem cells can be collected for

use in stem cell transplant. Stem cell transplant is a procedure used to restore the immune system of cancer patients who have had treatments that previously destroyed their immune cells.

Xylyl-bicyclam has also been shown in mice to reduce the severity of autoimmune collagen-induced arthritis, which is used as a model for rheumatoid arthritis in man.^{83, 86}

1.8 Aims of This Thesis

Xylyl-bicyclam is a CXCR4 receptor antagonist and metal complexation by xylyl-bicyclam greatly influences its activity. The aims of this thesis were to investigate solid and solution state structures of metal complexes of cyclam and bicyclam, and also of the new anti-HIV compound, AMD 3329 and its component macrocycle.

Specific aims were as follows.

1. To synthesize and characterise Pd^{2+} , Ni^{2+} , Co^{3+} and Cu^{2+} complexes of both cyclam and xylyl-bicyclam, using techniques such as X-ray crystallography and multidimensional NMR spectroscopy.
2. To synthesize and characterise $^{111}\text{Cd}^{2+}$ complexes of AMD 3329 and one of its component macrocycles, using ^{111}Cd NMR studies to obtain information on the solution structure of these novel complexes.
3. To investigate the interaction of metal-cyclam and metal-xylyl-bicyclam complexes with lysozyme, a model target protein, using X-ray crystallography and NMR spectroscopy.

1.9 References

- 1 B. Rosenberg, L. Van Camp, J. E. Trosko, and V. H. Mansour, *Nature*, 1969, **222**, 385-386.
- 2 Z. Guo and P. J. Sadler, *Angew. Chemie Int. Ed.*, 1999, **38**, 1512-1531.
- 3 Z. Guo and P. J. Sadler, *Ad. Inorg. Chem.*, 2000, **49**, 183-305.
- 4 J. Kasparikova, V. Marini, Y. Najajreh, D. Gibson, and V. Brabec, *Biochemistry*, 2003, **42**, 6321-6332.
- 5 N. Farrell, L. R. Kelland, J. D. Roberts, and M. Vanbeusichem, *Cancer Res.*, 1992, **52**, 5065-5072.
- 6 G. Natile and M. Coluccia, *Coord. Chem. Rev*, 2001, **216**, 383-410.
- 7 E. I. Montero, S. Diaz, A. M. Gonzalez-Vadillo, J. M. Perez, C. Alonso, and C. Navarro-Ranninger, *J. Med. Chem.*, 1999, **42**, 4264-4268.
- 8 A. M. Pizarro, V. P. Munk, C. Navarro-Ranninger, and P. J. Sadler, *Angew. Chem.-Int. Ed.*, 2003, **42**, 5339-5342.
- 9 P. Di Blasi, A. Bernareggi, G. Beggiolin, L. Piazzoni, E. Menta, and M. L. Formento, *Anticancer Res.*, 1998, **18**, 3113-3117.
- 10 H. Köpf and P. Köpf-Maier, *Angew. Chemie Int. Ed.*, 1979, **18**, 477-478.
- 11 P. Köpf-Maier and H. Köpf, 'Metal Compounds in Cancer Therapy', Chapman and Hall, London, 1994.
- 12 M. Friedrich, C. Villena-Heinsen, C. Farnhammer, and W. Schmidt, *Eur. J. Gynaecol. Oncol.*, 1998, **19**, 333-337.
- 13 C. Villena-Heinsen, M. Friedrich, A. K. Ertan, C. Farnhammer, and W.

- Schmidt, *Anti-Cancer Drugs*, 1998, **9**, 557-563.
- 14 C. V. Christodoulou, A. G. Eliopoulos, L. S. Young, L. Hodgkins, D. R. Ferry, and D. J. Kerr, *Br. J. Cancer*, 1998, **77**, 2088-2097.
- 15 M. J. Clarke, F. C. Zhu, and D. R. Frasca, *Chem. Rev.*, 1999, **99**, 2511-2533.
- 16 R. E. Aird, J. Cummings, A. A. Ritchie, M. Muir, R. E. Morris, H. Chen, P. J. Sadler, and D. I. Jodrell, *Br. J. Cancer*, 2002, **86**, 1652-1657.
- 17 R. E. Morris, R. E. Aird, P. D. Murdoch, H. M. Chen, J. Cummings, N. D. Hughes, S. Parsons, A. Parkin, G. Boyd, D. I. Jodrell, and P. J. Sadler, *J. Med. Chem.*, 2001, **44**, 3616-3621.
- 18 F. Y. Wang, J. Bella, J. A. Parkinson, and P. J. Sadler, *J. Biol. Inorg. Chem.*, 2005, **10**, 147-155.
- 19 H. M. Chen, J. A. Parkinson, S. Parsons, R. A. Coxall, R. O. Gould, and P. J. Sadler, *J. Am. Chem. Soc.*, 2002, **124**, 3064-3082.
- 20 H. M. Chen, J. A. Parkinson, R. E. Morris, and P. J. Sadler, *J. Am. Chem. Soc.*, 2003, **125**, 173-186.
- 21 C. F. Shaw, III, *Chem. Rev.*, 1999, **99**, 2589-2600.
- 22 D. Schuhmann, M. Kubickamuranyi, J. Mirtschewa, J. Gunther, P. Kind, and E. Gleichmann, *J. Immunology*, 1990, **145**, 2132-2139.
- 23 C. J. Anderson and M. J. Welch, *Chem. Rev.*, 1999, **99**, 2219-2234.
- 24 S. S. Jurisson and J. D. Lydon, *Chem. Rev.*, 1999, **99**, 2205-2218.
- 25 P. Caravan, J. J. Ellison, T. J. McMurry, and R. B. Lauffer, *Chem. Rev.*, 1999, **99**, 2293-2352.
- 26 G. G. Briand and N. Burford, *Chem. Rev.*, 1999, **99**, 2601-2658.
- 27 N. A. Campbell, 'Biology', Benjamin Cummings, California, 1996.

- 28 D. Schols, *Curr. Top. Med. Chem.*, 2004, **4**, 883-893.
- 29 E. De Clercq, *Pure Appl. Chem.*, 1998, **70**, 567-577.
- 30 E. De Clercq, *Nature Rev. Drug Dis.*, 2003, **2**, 581-587.
- 31 E. De Clercq, N. Yamamoto, R. Pauwels, J. Balzarini, M. Witvrouw, K. DeVreese, Z. Debyser, B. Rosenwirth, P. Peichl, R. Datema, D. Thornton, R. T. Skerlj, F. Paul, S. Padmanabhan, G. Bridger, G. Henson, and M. J. Abrams, *Antimicro. Agents. Chemother.*, 1994, **38**, 668-674.
- 32 L. O. Gerlach, R. T. Skerlj, G. J. Bridger, and T. W. Schwartz, *J. Biol. Chem.*, 2001, **276**, 14153-14160.
- 33 L. O. Gerlach, J. S. Jakobsen, K. P. Jensen, M. R. Rosenkilde, R. T. Skerlj, U. Ryde, G. Bridger, and T. W. Schwartz, *Biochemistry*, 2003, **42**, 710-717.
- 34 A.-Z. Decrion, A. Varin, J.-M. Estavoyer, and G. Herbein, *J. Gen. Virol.*, 2004, **85**, 1471-1478.
- 35 G. J. Bridger, R. T. Skerlj, D. Thornton, S. Padmanabhan, S. A. Martellucci, G. W. Henson, M. J. Abrams, N. Yamamoto, K. De Vreese, R. Pauwels, and E. De Clercq, *J. Med. Chem.*, 1995, **38**, 366-378.
- 36 G. J. Bridger, R. T. Skerlj, S. Padmanabhan, S. A. Martellucci, G. W. Henson, M. J. Abrams, H. C. Joao, M. Witvrouw, K. De Vreese, R. Pauwels, and E. De Clercq, *J. Med. Chem.*, 1996, **39**, 109-119.
- 37 G. J. Bridger, R. T. Skerlj, S. Padmanabhan, S. A. Martellucci, G. W. Henson, S. Struyf, M. Witvrouw, D. Schols, and E. De Clercq, *J. Med. Chem.*, 1999, **42**, 3971-3981.
- 38 G. Bridger and R. T. Skerlj, *Adv. Antiviral Drug Des.*, 1999, **3**, 161-229.
- 39 J. A. Este, C. Cabrera, E. De Clercq, S. Struyf, J. Van Damme, G. Bridger, R.

- T. Skerlj, M. J. Abrams, G. Henson, A. Gutierrez, B. Clotet, and D. Schols, *Mole. Pharm.*, 1999, **55**, 67-73.
- 40 X. Liang, J. A. Parkinson, M. Weishäupl, R. O. Gould, S. J. Paisey, H.-S. Park, T. M. Hunter, C. A. Blindauer, S. Parsons, and P. J. Sadler, *J. Am. Chem. Soc.*, 2002, **124**, 9105-9112.
- 41 K. Palczewski, T. Kumasaka, T. Hori, C. A. Behnke, H. Motoshima, B. A. Fox, I. Le Trong, D. C. Teller, T. Okada, and R. E. Stenkamp, et al., *Science*, 2000, **289**, 739-745.
- 42 J. Van Alphen, *Recl. Trav. Chim. Pays-Bas*, 1937, **56**, 343-350.
- 43 L. Messori, F. Abbate, G. Marcon, P. Orioli, M. Fontani, E. Mini, T. Mazzei, S. Carotti, T. O'Connell, and P. Zanello, *J. Med. Chem.*, 2000, **43**, 3541-3548.
- 44 E. Kimura, T. Shiota, T. Koike, M. Shiro, and M. Kodama, *J. Am. Chem. Soc.*, 1990, **112**, 5805-5811.
- 45 I. Taniguchi, N. Nakashima, and K. Yasukouchi, *J. Chem. Soc., Chem. Commun.*, 1986, **24**, 1814-1815.
- 46 T. R. Wagler, Y. Fang, and J. C. Burrows, *J. Org. Chem.*, 1989, **54**, 1584-1589.
- 47 H. Yoon and J. C. Burrows, *J. Am. Chem. Soc.*, 1988, **110**, 4087-4089.
- 48 J. D. Koola and J. K. Kochi, *Inorg. Chem.*, 1987, **26**, 908-916.
- 49 E. Kimura, *Tetrahedron*, 1992, **48**, 6175-6217.
- 50 F. P. Hinz and D. W. Margerum, *Inorg. Chem.*, 1974, **13**, 2941-2949.
- 51 M. Micheloni, A. Sabatini, and P. Paoletti, *J. Chem. Soc., Perkin Trans. II*, 1978, 828-830.
- 52 V. J. Thom, G. D. Hosken, and R. D. Hancock, *Inorg. Chem.*, 1985, **24**, 3378.

- 53 R. D. Hancock, R. J. Motekaitis, J. Mashishi, I. Cukrowski, J. H. Reibenspies, and A. E. Martell, *J. Chem. Soc., Perkin Trans.*, 1996, **2**, 1925-1929.
- 54 M. Kodama and E. Kimura, *J. Chem. Soc. Dalton Trans.*, 1977, **15**, 1473-1478.
- 55 M. Kodama and E. Kimura, *J. Chem. Soc. Dalton Trans.*, 1978, 1081-1085.
- 56 M. Kodama and E. Kimura, *J. Chem. Soc., Perkin Trans. II*, 1977, 2269-2276.
- 57 M. Kodama and E. Kimura, *J. Chem. Soc. Dalton Trans.*, 1980, 327-333.
- 58 E. Kimura, *Prog. Inorg. Chem.*, 1994, **41**, 443-491.
- 59 S. J. Paisey and P. J. Sadler, *Chem. Comm.*, 2004, 306-307.
- 60 P. J. Connolly and E. J. Billo, *Inorg. Chem.*, 1987, **26**, 3224-3226.
- 61 B. Bosnich, C. K. Poon, and M. L. Tobe, *Inorg. Chem.*, 1965, **4**, 1102-1108.
- 62 P. O. Whimp, M. F. Bailey, and N. F. Curtis, *J. Chem. Soc. A*, 1970, **11**, 1956-1963.
- 63 M. A. Donnelly and M. Zimmer, *Inorg. Chem.*, 1999, **38**, 1650-1658.
- 64 X. Liang and P. J. Sadler, *Chem. Soc. Rev.*, 2004, **33**, 246-266.
- 65 T. Kaden, *Helv. Chim. Acta*, 1970, **53**, 617-.
- 66 E. K. Barefield, A. Bianchi, E. J. Billo, P. J. Connolly, P. Paoletti, J. S. Summers, and D. G. Van Derveer, *Inorg. Chem.*, 1986, **25**, 4197-4202.
- 67 R. J. Pleus, H. Waden, W. Saak, and D. Haase, *J. Chem. Soc. Dalton Trans.*, 1999, **15**, 2601-2610.
- 68 X. Liang, M. Weishäupl, J. A. Parkinson, S. Parsons, P. A. McGregor, and P. J. Sadler, *Chem. Eur. J.*, 2003, **9**, 4709-4717.
- 69 X. Liang, J. A. Parkinson, S. Parsons, M. Weishaupl, and P. J. Sadler, *Inorg.*

- Chem.*, 2002, **41**, 4539-4547.
- 70 X. Chen, G. Long, R. D. Willett, T. Hawks, S. Molnar, and K. Brewer, *Acta Cryst.*, 1996, **C52**, 1924-1928.
- 71 E. Simon, P. L'Haridon, R. Pichon, and M. L'Her, *Inorg. Chim. Acta*, 1998, **282**, 173-179.
- 72 T. F. Lai and C. K. Poon, *Inorg. Chem.*, 1976, **15**, 1562-1566.
- 73 S. P. Sovilj, G. Vuckovic, K. Babic, N. Matsumoto, M. Avramov-Ivic, and V. M. Jovanovic, *J. Coord. Chem.*, 1994, **31**, 167-179.
- 74 J. F. Endicott, J. Lilie, J. M. Kuszaj, B. S. Ramaswamy, G. Schmonsees, M. G. Simic, M. D. Glick, and D. P. Rillema, *J. Am. Chem. Soc.*, 1977, **99**, 429-439.
- 75 A. S. Antsyshkina, M. A. Porai-Koshits, V. D. Makhaev, A. P. Borisov, N. S. Kedrova, and N. N. Mal'iseva, *Koord. Khim. (Russ.) (Coord. Chem.)*, 1992, **18**, 474-480.
- 76 R. D. Willett and A. Vij, *J. Chem. Cryst.*, 2000, **30**, 399-404.
- 77 Z. Wang, R. D. Willet, S. Molnar, and K. Brewer, *Acta Cryst.*, 1996, **C52**, 581-583.
- 78 J. Pickardt and I. Hoffmeister, *Z. Naturforsch., Teil B*, 1995, **50**, 828-832.
- 79 U. Heinl, U. Kleinitz, and R. Mattes, *Z. Anorg. Allg. Chem.*, 2002, **628**, 2409-2414.
- 80 M. Yamashita, H. Ito, K. Toriumi, and T. Ito, *Inorg. Chem.*, 1983, **22**, 1566-1568.
- 81 K. Toriumi, M. Yamashita, H. Ito, and T. Ito, *Acta Cryst.*, 1986, **C42**, 963-968.

- 82 J. W. Sibert, A. H. Cory, and J. G. Cory, *Chem. Comm.*, 2002, 154-155.
- 83 E. De Clercq, *Med. Res. Rev.*, 2002, **22**, 531-565.
- 84 N. A. Lack, B. Green, D. C. Dale, G. B. Calandra, H. Lee, R. T. MacFarland, K. Badel, W. C. Liles, and G. Bridger, *Clin. Pharmacol. Ther.*, 2005, **77**, 427-436.
- 85 E. De Clercq, *J. Med. Chem.*, 2005, **48**, 1297-1313.
- 86 P. Matthys, S. Hatse, K. Vermeire, A. Wuyts, G. Bridger, G. W. Henson, E. De Clercq, A. Billiau, and D. Schols, *J. Immunol.*, 2001, 4686-4692.

Chapter 2 Materials and Methods

2.1 Chemicals and Instruments

2.1.1 Chemicals

Cyclam (1,4,8,11-tetraazacyclotetradecane), palladium acetate, nickel nitrate hexahydrate, potassium tetrachloropalladate, cobalt acetate tetrahydrate, copper acetate monohydrate, cobalt chloride hexahydrate, ethyl trifluoroacetate, 2,6-pyridinemethanol, zinc acetate dihydrate, methane sulfonyl chloride, Raney nickel, (Aldrich Chemical Co.), α,α' -dibromo-*p*-xylene, diethyl chlorophosphate, diethanolamine, histidine (Fluka), nickel acetate tetrahydrate, (BDH Ltd.), nickel chloride hexahydrate, hexamethyl phosphoric triamide, cetyl trimethylammonium bromide, *p*-toluene sulfonyl chloride (Acros Chemical Company) and hen egg white lysozyme (Sigma Chemical Co.) were used as received. Isotopically enriched cadmium oxide (^{111}CdO , 95.29%) was purchased from Oak Ridge National Laboratory, TN.

Anhydrous solvents were prepared using standard methods. NMR solvents, deuterium oxide (Aldrich, 99.9 %) and chloroform-*d* (Aldrich, 99.9 %), were used as received.

2.1.2 IR Spectroscopy

Infrared spectra were recorded as KBr pellets in the range 4000 – 400 cm^{-1} on a Perkin-Elmer Paragon 1000 Fourier-transform spectrometer.

2.1.3 NMR Spectroscopy

NMR spectra were recorded on either Bruker DPX 360, DMX 500, AVA 600, BIO 600 or AVA 800 spectrometers using TBI [^1H , ^{13}C , X] or TXI [^1H , ^{13}C , X] probeheads, and equipped for z-gradients. All spectra were acquired at 298 K, unless otherwise stated, using standard pulse sequences in 5 mm NMR tubes. The ^1H shifts for aqueous solutions were referenced to 1, 4 – dioxane (3.75 ppm).¹ When DMSO- d_6 was used, peaks were referenced to 1, 4 – dioxane (3.57 ppm) and for CDCl_3 solutions, peaks were referenced to CHCl_3 (7.27 ppm).¹ NMR data was processed using XWIN-NMR (version 3.5, Bruker U.K. Ltd.).

2.1.4 X-ray Crystallography

X-ray crystallographic studies were carried out on a Bruker SMART-APEX CCD Stadi-4 diffractometer equipped with Oxford Cryosystems low-temperature devices by Dr. Simon Parsons and Dr. Andrew Parkin.

2.1.5 CHN Analysis

CHN elemental analysis was performed by the CHN service at the University of Edinburgh.

2.1.6 Electrospray Ionisation-Mass Spectrometry (ESI-MS)

Positive-ion electrospray ionisation mass spectra were obtained on a Platform II mass spectrometer (Micromass, Manchester, UK). The samples were infused at 8 $\mu\text{L}/\text{min}$. The source temperature was 383 K, and the drying gas flow rate was 300

L/h. A potential of 3.5 kV was applied to the probe tip, and cone voltages of 20 – 45 V over 200 – 1300 Da were used. Data were processed using Masslynx (v3.5) Windows XP PC data systems.

2.1.7 *Ultraviolet and Visible Spectroscopy (UV-Vis)*

UV-Vis absorption spectra were acquired on a Perkin-Elmer λ 16 UV-Vis recording spectrophotometer using 1 cm pathlength quartz cuvettes. The temperature was controlled using a PTPI Peltier Temperature Programmer. Spectra were processed with UVWinlab. Spectra were referenced to the solvent alone.

2.1.8 *pH Measurements:*

The pH values of solutions were determined using a Corning 145 pH meter equipped with a micro combination electrode, calibrated with Aldrich buffer solutions at pH 4, 7 and 10. No correction was made for deuterium isotope effects.

2.2 NMR Spectroscopy

Nuclear magnetic resonance (NMR) spectroscopy provides information about the types, number and connectivity of particular atoms.² NMR signals were first recorded in 1946 and can now routinely be detected for almost any magnetic resonance.³⁻⁵ Many textbooks have been published describing the theory and applications of NMR.^{3, 4, 6} The nuclei used in this thesis and their magnetic properties are shown in Table 2.1.

Table 2.1 NMR properties of nuclei studied in this thesis

Nucleus	Spin quantum number, I	Magnetic moment, μ (μ_N)	Gyromagnetic ratio, γ ($10^7 \text{ rad T}^{-1} \text{ s}^{-1}$)	Abundance (%)	Sensitivity (relative to ^1H)
^1H	$\frac{1}{2}$	4.84	26.75	99.99	1.000
^{13}C	$\frac{1}{2}$	1.22	6.73	1.11	0.016
^{15}N	$\frac{1}{2}$	0.49	-2.71	0.37	0.001
^{111}Cd	$\frac{1}{2}$	1.03	-5.70	12.80	0.0095

2.2.1 Nuclear Spin

For a nucleus to be NMR active, it must possess a magnetic moment. Nuclei possess magnetic moments when their spin quantum numbers are equal to or greater than $\frac{1}{2}$. The spin states of such nuclei are characterised by the magnetic quantum numbers $m_I = I, I-1, I-2, \dots, -I$. The spinning of a nucleus generates a magnetic moment. The magnetic moment is a vector, because it has both magnitude and direction. It is defined by its axis of spin. The NMR experiment utilises these magnetic properties of nuclei to provide structural information. The spin properties of the protons and neutrons in a nucleus combine to give the overall spin of the nucleus. Protons, neutrons and electrons all have a spin of $I=1/2$. When both the atomic number and the atomic mass are even, the nucleus has no magnetic properties and the spin quantum number is 0 ($I=0$). Every nucleus with a spin angular momentum I therefore also possesses a nuclear magnetic moment μ . The moment is proportional to the spin with a constant of proportionality, γ , called the magnetogyric ratio. Every isotope has a characteristic value of γ .

The energy of an NMR transition depends on the magnetic-field strength and

the magnetogyric ratio, γ . The frequency of a transition is given by:

$$\nu = (\gamma/2\pi)B_0 \quad (\text{Equation 2.1})$$

where ν is the frequency of the resonance radiation, and B_0 is the strength of the magnetic field.

Without a magnetic field, all $2I + 1$ orientations of a spin- I nucleus have the same energy. The degeneracy is removed when a magnetic field is applied. The magnetic field experienced by a nucleus in a molecule differs slightly from the external field in such a way that the exact resonance frequency (the chemical shift) is characteristic of the chemical environment of the nucleus. Nuclei with spins greater than $\frac{1}{2}$ are called quadrupolar nuclei and generally give broad NMR lines, making them difficult to study.

2.2.2 *Chemical Shift*

When an atom is placed in a magnetic field, its electrons circulate about the direction of the applied magnetic field (B_0). This circulation causes a small magnetic field at the nucleus which opposes the externally applied field.⁵

Chemical shifts arise because the field, B , actually experienced by a nucleus in an atom or a molecule differs slightly from the external field B_0 . In an atom, B is slightly smaller than B_0 because the external field causes the electrons to circulate about the direction of the applied magnetic field. This motion generates a small magnetic field B' at the nucleus which opposes the externally applied field. The nucleus is hence shielded from the external field by its surrounding electrons, as calculated from Equation 2.2. B' is proportional to B_0 .

$$B = B_0 - B' \quad (\text{Equation 2.2})$$

Similar effects occur for nuclei in molecules, referred to as nuclear shielding. Both the size and sign of the shielding constant are determined by the electronic structure of the molecule in the vicinity of the nucleus. The resonance frequency of a nucleus is therefore characteristic of its environment.

The chemical shift is defined in terms of the difference in resonance frequencies between the nucleus of interest (ν) and a reference nucleus (ν_{ref}), by δ ,

$$\delta = 10^6 [(\nu - \nu_{\text{ref}}) / \nu_{\text{ref}}] \quad (\text{Equation 2.3})$$

The factor 10^6 is introduced to scale the numerical value of δ to a convenient size, quoted in parts per million. The more heavily shielded nuclei appear on the right hand side of the spectrum, as they have smaller ν and smaller δ .

Hydrogen bonding can result in large observable deshielding effects in ^1H NMR.⁶ Intermolecular hydrogen bonds can produce small deshielding effects, but intramolecular hydrogen bonds can have a significant effect on the chemical shift of a nucleus, resulting in the resonance shifting upfield.

2.2.3 Spin-Spin Coupling

Nuclear spin-spin coupling arises from nuclei interacting with each other, and causes NMR lines to split into a small number of components with characteristic relative intensities and spacings.

Non-equivalent nuclei which are close to one another exert an influence on each other's effective magnetic field. If the distance between non-equivalent nuclei is less than or equal to three bond lengths, this effect is observable. This effect is called spin-spin coupling or J coupling.

In general, it is the s-character of the bonds between the coupling nuclei that

controls the magnitude J .⁷ The coupling between nuclei is transmitted via the bonding electrons rather than directly through space. Only s-electrons have a finite density at the nucleus so the amount of s-character in the valence hybrids used to form the chemical bond influences the strength of the coupling. The percentage s-character can be influenced by many factors. Increasing coordination number leads to a decrease in the coupling constant, the s-character of the bond to any given ligand decreases as the number of ligands increases. The coupling constant also increases with increasing electronegativity of the substituents, in line with a presumed increase in the s-character of the bond.

Interbond angles can also affect the coupling constant.⁷ For two bond couplings, *trans* couplings would normally be larger than *cis* couplings. The larger the interbond angle, the larger the coupling constant. For three bond couplings, the dihedral angle, ϕ , between planes containing a coupling nuclei and the bonds between them becomes important. The dihedral angle dependence of three bond couplings is calculated from the Karplus equation (Equation 2.4), which predicts that 3J will be greatest when ϕ is close to 0° or 180° .

$$^3J = C\cos^2\phi + B\cos\phi + A \quad (\text{Equation 2.4})$$

where $A = 4.22$, $B = -0.5$ and $C = 4.5$, for ^1H - ^1H couplings.

2.2.4 ^{15}N NMR Spectroscopy

It is possible to detect proton resonances from NH protons with ^{14}N present in natural abundance (99.6 %), but they are often broadened, as ^{14}N is a quadrupolar nucleus ($I = 1$), hence quadrupolar relaxation occurs. It is also necessary to work in H_2O (as opposed to D_2O) since NH protons usually exchange with deuterium rapidly.

However, ^{15}N ($I = 1/2$) can be detected despite its low natural abundance (0.37 %) and low NMR sensitivity. Its receptivity compared to ^1H is only 3.85×10^{-6} .⁸ The sensitivity of detection can be improved by the use of polarisation transfer from ^1H . ^1H -detected polarisation transfer methods are applicable to any system which contains a ^{15}N atom with a measurable spin-spin coupling to ^1H .

The intensity increase available by polarisation transfer from protons to an X nucleus is given by the ratio of magnetogyric ratios, $\gamma_{\text{H}}/\gamma_{\text{X}}$. For ^{15}N , the gain in signal intensity achievable by polarization transfer is 9.8 ($\gamma_{\text{H}}/\gamma_{\text{X}}$).⁸

2.2.5 *Quadrupolar Relaxation*

Relaxation refers to the processes which allow nuclear spins to lose energy and drop from the excited state to the ground state without emitting an NMR signal.⁷ Quadrupolar relaxation occurs when a quadrupolar nucleus is present, and depends on the size of the nuclear quadrupole and the electric field gradient at the nucleus. Quadrupolar relaxation has the effect of broadening signals, sometimes to the extent of making them NMR invisible. Signals can be broadened to thousands of hertz wide.

2.2.6 *1D NMR Spectroscopy*

A basic 1D NMR experiment consists of exciting the nuclei with a single pulse then receiving the free induction decay (FID), which is then Fourier transformed to produce the spectrum. The basic pulse sequence is shown in Figure 2.1. The single-pulse sequence to record a standard proton spectrum consists of three

steps. The first step is the relaxation period (d_1) which allows a pre-equilibrium state to be reached. The second step is to apply a radiofrequency pulse (p_1) to create transverse magnetization. The final step is the acquisition, during the t_2 period. Data are collected following the RF pulse. The pulse angle can be varied to optimise the signal. The two pulse sequence parameters shown in Figure 2.1, d_1 and p_1 , correspond to the length of the recycle delay and the length of the RF pulse, and $acq.$ is the acquisition time. After the acquisition is complete, a delay time is necessary to allow the nuclei to relax before the RF pulse is applied again.

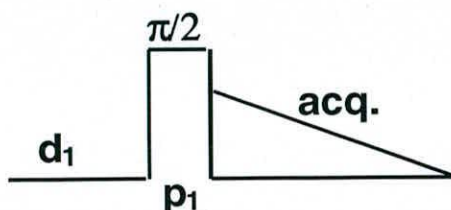


Figure 2.1 1D NMR pulse sequence

2.2.7 2D NMR Spectroscopy

2D NMR refers to an additional frequency axis, which can either be homonuclear or heteronuclear. Using this second dimension can allow for more detailed studies of structural connectivity, spatial proximity, or kinetic interchange. A 2D experiment has two detection periods, one directly detected, and one indirectly detected. Multiple pulse experiments can be used to transfer polarization selectively in a coupled spin system between the sensitive, S, and insensitive, I, spins in such a way that signals from the insensitive nuclei can be observed.

2.2.8 Correlation Spectroscopy (COSY)

COSY is a two-dimensional homonuclear (^1H , ^1H)-correlated NMR which is used to identify pairs of nuclei which are J -coupled to one another.^{9, 10} Through-bond connectivities between protons separated by two or three bonds can be established by COSY experiments. COSY experiments can be used to identify protons that have a mutual scalar coupling. A cross-peak in a COSY spectrum indicates that the protons giving the connected resonances on the diagonal are geminally or vicinally coupled. *Trans* couplings are generally larger than *cis* couplings. The pulse sequence used in this work was a magnitude COSY. A typical pulse sequence for a COSY experiment is shown in Figure 2.2. The 2D spectrum acquired in the magnitude COSY experiment has line-shapes in both F1 and F2 that have both absorption and dispersion contributions, which means that it is not possible to phase the spectrum so the peaks are purely absorptive, and the spectrum must be displayed in magnitude mode. Typical resolution is 3 Hz/pt.

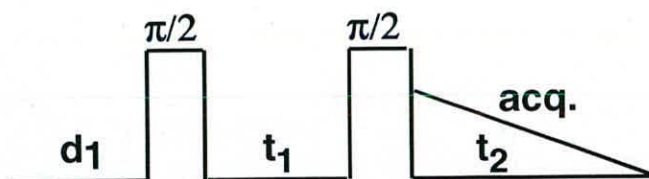


Figure 2.2 Pulse sequence for a two-dimensional COSY NMR experiment.

The resolution can be improved by using the double-quantum filtered COSY sequence (DQF-COSY),¹¹ shown in Figure 2.3. In this experiment, an extra 90° pulse is added after the second 90° COSY pulse. A DQF-COSY spectrum correlates

chemical shifts of the same nucleus in both dimensions. Both cross-peaks and diagonal multiplets have the same anti-phase absorption character. In DQF-COSY spectra, the diagonal signal size is reduced, allowing analysis of signals close to the diagonal.

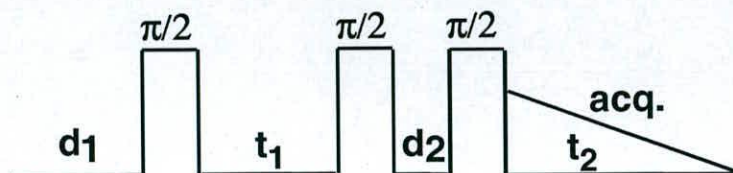


Figure 2.3 Pulse sequence for a two-dimensional DQF-COSY NMR experiment.

2.2.9 Nuclear Overhauser Effect Spectroscopy (NOESY)

Through-space connectivities between protons that are close in space can be established by NOESY experiments.^{12, 13} NOESY yields correlation signals, which are caused by dipolar cross-relaxation between nuclei (^1H , ^1H) in close spatially. A key feature of the NOESY experiment is the mixing time, τ . The pulse sequence for a NOESY experiment is shown in Figure 2.4. The cross-peaks are generated by magnetisation transfer that takes place during the mixing time, so the length of this delay must be chosen according to the rate of the transfer process. The intensities of the cross-peaks are inversely proportional to the sixth power of the distance between two nuclei, i and j , $\propto 1/r_{ij}^6$.¹⁴

2.2.10 Total Correlation Spectroscopy (TOCSY)

In TOCSY experiments, cross-peaks are generated between all members of a coupled spin network. Hence this can be useful in identifying how many different

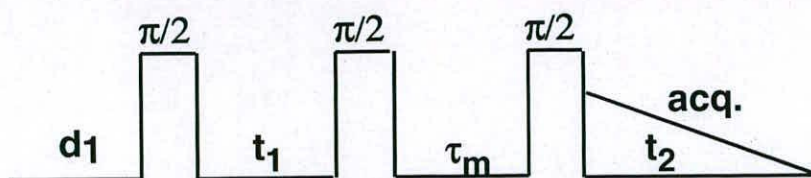


Figure 2.4 Pulse sequence for a two-dimensional NOESY experiment, τ_m is the mixing time.

products or isomers are present in a sample.^{6, 15} TOCSY experiments can be used to obtain the subspectrum characteristic of part of a molecule that has no scalar couplings to other spins in the molecules. TOCSY uses a different mechanism of coherence transfer from COSY for 2D correlation spectroscopy. In TOCSY, oscillatory exchange is established, which proceeds through the entire coupling network, so that there can be a net magnetisation transfer from one spin to another even without direct coupling. The pulse sequence for a TOCSY experiment is shown in Figure 2.5.

The coherence transfer period of the TOCSY sequence occurs during a multiple-phase spin-lock period.⁶ The multiple-phase spin-lock sequence most commonly used is MLEV-17 which contains a set of 17 $90/180^\circ$ pulses whose duration represents the mixing time τ_m . The length of the spin-lock period determines how far the spin-coupling network will be probed. The TOCSY spectrum can be phased so that all cross peaks and the diagonal peaks have positive intensity.

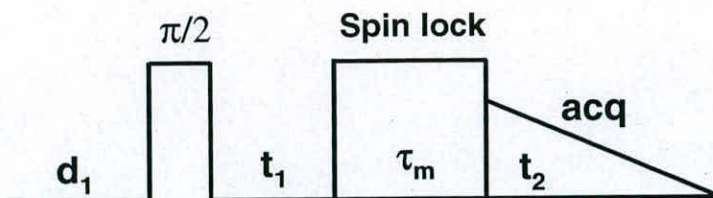


Figure 2.5 Pulse sequence for a two-dimensional TOCSY experiment.

2.2.11 Heteronuclear Single-Quantum Correlation (HSQC)

HSQC experiments allow identification of the chemical shifts of protons and X-nuclei that are directly coupled. This allows easy correlation of the assignments already made for one nuclear species to their corresponding X-nuclei. Another feature is that it allows proton resonances to be spread out according to the shifts of the heteronuclei to which they are coupled, which allows assignment of protons which may be overlapping in 1D or 2D proton NMR spectroscopy. An HSQC pulse sequence is shown in Figure 2.6.

HSQC spectroscopy uses indirect (or inverse) detection techniques. An important feature of this experiment is that the proton magnetisation which is detected during t_2 originated as proton magnetisation at the start of the sequence. The main advantage of this technique is the enhanced sensitivity with respect to direct detection, a theoretical maximum of $(|\gamma_H|/|\gamma_X|)^{5/2}$ (306 for ^{15}N).⁸

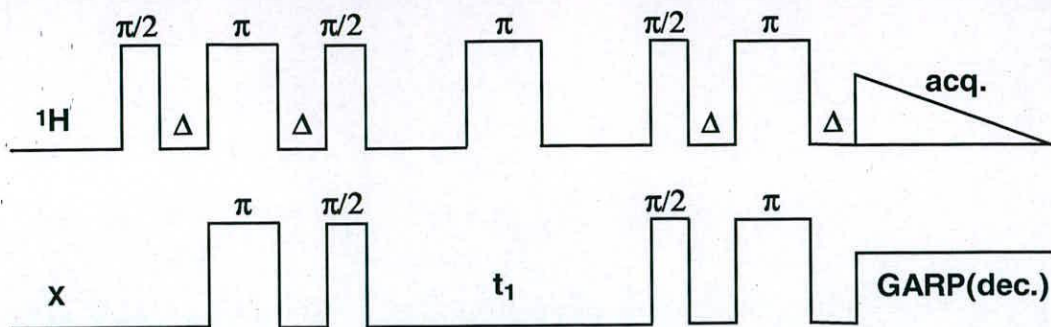


Figure 2.6 Basic [^1H , X] HSQC pulse sequence. The delays Δ and τ are $\frac{1}{4}J$ and $\frac{1}{2}J$ respectively, where J is the one-bond HX coupling constant.

2.3 IR Spectroscopy

Infrared spectra result from vibrations that occur naturally and predictably within molecules. The spectra produced can be used to provide a variety of information about a molecule's structure, particularly its symmetry and identity of its functional groups.⁶ The infrared spectra of compounds are unique and can be used as fingerprints to identify molecules. Vibrations of many functional groups always give rise to features within well defined regions of the spectra, regardless of the overall structure of the molecule. Hence, characteristic shifts for groups such as carbonyls and nitriles can be identified easily.

There are two types of fundamental vibrations in molecules, stretching, in which the distance between two atoms increases or decreases, but the atoms remain on the same bond axis, and bending, in which the position of the atoms changes relative to the original bond axis.⁶ The various stretching and bending vibrations of a bond occur at quantized frequencies. When infrared light of the same frequency is

incident on the molecule, energy is absorbed and the amplitude of that vibration is increased. A molecule can be said to be a system of balls of varying masses, and springs of varying strengths, corresponding to the chemical bonds of a molecule. This model can be used to account for the fundamental vibrations occurring between the nonvibrating state and vibrationally excited state in a simple diatomic molecule A-B. The vibrational frequency is given in cm^{-1} by Equation 2.5.

$$\nu = 1/2 \pi c(k/\mu)^{-2} \quad (\text{Equation 2.5})$$

Where k = the force constant of the bond

μ = the reduced mass of the molecule defined by $\mu = m_A m_B / (m_A + m_B)$

Bending vibrations generally require less energy and occur at a longer wavelength than stretching vibrations. Stretching vibrations are found to occur in the order of bond strengths. The triple bond (absorption at $2300 - 2000 \text{ cm}^{-1}$) is stronger than the double bond (absorption at $1900 - 1500 \text{ cm}^{-1}$), which is stronger than the single bond (absorption at $1300 - 800 \text{ cm}^{-1}$). When the single bond involves hydrogen, stretching vibrations occur at high frequencies (absorption at $3700 - 2630 \text{ cm}^{-1}$). Metal-ligand vibrations tend to appear in the low frequency region ($500 - 200 \text{ cm}^{-1}$).

2.4 Electrospray Ionisation Mass Spectrometry (ESI-MS)

A mass spectrometer determines the molecular weight of compounds by ionising, separating and measuring molecular ions according to their mass-to-charge ratio (m/z).⁶ A mass spectrometer consists of three major parts. These are a source

of gaseous ions, an evacuated dispersing region in which the ions of different mass-to-charge ratios are forced to travel different paths, and a detector that locates the paths followed by the different ions. A beam of electrons, produced from a heated filament collide with gaseous atoms of the sample, produces ions, some of which are fragments of the original molecules. The ions are then accelerated by an electric field, and these enter an evacuated flight tube in which they are subjected to a magnetic field. The different sized molecules are accelerated at different rates, and are detected. This records the position and intensity of each ion beam, and this is used to calculate the m/z of the ion.

Electrospray Ionization (ESI) generates ions directly from solution (usually an aqueous or aqueous/organic solvent system) by creating a fine spray of highly charged droplets in the presence of a strong electric field. As the droplet decreases in size, the electric charge density on its surface increases. The mutual repulsion between like charges on this surface becomes so great that it exceeds the forces of surface tension, and ions begin to leave the droplet. The ions are then electrostatically directed into the mass analyzer. Vaporization of these charged droplets results in the production of singly or multiply charged gaseous ions. Neutral fragments are lost using this technique. Because mass spectrometers measure the m/z ratio, the resultant ESI mass spectrum contains multiple peaks corresponding to the different charged states.

ESI is a highly sensitive technique, and since the ions are formed directly from solution, it has the advantage that it can be used in conjunction with liquid chromatography, commonly referred to as LCMS.

2.5 CHN Analysis

In CHN analysis, the carbon, hydrogen, and nitrogen content in organic and inorganic compounds can be determined.¹⁶ Combustion of the weighed sample occurs in pure oxygen under static conditions. Helium is used to carry the combustion products through the analytical system. Helium is used for this purpose because it is chemically inert relative to tube packing chemicals, and it has a very high co-efficient of thermal conductivity. The products of combustion are passed over suitable reagents in a combustion tube to assure complete oxidation and removal of undesirable by-products such as sulfur, phosphorous, and halogen gases. The next step is carried out in a reduction tube. In the reduction tube, oxides of nitrogen are converted to molecular nitrogen and residual oxygen is removed. This mixture is released into the thermal conductivity detector. Between the first of three pairs of thermal conductivity cells an absorption trap removes water from the sample gas. The differential signal read before and after the trap reflects the water concentration and, therefore, the amount of hydrogen in the original sample. A similar measurement is made of the signal output of a second pair of thermal conductivity cells, between which a trap removes carbon dioxide, thus determining the carbon content. The remaining gas now consists only of helium and nitrogen. This gas passes through a thermal conductivity cell and the output signal is compared to a reference cell through which pure helium flows. This gives the nitrogen concentration.

Drawbacks with this technique include the requirement for the sample to be very pure. If there are any solvents or moisture trapped in the sample, this will affect the accuracy of the results. This usually happens with samples that are oils. Also, if

the sample is not homogeneous, duplicate runs will not agree to within 0.3%. If a sample is extremely volatile, it may lose mass due to evaporation after it has been weighed out. This can also cause the results to be inaccurate. Furthermore, some compounds are inherently difficult to combust completely. Incomplete combustion can also cause inaccurate results.

2.6 References

- 1 H. E. Gottlieb, V. Kotlyar, and A. Nudelman, *J. Org. Chem.*, 1997, **62**, 7512-7515.
- 2 J. K. M. Sanders and B. K. Hunter, 'Modern NMR Spectroscopy', Oxford University Press, New York, 1987.
- 3 P. J. Hore, 'Nuclear Magnetic Resonance', Oxford University Press, New York, 1995.
- 4 R. J. Abraham, J. Fisher, and P. Loftus, 'Introduction to NMR Spectroscopy', John Wiley and Sons Ltd., Chichester, 1988.
- 5 H. Günther, 'NMR Spectroscopy', John Wiley and Sons Ltd, New York, 1995.
- 6 J. B. Lambert, H. F. Shurvell, D. A. Lightner, and R. Graham Cooks, 'Organic Structural Spectroscopy', Prentice-Hall, New Jersey, 1998.
- 7 J. A. Iggo, 'NMR: Spectroscopy in Inorganic Chemistry', Oxford University Press, New York, 2004.
- 8 S. J. Berners-Price and P. J. Sadler, *Coord. Chem. Rev.*, 1996, **151**, 1-40.
- 9 W. P. Aue, E. Bartholdi, and R. R. Ernst, *J. Chem. Phys.*, 1976, **64**, 2229-2246.
- 10 K. Nagayama, A. Kumar, K. Wuthrich, and R. R. Ernst, *J. Magn. Res.*, 1980, **40**, 321-334.
- 11 M. Rance, O. W. Sorensen, G. Bodenhausen, G. Wagner, R. R. Ernst, and K. Wüthrich, *Biochem. Biophys. Res. Commun.*, 1983, **117**, 479-485.

- 12 J. Jeener, B. H. Meier, P. Bachmann, and R. R. Ernst, *J. Chem. Phys.*, 1979, **71**, 4546-4553.
- 13 A. Kumar, R. R. Ernst, and K. Wuthrich, *Biochem. Biophys. Res. Commun.*, 1980, **95**, 1-6.
- 14 A. E. Derome, 'Modern NMR Techniques for Chemistry Research', Pergamon, Oxford, 1987.
- 15 L. Braunschweiler and R. R. Ernst, *J. Magn. Res.*, 1983, **53**, 521-528.
- 16 (a) <http://www.chnos.com/> (b) www.perkinelmer.com

Chapter 3 Synthesis and Characterisation of Metallocyclam Complexes

3.1 Introduction

Cyclam can complex a variety of cations, including transition metals, often with high thermodynamic and kinetic stability with respect to metal ion dissociation. As cyclam is flexible enough to coordinate a wide variety of metal ions, it is of little use as a selective metal chelating agent. There has been extensive work on tetra N-substituted cyclams, with more work been done in recent years on mono-, di- and tri-N-substituted cyclams.¹

There are five configurational *trans* isomers of metal-cyclam adducts, which differ in the chirality of the N atoms (Figure 1.12).^{2,3} Semi-quantitative analysis of the relative strain energies of the five *trans* isomers indicates that the *trans*-III form is the most stable.^{3,4} However, it has been shown that square-planar complexes prefer to adopt the *trans*-I configuration, as opposed to octahedral complexes, which prefer *trans*-III.⁵ Key configurations are shown in Figure 3.1.

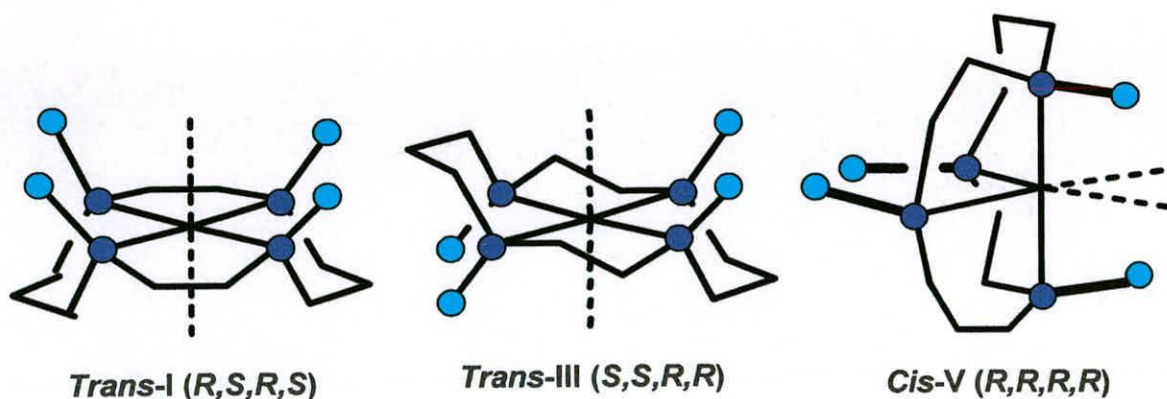
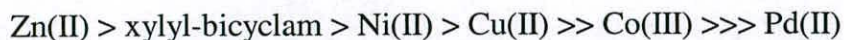


Figure 3.1 Major configurational isomers of metal-cyclam

Complexation of metals to xylyl-bicyclam affects its anti-HIV activity in the following series:



As there are free metals in the blood, there is a possibility that xylyl-bicyclam picks up metals, especially zinc, from the blood, and that this is the active form of the drug. There has been a lot of work done on the configurations of Zn-cyclam and Zn(II)₂-xylyl-bicyclams, but not much work on the other metal complexes.^{6,7}

In the X-ray crystal structures of [Zn(cyclam)(H₂O)₂](OAc)₂ the macrocycle adopts the *trans*-III configuration and the axial Zn–OH₂ bonds are long (2.27 Å).⁶ Similarly the phthalate bridged complex [Zn(cyclam)(phthalate)]_n(CH₃OH)_{2n} is also *trans*-III. In aqueous solution these carboxylato Zn(II) cyclam complexes exist as mixtures of *trans*-I, *trans*-III and *cis*-V configurations.⁶

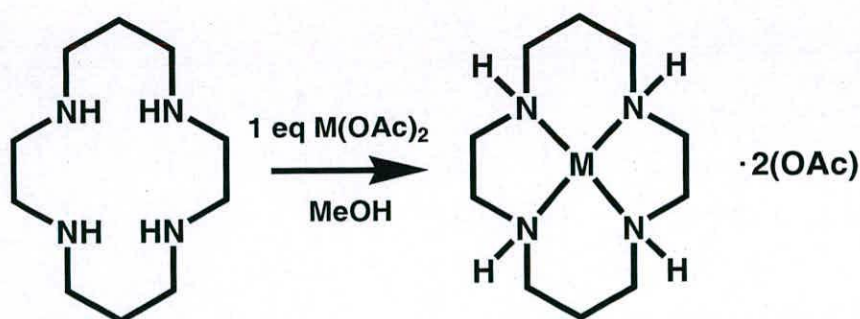
The X-ray crystal structure of a Zn(II) complex of AMD3100, [Zn₂(xylyl-bicyclam)₂](OAc)₂·2CH₃OH showed that both the cyclam rings were in the *cis*-V configuration with chelation by acetate on one cyclam face, and double H-bonding on the other.⁷ Detailed NMR studies of this complex showed it to be *cis*-V/*trans*-I in aqueous solution, in contrast to the perchlorate complex which was largely *trans*-I and *trans*-III. Addition of acetate to the perchlorate complex induced a rapid, major structural change, significantly increasing the amount of *cis*-V/*cis*-V and *cis*-V/*trans*-I species. Liang *et al.*⁸ carried out NMR solution studies on Cd(cyclam)(ClO₄)₂, Cd(cyclam)Cl₂ and [Cd₃(cyclam)₃(CO₃)](ClO₄)₄·3H₂O and used these to identify key markers for various configurations adopted by these complexes. Cadmium was used for this study because its isotopes (¹¹¹Cd and ¹¹³Cd, *I* = ½) are favourable for NMR studies, unlike those of zinc. A variety of solution conditions were analysed using 1D

and 2D ^1H , ^{13}C , ^{15}N and ^{111}Cd NMR spectroscopy, including Karplus-type analyses of ^1H , ^1H and ^1H , ^{111}Cd coupling constants. Only the *trans*-I and *trans*-III configurations have six non-equivalent protons and hence give rise to six proton resonances, while the *trans*-IV, *trans*-V and *cis*-V configurations have five non-equivalent protons and give rise to five proton resonances. The X-ray crystal structure of $[\text{Cd}_3(\text{cyclam})_3(\text{CO}_3)](\text{ClO}_4)_4 \cdot 3\text{H}_2\text{O}$ showed it to be in the uncommon folded *cis*-I configuration with all of the N-H bonds oriented upwards, while the NMR studies suggested that it adopts the *trans*-I configuration in solution.

In order to understand this order of anti-HIV activity via interaction with the coreceptor CXCR4, the properties of Co(III), Pd(II), Ni(II) and Cu(II) cyclam complexes are investigated. The most common configuration of metalocyclam complexes in the solid state is *trans*-III, but little is known about the solution structure of these complexes.

3.2 Experimental

Metal-cyclam complexes were synthesised using the general scheme shown in Scheme 3.1.



Scheme 3.1 General preparative route to metal cyclam acetate complexes.

3.2.1 Synthesis of Palladium(II) Cyclam Complexes

[Pd(cyclam)]Cl₂ (1). A solution of K₂PdCl₄ (489.6 mg, 1.5 mmol) in water (75 mL) was added dropwise to a solution of cyclam (300.5 mg, 1.5 mmol) in water (75 mL) under N₂ over a period of 2.5 h. The clear yellow/brown solution was left to stir overnight and then the solvent removed under high vacuum to give a pale yellow powder. The powder was dried in vacuo (685.5 mg), and then dissolved in methanol (1 mL) to give a yellow solution leaving a white precipitate (KCl). The mixture was centrifuged and the yellow solution was pipetted off, leaving behind the KCl. The solvent was removed under reduced pressure and the powder was dried in vacuo. This produced a yellow powder of [Pd(cyclam)]Cl₂, (251.8 mg, 0.66 mmol, 45 % yield). 1D and 2D NMR spectra (COSY, TOCSY, NOESY and [¹H, ¹³C] HSQC) were recorded on this product on a 500 MHz spectrometer in 90 % H₂O / 10 % D₂O. ES-MS : m/z = 340.9 [M-Cl]⁺, 304.9 ([M-2Cl-H]⁺).

Anal. Calcd for C₁₀H₂₄N₄PdCl₂: C, 31.80, N, 14.84, H, 6.41 %, found C, 31.48, N, 14.55, H, 6.74 %.

Selected IR (KBr, cm⁻¹): 3410 m (NH), 3152 s (NH), 2932 m (CH), 2869 s (CH).

[Pd(cyclam)](OAc)₂·2H₂O (2). Pd(OAc)₂ (236.3 mg, 1.05 mmol) was reacted with cyclam (200.3 mg, 1 mmol) in water (100 mL) under N₂ with stirring for 8 h and addition of CH₃CO₂H to maintain a pH of ca. 4.4. The cloudy black solution was filtered and gave a yellow powder after the solvent was removed under high vacuum. Yellow crystals suitable for X-ray diffraction were obtained by slow diffusion of diethyl ether into a MeOH solution of this powder. (408.1 mg, 0.66 mmol, 85 % yield). 1D and 2D NMR spectra (COSY, TOCSY, NOESY and [¹H, ¹³C] HSQC)

were recorded on this product on a 500 MHz spectrometer in 90 % H₂O / 10 % D₂O.

ES-MS : $m/z = 365.0$ [M-OAc-2(H₂O)]⁺, 305.0 [M-OAc-2(H₂O)-H]⁺.

Anal. Calcd for C₁₄H₃₄N₄PdO₆: C, 36.48, N, 7.44, H, 12.16 %, found C, 36.93, N, 7.24, H, 12.60 %.

Selected IR (KBr, cm⁻¹): 3411 m (NH), 2947 m (CH), 2867 s (CH), 1621 m (OH), 1455 m (CO), 1429 m (CO).

[Pd(cyclam)](ClO₄)₂ (3). Warning - Perchlorate salts of complexes with organic ligands are potentially explosive and should be treated with great care. [Pd(cyclam)](OAc)₂ (51.2 mg, 0.12 mmol) was dissolved in HClO₄ (2 molar equiv, 120 μL, 1 M) to give a clear, pale yellow solution. The solution was left in a refrigerator at 277 K to allow slow evaporation to occur. Yellow crystals formed after 4 days (pH=1.00). The acid was filtered off and the crystals were dried under high vacuum. (60.6 mg, 0.09 mmol, 77 % yield).

1D and 2D NMR spectra (COSY, TOCSY, NOESY and [¹H, ¹³C] HSQC) were recorded on this product on a 600 MHz spectrometer in 90 % H₂O / 10 % D₂O.

ES-MS : $m/z = 406.9$ [M-ClO₄]⁺, 304.9 [M-2(ClO₄)-H]⁺.

Anal. Calcd for C₁₀H₂₄N₄PdO₈Cl₂: C, 23.75, N, 11.05, H, 4.78 %, found C, 23.91, N, 10.99, H, 4.51 %.

Selected IR (KBr, cm⁻¹): 3271 s (NH), 3214 m (NH), 2935 m (CH), 2876 s (CH).

3.2.2 Synthesis of Nickel (II) Cyclam Complexes

[Ni(cyclam)](OAc)₂·H₂O (4). Cyclam (400.85 mg, 2 mmol) was dissolved in methanol (50 mL) and Ni(OAc)₂·4H₂O (363.46 mg, 2 mmol) was added. The

reaction was stirred overnight under N₂. The resulting purple solution was filtered and concentrated to dryness to give a purple powder. This was recrystallized by slow evaporation from methanol into diethyl ether to give [Ni(cyclam)](OAc)₂·H₂O (422 mg, 1.12 mmol, 56 % yield). 1D and 2D NMR spectra (COSY, TOCSY, NOESY and [¹H, ¹³C] HSQC) were recorded on this product on a 600 MHz spectrometer in 100 % D₂O and 90 % H₂O / 10 % D₂O.

ES-MS : m/z = 376.9 [M+H-H₂O]⁺, 316.8 [M-OAc-H₂O]⁺, 256.7 [M-2(OAc)-H₂O-H]⁺.

Anal. Calcd for C₁₄H₃₂N₄NiO₅: C, 42.56, N, 14.18, H, 8.16 %, found C, 40.15, N, 14.19, H, 7.84 %.

Selected IR (KBr, cm⁻¹): 3528 b (OH), 3457 m (NH), 3246 s (NH), 2939 m (CH), 2875 s (CH), 1636 m (OH), 1571 s (CO), 1406 s (CO).

[Ni(cyclam)]Cl₂ (5). Cyclam (50.7 mg, 0.25 mmol) was dissolved in methanol (20 mL) and NiCl₂·6H₂O (59.74 mg, 0.25 mmol) was added. The reaction was stirred overnight under N₂. The resulting orange/brown solution was filtered and concentrated to dryness to give a green powder. Upon drying under high vacuum, the powder turned purple. (63.3 mg, 0.19 mmol, 77 % yield)

1D and 2D NMR spectra (COSY, TOCSY, NOESY and [¹H, ¹³C] HSQC) were recorded on this product on a 600 MHz spectrometer in 90 % H₂O / 10 % D₂O.

ES-MS : m/z = 332.7 [M+H]⁺, 292.6 [M-Cl]⁺, 256.6 [M-2Cl-H]⁺.

Anal. Calcd for C₁₀H₂₄N₄NiCl₂: C, 36.40, N, 16.98, H, 7.33 %, found C, 36.55, N, 17.12, H, 7.30 %.

Selected IR (KBr, cm⁻¹): 3262 m (NH), 3211 s (NH), 2926 m (CH), 2857 s (CH).

[Ni(cyclam)](NO₃)₂ (6). Cyclam (104.65 mg, 0.52 mmol) was dissolved in methanol (20 mL) and Ni(NO₃)₂·6H₂O (150.21 mg, 0.52 mmol) was added. The reaction was stirred overnight under N₂. The resulting orange solution was filtered and concentrated to dryness to give a purple powder, which was dried under high vacuum. (140.4 mg, 0.43 mmol, 83 % yield).

1D and 2D NMR spectra (COSY, TOCSY, NOESY and [¹H, ¹³C] HSQC) were recorded on this product on a 600 MHz spectrometer in 90 % H₂O / 10 % D₂O.

ES-MS : m/z = 319.7 [M-NO₃]⁺, 256.7 [M-2(NO₃)-H]⁺.

Anal. Calcd for C₁₀H₂₄N₆NiO₆: C, 31.36, N, 21.94, H, 6.32 %, found C, 31.25, N, 22.21, H, 6.28 %.

Selected IR (KBr, cm⁻¹): 3261 s (NH), 3212 s (NH), 2927 m (CH), 2871 s (CH), 1381 b (NO).

3.2.3 Synthesis of a Cobalt(III) Cyclam Complex

[Co(cyclam)(OAc)₂](BPh₄) (7). Cyclam (404.9 mg, 2 mmol) was dissolved in methanol (20 mL) with stirring. To this, a solution of Co(OAc)₂·4H₂O (498.1 mg, 2 mmol) in methanol (30 mL) was added dropwise with stirring over 10 minutes. Air was bubbled through the orange/brown solution for 30 minutes. Acetic acid (1 M, 2 molar equiv, 20 mL) was added and air was bubbled through for a further 30 minutes. The brown solution was filtered and concentrated to dryness to give an orange/pink oil (654.2 mg). This oil (100 mg, 0.2 mmol) was then dissolved in methanol (5 mL) and NH₄BPh₄ (134.82 mg, 0.4 mmol) was added with stirring. The cloudy orange solution was stirred overnight at room temperature. The resulting cloudy pink solution was filtered and concentrated to dryness to give pink crystals of

[Co(cyclam)(OAc)₂](BPh₄) (124 mg, 65 % yield).

1D and 2D NMR spectra (COSY, TOCSY, NOESY, [¹H, ¹³C] HSQC and [¹H, ¹⁵N] HSQC) were recorded on this product on a 600 MHz spectrometer in DMSO-d₆.

ES-MS : m/z = 377.0 [M-(BPh₄)]⁺, 318.1 [M-(OAc)-(BPh₄)-H]⁺, 258.1 [M-2(OAc)-(BPh₄)-H]⁺.

Selected IR (KBr, cm⁻¹): 3432 m (NH), 3215 s (NH), 2932 m (CH), 2871 s (CH), 1570 m (CO), 1376 m (CO).

3.2.4 Synthesis of a Copper(II) Cyclam Complex

Synthesis of [Cu(cyclam)(H₂O)₂](OAc)₂·2MeOH (8). Cyclam (400.85 mg, 2 mmol) was dissolved in methanol (50 mL) and Cu(OAc)₂·H₂O (363.46 mg, 2 mmol) was added. The reaction was heated to reflux for two hours. The resulting purple solution was filtered and concentrated to dryness to give a purple powder. This was recrystallized by slow evaporation from methanol into diethyl ether to give [Cu(cyclam)(H₂O)₂](OAc)₂·2MeOH.

1D and 2D NMR spectra ([¹H, ¹³C] HSQC) were recorded on this product on a 360 MHz spectrometer in 90 % H₂O / 10 % D₂O.

ES-MS : m/z = 322.2 [M-OAc-2(H₂O)]⁺, 262.0, [M-2(OAc)-2(H₂O)-H]⁺.

Anal. Calcd for C₁₄H₃₄N₄CuO₆: C, 40.23, N, 13.40, H, 8.20 %, found C, 40.24, N, 13.36, H, 8.14 %.

Selected IR (KBr, cm⁻¹): 3229 m (NH), 3164 m (NH), 2938 m (CH), 2878 s (CH), 1644 m (OH), 1565 m (CO), 1428 m (CO).

3.2.5 NMR Studies of [Ni(cyclam)](OAc)₂, 4

Firstly, 1D and 2D (¹H, ¹³C] HSQC, COSY, TOCSY and NOESY) spectra were recorded of complex 4 in 100 % D₂O, (5 mM, 600 μL). Dioxane was added as a reference (2 μL). The solvent was removed and the powder was re-dissolved in 90 % H₂O / 10 % D₂O (600 μL) and left to equilibrate for 24 hours. Then, the 1D and 2D spectra were re-recorded. Two molar equivalents of NaOAc (an aliquot of a 1 M solution) were added and again left to equilibrate for 24 hours and the 1D and 2D spectra were recorded. The procedure was repeated again with 10 molar equivalents of NaOAc.

3.2.6 UV-Vis Spectroscopy

UV-vis spectroscopy was carried out on complexes 4-8 at 2.5 mM in water, except for complex 7, which was recorded in DMSO. All spectra were recorded at 25 °C in 1 cm cells.

3.3 Results

3.3.1 NMR Studies of Pd(II) Cyclam Complexes

2D NMR methods were used to identify the configurations present in solution for the three palladium cyclam complexes. The chemical shifts of all three complexes are shown in Table 3.1.

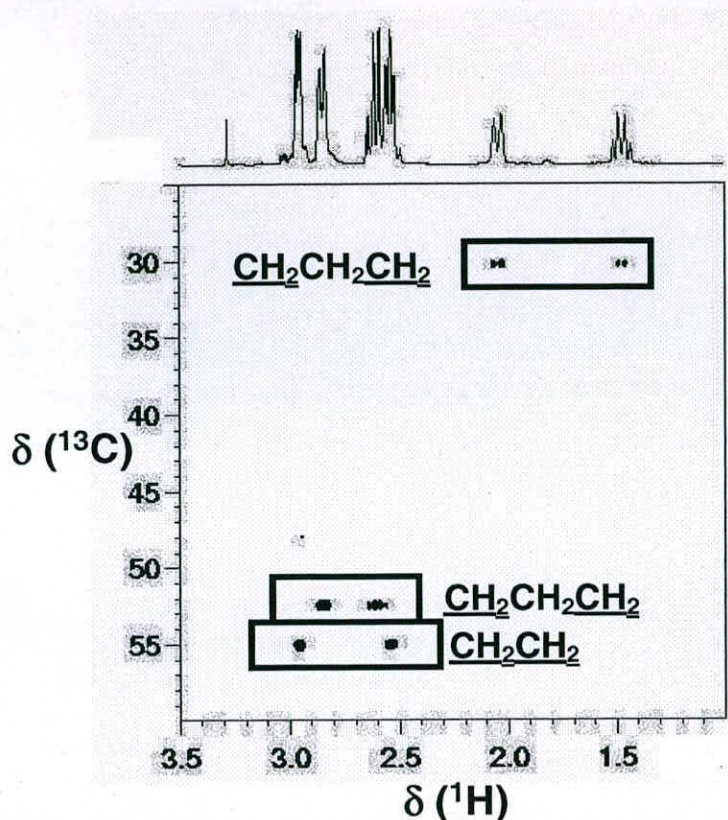


Figure 3.2 2D [^1H , ^{13}C] HSQC and 1D NMR spectra of $[\text{Pd}(\text{cyclam})]\text{Cl}_2$ in 90 % H_2O / 10% D_2O . The protons that are on the same carbon atoms can clearly be seen.

$[\text{Pd}(\text{Cyclam})]\text{Cl}_2$ (**1**). 2D [^1H , ^{13}C] HSQC (Figure 3.2) and [^1H , ^1H] COSY, NOESY and TOCSY (Figure 3.3) NMR spectra were recorded. There is a singlet at 5.15 ppm which can be assigned to the NH protons, as it is absent in the 2D [^1H , ^{13}C] HSQC NMR spectrum. The 2D COSY NMR spectrum shows this signal has cross-peaks to four other signals. These are at 2.92, 2.82, 2.73 and 2.55 ppm. These signals must be either the $-\text{CH}_2-\text{CH}_2-\text{CH}_2-$ or the $-\text{CH}_2-\text{CH}_2-$ protons. The signals at 2.82 and 2.73 ppm show cross-peaks to the signals at 1.53 and 2.02 ppm. This implies that the signals at 2.82 and 2.73 ppm correspond to the $-\text{CH}_2-\text{CH}_2-\text{CH}_2-$ protons and the signals at 1.53 and 2.02 ppm correspond to the $-\text{CH}_2-\text{CH}_2-\text{CH}_2-$ protons (^{13}C shift =

30.2 ppm). Hence the signals at 2.92 and 2.55 ppm arise from the $-\text{CH}_2-\text{CH}_2-$ protons (^{13}C shift = 55.0 ppm). This assignment is confirmed by 2D [^1H , ^{13}C] HSQC NMR spectrum as the signals at 2.82 and 2.73 ppm in the ^1H dimension have the same ^{13}C chemical shift (52.2 ppm). There is a small amount of free cyclam present, giving rise to signals at 1.8 and 3.0 ppm.

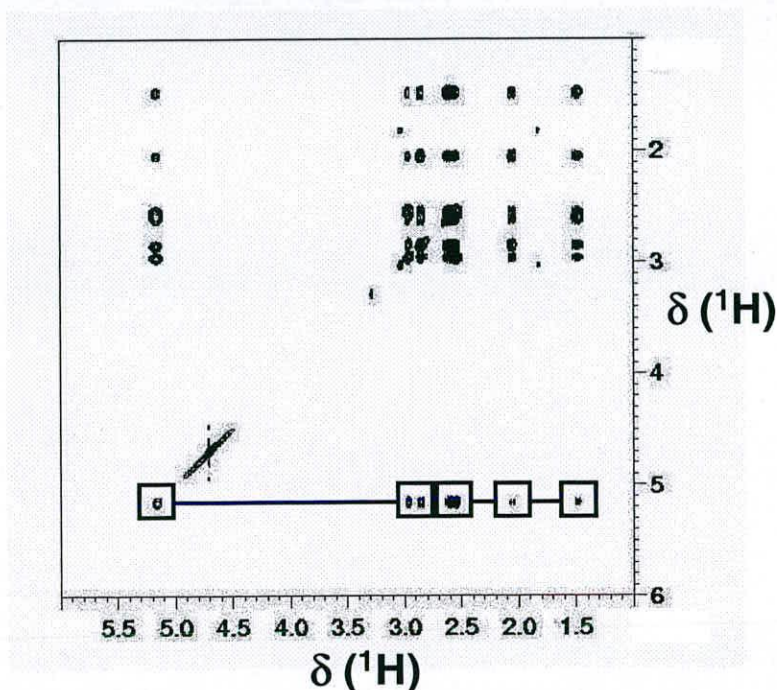


Figure 3.3 2D [^1H , ^1H] TOCSY NMR spectrum of $[\text{Pd}(\text{cyclam})]\text{Cl}_2$ in 90 % H_2O / 10 % D_2O , in which the NH peak at 5.15 ppm shows TOCSY cross peaks to all the proton signals in the complex.

The 2D [^1H , ^1H] TOCSY NMR spectrum (Figure 3.3) demonstrates that there is only one isomer present, along with a small amount of cyclam. The 2D [^1H , ^1H] NOESY NMR spectrum can be used to assign which protons are axial and which are equatorial in the six-membered chelate rings. The signal at 1.53 ppm shows a cross-peak to the peak at 5.15 ppm, whereas the signal at 2.02 ppm does not. This means

that the signal at 1.53 ppm is from an axial proton, and the signal at 2.02 ppm is from an equatorial proton. For the $-\underline{\text{CH}_2}-\text{CH}_2-\underline{\text{CH}_2}-$ protons, the signal at 2.82 ppm has a crosspeak to the $-\text{NH}$ proton signal, and therefore must be the axial proton signal. For the $-\underline{\text{CH}_2}-\underline{\text{CH}_2}-$ protons, both have cross-peaks to the $-\text{NH}$ protons. Because this forms a five-membered ring, it is not possible to assign the protons as axial or equatorial.

[Pd(Cyclam)](OAc)₂ (2). There is only one NH proton signal present, at 5.27 ppm, indicating that there is only one isomer present. There is a peak from the acetate group at 1.84 ppm. The peaks at 1.51 ppm and 2.00 ppm are attributed to the $\text{CH}_2-\underline{\text{CH}_2}-\text{CH}_2$. The $\underline{\text{CH}_2}-\text{CH}_2-\underline{\text{CH}_2}$ protons gave peaks at 2.57 and 2.96 ppm. The $\underline{\text{CH}_2}-\underline{\text{CH}_2}$ protons gave signals at 2.69 and 2.85 ppm.

[Pd(Cyclam)](ClO₄)₂ (3). This has a peak at 1.52 ppm and another peak at 2.31 ppm, which is assigned to the $\text{CH}_2-\underline{\text{CH}_2}-\text{CH}_2$ protons. There are two peaks from the $\underline{\text{CH}_2}-\text{CH}_2-\underline{\text{CH}_2}$ protons, at 2.61 and 3.01 ppm. The $\underline{\text{CH}_2}-\underline{\text{CH}_2}$ protons give two peaks, at 2.68 and 2.91 ppm. The single NH peak at 5.21 ppm shows that there is only one isomer present.

Table 3.1 ¹H NMR Chemical shifts of Pd(II)-cyclam complexes, recorded in 90 % H₂O / 10 % D₂O at 25 °C at 5 mM.

Complex	δ ¹ H / ppm			
	$\underline{\text{NCH}_2\text{CH}_2\text{N}}$	$\text{NCH}_2\underline{\text{CH}_2}\text{CH}_2\text{N}$	$\underline{\text{NCH}_2\text{CH}_2}\underline{\text{CH}_2\text{N}}$	NH
1	2.92, 2.55	1.53, 2.02	2.73, 2.82	5.15
2	2.69, 2.85	1.51, 2.00	2.57, 2.96	5.27
3	2.68, 2.91	1.52, 2.31	2.61, 3.01	5.21

3.3.2 NMR Studies of Ni(II) Cyclam Complexes

The 1D spectra of all three Ni(II) cyclam complexes (**4-6**) showed a mixture of sharp and broad peaks (Figure 3.4). The broad shifted peaks can be attributed to one or more paramagnetic forms of the complex. As paramagnetic species are

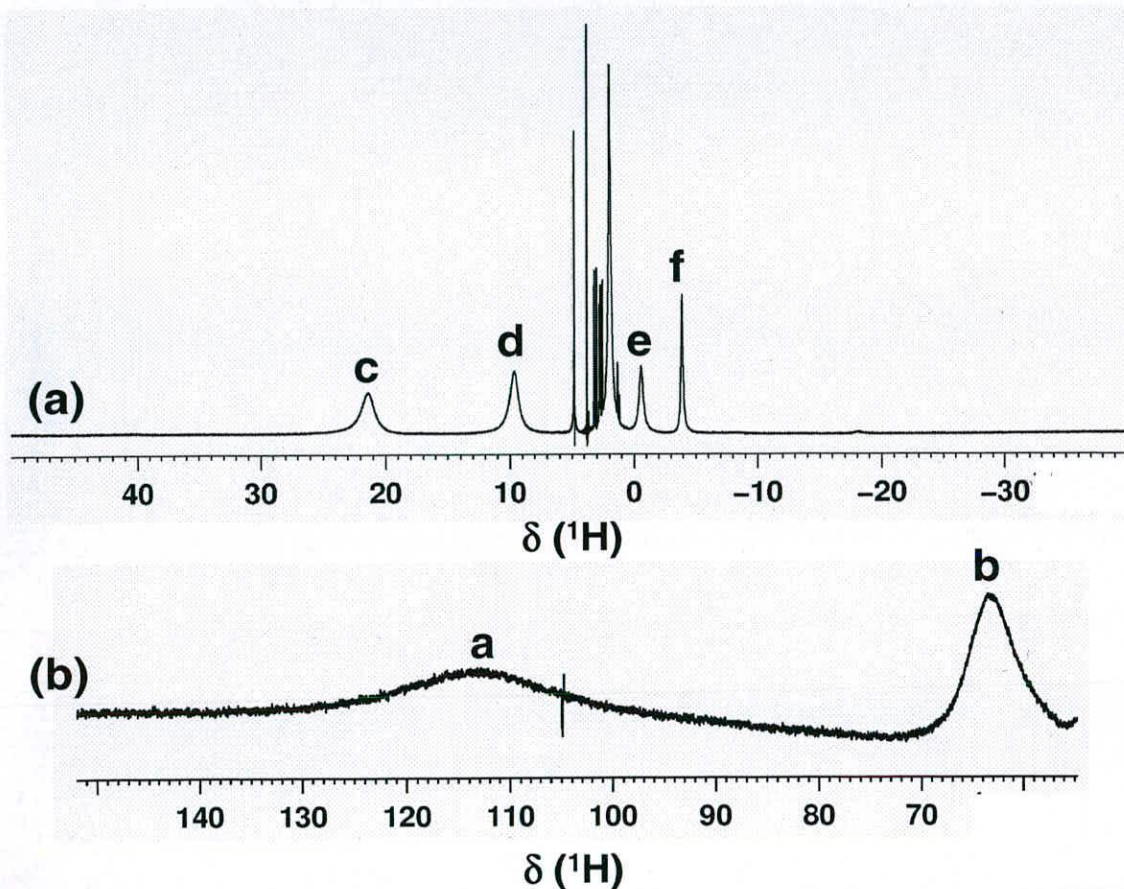


Figure 3.4 Proton NMR spectra of [Ni(cyclam)](OAc)₂, complex **4**. (a) Over the range -40 ppm to +50 ppm. (b) From 55 ppm to 155 ppm. This shows there is a mixture of peaks from diamagnetic (between 0 – 4 ppm) and paramagnetic species. The scale of the vertical axis in (b) is increased by 2⁴.

known to have shifted peaks in NMR spectra, the spectra were recorded over a large sweep width from -150 ppm to 300 ppm. Peaks were observed in the spectrum

between -50 ppm and +150 ppm. Peaks for diamagnetic forms of the complexes were observed between 1 ppm and 4 ppm. The shifts observed for the paramagnetic species are summarised in Table 3.2, and the diamagnetic shifts shown in Table 3.3.

Table 3.2 ^1H NMR Chemical shifts for paramagnetic Nickel(II) cyclam complexes recorded in 90 % H_2O , 10 % D_2O at 25 °C at 5 mM.

Peak	Complex		
	4*	5	6
a	113.82	54.69	55.19
b	63.02	19.01	18.64
c	21.54	8.74	8.66
d	9.62	-0.35	-0.32
e	-0.58	-3.18	-3.22
f	-3.08		-52.56

*The peaks for complex 4 are labelled in Figure 3.4.

[Ni(cyclam)](OAc)₂, 4. The 1D and 2D spectra of the acetate complex, 4, recorded in 100 % D_2O show peaks for 6 non-equivalent protons and 3 corresponding non-equivalent carbon signals. Therefore in the diamagnetic complex the cyclam ring must be in a symmetrical configuration.

From the 2D [^1H , ^1H] TOCSY NMR spectrum it can be seen that there are cross-peaks between non-equivalent protons on the same carbon and also cross peaks between protons on neighbouring carbons. Cross-peaks between protons separated by a NH group are not seen in this spectrum.

The 1D and 2D NMR spectra were also recorded in a mixture of 90% H_2O / 10% D_2O in order to assign the NH shift. A new peak at 3.60 ppm was observed in

the 1D spectrum and the 2D [$^1\text{H}, ^1\text{H}$] TOCSY NMR spectrum and not in the 2D [$^1\text{H}, ^{13}\text{C}$] HSQC NMR spectrum, therefore this signal was assigned as a signal from the NH proton. Only one signal was seen for an NH proton therefore all the NH groups in the diamagnetic configuration must be equivalent, and only one diamagnetic configuration is present.

In order to confirm the position of the acetate peak in the ^1H NMR spectrum, 2 and 10 molar equivalents of Na(OAc) were added to the solution. This would have the effect of moving the equilibrium of the system and increasing the intensity of acetate signal observed in the ^1H NMR spectrum. The signal at 1.9 ppm increased in intensity (Figure 3.5) and was therefore assigned as the acetate signal. As the signal is quite broad, both before and after the addition of excess acetate, it is likely that the bound acetate is in fast exchange with the non-bound acetate, as if this was not the case, two signals would be expected, one broad one for bound acetate and one sharper one for unbound acetate. The signal for the bound acetate is broadened as it is directly bonded to the paramagnetic octahedral Ni^{2+} centre.

Using the 1D and 2D spectra, the peaks for the diamagnetic configuration have been assigned (Table 3.3). It was found that there were 6 peaks for protons in complex **4**. These corresponded to 3 carbons in the HSQC spectra (Table 3.3). Two isomers have the correct symmetry to give rise to six non-equivalent protons: *trans*-I and *trans*-III. Only one NH signal was observed, which also supports either a *trans*-I or a *trans*-III configuration.

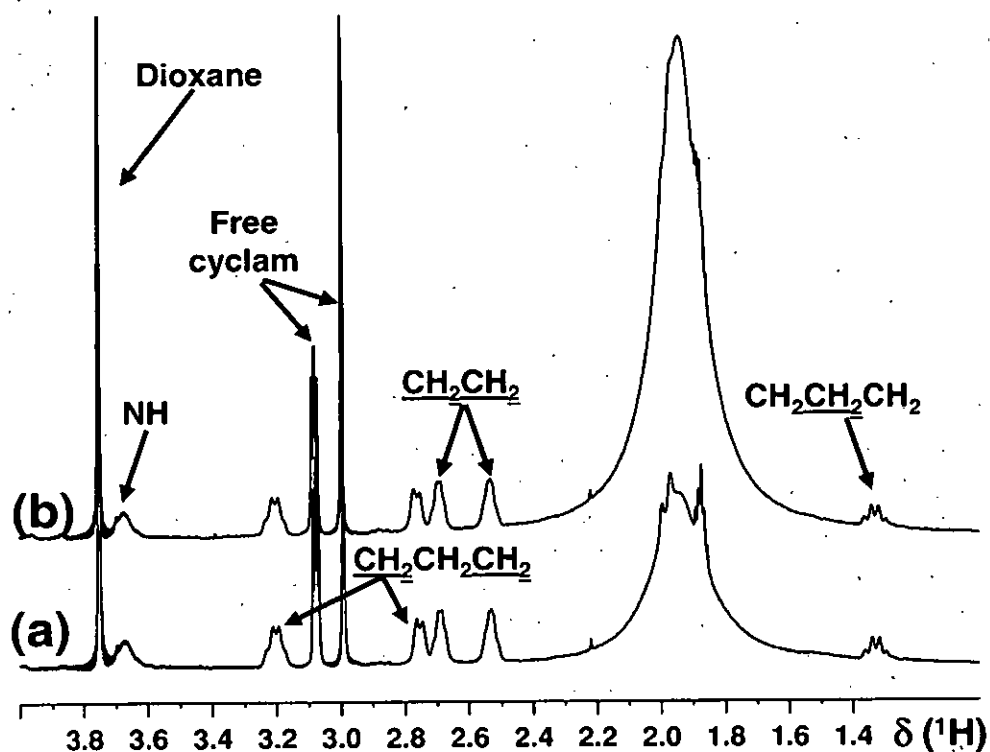


Figure 3.5 $[\text{Ni}(\text{cyclam})](\text{OAc})_2$, complex 4, in 90 % H_2O / 10 % D_2O (a) before and (b) after the addition of 10 equivalents of NaOAc . The assignments for the peaks are shown. There are peaks present for complex 4 and free cyclam present. The peak at 1.9 ppm increases significantly, showing it is from the acetate.

$[\text{Ni}(\text{cyclam})]\text{Cl}_2$, 5. No free cyclam was observed in solutions of the complex. There was only one NH peak present in the 1D ^1H NMR spectrum, at 3.67 ppm, implying only one diamagnetic isomer was present. There is a peak at 1.34 ppm and another peak at 1.98 ppm, which are assigned as from the $\text{CH}_2\text{-CH}_2\text{-CH}_2$ protons, with a corresponding ^{13}C shift of 28.7 ppm. There are two peaks from the $\text{CH}_2\text{-CH}_2\text{-CH}_2$ protons, at 2.71 and 3.21 ppm, connected to the same ^{13}C signal at 50.7 ppm. The $\text{CH}_2\text{-CH}_2$ protons give two peaks, at 2.52 and 2.68 ppm, with a ^{13}C shift of 53.1

ppm. The data are summarised in Table 3.3.

[Ni(cyclam)](NO₃)₂, **6**. Again, there is only one NH peak observed, at 3.67 ppm. The CH₂-CH₂-CH₂ protons were observed at 1.33 ppm and 1.98 ppm. The CH₂-CH₂-CH₂ protons were found to be at 2.71 ppm and 3.19 ppm, with the CH₂-CH₂ protons being found at 2.52 ppm and 2.68 ppm. The ¹³C shifts for this complex are shown in Table 3.3.

Table 3.3 ¹H and ¹³C Chemical shifts of diamagnetic Ni(cyclam)²⁺ complexes recorded in 90 % H₂O, 10 % D₂O at 25 °C at 5 mM.

Complex		¹ H and ¹³ C assignment / ppm									
		NCH ₂ CH ₂ N			NCH ₂ CH ₂ CH ₂ N			NCH ₂ CH ₂ CH ₂ N			NH
4	¹ H	2.69		2.53	1.32		1.98	2.76		3.20	3.60
	¹³ C		53.0			28.7			50.7		
5	¹ H	2.52		2.67	1.34		1.98	2.71		3.20	3.67
	¹³ C		53.1			28.7			50.7		
6	¹ H	2.52		2.67	1.33		1.98	2.71		3.19	3.67
	¹³ C		53.2			28.8			50.8		

3.3.3 NMR Studies of Co(III) Cyclam Complex, **7**

The 1D ¹H spectrum of this complex is very complicated (Figure 3.6). No free cyclam was observed in solutions of the complex. There were four peaks observed in the 2D [¹H, ¹⁵N] NMR HQSC spectrum (Figure 3.7). Two of these peaks show a TOCSY peak to each other, while the other two show no interaction

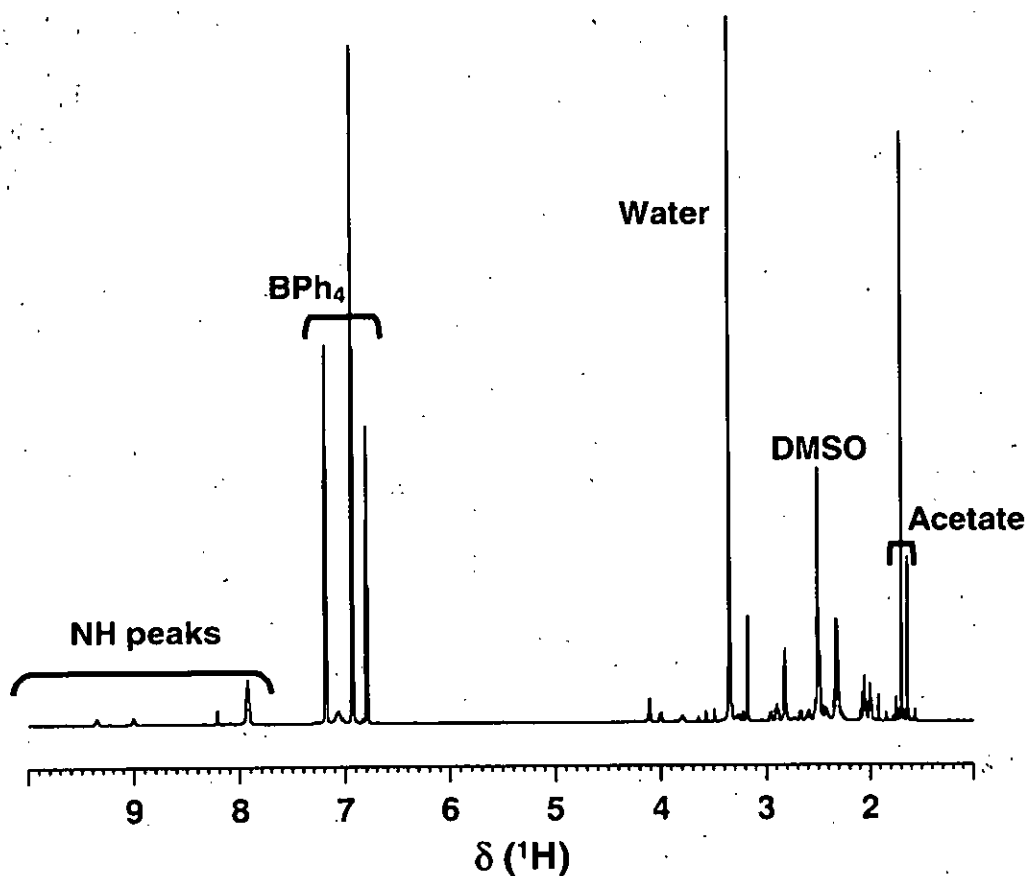


Figure 3.6 ^1H NMR spectrum of $\text{Co}(\text{cyclam})(\text{OAc})_2(\text{BPh}_4)$ in DMSO-d_6 at 25 °C.

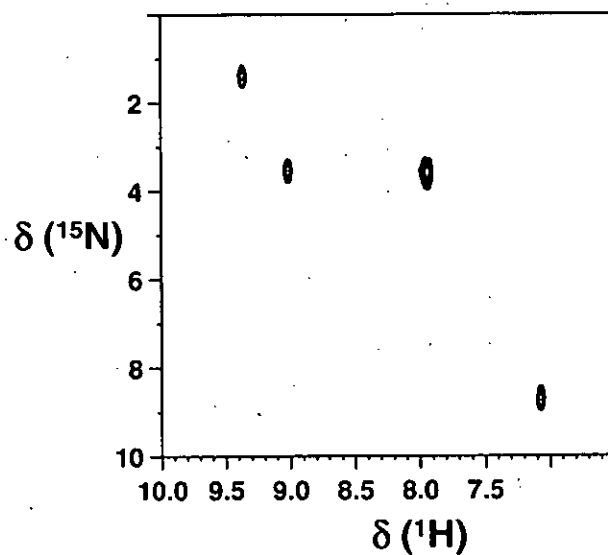


Figure 3.7 2D [^1H , ^{15}N] HSQC NMR spectrum of $[\text{Co}(\text{cyclam})(\text{OAc})_2](\text{BPh}_4)$ in DMSO-d_6 at 25 °C. Four NH signals are clearly observed.

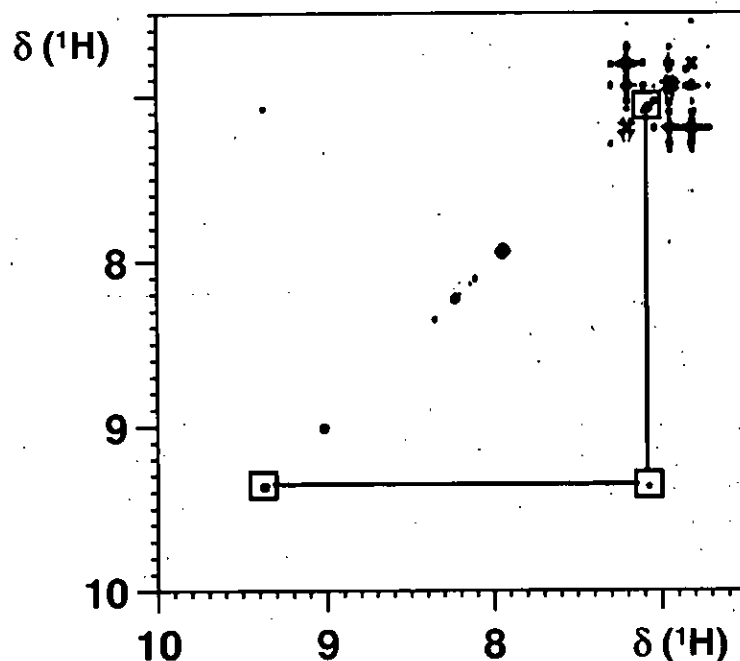


Figure 3.8 2D [^1H , ^1H] TOCSY NMR spectrum of $[\text{Co}(\text{cyclam})(\text{OAc})_2](\text{BPh}_4)$ in DMSO-d_6 at $25\text{ }^\circ\text{C}$. Two NH signals show a TOCSY cross peak to each other, showing that they are from the one species, whereas none of the other NH signals interact with each other.

with each other, implying that there are three configurations present, as shown in Figure 3.8. Three acetate signals are observed, all in the region of bound acetate, further confirming the presence of three configurations (Figure 3.9). This suggests that all three are *trans* configurations, as if there was a *cis* configuration with a chelated acetate, there would also be a signal present for free acetate. The major configuration has an NH peak at 7.94 ppm (^1H dimension). As this is the major configuration, and the crystal structure shows that the complex is in the *trans*-III configuration, this major form in solution is likely to be in the *trans*-III

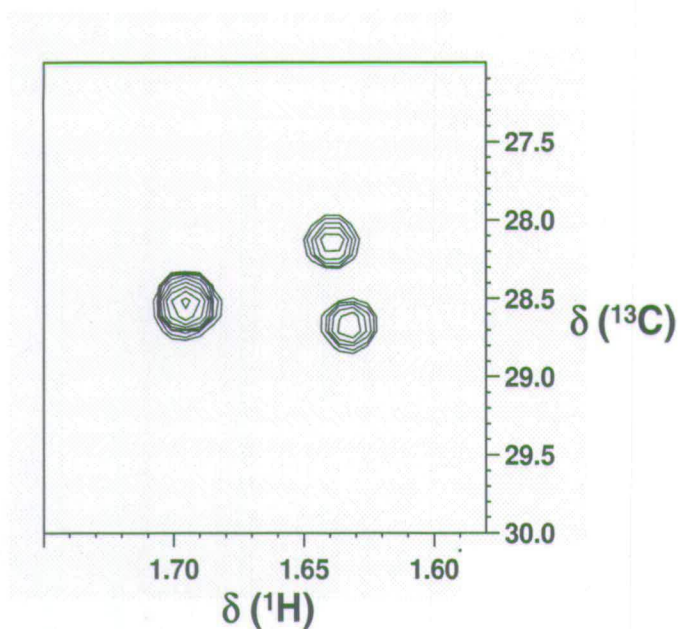


Figure 3.9 2D [^1H , ^{13}C] HSQC NMR spectrum of $[\text{Co}(\text{cyclam})(\text{OAc})_2](\text{BPh}_4)$ in DMSO at 25 °C.

configuration. Three sets of CH_2 peaks for this species (seen by 2D [^1H , ^1H] TOCSY and [^1H , ^{13}C] HSQC NMR spectra) support this. Full characterisation for this species (species A) is given in Table 3.4. There is a second species with an NH peak at 8.99 ppm, species B. This can also be found to have three sets of CH_2 peaks, again suggesting a *trans* configuration. This one is likely to be *trans*-I, as the *trans*-I is the most favoured configuration after *trans*-III. The third species, C, has two NH signals which show a TOCSY cross-peak to each other. Six sets of CH_2 peaks were observed in the 2D NMR spectra for this complex. The data for all three species are summarised in Table 3.4.

Table 3.4 ^1H , ^{13}C and ^{15}N Chemical shifts of $[\text{Co}(\text{cyclam})(\text{OAc})_2]^+$ (7) recorded in DMSO at 25 °C at 5 mM.

Species		δ / ppm									
		$\text{NCH}_2\text{CH}_2\text{N}$			$\text{NCH}_2\text{CH}_2\text{CH}_2\text{N}$			$\text{NCH}_2\text{CH}_2\text{CH}_2\text{N}$			NH
A	^1H	2.32		2.82	1.99		2.06	2.32		2.49	7.94
	^{13}C		55.1			29.7			50.2		
	^{15}N										-21.62
B	^1H	2.96		2.52	2.05		2.37	2.66		*	8.99
	^{13}C		55.0			30.0			50.2		
	^{15}N										-21.67
C	^1H	2.44		2.90	3.21		3.27	2.52		2.59	9.35
	^{13}C		55.7			35.8			45.4		
	^{15}N										-23.78
	^1H	2.43		2.89	2.05		*	2.47		2.27	7.06
	^{13}C		53.1			30.1			50.6		
	^{15}N										-16.5

* Peaks not observed due to overlap.

3.3.4 NMR Studies of Cu(II) Cyclam Complex, 8

1D ^1H NMR and 2D [^1H , ^{13}C] HSQC NMR spectra were recorded in 90 % H_2O / 10 % D_2O at 25 °C, at 5 mM, on this complex (Figure 3.10). Only one sharp peak was observed, at 1.8 ppm in the ^1H dimension, and 23.52 ppm in the ^{13}C dimension. Two broad peaks, at 16 ppm and -12 ppm, were observed in the ^1H dimension, but had no connectivity in the ^{13}C dimension.

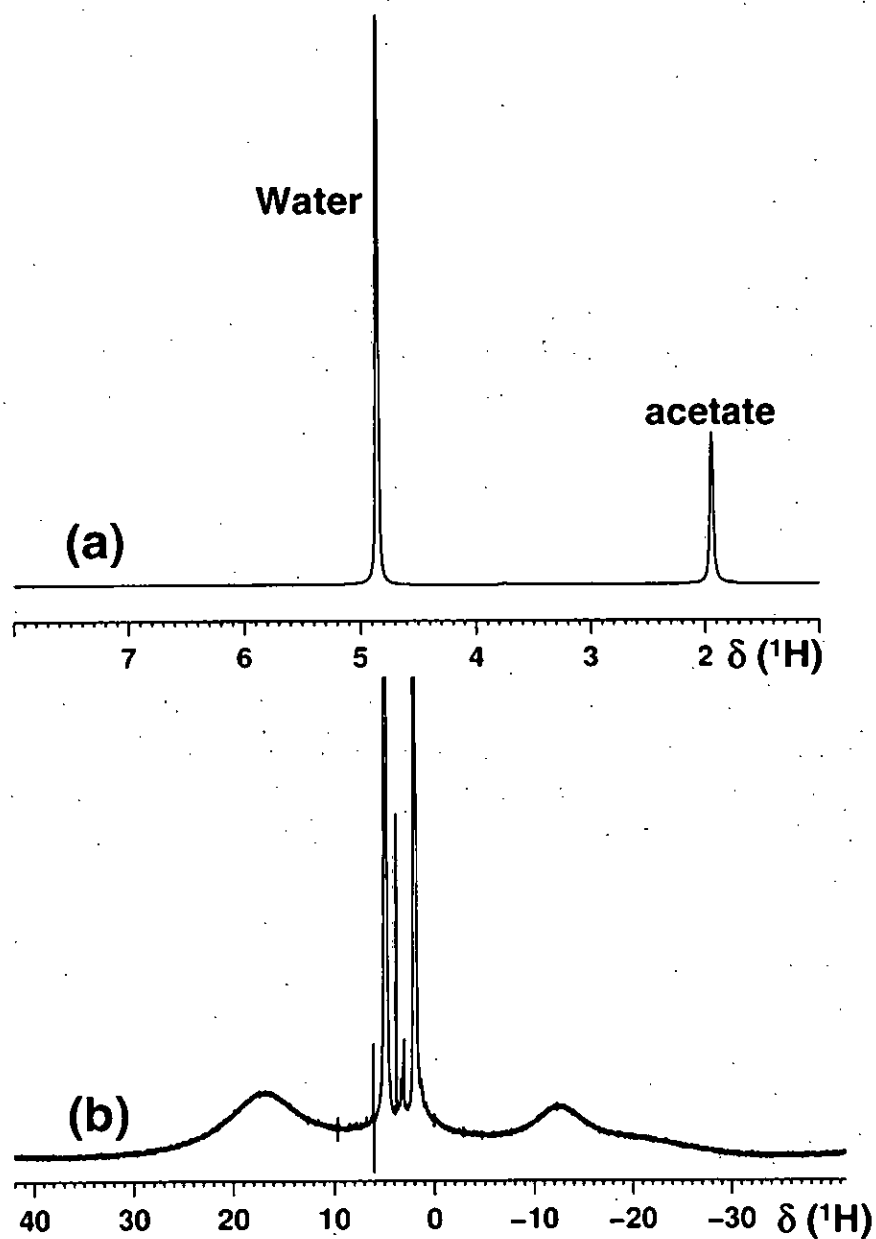


Figure 3.10 1D ¹H NMR spectrum of [Cu(cyclam)(H₂O)₂](OAc)₂, recorded in 90 % H₂O / 10 % D₂O, at 25 °C, (a) over the range 1 – 8 ppm, there is a signal for acetate in this region, (b) over the range -40 – 40 ppm, showing two broad peaks at 16 ppm and -12 ppm.

3.3.5 X-Ray Crystallography

Four crystal structures of metal cyclam acetate complexes were obtained in this work. These were [Pd(cyclam)](OAc)₂·2H₂O (Figure 3.11), [Ni(cyclam)](OAc)₂·H₂O (Figure 3.13), [Co(cyclam)(OAc)₂](BPh₄) (Figure 3.15) and [Cu(cyclam)(H₂O)₂](OAc)₂·2MeOH (Figure 3.17). The cyclam ring was found to be in the *trans*-III configuration in all cases. A comparison of key bond lengths and angles is shown in Table 3.5. There are two independent Pd²⁺ units in [Pd(cyclam)](OAc)₂·2H₂O and two independent Co³⁺ units in [Co(cyclam)(OAc)₂](BPh₄); indicated by a "A" in the table. Crystallographic data for these complexes are shown in Table 3.6.

Table 3.5 Comparison of bond lengths (Å) and angles (°) for metal cyclam acetate complexes

Complex	[Pd(cyclam)] (OAc) ₂ ·2H ₂ O, 2	[Ni(cyclam)] (OAc) ₂ ·H ₂ O, 4	[Co(cyclam)] (OAc) ₂](BPh ₄), 7	[Cu(cyclam)] (H ₂ O) ₂](OAc) ₂ ·2MeOH, 8
N-M bond lengths	2.038(4)	2.0678(14)	1.932(5)	2.018(2)
	2.043(3)	2.0746(15)	1.959(5)	2.012(2)
	2.036(4)A		1.988(6)A	
	2.037(3)A		1.979(6)A	
N(1)-M-N(1) bond angles	180.0(3)	180.0(7)	180.0(7)	180.0(3)
	180.0(1)A		180.0(7)A	
N(1)-M-N(2) bond angles	95.05(15)	94.49(6)	93.5(2)	94.04(10)
	95.28(15)A		94.2(2)A	
N(2)-M-N(1) bond angles	84.95(15)	85.51(6)	86.5(2)	85.96(10)
	84.72(15)A		85.8(2)A	

Table 3.6 X-ray Crystallographic Data for Metal Cyclam Acetate Crystal Structures

Complex	[Pd(cyclam)] (OAc) ₂ ·2H ₂ O, 2	[Ni(cyclam)] (OAc) ₂ ·H ₂ O, 4	[Co(cyclam)] (OAc) ₂](BPh ₄), 7	[Cu(cyclam)] (H ₂ O) ₂](OAc) ₂ · 2MeOH, 8
Formula	C ₁₄ H ₃₄ N ₄ O ₆ Pd	C ₁₄ H ₃₂ N ₄ NiO ₅	C ₃₈ H ₅₂ BCoN ₄ O ₄	C ₁₆ H ₄₂ CuN ₄ O ₈
Formula weight	460.85	395.15	698.60	482.08
Crystal system	Triclinic	Monoclinic	Monoclinic	Orthorhombic
Space group	P-1	C 2/c	P 2 ₁ /n	Pbca
<i>a</i> / Å	8.5829(10)	13.1311(5)	11.0919(8)	15.9421(7)
<i>b</i> / Å	9.7811(12)	12.5959(5)	23.1481(17)	7.0819(3)
<i>c</i> / Å	11.6962(14)	11.6830(5)	14.566(1)	20.9833(10)
α / °	83.521	90	90	90
β / °	86.559	99.906(3)	109.655(2)	90
γ / °	89.682	90	90	90
Cell vol. / Å ³	973.9(2)	1903.54(13)	3521.9(4)	2369.02
<i>Z</i>	2	4	4	4
Density(Calc) mg/m ³	1.572	1.379	1.317	1.352
Abs. coeff. mm ⁻¹	0.989	1.049	0.533	0.967
Unique reflections	3947	2584	6155	2329
Observed reflections	7978	10647	18105	14118
R1 (obs/all refl)	0.0428	0.0360	0.0663	0.0341
wR2 (obs/all refl)	0.1014	0.0909	0.1771	0.1059

[Pd(cyclam)](OAc)₂·2H₂O, 2. The cyclam ring is in the *trans*-III configuration, with the Pd²⁺ ion being square-planar (Figure 3.11). The unit cell of [Pd(cyclam)](OAc)₂·2H₂O contains 2 molecules, consisting of half molecules of [Pd(cyclam)] in an asymmetric unit along with 2 acetate ions and 2 water molecules. Each [Pd(cyclam)]²⁺ ion appears to form an infinite hydrogen bonded sheet structure with the acetate and water molecules (Figure 3.12). There is no axial interaction between the acetate and the Pd(II), the shortest Pd-O distance being 4.0 Å. The acetate does interact with the NH protons, forming hydrogen bonds, ranging in length from 2.0 Å to 2.2 Å. There is further hydrogen bonding between the acetate and the water molecules, with distances between 1.9 Å - 2.1 Å.

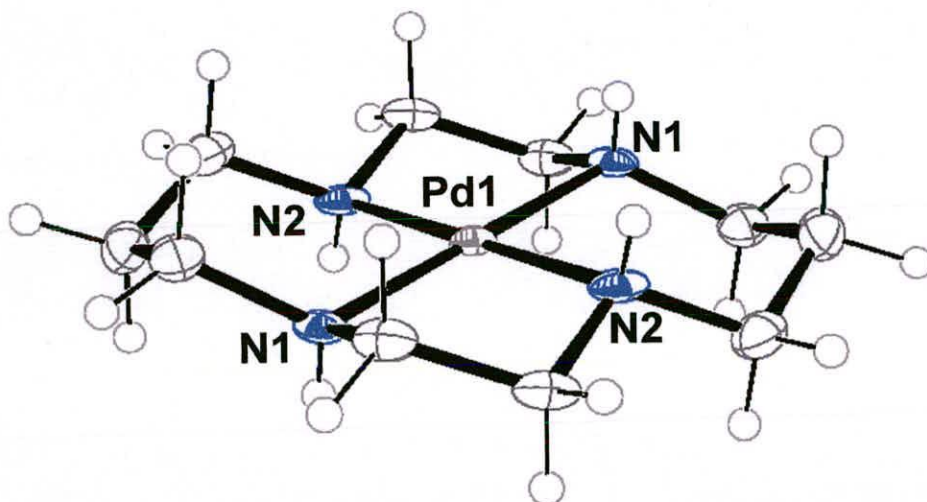


Figure 3.11 [Pd(II)-cyclam]²⁺ from [Pd(cyclam)](OAc)₂·2H₂O. The cyclam ring is in the *trans*-III configuration, and the Pd(II) is square planar.

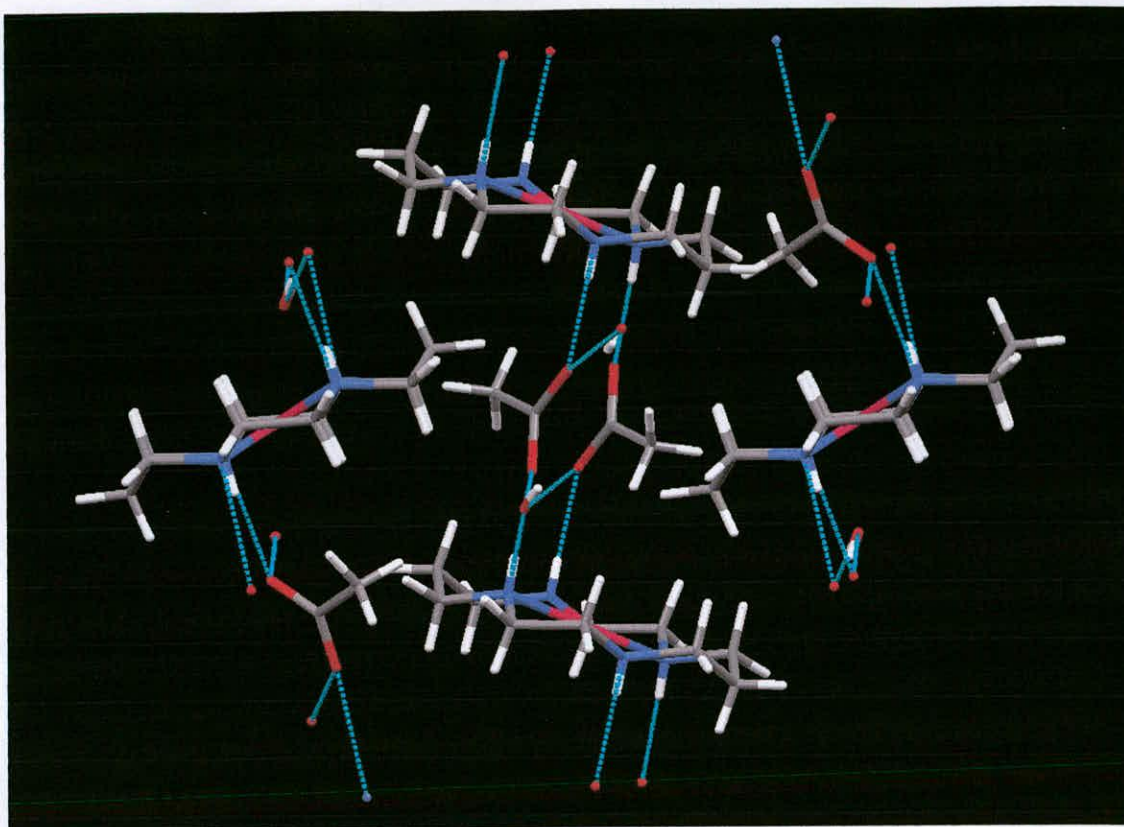


Figure 3.12 Crystal packing of $[\text{Pd}(\text{cyclam})](\text{OAc})_2 \cdot 2\text{H}_2\text{O}$, showing the hydrogen bonding network (in cyan) between the acetate groups and the water molecules.

$[\text{Ni}(\text{cyclam})(\text{OAc})_2] \cdot \text{H}_2\text{O}$, **4**. The nickel is octahedral, with monodentate acetate in each of the axial positions (Figure 3.13). The bond length of the Ni-O bond is 2.106 Å. The cyclam ring is in the *trans*-III configuration. The molecules are held together in layers by a network of hydrogen bonds (Figure 3.14). The O of the acetate ligand is found to form an internal hydrogen bond to the NH of the cyclam ring, bond length 2.1 Å, stabilising the *trans*-III configuration. The structure also contains a water molecule that hydrogen bonds to the acetate ligands on adjacent molecules (2.0 Å) holding the layers of the crystal together.

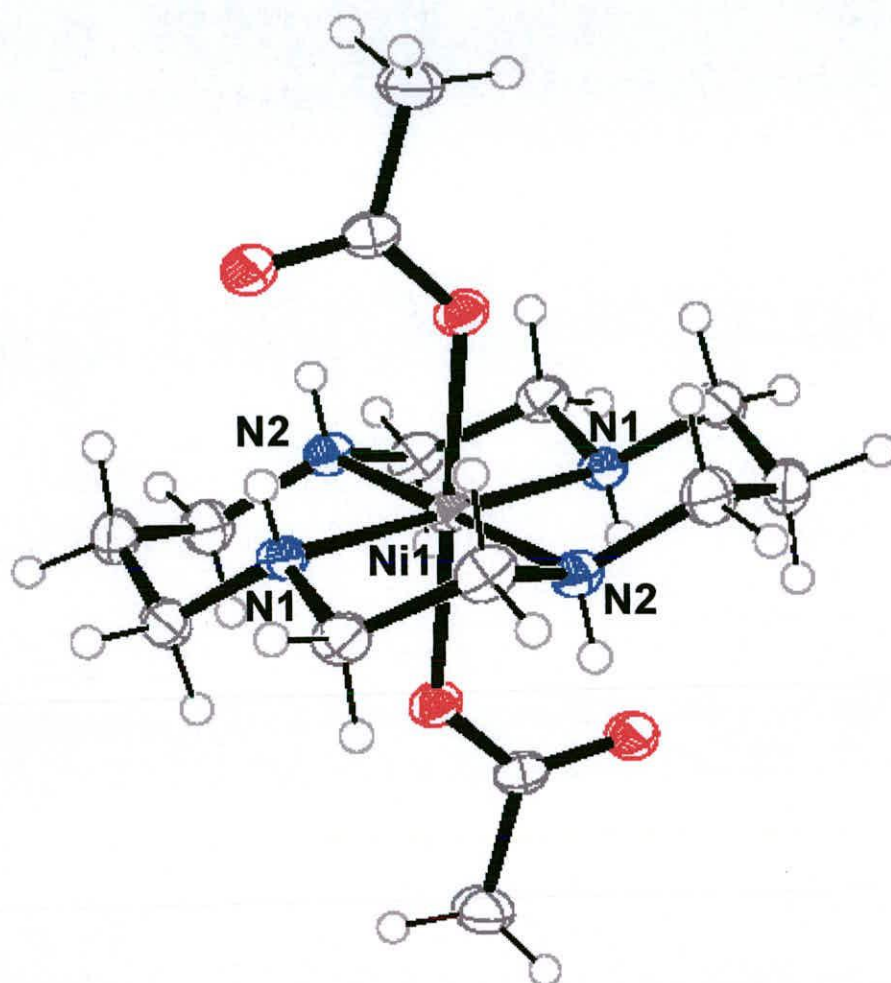


Figure 3.13 [Ni(cyclam)(OAc)₂] from [Ni(cyclam)(OAc)₂] \cdot H₂O. This structure is similar to that of the Co(III) complex, with the acetates forming H-bonds to the NH groups.

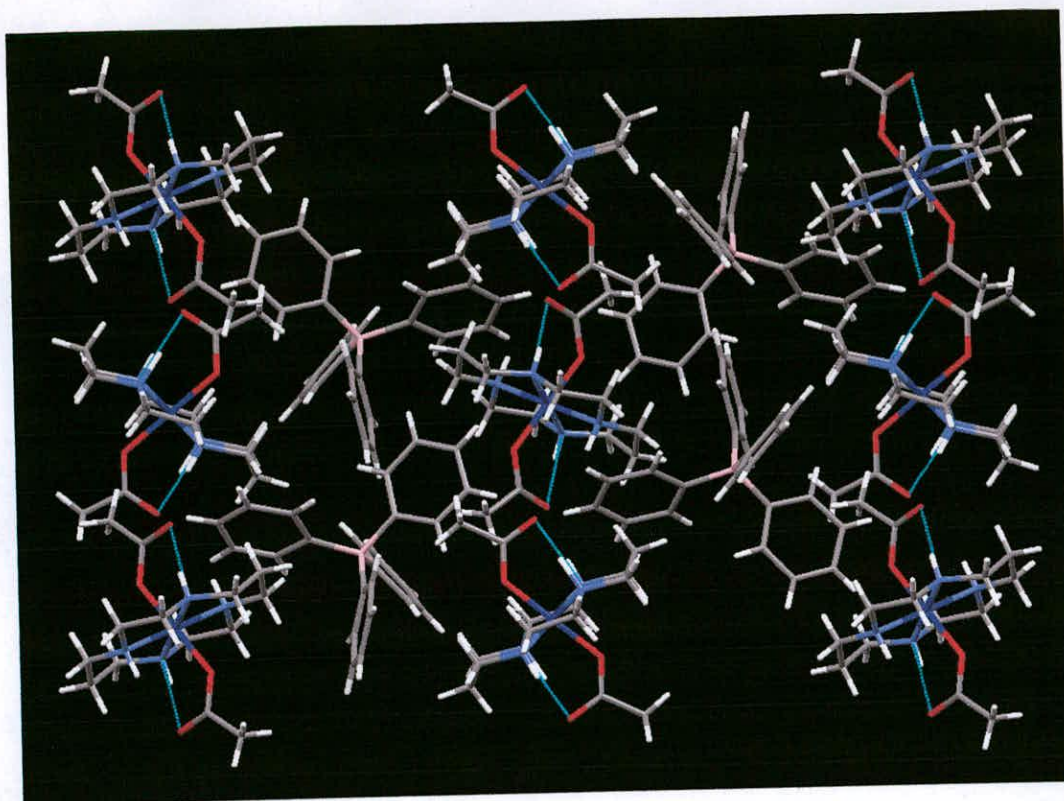


Figure 3.16 Crystal packing of $[\text{Co}(\text{cyclam})(\text{OAc})_2](\text{BPh}_4)$. There is no interaction between axial acetate groups and neighbouring cyclam rings. There is a hydrogen bond (shown in cyan) between the acetate group and an NH group on both sides of the ring.

$[\text{Cu}(\text{cyclam})(\text{H}_2\text{O})_2](\text{OAc})_2 \cdot 2\text{MeOH}$, 8. Again, the cyclam ring is found to be in the *trans*-III configuration (Figure 3.17). The acetate is not coordinated, and there are two water molecules coordinated to Cu^{2+} instead. The molecule forms H-bonds to give a 1D strand (Figure 3.18). The Cu^{2+} ion has a Jahn–Teller-distorted octahedral configuration with four short equatorial Cu–N(cyclam) bonds of 2.012 Å and 2.018 Å, and two long axial Cu–OH₂ bonds of 2.546 Å. One of the carboxylate O atoms from the acetate is H-bonded to a cyclam NH. The hydrogen bonds from the N–H...O of the acetate are approximately 2.1 Å in length. This O atom also

forms hydrogen bonds to the HO from a methanol molecule, with a length of 1.9 Å. The other carboxylate O atom is H bonded to bound water molecule, at a length of 1.9 Å and 2.0 Å.

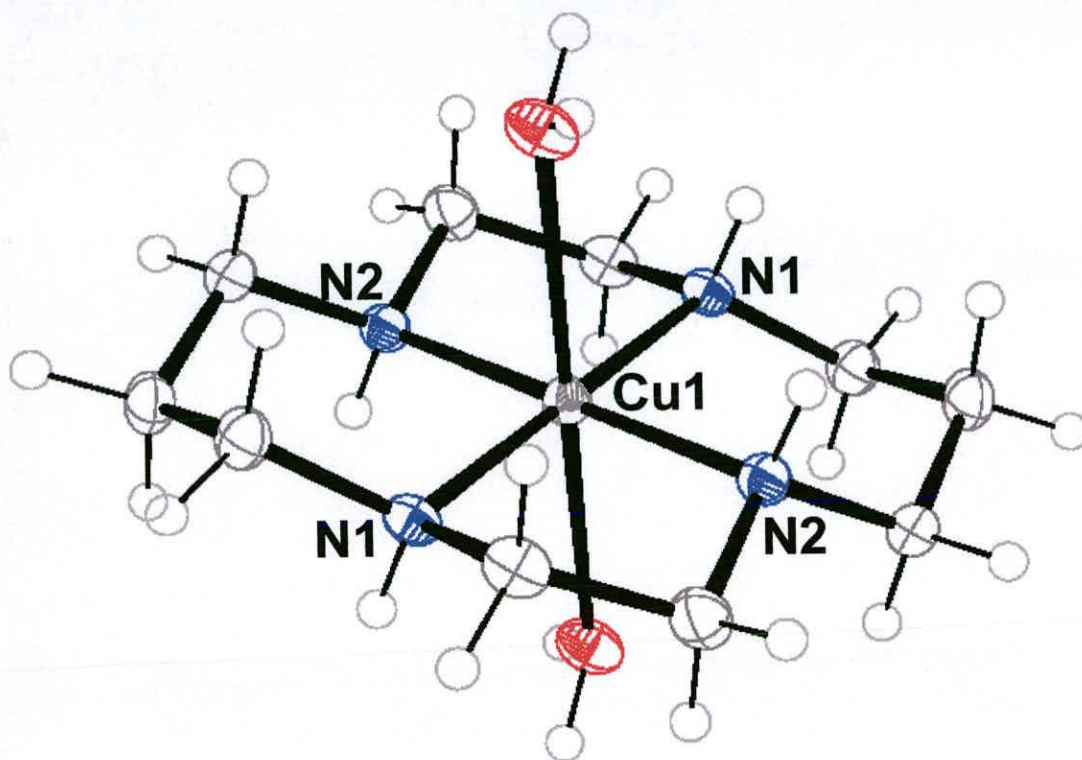


Figure 3.17 $[\text{Cu}(\text{cyclam})(\text{H}_2\text{O})_2]^{2+}$ from $[\text{Cu}(\text{cyclam})(\text{H}_2\text{O})_2](\text{OAc})_2 \cdot 2\text{MeOH}$. The cyclam ring is *trans*-III.

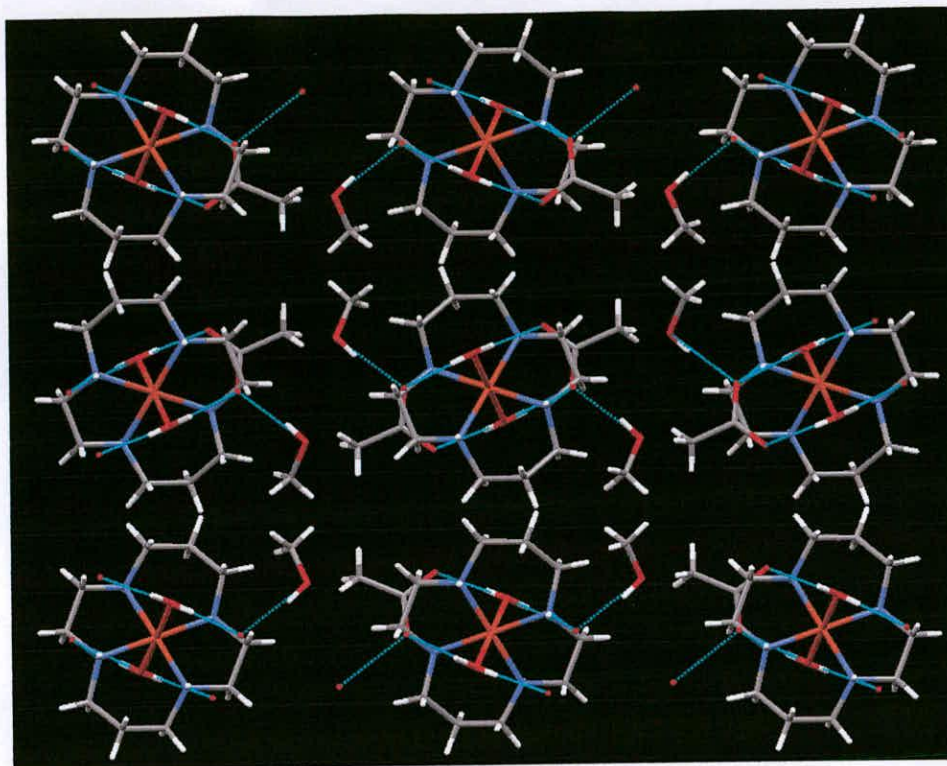


Figure 3.18 Crystal packing of $[\text{Cu}(\text{cyclam})(\text{H}_2\text{O})_2](\text{OAc})_2 \cdot 2\text{MeOH}$, showing the hydrogen bonding (in cyan) from the unbound acetate groups and methanol units to the axial water molecules.

3.3.6 UV-Vis Spectroscopy

The extinction coefficients of the complexes were calculated and are listed in the Table 3.7 below. The extinction coefficients were calculated using :

$$A = \epsilon cl, \quad \text{Equation 3.1}$$

where A = absorbance,

c = concentration / M,

l = cell path length / cm, and

ϵ = extinction coefficient / $\text{M}^{-1} \text{cm}^{-1}$.

lengths range from 1.933 Å to 1.988 Å. There appears to be no interaction between axial ligands and a neighbouring cyclam ring, the tetraphenyl borate blocks any such interaction (Figure 3.16).

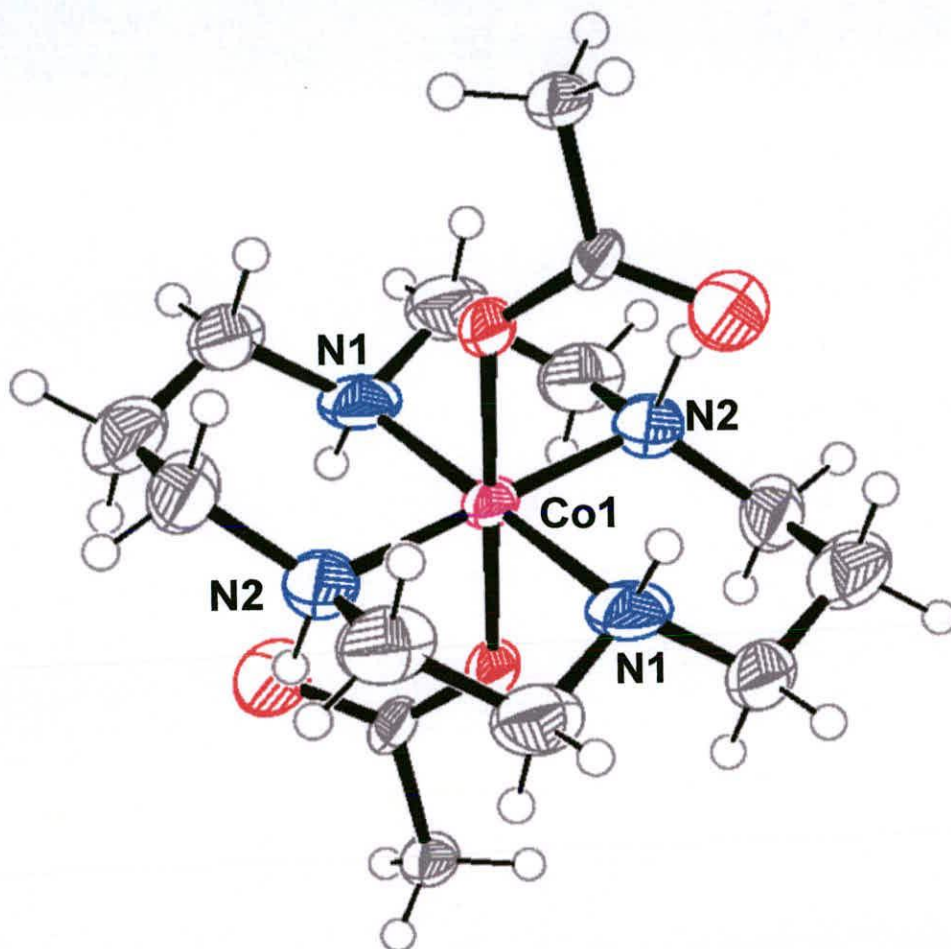


Figure 3.15 $[\text{Co}(\text{cyclam})(\text{OAc})_2]^+$ from $[\text{Co}(\text{cyclam})(\text{OAc})_2](\text{BPh}_4)$. The cobalt ion is octahedral, and the cyclam ring is *trans*-III. The O atoms from the acetate groups form H-bonds to the NH groups.

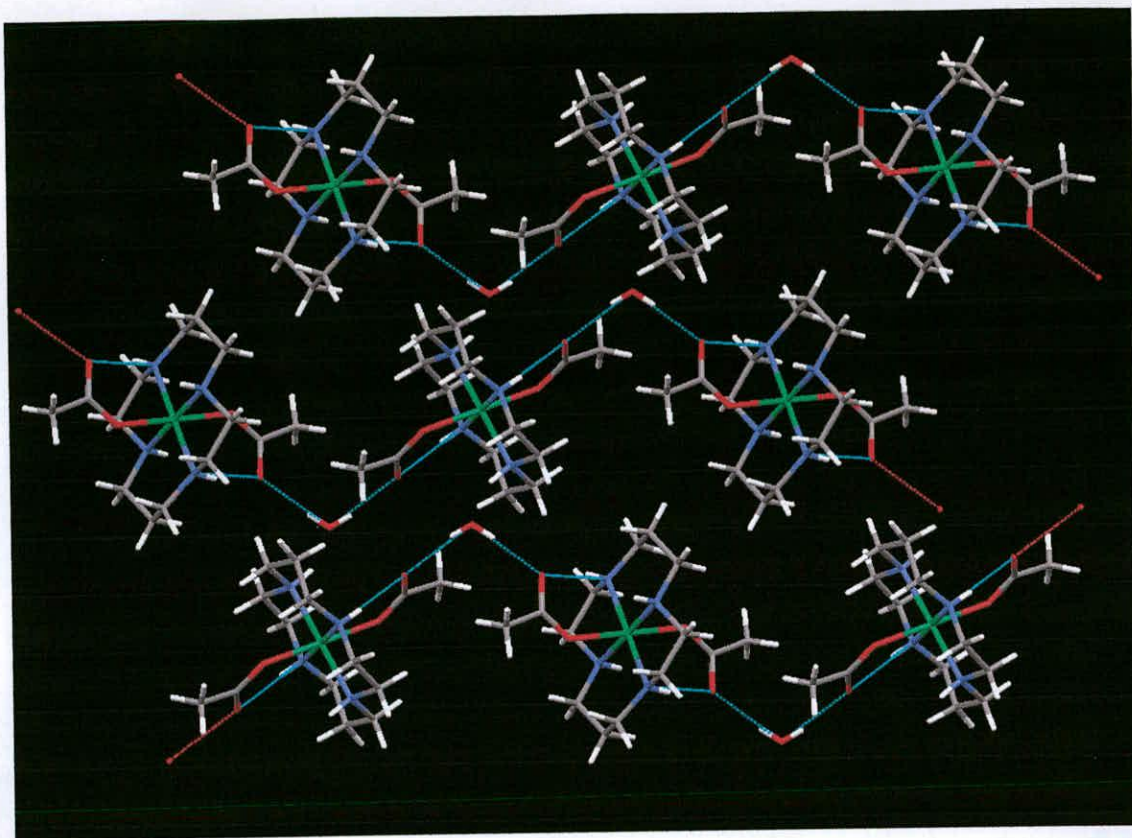


Figure 3.14 Crystal packing of $[\text{Ni}(\text{cyclam})(\text{OAc})_2] \cdot \text{H}_2\text{O}$, showing the H-bonding (in cyan) between the acetate groups, water molecules and NH groups, stabilising the configuration.

$[\text{Co}(\text{cyclam})(\text{OAc})_2](\text{BPh}_4)$, 7. The Co(III) is octahedral, with an acetate molecule in each of the axial positions (Figure 3.15). The cyclam ring is in the *trans*-III configuration. The configuration is stabilised by a hydrogen bond from the NH to the carboxylate group of the bound acetate. The unit cell has two cobalt atoms in it. In one of the Co-cyclam units, the $\text{NH} \cdots \text{O}$ bond lengths are quite similar (2.2 Å), whereas in the other Co-cyclam unit, there is a large difference between them (2.2 Å and 2.6 Å). In the second unit, the acetate seems to sit a lot closer to the NH, causing this difference. The Co-O bond lengths are 1.917 Å and 1.906 Å. The Co-N bond

Table 3.7 Extinction Coefficients for Metal-Cyclam Complexes, recorded in water at 2.5 mM, 25 °C, except 8, recorded in DMSO.

Complex	λ_{\max}	A	$\epsilon / M^{-1} \text{ cm}^{-1}$
Ni(cyclam)(OAc) ₂ , 4	448	0.0893	35.7
Ni(cyclam)Cl ₂ , 5	451	0.0601	24.0
Ni(cyclam)(NO ₃) ₂ , 6	448	0.0770	30.8
[Co(cyclam)(OAc) ₂](BPh ₄), 7	362	0.1768	70.7
	552	0.0864	34.5
	443	0.0720	28.8
[Cu(cyclam)(H ₂ O) ₂](OAc) ₂ , 8	505	0.1830	73.2

The cobalt complex was only complex to have more than one absorption maximum in the range 300 – 800 nm. All the values of ϵ are of the order expected for d-d transitions.

3.4 Discussion

3.4.1 Comparison of Metal-Cyclam Complexes in the Solid State

In the complexes **2**, **4**, **7** and **8**, the cyclam rings are all in the common *trans*-III configuration. The metals all sit in the centre of the 4 nitrogen atoms, with the angles N-M-N all being within 84 ° – 96 °.

There are 9 Pd-cyclam structures in the CSD. These are all in the *trans*-III configuration. The Pd-N bond lengths range from 2.037 Å⁷ to 2.066 Å.^{9, 10} In this work, the Pd-N bond lengths in complex **2** range from 2.036 Å to 2.043 Å. There are two reported octahedral Pd-cyclam complexes, both of these involve Pd(IV). All the

reported Pd(II)-cyclam complexes are square planar. Crystal data for complex **2** are shown in Table 3.6, with key bond lengths and angles shown in Table 3.5.

There are 36 Cu(II) cyclam complexes in the CSD. All of these are in the *trans*-III configuration. Of these, five involve copper binding directly to oxygen. The bonds lengths range from 2.351 Å¹¹ to 2.567 Å.¹² All five of these contain 6-coordinate Cu(II). The Cu-N distances range from 1.922 Å¹³ to 2.031 Å¹¹. Two of these Cu(II) cyclam complexes form polymers, with chains linked through O-Cu-O bonds. In the case of complex **8**, the Cu-O bond length is 2.546 Å, and the Cu-N bond lengths are 2.012 Å and 2.018 Å. The copper is bound to water molecules, and there are hydrogen bonds from the NH protons to the acetate molecules. Again, the cyclam ring is in the *trans*-III configuration. The copper is in a Jahn-Teller-distorted octahedral configuration, with two long bonds to the oxygen from two water molecules in the axial positions. The acetate oxygen atoms are H bonded to cyclam NH groups on adjacent rings and to coordinated water. The cyclam ring adopts the common *trans*-III configuration.

This Cu-cyclam acetate complex (**8**) is very similar to that of Zn-cyclam acetate, which also has two water molecules in the axial positions, and acetate as the counter ion.⁶ In this zinc complex, there are two types of hydrogen bonds, OH...O and N-H...O. Both the carboxylate oxygen atoms of the acetate act as acceptors. All four H atoms of the amine groups and all four of the H atoms from the coordinated water molecules act as hydrogen bond donors. The hydrogen bonds range in length from 1.84Å to 2.24Å.

There are 22 Co-cyclam structures found in the CSD. Five of these are in the *cis*-V configuration, while the remainder are all in the *trans*-III configuration. Of

these 22 complexes, 9 involve direct bonding between Co and O. The Co-O bond lengths range from 1.840 Å¹⁴ to 2.319 Å¹⁵, with the Co-N bond lengths ranging between 1.919 Å and 2.102 Å.¹⁴ The longest and shortest Co-N bonds are both found in a *cis*-V configuration. In the *trans*-III complex **7**, the Co-O bond lengths are 1.906 Å and 1.917 Å, while the Co-N bond lengths range between 1.933 Å and 1.988 Å. Comparing the 4 crystal structures in this work, the M-O and M-N bond lengths are the shortest in this Co³⁺ complex, **7**. This is likely to be the result of this being Co³⁺, whereas the other metals are all M²⁺.

There are 61 Ni-cyclam structures in the CSD. One of these is the unusual *trans*-V configuration,¹⁶ six are *cis*-V, one is a mixture of two structures, a *cis*-V and a *trans*-III,¹⁷ and the remainder are *trans*-III. 28 of these involve the direct bonding of nickel to oxygen, with six of these involving water. The Ni-O bond lengths in these complexes range from 2.070 Å¹⁸ to 2.457 Å,¹⁹ with the Ni-N bond lengths varying from 1.963 Å¹⁹ to 2.109 Å.¹⁸ In the case of **4**, the Ni-O bond lengths are 2.106 Å and the Ni-N are 2.068 Å and 2.075 Å.

3.4.2 NMR Studies

In these NMR studies, the central methylene protons in the six membered rings were easily identified by their chemical shift, as these are often the highest shifted peaks in the spectra. Cyclam can adopt 5 *trans* configurations depending on the spatial alignment of the NH protons. The configurations that can fold along the diagonal can interconvert to give *cis* configurations. It has been stated that only *trans*-I and *trans*-III can produce six -CH₂- protons signals, two of them being from the central methylene of the six membered rings.⁶ In the *trans*-I and *trans*-III

configurations, the six-membered rings adopt the stable chair configuration, which results in the two central methylene protons being inequivalent and hence these give rise to two ^1H NMR resonances.

Configurational analysis also shows that *trans*-IV and *trans*-V configurations have only 5 non-equivalent $-\text{CH}_2-$ protons, one of them being from the central methylene of the six membered rings.¹ Both six-membered rings in the *trans*-IV and *trans*-V adopt twist-boat conformation and the middle two $-\text{CH}_2-$ protons are equivalent and hence give rise to one ^1H NMR signal. However, as these two configurations contain highly strained six-membered rings, these configurations are unlikely to form. The *trans*-V configuration can easily fold along the diagonal to give the *cis*-V configuration, in which the six-membered rings are in the more stable chair configuration.

[Pd(cyclam)]²⁺ Complexes, 1-3

2D [^1H , ^1H] TOCSY NMR spectra showed that each of these only had one configuration present in solution. There were no changes in the NMR spectra with time, showing the structures to be kinetically stable. As no change occurs, it was concluded that the solution structure was the same as the solid state structure, which is *trans*-III. The three [Pd(cyclam)]²⁺ complexes, **1-3**, were found to all be in the same configuration in solution. This shows that the counter ion has little effect on the overall structure of the [Pd(cyclam)]²⁺, and the configuration cannot easily be changed by varying the counterion. It is notable that Pd(II)-cyclam complexes are inactive as anti-HIV agents, which can be attributed to the inability of Pd(II) to bind to axial ligands and possibly due to its inability to adopt configurations other than

trans-III.

[Cu(Cyclam)]²⁺, 8

The ¹H NMR spectrum of this complex showed only one unbroadened peak at 1.8 ppm, (¹³C shift = 23.52 ppm) corresponding to unbound acetate, which agrees with the solid state structure. In the solid state, water is bound in the axial positions, and the acetate is a non bonded counterion. If the acetate was directly bound to the copper, this peak would have been significantly broadened. There are very small peaks present from cyclam, implying that some dissociation occurs. The spectrum was recorded from -400 ppm to + 400 ppm, and only two broad peaks were observed. These were at 16 ppm and -12 ppm. The assignment of these peaks is unknown. The broadening of these peaks is caused by paramagnetic Cu²⁺, which has the configuration 3d⁹, hence always has one unpaired electron.

[Co(Cyclam)]³⁺, 7

Three configurations were identified for this complex. Two of these showed two resonances for the central methylene -CH₂- groups, hence it was concluded that these were either *trans*-I or *trans*-III.⁶ As the complex is *trans*-III in the solid state, it was concluded that the major configuration in solution is also *trans*-III, and the other configuration would be *trans*-I. The third configuration was shown to have 2 NH signals. This could be a result of strong hydrogen bonding between one NH and the acetate group, resulting in a high shift of this NH group (9.35 ppm) and a low shift of the other NH group (7.06 ppm). This also makes the cyclam ring inequivalent, hence six ¹³C signals are observed for this species in total. However the exact

configuration of this configuration could not be determined.

Ni(Cyclam)]²⁺ Complexes, 4-6

Work has been reported on substituted nickel-cyclams, such as cyclam with 8 methyl groups substituted on various CH₂ groups on the ring,²⁰ when substitution at the CH₂ groups gave all *trans*-I structures in solution. Much work has also been carried out on Ni(II) complexes of tetramethyl-cyclam (tmc), where methyl groups are attached to each of the NH groups. It has been shown that [Ni(tmc)(ClO₄)₂] is high spin and octahedral, with *trans*-I and *trans*-III species being isolated.²¹⁻²³ Isomerisation between *trans*-III and *trans*-I configurations has been shown to occur in Ni(tmc)²⁺ in non-aqueous solvents such as DMSO.²⁴ However, a *trans*-II isomer has been observed by ¹H NMR in nitromethane.²⁵ This was shown to isomerise to the *trans*-I isomer. Since Ni(II) is relatively labile, N-substitution of the cyclam makes isomerisation slower and aids isolation of unusual species, such as this *trans*-II isomer.² The less common *cis*-V structures have been isolated from Ni(II) complexes of cyclam substituted with two pyridyl methyl groups at the N positions.²⁶

It has been shown that in CDCl₃, Ni(cyclam)Cl₂ exists entirely as the paramagnetic *trans*-III configuration, at 34 °C.²⁷ In the same work, cyclams substituted at various CH₂ groups with methyl groups were found to exist in either *trans*-I or *trans*-III, depending on the position of the substitution. *Trans*-I, *trans*-III and *cis*-V isomers of Ni(cyclam)²⁺ have all been observed in solution.^{2, 28-30} The *trans*-III isomer was shown to be in rapid diamagnetic-paramagnetic equilibrium by ¹⁷O NMR studies, in both Ni(cyclam)²⁺ and Ni(cyclen)²⁺.^{30, 31} Detailed ¹H NMR studies have shown that the diamagnetic, square planar *trans*-I configuration can

isomerise to the paramagnetic, octahedral *trans*-III configuration under basic conditions.² However, at pH = 3, the *trans*-I isomer was found to be extremely stable, and the half life at pH = 2 was estimated at 20 years at room temperature. This isomerisation between the *trans*-I and *trans*-III isomers can be catalysed by the oxidation of Ni(II) to Ni(III) at low pH values, to give a half life of 400 ms, which produced a *trans*-III isomer.²⁸ The isomerisation between *cis* and *trans* Ni(cyclam)²⁺ complexes has been studied, and has been found to be rapid at pH = 10, and very slow at pH = 3.²⁹ Molecular mechanics investigations and density functional theory have both been used to show that *trans*-I and *trans*-III are the most stable Ni-cyclam configurations, with there being little difference in energy between the two configurations.^{2, 32, 33}

The 1D spectra of all three Ni(II) cyclam complexes (**4-6**) show a large number of peaks. In solution it is possible for a mixture of complexes of cyclam molecules to exist. Both paramagnetic and diamagnetic species may exist in equilibrium with unbound cyclam, nickel and unbound ligands. The broad shifted peaks can be attributed to one or more paramagnetic forms of the complex. As paramagnetic species are known to have shifted peaks in NMR spectra, the spectra were recorded over a large sweep width -150 ppm to 300 ppm. Peaks were observed in the spectrum between -50 ppm and +150 ppm. Peaks for diamagnetic forms of the complexes were observed between 1 ppm and 4 ppm.

The diamagnetic peaks were assigned using 1D and 2D spectra. Peaks are seen in the spectra for unbound cyclam suggesting that an equilibrium exists between the nickel complex and unbound cyclam, although previous studies have shown that

metal cyclam complexes have high thermodynamic and kinetic stability with respect to metal dissociation.

The 1D and 2D spectra show peaks for 6 non-equivalent protons and 3 corresponding non-equivalent carbon signals. Therefore in the diamagnetic complex the cyclam ring must be in a symmetrical configuration with equivalent positions that are related by symmetry.

The spectra for complex **4**, Ni(cyclam)(OAc)₂, were initially recorded in 100 % D₂O. When the spectra were recorded in 90 % H₂O / 10 % D₂O, a new peak at 3.6 ppm was observed in the 1D NMR spectrum and the 2D [¹H,¹H] TOCSY NMR spectrum but not in the 2D [¹H,¹³C] HSQC NMR spectrum, therefore this signal was assigned as a signal from an NH proton. Only one signal was seen for an NH proton, and therefore all the NH groups in the diamagnetic configuration must be equivalent. The new peak shows cross-peaks to all the protons in the diamagnetic region in the 2D [¹H,¹H] TOCSY NMR spectrum showing that there is only one diamagnetic configuration present. In a previously reported ¹H NMR characterisation of diamagnetic [Ni(cyclam)](ClO₄)₂, the NH proton gave a signal at 3.62 ppm, similar to the value found here.²⁸

In order to confirm the position of the acetate peak in the ¹H NMR spectrum, 10 molar equivalents of Na(OAc) were added to the solution. The signal at 1.9 ppm increased in intensity and was assigned to acetate. Only one broad signal for acetate was observed, hence it is likely that bound acetate is in fast exchange with free acetate.

Due to the presence of only one NH signal, and based on the previously published results on the nickel cyclam perchlorate complex,^{2, 34} it was deduced that

the conformation of the diamagnetic component was square-planar *trans*-I, as is the previously published perchlorate complex. All three $[\text{Ni}(\text{cyclam})]^{2+}$ complexes were found to be in the same configuration, showing that the counterion has little effect on the overall structure of $[\text{Ni}(\text{cyclam})]^{2+}$ in solution.

3.4.3 UV-Vis Spectroscopy

For the cobalt complex, **7**, the UV-vis spectrum clearly indicates that it is in a *trans* configuration. For Co(III) complexes, the UV-vis absorptions consists of transitions from the $^1A_{1g}$ ground state to other singlet states.³⁵ In octahedral Co(III) complexes, two absorption bands are observed, corresponding to transitions to the upper states $^1T_{1g}$ and $^1T_{2g}$. However, in *trans* complexes, the $^1T_{1g}$ state splits markedly, resulting in the appearance of a third absorption band, as seen here. This shows there is no interconversion from *trans* to *cis* configurations on going from the solid state to the solution state.

For the nickel complexes **4-6**, the UV-vis spectra show that the majority of them adopt a planar configuration. Tetrahedral Ni(II) complexes have a strong absorption band of the order $\epsilon = 10^2 \text{ M}^{-1} \text{ cm}^{-1}$, at approximately 670 nm, absent in these complexes.³⁵ Furthermore, octahedral Ni(II) complexes show three absorption bands, corresponding to the three spin-allowed transitions $^3A_{2g} \rightarrow ^3T_{2g}$, $^3A_{2g} \rightarrow ^3T_{1g}(F)$ and $^3A_{2g} \rightarrow ^3T_{1g}(P)$.³⁵ The complexes studied here all just had one absorption band, at 448 nm or 451 nm, of the order $\epsilon = 24\text{-}35 \text{ M}^{-1} \text{ cm}^{-1}$. For Ni(II) complexes, planar geometry is generally preferred, since in the d^8 configuration, the planar ligand set causes one of the d orbitals, $d_{x^2-y^2}$, to be uniquely high in energy and the 8 electrons can occupy the other four d orbitals without interacting with the

strongly antibonding $d_{x^2-y^2}$ orbital. However, in tetrahedral geometries, the occupation of anti-bonding orbitals is unavoidable. For tetra aza ligands, it has been reported that nickel complexes are blue when paramagnetic and octahedral and yellow when diamagnetic and square planar.³⁶ Linear tetra aza Ni(II) complexes are generally blue, and as such favour octahedral configuration,³⁷ whereas Ni(II)-cyclam complexes favour the square planar configuration.³⁸ There are reported Ni(cyclam)²⁺ complexes with absorption bands in the region of 445 nm, and were all found to be diamagnetic, square-planar configurations.^{28,39} Furthermore, octahedral Ni(cyclam)²⁺ complexes have been shown to have three absorption bands and to be in *trans* configurations.^{40, 41} The UV-vis spectroscopy carried out here show that there is a square-planar [Ni(cyclam)]²⁺ configuration present in solution.

The UV-vis spectrum of the copper complex, **8**, shows only one absorption band. Its intensity is that of a d-d transition.

3.5 Conclusions

NMR spectroscopy, UV-vis spectroscopy and X-ray crystallography were used to identify the configurations of Pd(II)-, Ni(II)-, Co(III)- and Cu(II)-cyclam complexes. Palladium was found to form only square-planar *trans*-III complexes with cyclam, and the counterion has little effect on the overall structure. Acetate does not bind to Pd(II)-cyclam directly, nor does it induce configurational changes, a lack of direct coordination of Pd(II)-cyclam to carboxylates may be a major factor in its lack of anti-HIV activity. A further factor could be its apparent lack of ability to change configuration, unlike the active Zn(II) complex, which can change from

trans-III to *cis*-V.

In the solid state, Ni(II)-cyclam is found to adopt the *trans*-III configuration, with axial counterions, whereas in solution, Ni(II) cyclam can also be found in the diamagnetic, square-planar *trans*-I configuration. A paramagnetic configuration is also present in solution, as revealed by the NMR, likely to be the octahedral *trans*-III isomer, but this could not be fully characterised.

Cu(II)-cyclam was found to be *trans*-III in the solid state, with water bound in the axial positions, and acetate as a counterion. The solution NMR supported this, with the acetate peak being the only non-broadened peak in the spectrum, showing that there is no configurational change between the solid and the solution state.

Co(III)-cyclam adopts a *trans*-III configuration in the solid state, with acetate in the axial positions. Three configurations were observed in solution, *trans*-III, *trans*-I and a further unidentified *trans* configuration. All the acetate was bound directly to the cobalt in solution, as no peaks were observed for free acetate.

The antiviral activity of cyclam and its derivatives is greatly influenced by metal complexation. The biological target for these complexes is the membrane co-receptor protein CXCR4. Therefore it is important to gain an understanding of the factors which influence the interaction between the protein and the metal macrocycle. It is clear that the nature of the metallocyclams and their stereochemistry (*trans* or *cis*), as well as the substituents on the ring nitrogen atoms and on the periphery can also exert a major effect. Importantly the configuration found in the solid state is not necessarily the only configuration found in solution, and the availability of low-energy pathways for interconversion between configurations may be important in receptor recognition and antiviral activity. In

particular for Zn(II)-cyclams (active) interconversions between configurations are often facile, whereas for Pd(II)-cyclams (inactive) and Co(III)-cyclams (very low activity) they are not.

3.6 References

- 1 X. Liang and P. J. Sadler, *Chem. Soc. Rev.*, 2004, **33**, 246-266.
- 2 P. J. Connolly and E. J. Billo, *Inorg. Chem.*, 1987, **26**, 3224-3226.
- 3 B. Bosnich, C. K. Poon, and M. L. Tobe, *Inorg. Chem.*, 1965, **4**, 1102-1108.
- 4 P. O. Whimp, M. F. Bailey, and N. F. Curtis, *J. Chem. Soc. A*, 1970, **11**, 1956-1963.
- 5 M. A. Donnelly and M. Zimmer, *Inorg. Chem.*, 1999, **38**, 1650-1658.
- 6 X. Liang, M. Weishäupl, J. A. Parkinson, S. Parsons, P. A. McGregor, and P. J. Sadler, *Chem. Eur. J.*, 2003, **9**, 4709-4717.
- 7 X. Liang, J. A. Parkinson, M. Weishäupl, R. O. Gould, S. J. Paisey, H.-S. Park, T. M. Hunter, C. A. Blindauer, S. Parsons, and P. J. Sadler, *J. Am. Chem. Soc.*, 2002, **124**, 9105-9112.
- 8 X. Liang, J. A. Parkinson, S. Parsons, M. Weishaupl, and P. J. Sadler, *Inorg. Chem.*, 2002, **41**, 4539-4547.
- 9 M. Yamashita, H. Ito, K. Toriumi, and T. Ito, *Inorg. Chem.*, 1983, **22**, 1566-1568.
- 10 K. Toriumi, M. Yamashita, H. Ito, and T. Ito, *Acta Cryst.*, 1986, **C42**, 963-968.
- 11 M. Kato and T. Ito, *Bull. Chem. Soc. Jpn.*, 1986, **59**, 285-294.
- 12 P. A. Tasker and L. Sklar, *J. Cryst. Mol. Struct.*, 1975, **5**, 329-344.
- 13 L. F. Lindoy, M. S. Mahinay, B. W. Skelton, and A. H. White, *J. Coord. Chem.*, 2003, **56**, 1203-1213.
- 14 E. Simon, P. L'Haridon, R. Pichon, and M. L'Her, *Inorg. Chim. Acta*, 1998,

- 282, 173-179.
- 15 A. Bakac, J. H. Espenson, and V. G. Young Junior, *Inorg. Chem.*, 1992, **31**, 4959-4964.
 - 16 E. K. Barefield, A. Bianchi, E. J. Billo, P. J. Connolly, P. Paoletti, J. S. Summers, and D. G. Van Derveer, *Inorg. Chem.*, 1986, **25**, 4197-4202.
 - 17 R. J. Pleus, H. Waden, W. Saak, and D. Haase, *J. Chem. Soc. Dalton Trans.*, 1999, **15**, 2601-2610.
 - 18 L. P. Battaglia, A. Bianchi, A. B. Corradi, E. Garciaespana, M. Micheloni, and M. Julve, *Inorg. Chem.*, 1988, **27**, 4174-4179.
 - 19 J. W. Cai, C. H. Chen, and J. S. Zhou, *Chin. J. Inorg. Chem.*, 2003, **19**, 81-85.
 - 20 J.-W. Chen, C.-C. Chang, and C.-S. Chung, *Inorg. Chem.*, 1986, **25**, 4794-4797.
 - 21 E. K. Barefield and F. Wagner, *Inorg. Chem.*, 1973, **12**, 2435-2439.
 - 22 F. Wagner, M. T. Mocella, M. J. D'Aniello, A. H. J. Wang, and E. K. Barefield, *J. Am. Chem. Soc.*, 1974, **96**, 2625.
 - 23 F. Wagner and E. K. Barefield, *Inorg. Chem.*, 1976, **15**, 408-417.
 - 24 P. Moore, J. Sachinidis, and G. R. Willey, *J. Chem. Soc., Chem. Comm.*, 1983, 522-523.
 - 25 S. F. Lincoln, J. H. Coates, D. A. Hadi, and D. L. Pisaniello, *Inorg. Chim. Acta*, 1984, **81**, L9-L10.
 - 26 A. S. Batsanov, A. E. Goeta, J. A. K. Howard, D. Maffeo, H. Puschmann, and J. A. G. Williams, *Polyhedron*, 2001, **20**, 981-986.
 - 27 A. Dei, *Inorg. Chem.*, 1979, **18**, 891-894.
 - 28 D. T. Pierce, T. L. Hatfield, E. J. Billo, and Y. Ping, *Inorg. Chem.*, 1997, **36**,

- 2950-2955.
- 29 E. J. Billo, *Inorg. Chem.*, 1981, **20**, 4019-4021.
- 30 R. J. Pell, H. W. Dodgen, and J. P. Hunt, *J. Am. Chem. Soc.*, 1983, **22**, 529-532.
- 31 J. H. Coates, D. A. Hadi, S. F. Lincoln, H. W. Dodgen, and J. P. Hunt, *Inorg. Chem.*, 1981, **20**.
- 32 K. R. Adam, M. Antolovich, L. G. Brigden, A. J. Leong, L. F. Lindoy, P. J. Baillie, D. K. Uppal, M. Mcpartlin, B. Shah, D. Proserpio, L. Fabbrizzi, and P. A. Tasker, *J. Chem. Soc. Dalton Trans.*, 1991, 2493-2501.
- 33 K. R. Adam, I. M. Atkinson, and L. F. Lindoy, *Inorg. Chem.*, 1997, **36**, 480-481.
- 34 E. J. Billo, P. J. Connolly, D. J. Sardella, J. P. Jasinski, and R. J. Butcher, *Inorg. Chim. Acta*, 1995, **230**, 19-28.
- 35 F. A. Cotton and G. Wilkinson, 'Advanced Inorganic Chemistry', John Wiley and Sons, New York, 1988.
- 36 P. Paoletti, L. Fabbrizzi, and R. Barbucci, *Inorg. Chim. Acta Rev.*, 1973, **7**, 43.
- 37 R. G. Wilkins, R. Yelin, D. W. Margerum, and D. C. Weatherburn, *J. Am. Chem. Soc.*, 1969, **91**, 4326.
- 38 F. P. Hinz and D. W. Margerum, *Inorg. Chem.*, 1974, **13**, 2941-2949.
- 39 A. Anichini, L. Fabbrizzi, P. Paoletti, and R. M. Clay, *Inorg. Chim. Acta*, 1977, **24**, 21.
- 40 K. Mochizuki and T. Kondo, *Inorg. Chem.*, 1995, **34**, 6241-6243.
- 41 A. Ito, M. Kato, and H. Ito, *Bull. Chem. Soc. Jpn.*, 1984, **57**, 2641-2649.

Chapter 4 Synthesis and Reactions of Xylyl-Bicyclam and its Metal Complexes

4.1 Introduction

4.1.1 Discovery of AMD 3100

In 1985, Rozenbaum *et al.* reported evidence of the anti HIV activity of a polyoxometalate.¹ Polyoxometalates are globular polyanionic structures, with peripherally located oxygen atoms that give them their anionic charge. This led to the testing of many other polyoxometalates were tested, to see if the activity could be matched or improved.² However, they were never really pursued as long term potential treatments for HIV, as it was thought that they would be deposited in organs, such as the liver, over time. It was suggested that instead of incorporating a metal into the globular shell, that metal complexes of organic compounds could be tested. This led to the investigation of cyclam, with its 4 nitrogen atoms that can readily coordinate metal ions.³ However, before testing on metallocyclams began, testing was carried out on the ligand alone to ensure the activity would come from the addition of the metal. It was found that the majority of the commercially available samples of cyclam had little anti-HIV activity, as expected. However, there was one sample which showed distinct activity, it was found to have an EC₅₀ value of 10 µg per ml, compared to the other samples, in which the EC₅₀ values were all greater than 100 µg per ml. As this sample was the only one to have such activity, the purity of it was questioned. High pressure liquid chromatography (HPLC) analysis was carried out on it, and it was found that there was an impurity present, of

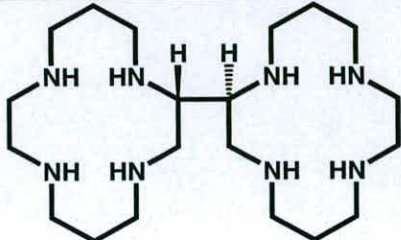
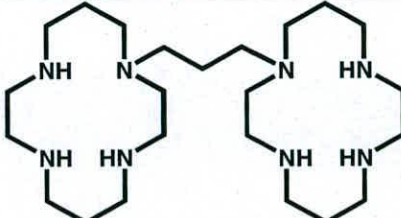
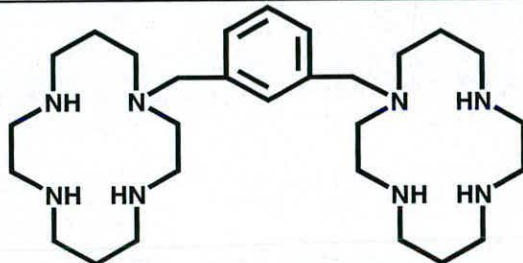
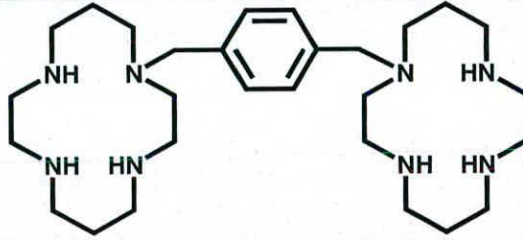
about 1 - 2 %. When the impurity was purified and isolated, it was found to have an EC_{50} of 0.1-0.2 μg per ml. This was eventually characterised as the bicyclam JM1657, consisting of two cyclam rings, joined by a carbon-carbon bridge (structure shown in Table 4.1).

However, a major drawback was encountered when it proved impossible to resynthesise this compound. This was tackled by synthesising derivatives of this molecule, where the cyclam rings were joined by aliphatic bridges through the nitrogen groups. This led to the discovery of JM2763, with an aliphatic bridge consisting of three CH_2 groups, which was found to have an activity similar to that of JM1657.⁴ However, it was thought that the activity of this compound could be further improved, so many derivatives were tested. The most significant improvement was found when an aromatic bridge was introduced to replace the aliphatic bridge. This led to JM2987 and JM3100 (renamed AMD3100 at a later date, referred to as xylyl-bicyclam in this work, shown in Figure 4.1).⁵ Both were active at a concentration of $\sim 0.005 \mu\text{g}$ per ml, and were not toxic to host cells at $> 500 \mu\text{g}$ per ml. As AMD3100 had the slightly better activity, this one was pursued further and eventually taken to clinical trials.



Figure 4.1 Xylyl-bicyclam, **9**

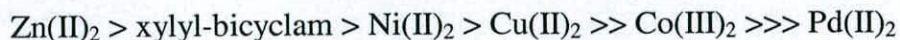
Table 4.1 Anti-HIV activity of Bicyclams³

Compound Number	Structure	EC ₅₀ /μM		CC ₅₀ /μM
		HIV-1 (III _B)	HIV-2 (ROD)	
JM1657		0.144	1.01	319
JM2763		0.248	1.00	>622
JM2987		0.005	0.010	>500
JM3100 (renamed AMD3100)		0.003	0.009	>500

AMD3100 is also in clinical trials for stem cell transplantation used in the treatment of patients who have cancers involving the blood and the immune system.³ AMD3100 blocks the entry of T-lymphotropic HIV-1 and HIV-2 strains by specifically binding to the CXCR4 co-receptor.⁶

4.1.2 Metal Complexation

The effect of metal complexation on the activity of xylyl-bicyclam has been investigated.⁷ It has been shown that zinc increased the activity compared to xylyl-bicyclam, while other metals decrease the activity, with the palladium complex having no activity at all. The overall order of activity is :



It has been suggested that xylyl-bicyclam could pick up zinc from the blood, and that this could be the active form of the drug in the body.⁷ It is therefore important to consider the solution structure of these metallobicyclams, to gain understanding as to why the zinc complex is active, but other metals reduce the activity. The concentration of zinc in blood plasma is *ca* 20 μM .⁸ The most common ligands for zinc in the Protein Data Bank are histidine and cysteine.⁹ As such, it is possible that xylyl-bicyclam could extract zinc from carrier proteins.

4.1.3 Zinc Histidine

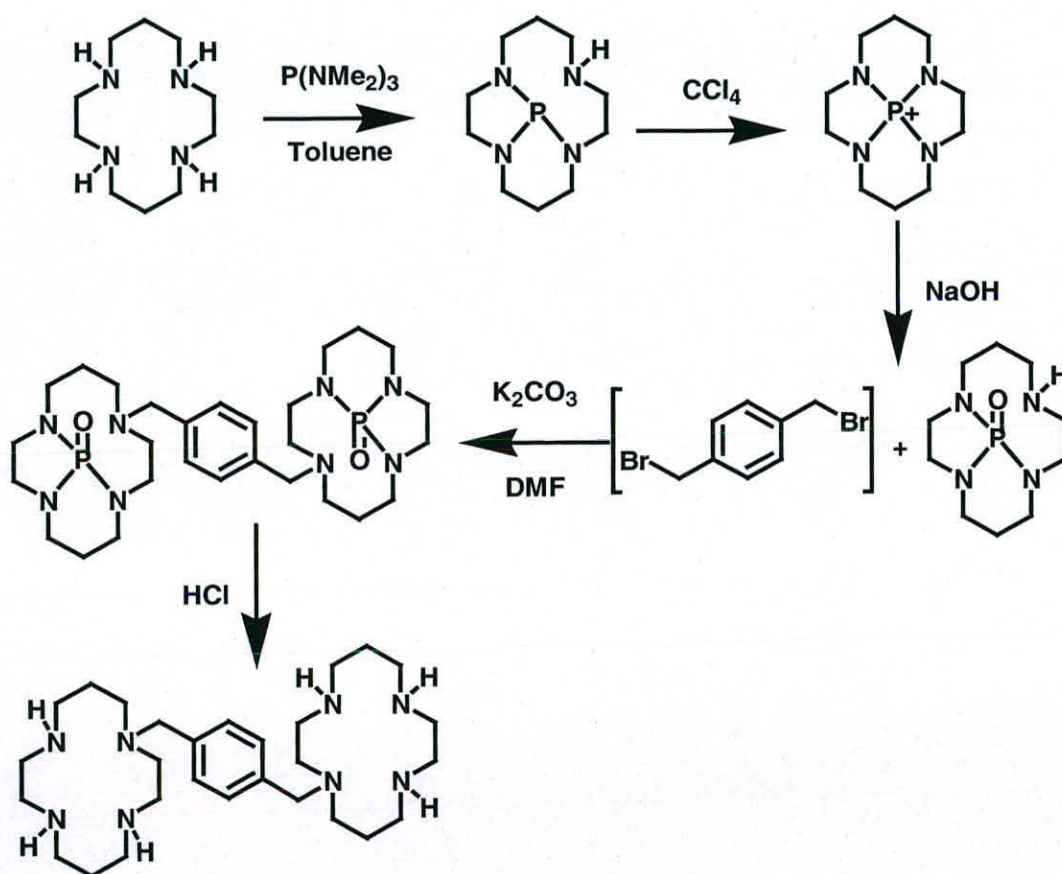
Much work has been carried out investigating the properties of zinc histidine. It has been shown that at $\text{pH} = 7$, $[\text{Zn}(\text{Hist})]^+$ and $[\text{Zn}(\text{Hist})_2]$ are the principal forms in solution.¹⁰ Two crystal structures of zinc histidine have been reported.^{11, 12} The first one has is a pentahydrate complex, with two histidines coordinated to one zinc, with the zinc coordinated in a distorted tetrahedral manner, consisting of an amino nitrogen and an imidazole nitrogen from each histidine group.¹¹ The second structure has a similar structure, except it crystallised as the dihydrate form. However, it has been argued by Couves *et al.*,¹¹ that the zinc in both of these complexes are in fact in distorted octahedral coordination. This is due to the fact that

both of these complexes have two carboxylate groups in close proximity to the zinc (2.8 – 2.9 Å).¹¹

4.2 Synthesis

4.2.1 Synthesis of Xylyl-Bicyclam, 9, Route 1

The first attempted synthesis of xylyl-bicyclam uses a phosphoryl-protected cyclam,¹³ as shown in Scheme 4.1.



Scheme 4.1 Synthetic route 1 to xylyl-bicyclam.

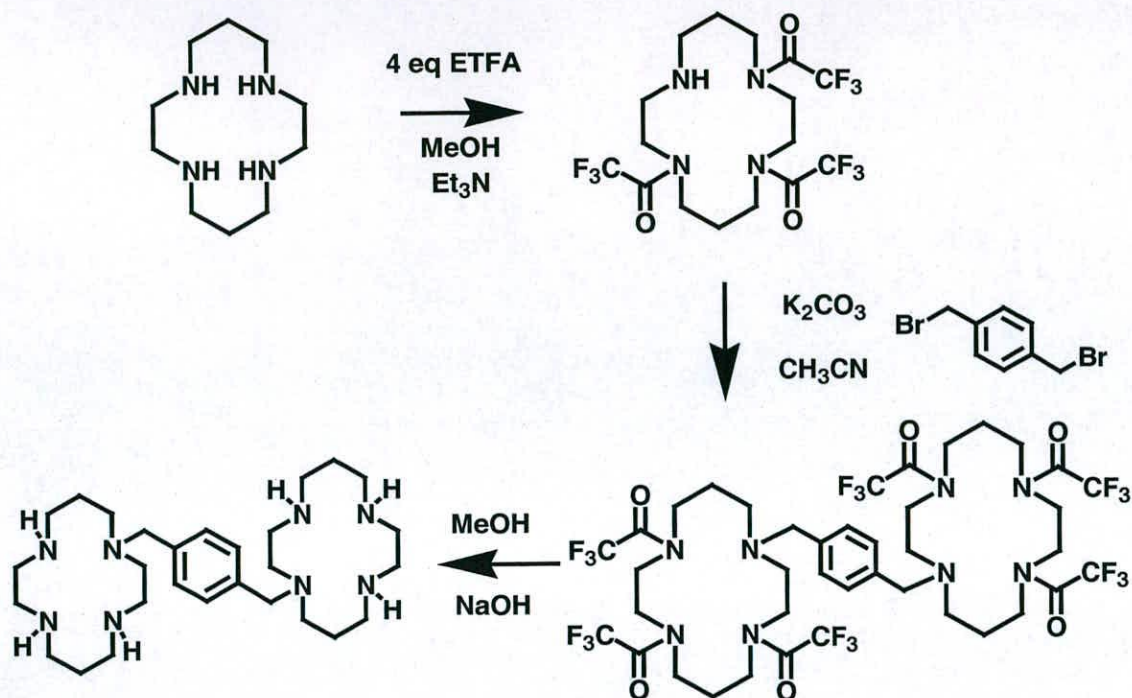
Cyclam (501 mg, 2.5 mmol) was suspended in dry toluene (100 mL) and hexamethylphosphoric triamide (454 μ L, 2.5 mmol) was added. The mixture was

stirred for 4 hours at room temperature and then heated overnight under reflux. The resulting clear solution was cooled to 0 °C, which resulted in some white precipitate forming. Carbon tetrachloride (375 μ L, 3.9 mmol) was added which resulted in further precipitation. This mixture was stirred at room temperature overnight. The mixture was then concentrated to dryness and 10% sodium hydroxide (25 mL) was added. This was then left to stir overnight. The reaction mixture was extracted with chloroform (5 x 100 mL) and the combined organic layers were dried over MgSO₄. This was then filtered and dried under high vacuum to give protected cyclam as a white powder (575 mg, 2.35 mmol, 94 % yield).

Protected cyclam (570 mg, 2.33 mmol) was suspended in dry DMF (70 mL) and α,α' -dibromo-*p*-xylene (0.5 molar equiv, 308 mg, 1.17 mmol) and sodium carbonate (580 mg, 1.83 mmol) were added. This was stirred at 120 °C for 24 hours. The solvent was removed under high vacuum and the white residue was reacted with 10 % hydrochloric acid (40 mL). The resulting yellow solution was heated under reflux for 2.5 days. The pH was adjusted to pH \geq 13 using sodium hydroxide pellets. This aqueous phase was then extracted with chloroform (3 x 100 mL). The combined organic layers were then dried over NaSO₄. The solution was filtered and the solvent was removed under high vacuum to give a pale yellow powder (520 mg, 44 % yield).

4.2.2 *Synthesis of Xylyl-Bicyclam, 9, Route 2*

The second synthetic route used for xylyl-bicyclam starts from cyclam, and uses trifluoroacetate protecting groups, shown in Scheme 4.2.¹⁴



Scheme 4.2 Synthetic route 2 to xylyl-bicyclam

Part (a) Protection of Three NH Groups on Cyclam

Cyclam (2.02 g, 10.08 mmol) was dissolved in methanol (8 mL) under N_2 with stirring and triethylamine (1.4 mL, 1 molar equiv) was added to give a pale yellow solution. Ethyl trifluoroacetate (4 molar equiv, 40.32 mmol, 4.82 mL) was added dropwise over 10 minutes whilst the cyclam solution was cooled in an ice bath. Once the addition was complete, the ice bath was removed and the reaction was left to stir at room temperature for four hours. The solvent was then removed under high vacuum. The residue, dissolved in ethyl acetate, was then passed through a silica plug (8 g) and the resulting solution was then concentrated to dryness under high vacuum to give a white foam (2.01 g, 4.12 mmol, 41 % yield).

1H NMR (250 MHz, $CDCl_3$) : 3.91-3.47 (m, 12H), 3.17-2.65 (m, 4H), 2.30-1.73 (m, 4H), 1.20-0.8 (bs, 1H).

ES-MS : $m/z = 489.2 [M+H]^+$.

Part (b) Dimerisation

Tri-protected cyclam (2.01 g, 4.12 mmol) was dissolved in anhydrous CH_3CN (100 mL) under an N_2 atmosphere and potassium carbonate (3 molar equiv, 12.36 mmol, 1.72 g) was added. To this, α,α' -dibromo-*p*-xylene (2.06 mmol, 545 mg, 0.5 molar equiv) was added and the reaction was heated to reflux for 22 hours. The resulting cloudy mixture was dried under high vacuum to give a white solid. This was partitioned between water (30 mL) and dichloromethane (100 mL) and the aqueous layer was extracted with dichloromethane (3 x 50 mL). The combined organic layers were dried over $MgSO_4$, which was filtered off and the solvent removed to give a pale yellow powder. The product was then purified by column chromatography on silica gel using ethyl acetate : hexane (9:1 ratio). The solvent was removed under high vacuum to give a white solid (2.75 g, 2.55 mmol, 62 % yield).

1H NMR (250 MHz, $CDCl_3$) : 7.23-7.10 (m, 4H), 3.83-3.25 (m, 24H), 2.85-1.54 (m, 20H).

ES-MS : $m/z = 1079.8 [M+H]^+$.

Part (c) Deprotection

The hexa-protected bicyclam (2.75 g, 2.55 mmol) was dissolved in methanol (15 mL) and 10 % NaOH (15 mL). Immediately a white precipitate formed. The solution was stirred for 6 hours at room temperature to give a clear colourless solution. The aqueous layer was then extracted with chloroform (3 x 50 mL), and the

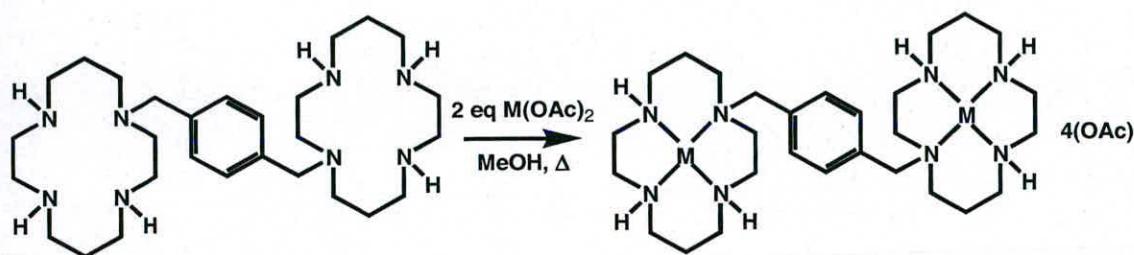
organic layer was dried with sodium sulphate. This was removed by filtration, and the solvent was removed under high vacuum to give a white powder (1.10 g, 2.19 mmol, 86 % yield).

^1H NMR (250 MHz, CDCl_3) : 7.50-7.32 (m, 4H), 3.83 (s, 4H), 3.32-2.70 (m, 32H), 2.18-2.08 (m, 4H), 1.92-1.78 (m, 4H).

ES-MS : $m/z = 504.2$ $[\text{M}+\text{H}]^+$.

4.2.3 Synthesis of Metal-Xylyl-Bicyclam Complexes

The metal-xylyl-bicyclam complexes **10-13** were synthesised using the general route shown in Scheme 4.3.



Scheme 4.3 General route to metal-xylyl-bicyclams

$\text{Ni}_2(\text{Xylyl-bicyclam})(\text{OAc})_4$, **10**

$\text{Ni}(\text{OAc})_2 \cdot 4\text{H}_2\text{O}$ (11.1 mg, 0.04 mmol) was dissolved in methanol (5 mL) and added to a solution of xylyl-bicyclam (0.5 molar equiv, 11.2 mg, 0.02 mmol) in methanol (10 mL). The mixture was stirred for while refluxing for 2 hours. The solvent was then removed by under reduced pressure and the resulting purple solid was dried under vacuum. The product was dissolved in methanol and set up for slow diffusion into diethyl ether, which produced a purple powder (10.3 mg, 0.012 mmol, 60 % yield). 1D and 2D NMR spectra (^1H , ^{15}N] HSQC) were recorded on this

product on a 800 MHz spectrometer in 90 % H₂O / 10 % D₂O.

ES-MS : $m/z = 368.2$ [M-2OAc]²⁺, 368.2 [M-3OAc-H]²⁺, 308.2 [M-4OAc-2H]²⁺.

Selected IR (KBr, cm⁻¹): 3423 s (NH), 2927 m (CH), 2869 s (CH), 1565 m (CO), 1412 m (CO).

Cu₂(Xylyl-bicyclam)(OAc)₄, 11

Cu(OAc)₂.H₂O (36.3 mg, 0.18 mmol) was dissolved in methanol (2 mL) and added to a solution of xylyl-bicyclam (0.5 molar equiv, 46.1 mg, 0.09 mmol) in methanol (10 mL). The mixture was stirred for while refluxing for 2 hours. The solvent was then removed under reduced pressure and the resulting purple solid was dried under vacuum. The product was dissolved in methanol and set up for slow diffusion into diethyl ether, which produced a blue/purple powder (65.2 mg, 0.075 mmol, 83 % yield). 1D and 2D NMR spectra ([¹H, ¹³C] HSQC) were recorded on this product on a 800 MHz spectrometer in 90 % H₂O / 10 % D₂O.

ES-MS : $m/z = 373.3$ [M-2OAc]²⁺, 343.2 [M-3OAc-H]²⁺, 314.2 [M-4OAc-2H]²⁺.

Selected IR (KBr, cm⁻¹): 3440 s (NH), 2917 m (CH), 1417 m (CO).

[Pd₂(Xylyl-bicyclam)](OAc)₄, 12

Xylyl-bicyclam (10.1 mg, 0.02 mmol) was dissolved in methanol (1 mL) and Pd(OAc)₂ (2 molar equiv, 9.0 mg, 0.04 mmol) was added and the solution immediately turned brown. The reaction was heated under reflux for two hours, then filtered and concentrated to dryness. The product was dissolved in methanol and set up for slow diffusion into diethyl ether, which produced a yellow powder (8.9 mg, 0.0099 mmol, 50 % yield). 1D and 2D NMR spectra (COSY, TOCSY, NOESY, [¹H,

^{15}N] HSQC and [^1H , ^{13}C] HSQC) were recorded on this product on a 800 MHz spectrometer in 90 % H_2O / 10 % D_2O .

ES-MS : $m/z = 357.2$ [$\text{M}-3\text{H}$] $^{2+}$.

Selected IR (KBr, cm^{-1}): 3446 s (NH), 2360 m (CH), 2341 s (CH), 1560 m (CO), 1412 m (CO).

[$\text{Co}_2(\text{Xylyl-bicyclam})\text{Cl}_4$] Cl_2 , 13

Xylyl-bicyclam (9.5 mg, 0.019 mmol) was dissolved in methanol (1 mL) with stirring to give a clear, colourless solution. $\text{CoCl}_2 \cdot 6\text{H}_2\text{O}$ (2 molar equiv, 9.0 mg, 0.038 mmol) was dissolved in methanol (1 mL) with stirring. This resulted in a clear, purple/blue solution. The cobalt solution was added dropwise to the xylyl-bicyclam solution with stirring. This gave a clear, yellow/brown solution. Air was bubbled through the solution for 10 minutes and 1 M HCl (1 mL) was added until the solution became dark green. Air was bubbled through the solution for a further 10 minutes. The dark green solution was filtered. This resulted in a clear green solution with a small amount of precipitate (a green powder). The green solution was concentrated to dryness to give a green powder. The powder was dissolved in the minimum amount of hot water, which produced a black solution. Once cooled, green needle crystals formed. These were filtered and washed with diethyl ether (9.2 mg, 0.011 mmol, 58 % yield). 1D and 2D NMR spectra (COSY, TOCSY, NOESY, [^1H , ^{15}N] HSQC and [^1H , ^{13}C] HSQC) were recorded on this product on a 800 MHz spectrometer in 90 % H_2O / 10 % D_2O .

ES-MS : $m/z = 381.2$ [$\text{M}-2\text{Cl}$] $^{2+}$, 363.2 [$\text{M}-3\text{Cl}-\text{H}$] $^{2+}$, 346.2 [$\text{M}-4\text{Cl}-2\text{H}$] $^{2+}$.

Selected IR (KBr, cm^{-1}): 3418 s (NH), 2925 m (CH), 2360 s (CH), 1623 m (OH),

1459 m (CO).

4.2.4 UV-Vis Spectroscopy

UV-vis spectra were recorded for complexes **10**, **11** and **13** in H₂O at 25 °C, between 300-800 nm.

4.2.5 Zinc Uptake of Xylyl-Bicyclam at 37 °C

Xylyl-bicyclam (3.1 mg) was dissolved in D₂O (500 µL, 10 mM) and dioxane (2 µL) was added. The pH was adjusted using DNO₃ (1 M) until pH=7.28. A ¹H NMR spectrum at 37 °C was recorded. The reaction was maintained at 37 °C and Zn₂(OAc)₂·2H₂O (2 molar equiv, 2.6 mg, 20 mM) was added. The pH was adjusted to pH=7.28 and another NMR spectrum was recorded 5 minutes 12 seconds after the addition. Spectra were recorded every 10 minutes for 3 hours and then every 30 minutes for 21 hours. A 2D [¹H, ¹³C] HSQC NMR spectrum was then recorded on this product on a 800 MHz spectrometer in 90 % H₂O / 10 % D₂O.

4.2.6 Reaction of Zn(histidine)₂ with Xylyl-Bicyclam at 37 °C

Histidine (31.02 mg, 0.1 mmol) was dissolved in D₂O (10 mL). Zinc chloride (0.5 molar equiv, 6.81 mg, 0.05 mmol) was added and the mixture was stirred at room temperature for one hour. The solution was concentrated until white precipitate formed, which was then filtered off and washed with diethyl ether. This was then made up to 10 mL with D₂O. The resulting clear solution (pH=6.02) was adjusted to pH=7.17 using NaOD.

^1H NMR – 7.81 (1H, s), 7.07 (1H, s), 3.99 (1H, t, J = 4 Hz), 3.17 (s, 2H).

ES-MS : $m/z = 375.7 [\text{Zn} + 2\text{hist} + 3\text{H}]^+$, $329.6 [\text{Zn} + 2\text{hist} - \text{COOH}]^+$, $218.4 [\text{Zn} + \text{hist} - \text{H}]^+$, $157.3 [\text{Zn} + \text{hist} - \text{COOH}]^+$.

A ^1H NMR spectrum of $\text{Zn}(\text{hist})_2$ (600 μL , 5 mM) in D_2O at pH = 7.17 and 37 $^\circ\text{C}$ was recorded with dioxane (2 μL) added as a reference. Xylyl-bicyclam (0.5 molar equiv, 300 μL , 5 mM, pH=7.2) in D_2O was added and a spectrum was recorded at 37 $^\circ\text{C}$, 2 minutes 56 seconds after addition. 1D ^1H NMR spectra were then recorded every 10 minutes for 2 hours, then every 30 minutes for the following 22 hours. 2D NMR spectra ($[^1\text{H}, ^1\text{H}]$ COSY, TOCSY, NOESY and $[^1\text{H}, ^{13}\text{C}]$ HSQC) were recorded at the end of this period.

To identify the products of this reaction, HPLC-MS was carried out on the product. A polymer reverse phase column was used and water and acetonitrile solvents were used with 0.1% TFA added as an ion pairing agent.

HPLC conditions : 30 μL portions, flow rate = 0.6 mL / min, gradient: 0 – 5 minutes, 90 % water / 10 % acetonitrile; 5 – 15 minutes, 50 % water / 50 % acetonitrile; 15 – 20 minutes, 50 % water / 50 % acetonitrile; 20 – 21 minutes, 90 % water / 10 % acetonitrile; 21-27 minutes, 90 % water / 10 % acetonitrile. The total separation time was 27 minutes. The absorbance was measured at 254 nm.

4.2.7 Addition of Acetate to $\text{Pd}_2(\text{xylyl-bicyclam})(\text{OAc})_4$

A solution of $\text{Pd}_2(\text{xylyl-bicyclam})(\text{OAc})_4$ (4 mg, 0.0044 mmol) in 90 % H_2O / 10 % D_2O (600 μL , 7.5 mM) with dioxane (2 μL) added as a reference was prepared. This was used to record 1D ^1H NMR and 2D $[^1\text{H}, ^1\text{H}]$ TOCSY, COSY and NOESY and $[^1\text{H}, ^{13}\text{C}]$ and $[^1\text{H}, ^{15}\text{N}]$ HSQC were recorded. Sodium acetate (1 M,

17.6 μL , 4 molar equiv) was added and 1D ^1H NMR spectra were recorded every 30 minutes for 24 hours and then the 2D NMR spectra were re-recorded.

4.2.8 Addition of Acetate to $\text{Co}_2(\text{xylyl-bicyclam})\text{Cl}_4\text{Cl}_2$

A solution of $\text{Co}_2(\text{xylyl-bicyclam})\text{Cl}_4\text{Cl}_2$ (3 mg, 0.0036 mmol) in 90 % H_2O / 10 % D_2O with dioxane (2 μL) added as a reference was prepared. This was used to record 1D ^1H NMR and 2D [^1H , ^1H] TOCSY, COSY and NOESY and [^1H , ^{13}C] and [^1H , ^{15}N] HSQC spectra. Sodium acetate (1 M, 21.6 μL , 6 molar equiv) was added. A 1D ^1H proton spectrum was recorded 5 minutes after the first addition and every 10 minutes for 2 hours and every 30 minutes for 45 hours. 2D [^1H , ^1H] TOCSY, COSY and NOESY and [^1H , ^{13}C] and [^1H , ^{15}N] HSQC spectra were then recorded on the product. UV-vis spectroscopy, (300-800 nm, 25 $^\circ\text{C}$, in 90 % H_2O / 10 % D_2O) and ES MS were also carried out on the product.

ES-MS : $m/z = 457.7$ [$\text{Co}_2(\text{xylyl-bicyclam})(\text{OAc})_5$] $^{2+}$, 428.7 [$\text{Co}_2(\text{xylyl-bicyclam})(\text{OAc})_4$] $^{2+}$, 368.1 [$\text{Co}_2(\text{xylyl-bicyclam})(\text{OAc})_2$] $^{2+}$

4.3 Results

4.3.1 Synthesis of Xylyl-bicyclam, 9

The ^1H NMR spectrum produced from route 1 shows that there is a mixture of cyclam and xylyl-bicyclam present. There are two main areas during the synthesis which could have caused it to give poor results. The first is the DMF, which was difficult to obtain in a completely anhydrous form, giving residual water in the reaction, hence causing a poor yield. The second is the highly air sensitive

phosphine protecting group, which can easily decompose. Xylyl-bicyclam (**9**) was successfully synthesised using route 2, and characterised using ES-MS and ^1H NMR. The xylyl-bicyclam produces a characteristic multiplet at 7.50-7.32 ppm, which arises from the aromatic linker protons. The aliphatic linker protons give the broad singlet at 3.83 ppm. The 2 sets of $\text{CH}_2\text{CH}_2\text{CH}_2$ protons give signals at 1.92-1.78 ppm and 2.18-2.08 ppm. There is a large multiplet between 2.70 ppm and 3.32 ppm which arise from $\text{CH}_2\text{CH}_2\text{CH}_2$ protons.

4.3.2 $[\text{Ni}_2(\text{Xylyl-Bicyclam})](\text{OAc})_4$, **10**

The 1D ^1H NMR spectrum (Figure 4.2) for the nickel(II)-xylyl-bicyclam acetate complex **10** is extremely complicated. It is likely that there is a large number of species present in solution. There is a mixture of peaks for paramagnetic and diamagnetic species. Spectra were recorded over a spectral width of -400 ppm to +400 ppm. Peaks were observed between -20 ppm and 250 ppm. The region 55 ppm to -45 ppm is shown in Figure 4.3. The broadened peaks are shown in Figure 4.4, and the data are summarised in Table 4.2. A [^1H , ^{15}N] HSQC spectrum was recorded, but no NH signals were observed. The two cyclam rings in the xylyl-bicyclam molecule may be in different configurations and be either paramagnetic or diamagnetic giving molecules with both paramagnetic and diamagnetic components. Paramagnetic-paramagnetic, paramagnetic-diamagnetic and diamagnetic-diamagnetic components may all be present in solution and affect the NMR spectrum obtained. Further experimentation would be required in order to assign the peaks seen in the spectrum.

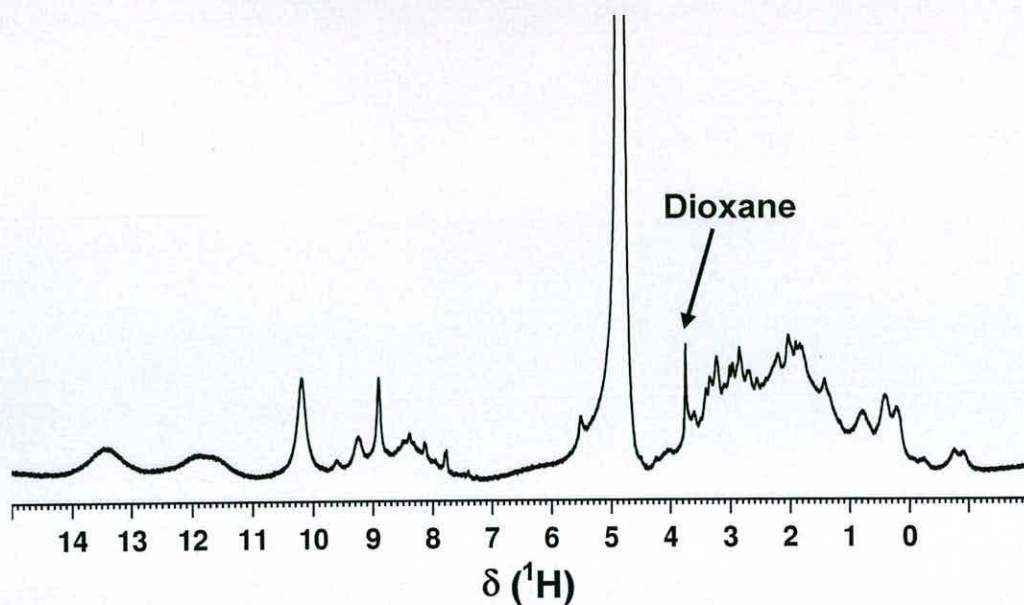


Figure 4.2 1D ^1H NMR spectrum of $\text{Ni}_2(\text{bicyclam})(\text{OAc})_4$, **10**, recorded in 90 % H_2O / 10 % D_2O , at 25 °C.

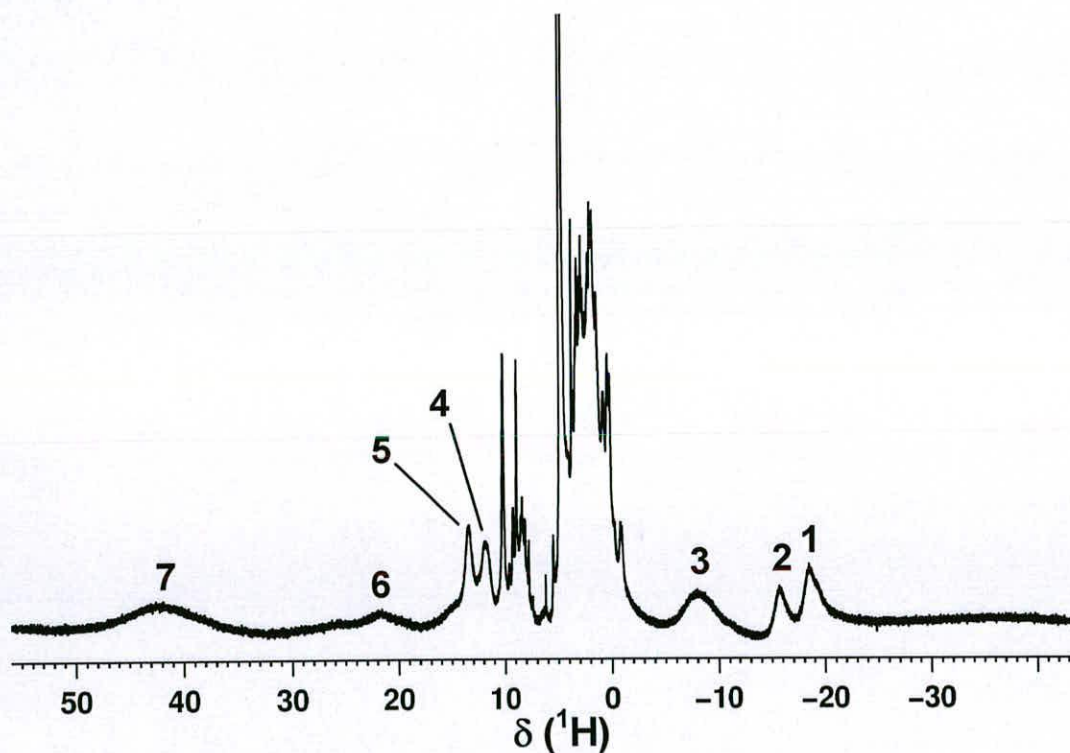


Figure 4.3 1D ^1H NMR spectrum of $\text{Ni}_2(\text{bicyclam})(\text{OAc})_4$, **10**, recorded in 90 % H_2O / 10 % D_2O , at 25 °C, over a sweep width of 55 ppm to -45 ppm, showing the broad peaks observed in this region. Peak labels correspond to those in Table 4.2.

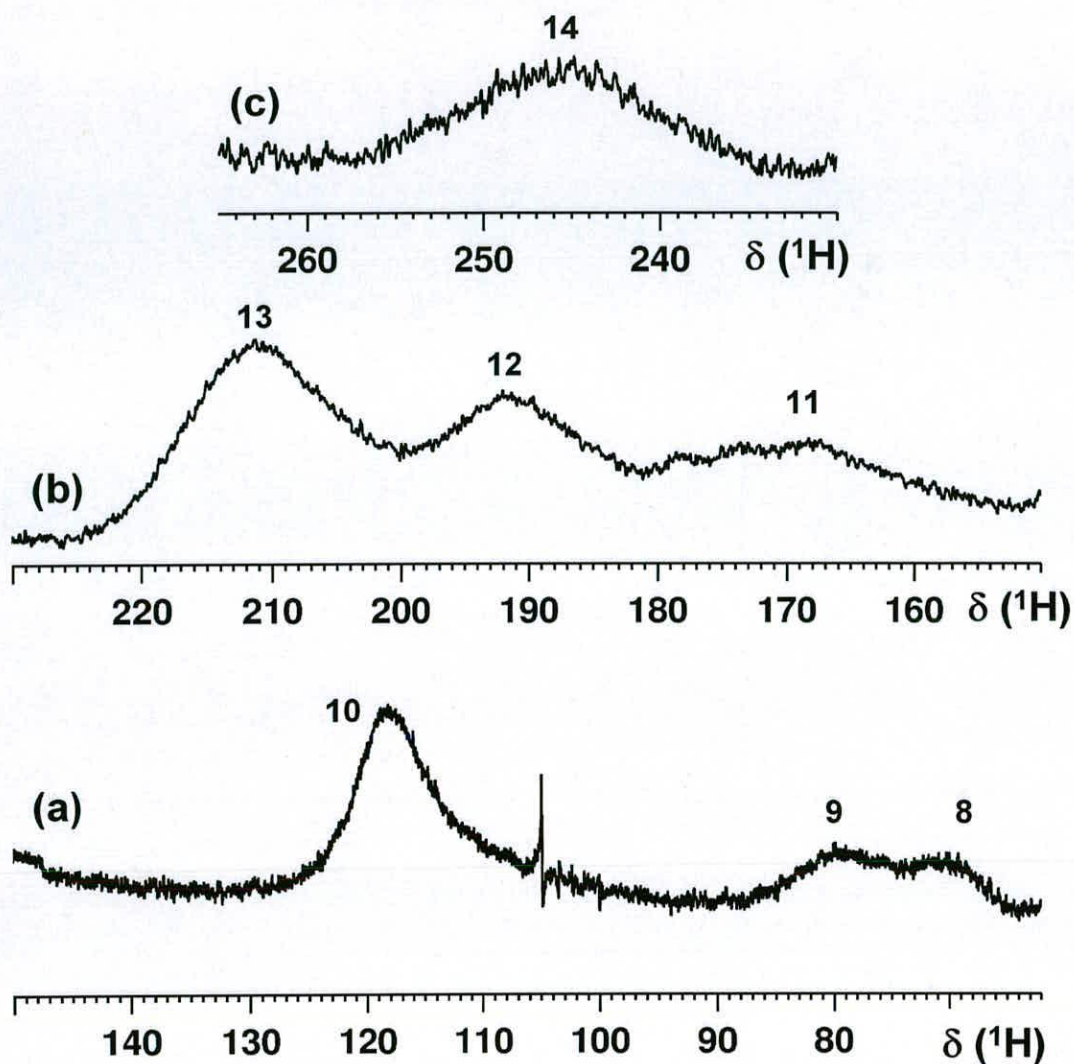


Figure 4.4 1D ^1H NMR spectrum of $\text{Ni}_2(\text{bicyclam})(\text{OAc})_4$, **10**, recorded in 90 % H_2O / 10 % D_2O , at 25 °C, (a) over a spectral width of 60 ppm to 150 ppm, (b) over a spectral width of 150 ppm to 230 ppm and (c) over a spectral width of 230 ppm to 265 ppm showing the broad peaks observed in this region. Peak labels correspond to those in Table 4.2.

Table 4.2 Para magnetically-shifted peaks for Ni₂(xylyl-bicyclam)(OAc)₄, complex 10. (See Figure 4.3 and Figure 4.4)

Peak	¹ H / ppm	Peak	¹ H / ppm
1	-18.2	8	69.7
2	-15.5	9	80.3
3	-7.5	10	117.7
4	11.7	11	169.0
5	13.3	12	191.8
6	21.4	13	211.8
7	42.1	14	245.5

4.3.3 [Cu₂(Xylyl- Bicyclam)](OAc)₄, 11

A one dimensional ¹H NMR spectrum was recorded for this complex in 90 % H₂O / 10 % D₂O, and a 2D [¹H, ¹³C] HQSC. Six peaks were observed in the 1D ¹H NMR spectra (recorded over a spectral width of -400 ppm to +400 ppm). There was one unbroadened peak at 1.94 ppm, (23.6 ppm in ¹³C dimension), likely to be from free acetate. The other five peaks were found to be broadened significantly by the two paramagnetic Cu²⁺ centres (Figure 4.5). The data are summarised in Table 4.3.

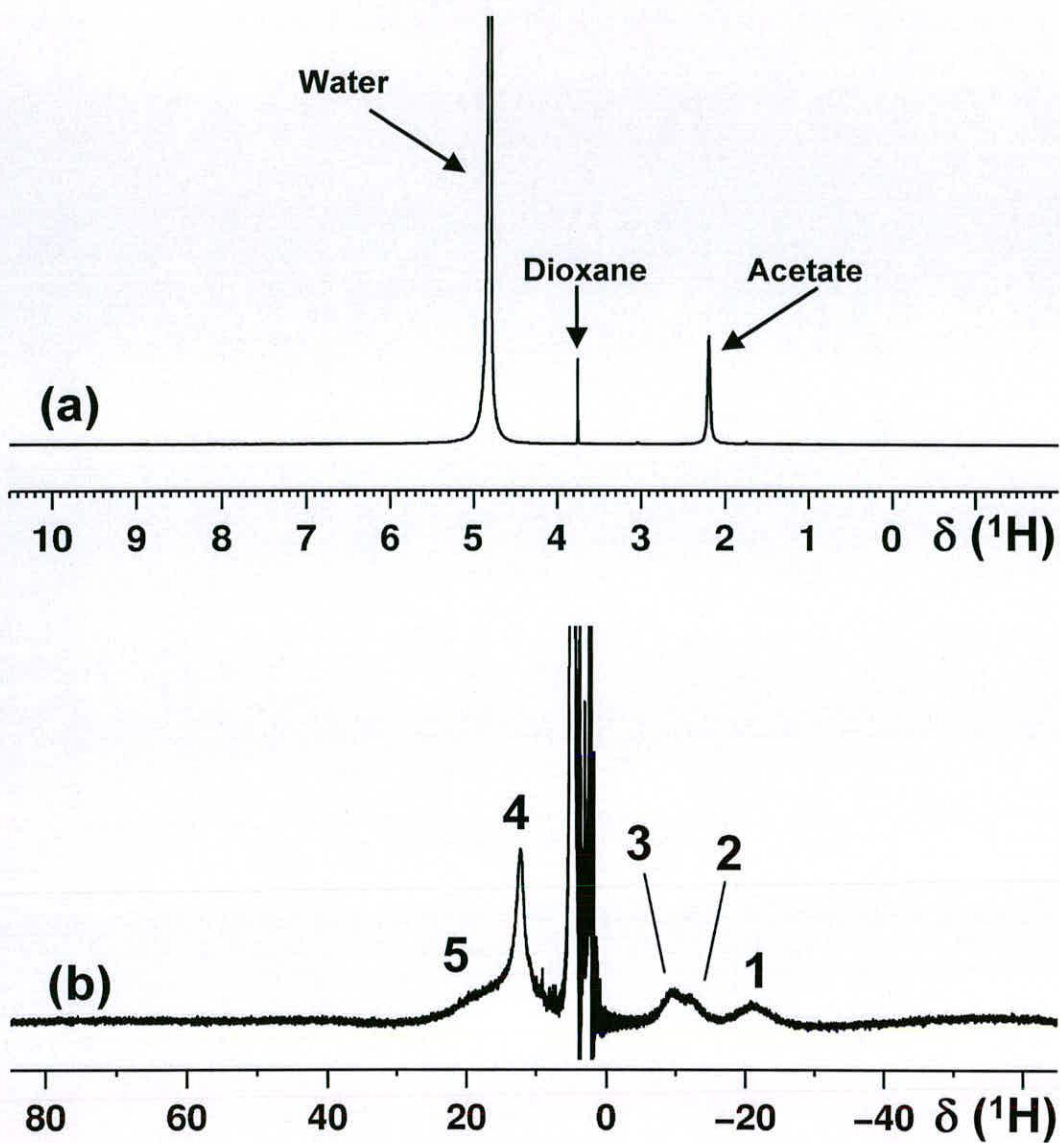


Figure 4.5 1D ^1H NMR spectrum of $[\text{Cu}_2(\text{Xylyl-Bicyclam})](\text{OAc})_4$, 11, recorded in 90 % H_2O / 10 % D_2O , at 25 $^\circ\text{C}$ (a) from -1 to 11 ppm, (b) from -70 to 80 ppm. Five broad peaks are seen in (b), labelled 1-5.

Table 4.3 Para magnetically-shifted peaks for $\text{Cu}_2(\text{xylyl-bicyclam})(\text{OAc})_4$, complex 11. (See Figure 4.5)

Peak	^1H / ppm
1	-21
2	-12
3	-9
4	12
5	18

4.3.4 $[\text{Pd}_2(\text{xylyl-bicyclam})](\text{OAc})_4$, 12

The ^1H NMR spectrum of $[\text{Pd}_2(\text{xylyl-bicyclam})](\text{OAc})_4$, 12, in 90 % H_2O / 10 % D_2O is shown in Figure 4.6. The resonances in the spectrum can be split into 4 groups: resonances from the aromatic protons, resonances from the protons in the bridging linker CH_2 groups, resonances from NH protons and resonances from the protons in the cyclam rings. In order to aid full characterisation of the ^1H NMR spectrum, $[\text{H}, \text{H}]$ TOCSY, COSY and NOESY and $[\text{H}, \text{C}]$ and $[\text{H}, \text{N}]$ HSQC spectra were acquired. There is one acetate signal, at 1.91 ppm, showing that all the acetate is in the one configuration. The acetate peak does not show TOCSY peaks to any other proton peaks, showing that it is not bound to the Pd^{2+} .

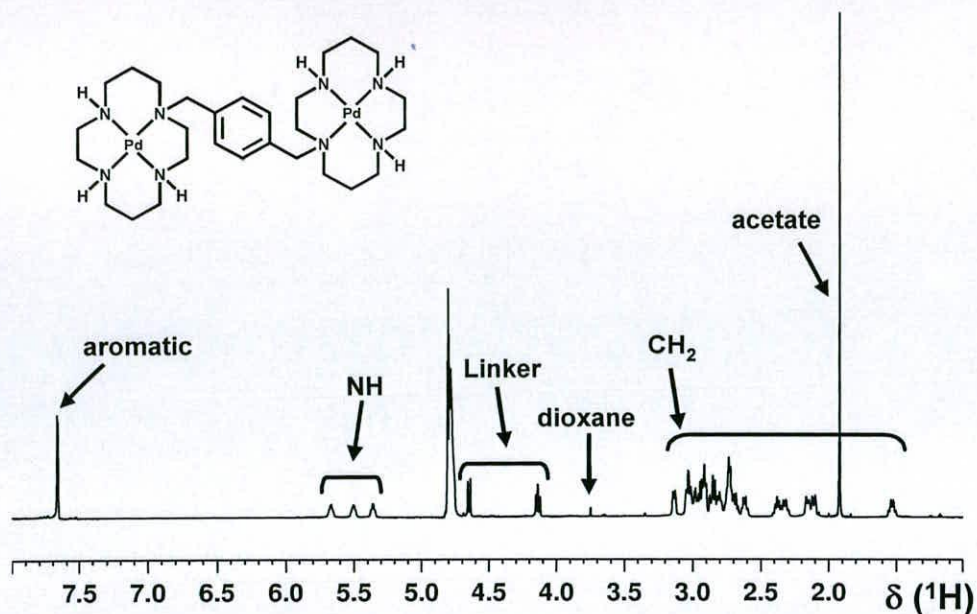


Figure 4.6 1D ^1H NMR spectrum of complex **12**, $[\text{Pd}_2(\text{xylyl-bicyclam})](\text{OAc})_4$, in 90 % H_2O / 10 % D_2O at 25 $^\circ\text{C}$, with the different regions labelled.

NH Proton Resonances

There are only 3 NH signals present in the $[\text{H}, \text{N}]$ -HSQC (Figure 4.7). This shows that there is only one configuration present, hence both cyclam rings must be in the same configuration.

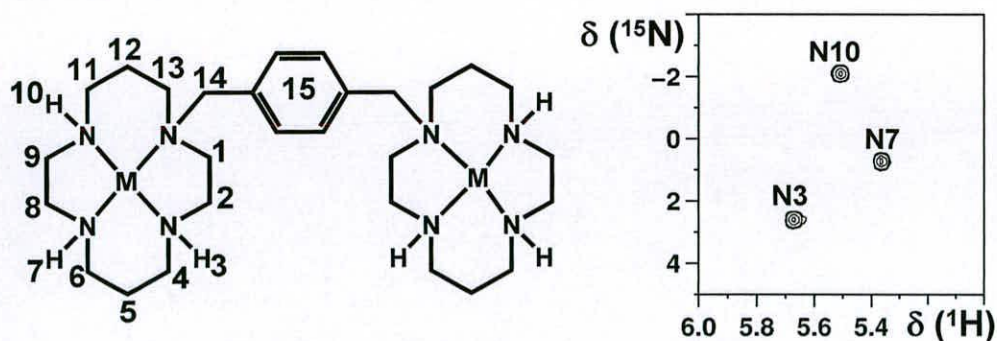


Figure 4.7 2D $[\text{H}, \text{N}]$ HSQC NMR spectrum of complex **12**, recorded in 90 % H_2O / 10 % D_2O at 25 $^\circ\text{C}$. Three NH signals are observed.

Bridging Methylene Proton Resonances

Only one pair of resonances for the bridging methylene protons is observed in the 2D [^1H , ^{13}C] HSQC NMR spectrum, shown in Figure 4.8. One of the linker protons (4.15 ppm) shows a NOESY peak to one of the NH proton signals (5.67 ppm) showing that they are on the same face of the cyclam ring. There is no interaction between the linker protons and either of the other two NH resonances, which is indicative of a *trans*-III configuration.

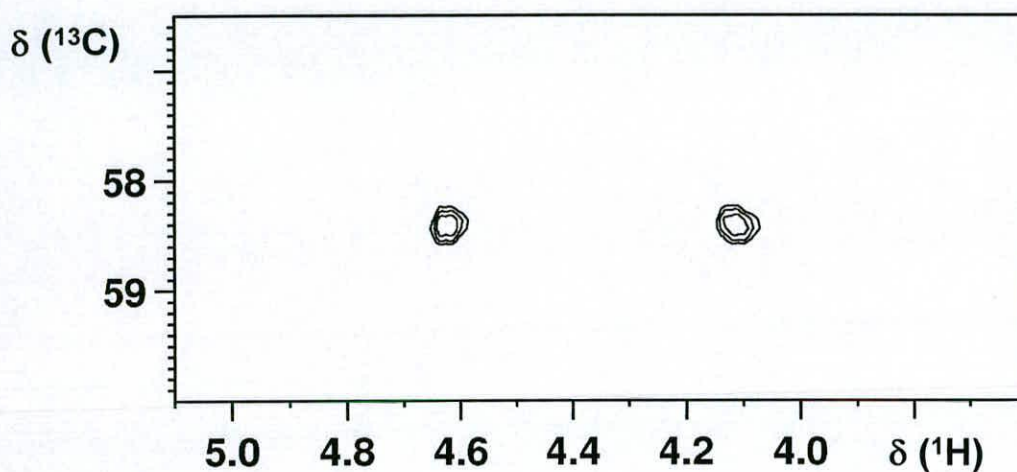


Figure 4.8 Linker region of the 2D [^1H , ^{13}C] HSQC NMR spectrum of complex **12**, $[\text{Pd}_2(\text{xylyl-bicyclam})](\text{OAc})_4$, recorded in 90 % H_2O / 10 % D_2O , showing only two linker protons, hence only one configuration of the macrocycle must be present.

Aromatic Resonances

There is only one signal in the aromatic region of the [^1H , ^{13}C] HSQC spectrum, this means that both rings have to be in the same configuration, as if they were in different ones, the aromatic protons would be in different environments and

the signals would become inequivalent. There is a peak in the [^1H , ^1H] NOESY spectrum between the aromatic signal and one of the linker protons, 14b. The aromatic resonance shows NOESY cross peaks to one of the central methylene protons of one of the 3-carbon bridges, 9a, and also to protons 1a and 13b, supporting that these are the groups closest to the linker. For the numbering scheme, see Figure 4.7,

Proton Resonances from the Cyclam Rings

Only one set of NH peaks and one set of linking CH_2 groups shows that there is only one type of cyclam ring present in solution for $[\text{Pd}_2(\text{xylyl-bicyclam})](\text{OAc})_4$. This is supported by the fact that there are 10 pairs of signals in the aliphatic region of the 2D [^1H , ^{13}C] HSQC NMR spectrum, shown in Figure 4.9. Two of the NH peaks (protons 5 and 7) show NOESY cross peaks to the same central methylene resonance (proton 2a), showing that they are both on the same side of the ring as proton 2a. Proton 2a must therefore be an axial proton. The other NH, proton 10, shows a NOESY cross peak to the linker proton 14a, showing that proton 10 and the linker are on the same face of the ring. These two interactions are strongly indicative of a *trans*-III configuration. Proton 10 also shows a NOESY cross-peak to proton 9a, which is the axial central methylene proton in the other 3-carbon bridge. The fully assigned 2D [^1H , ^{13}C] HSQC NMR spectrum is shown in Figure 4.9, along with the numbering scheme. The data are summarised in Table 4.4.

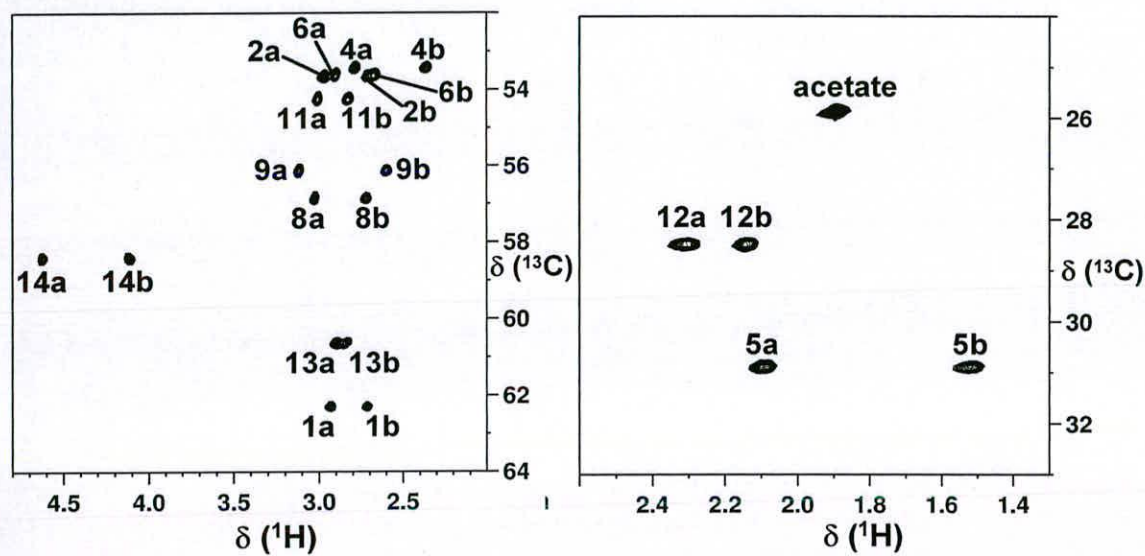
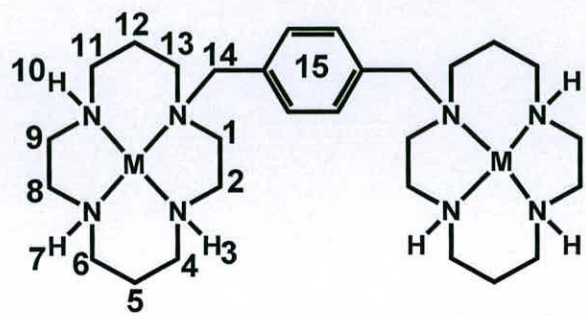


Figure 4.9 2D [^1H , ^{13}C] HSQC NMR spectrum of complex **12**, $[\text{Pd}_2(\text{xylyl-bicyclam})](\text{OAc})_4$, recorded in 90 % H_2O / 10 % D_2O . Ten sets of CH_2 protons are from the macrocycle, and one set from the linker protons. Only one acetate signal is observed. The numbering scheme is included. Protons on the same carbon atom are referred to as a and b.

Table 4.4 ^1H , ^{13}C and ^{15}N Chemical shifts of $\text{Pd}_2(\text{xylyl-bicyclam})](\text{OAc})_4$, **12**, recorded in 90 % H_2O / 10 % D_2O at 25 °C. For numbering scheme, see Figure 4.9.

Assignment	^1H / ppm	^{13}C / ppm	^{15}N / ppm	Assignment	^1H / ppm	^{13}C / ppm	^{15}N / ppm
1a	2.96	62.3		8b	2.74	56.2	
1b	2.74			9a	3.14		
2a	2.99	9b		2.62			
2b	2.73	53.7		10	5.67	2.6	
3	5.51		2.1	11a	3.03	54.3	
4a	2.79	53.4		11b	2.84		
4b	2.38			12a	2.33	28.5	
5a	2.12	30.9		12b	2.17		
5b	1.54			13a	2.92	60.6	
6a	2.91	53.6		13b	2.84		
6b	2.69			14a	4.65	58.5	
7	5.37		0.7	14b	4.14		
8a	3.05	56.9		15	7.65	135.0	

4.3.5 $[\text{Co}_2(\text{Xylyl-Bicyclam})\text{Cl}_4]\text{Cl}_2$, **13**

The ^1H NMR spectrum of $[\text{Co}_2(\text{xylyl-bicyclam})\text{Cl}_4]\text{Cl}_2$, **13**, in 90 % H_2O / 10 % D_2O is shown in Figure 4.10. Dioxane was added as a reference. In order to aid full characterisation of the ^1H NMR spectrum, 2D [^1H , ^1H] TOCSY, COSY and NOESY and [^1H , ^{13}C] and [^1H , ^{15}N] HSQC NMR spectra were acquired.

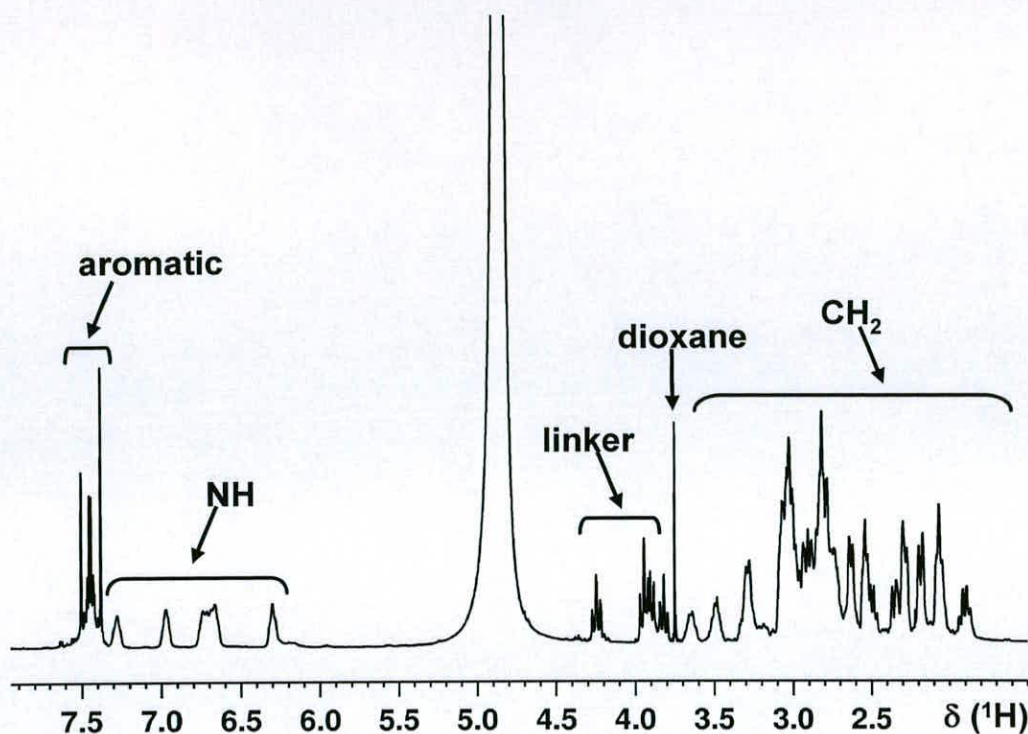


Figure 4.10 1D ^1H NMR spectrum of $[\text{Co}_2(\text{xylyl-bicyclam})\text{Cl}_4]\text{Cl}_2$, **13**, recorded in 90 % H_2O / 10 % D_2O at 25 $^\circ\text{C}$. Key regions are highlighted.

NH Proton Resonances

There are 6 NH signals present in the 2D [^1H , ^{15}N] HSQC spectrum (Figure 4.11). This shows that there are two configurations present. From this HSQC spectrum alone, it is impossible to tell if they are from one xylyl-bicyclam molecule with the rings in different configurations or if there are two xylyl-bicyclam molecules present. The 2D [^1H , ^1H] TOCSY spectrum can be used here to show that the peaks at 6.97 ppm, 6.66 ppm and 6.29 ppm show TOCSY peaks to each other, indicating that they are from the same cyclam ring, (system A) and the peaks at 7.28 ppm and 6.75 ppm and 6.69 ppm show TOCSY peaks to one another, so they must also be from the same cyclam ring (system B) (Figure 4.12). The integrations of the

peaks in the 2D [^1H , ^{15}N] HSQC NMR spectrum show that the peaks from system A all integrate to similar values, as do those of system B. From the integrals, it can be calculated that the ratio of system A : system B is approximately 60:40. The shifts are summarised in Table 4.5.

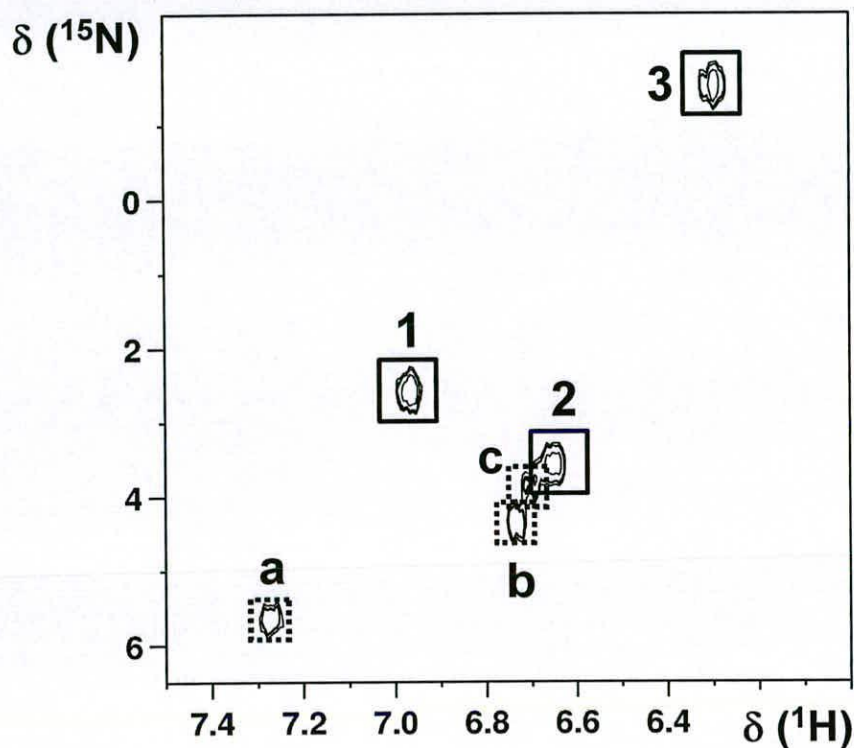


Figure 4.11 2D [^1H , ^{15}N] HSQC NMR spectrum of $[\text{Co}_2(\text{xylyl-bicyclam})\text{Cl}_4]\text{Cl}_2$, **13**, recorded in 90 % H_2O , 10 % D_2O at 25 °C. Six signals are observed, three are from system A, shown in solid lines, and three are from system B, shown in dotted lines, showing that there are two configurations of cyclam present. The ^1H and ^{15}N peak shifts are summarised in Table 4.5.

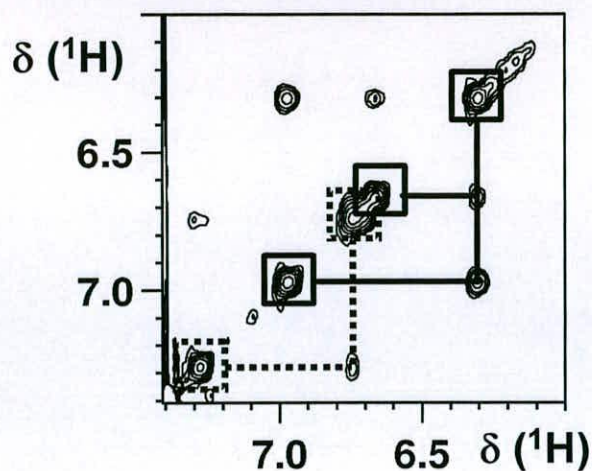


Figure 4.12 2D [^1H , ^1H] TOCSY NMR spectrum of $[\text{Co}_2(\text{xylyl-bicyclam})\text{Cl}_4]\text{Cl}_2$, **13**, recorded in 90 % H_2O / 10 % D_2O at 25 °C, showing the TOCSY interactions between the NH protons. There are 6 NH signals, three of which show connectivity to each other, (solid black lines) therefore must be one system (system A). The other three also show TOCSY cross-peaks to each other, (dotted lines, system B), although two overlap in the proton axis and can only be seen as one signal here.

Table 4.5 ^1H and ^{15}N Shifts for the NH protons from $[\text{Co}_2(\text{xylyl-bicyclam})\text{Cl}_4]\text{Cl}_2$ in 90 % H_2O / 10 % D_2O at 25 °C. (See Figure 4.11).

System	Proton*	^1H / ppm	^{15}N / ppm
A	NH1	6.97	2.6
	NH2	6.66	3.5
	NH3	6.29	-1.5
B	NHa	7.28	5.7
	NHb	6.75	4.3
	NHc	6.69	3.9

* No specific assignment

Bridging Methylene Proton Resonances

There are two pairs of resonances for the bridging methylene protons is observed in the 2D [^1H , ^{13}C] HSQC NMR spectrum, further supporting the presence of two cyclam configurations (Figure 4.13). There is one set at 55.6 ppm (^{13}C dimension) and one set at 58.8 ppm. These integrate in the ratio 40:60, showing that the set at 55.6 ppm corresponds to system B, and the set at 58.8 ppm corresponds to system A. The data are summarised in Table 4.6.

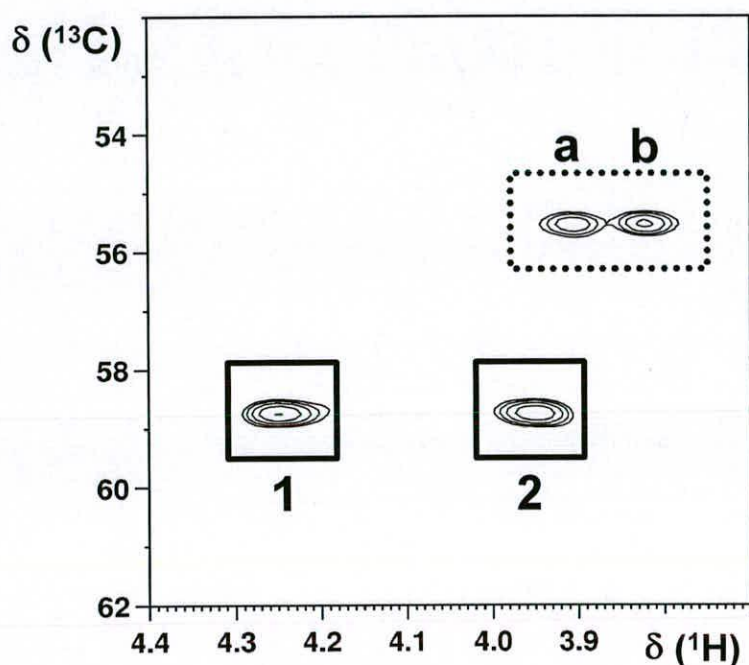


Figure 4.13 2D [^1H , ^{13}C] HSQC spectrum of $[\text{Co}_2(\text{xylyl-bicyclam})\text{Cl}_4]\text{Cl}_2$, **13**, recorded in 90 % H_2O / 10 % D_2O at 25 $^\circ\text{C}$, showing two sets of linker protons. The ^1H and ^{13}C NMR shifts are given in Table 4.6.

Table 4.6 ^1H and ^{13}C Shifts for the linker protons from $[\text{Co}_2(\text{xylyl-bicyclam})\text{Cl}_4]\text{Cl}_2$ in 90 % H_2O / 10 % D_2O at 25 $^\circ\text{C}$. (See Figure 4.13).

System	Proton*	^1H / ppm	^{13}C / ppm
A	CH1	4.24	58.8
	CH2	3.94	
B	CHa	3.89	55.6
	CHb	3.81	

* No specific assignment

Proton Resonances from the Cyclam Rings

Two sets of NH peaks and two sets of linking CH_2 groups shows that there are two types of cyclam ring present in solution for $[\text{Co}_2(\text{xylyl-bicyclam})\text{Cl}_4]\text{Cl}_2$. Four sets of protons are observed with corresponding ^{13}C NMR shifts between 25 ppm and 32 ppm (^{13}C dimension, Figure 4.14), these are from the central methylene protons in the 3-carbon bridge. Four sets of signals in this region again suggest that there are two configurations of cyclam present. However, the remainder of the peaks in the 2D [^1H , ^{13}C] HSQC NMR spectrum, from the CH_2 groups around the cyclam rings could not be fully characterised, due to overlapping signals in both the proton and the carbon dimensions.

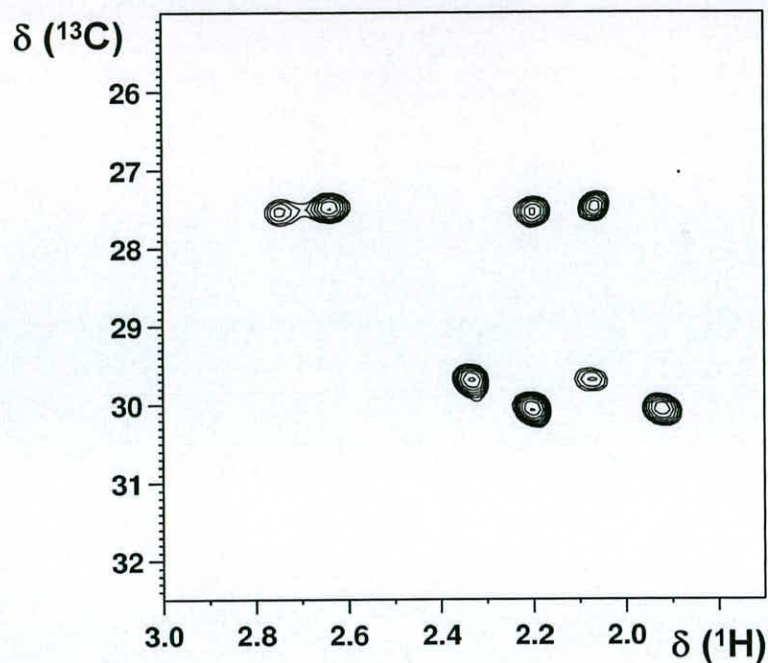


Figure 4.14 2D [^1H , ^{13}C] HSQC spectrum of $[\text{Co}_2(\text{xylyl-bicyclam})\text{Cl}_4]\text{Cl}_2$, **13**, recorded in 90 % H_2O / 10 % D_2O at 25 °C, showing four sets of $\text{CH}_2\text{CH}_2\text{CH}_2$ protons.

Aromatic Resonances

The xylyl aromatic resonances are sensitive to both of the attached cyclam units, being singlets when the two units are the same but AB quartets when they are different. In this case, there are two singlets, and one AB quartet present, (Figure 4.15) which suggests there are three xylyl-bicyclam isomers present, two with both the cyclam rings in same configuration, and one with the cyclam rings in two configurations.

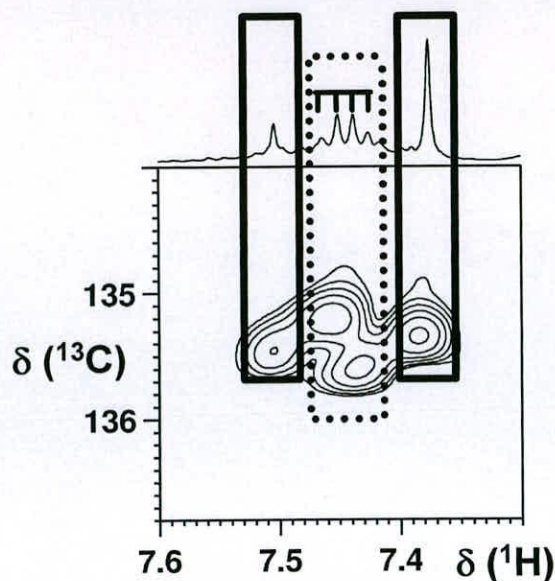


Figure 4.15 2D [^1H , ^{13}C] HSQC NMR spectrum of $[\text{Co}_2(\text{xylyl-bicyclam})\text{Cl}_4]\text{Cl}_2$, **13**, recorded in 90 % H_2O / 10 % D_2O , at 25 °C. Two singlets are present, marked by solid boxes, which shows that there are two species present in which the both the cyclam rings are in the same configuration. One AB quartet is observed, marked by a dotted box, which means that there is one species present which has the cyclam rings in different configurations.

4.3.6 UV-Vis Spectroscopy

UV-vis spectroscopy was carried out on complexes **10**, **11**, **13** and **13** + 6 molar equivalents of NaOAc. One absorption band was found for the Ni(II) and the Cu(II) complexes, while three bands were observed for the Co(III) complexes. The extinction coefficients were calculated using Equation 3.1, and the results are shown in Table 4.7.

Table 4.7 Extinction Coefficients for Metal-Bicyclam complexes, recorded in H₂O, at 25 °C.

Complex	Conc. / mM	λ_{\max} / nm	A	ϵ / M ⁻¹
Ni ₂ (xylyl-bicyclam)(OAc) ₄ , 10	0.934	456	0.0796	85.2
Cu ₂ (xylyl-bicyclam)(OAc) ₄ , 11	2.23	513	0.1927	86.4
Co ₂ (xylyl-bicyclam)Cl ₆ , 13	1.4	641	0.03400	24.3
		466	0.04962	35.4
		383	0.1143	81.6
13 + 6 molar equiv NaOAc *	5.0	571	0.2332	44.6
		475	0.1826	36.5
		373	0.3967	79.3

* Recorded in 90 % H₂O / 10 % D₂O. Assumed final product was Co₂(xylyl-bicyclam)(OAc)₆ for concentration calculation, based on the ES-MS data.

4.3.7 Zinc Uptake of Xylyl-Bicyclam at 37 °C

The first ¹H NMR spectrum after the addition of Zn²⁺ from zinc acetate (2 molar equiv) recorded showed an immediate change from that of the initial xylyl-bicyclam (Figure 4.16). There was no observable change in the ¹H NMR spectrum recorded over a 24-hour period. The structure of Zn₂(xylyl-bicyclam)(OAc)₄ has been well studied by NMR spectroscopy, and shifts of particular protons can be used to identify the configuration of the cyclam rings.¹⁵ In this case, the methylene linker protons were used to identify the configurations. There are three identifiable sets of methylene linker proton peaks observable in the [¹H, ¹³C] HSQC spectrum (Figure 4.17). These were attributed to a *trans*-III configuration, a *trans*-I configuration and

a *cis*-V configuration. There is also a peak present from unreacted xylyl-bicyclam. Looking at the integrals of the peaks in this region, 12 % of the complex is *trans*-III, 15 % is *cis*-V and 28 % is *trans*-I. Integration showed that 45 % of xylyl-bicyclam remained uncomplexed.

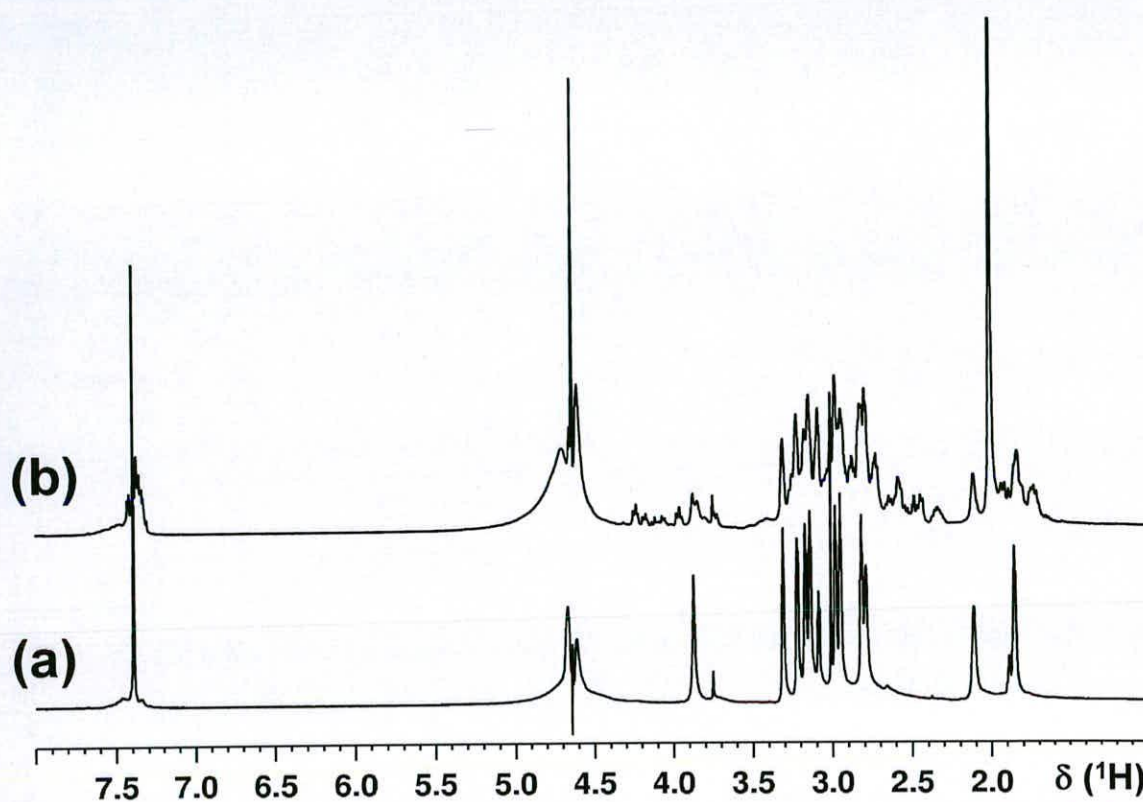


Figure 4.16 Stacked plot of (a) xylyl-bicyclam in 90 % H₂O, 10 % D₂O, pH = 7.2, temp = 37 °C, (b) after the addition of ZnOAc₂ (2 molar equiv), spectrum recorded 5 minutes 12 seconds after addition. The changes occur before the first spectrum could be recorded and the spectrum did not change over 24 hours.

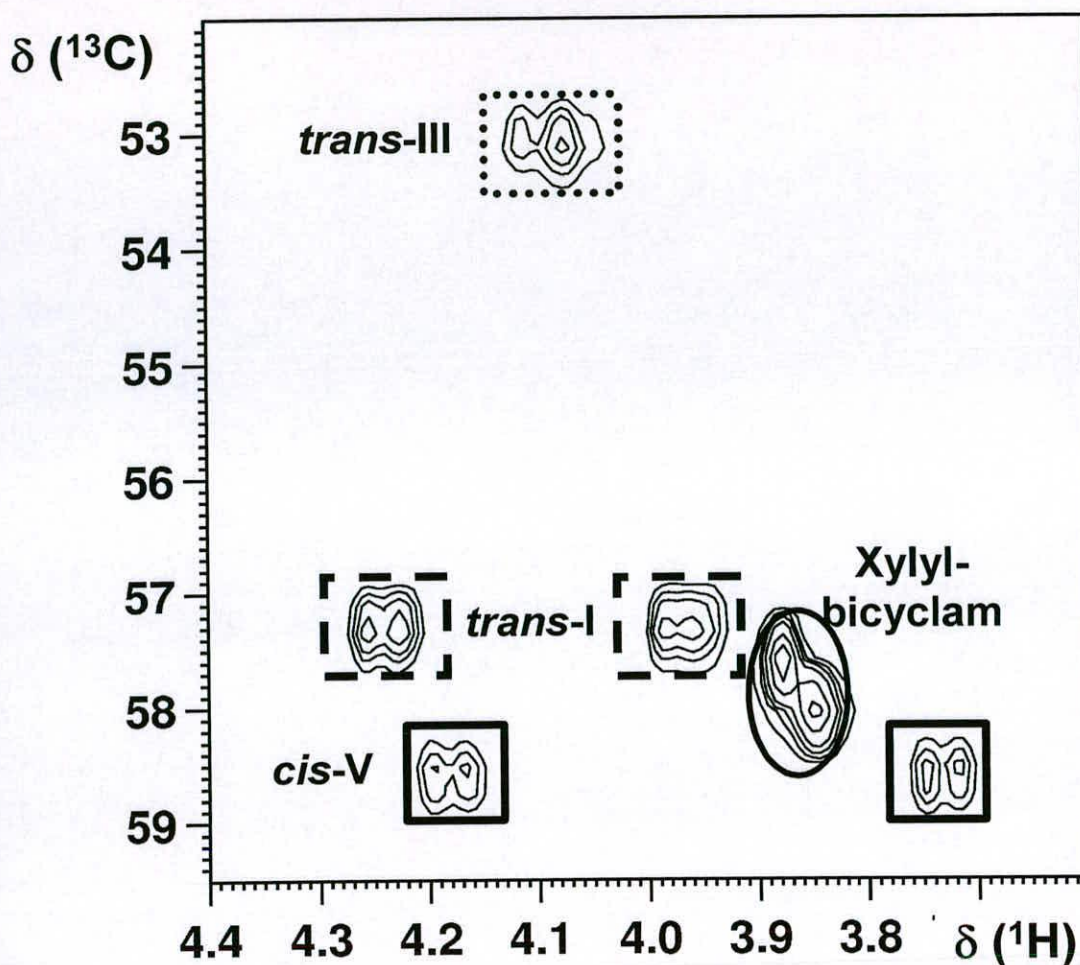


Figure 4.17 The methylene linker region of the [^1H , ^{13}C]-HSQC spectrum of xylyl-bicyclam after the addition of $\text{Zn}(\text{OAc})_2$. There is some unreacted xylyl-bicyclam left (in circle), but new signals from the linker protons are clearly observed. This region can be used to identify the configurations of the cyclam rings, with three configurations identified. *Trans*-III (dots) – 12 %, *trans*-I (dashes) – 28 % and *cis*-V – 15 %.

4.3.8 Reaction of Xylyl-Bicyclam With Zinc Histidine

Upon the mixing of xylyl-bicyclam with $\text{Zn}(\text{hist})_2$, there was an immediate

change in the spectrum. New peaks appeared in the aromatic region and the linker region of the bicyclam spectrum (Figure 4.18). However, these peaks remained stable over a 24 hour period, showing that the products that were immediately formed were stable.

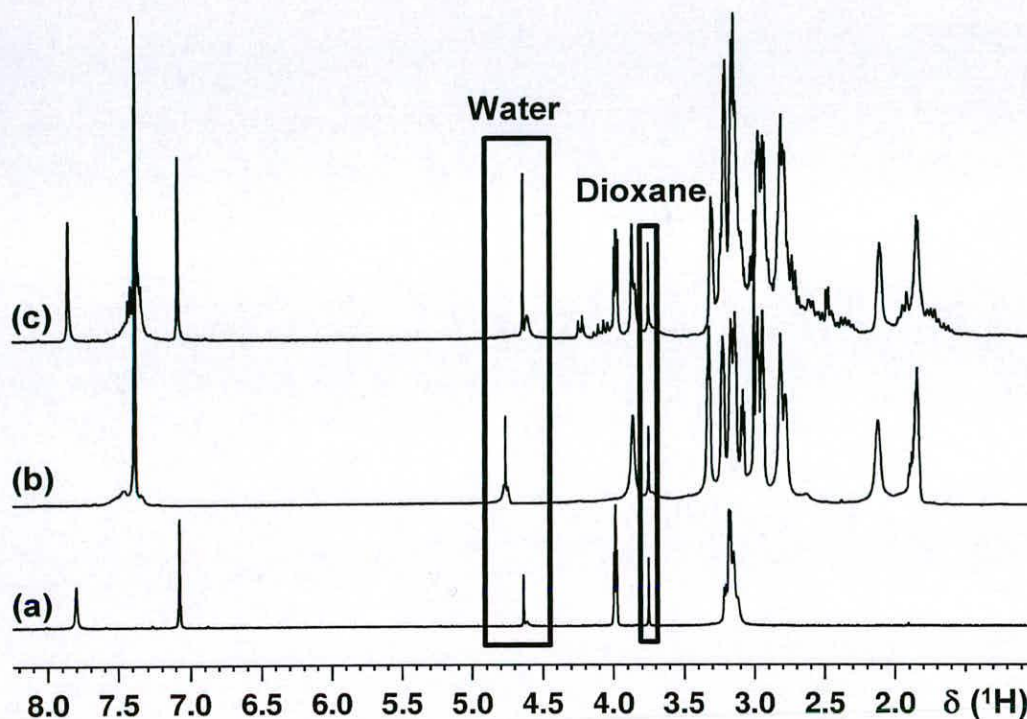


Figure 4.18 1D ^1H NMR spectra showing (a) $\text{Zn}(\text{hist})_2$, (b) xylyl-bicyclam and (c) 24 hours after the addition of $\text{Zn}(\text{hist})_2$ to xylyl-bicyclam. All spectra were recorded in 90 % H_2O / 10 % D_2O at 37 $^\circ\text{C}$.

The linker region of the spectrum can be used to assign configurations of the cyclam rings.¹⁵ The *trans*-I and *trans*-III isomers were found to be present, along with some unreacted xylyl-bicyclam, shown in Figure 4.19. The HPLC-MS results showed the formation of TFA adducts of zinc-bicyclam. There is no evidence for histidine being present based on the LC-MS data. This could be as a result of the

change in pH caused by the addition of TFA as an ion pairing agent, causing displacement of the histidine with TFA. This is also likely to influence the configuration of the macrocycles, as it has been shown that pH can change the ratio of isomers in $\text{Zn}(\text{cyclam})^{2+}$.⁸ There were peaks at 3.04 min and 4.85 min which were unidentified. There was a peak at 12.08 min, which was found to be $[\text{Zn}(\text{cyclam})(\text{TFA})]^+$, one at 12.32 min which corresponded to $[\text{xylyl-bicyclam}]^+$, one at 13.28 min which was found to be $[\text{Zn}(\text{xylyl-bicyclam})(\text{TFA})]^+$, and one at 14.24 min which was found to be $[\text{Zn}_2(\text{xylyl-bicyclam})(\text{TFA})_3]^+$. Formic acid was tried as an ion pairing agent, but good separation could not be achieved. Also, the HPLC-MS was recorded with no ion pairing agent, but this also resulted in poor separation.

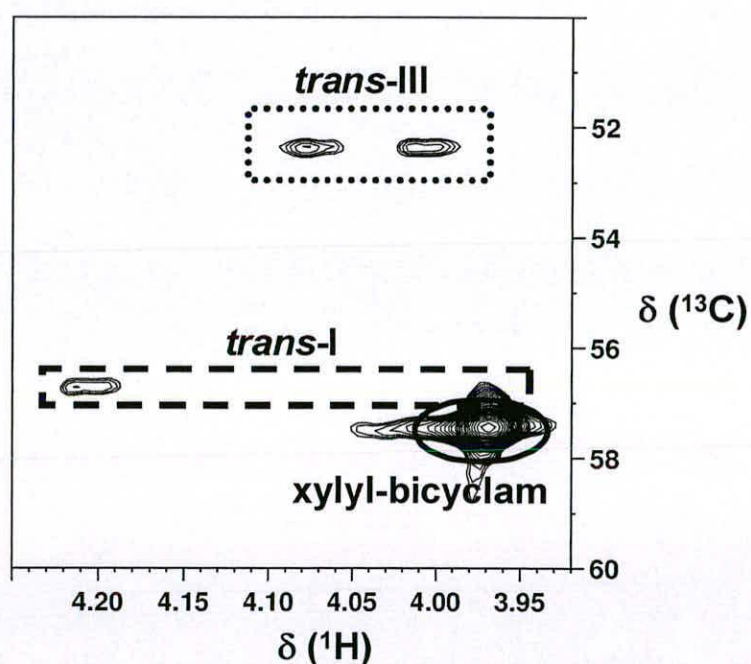


Figure 4.19 2D [^1H , ^{13}C] HSQC NMR spectrum of the product of the reaction of $\text{Zn}(\text{Hist})_2 + \text{xylyl-bicyclam}$. Two configurations of cyclam can be identified from the position of the linker protons shown here, a *trans*-III configuration and a *trans*-I configuration were found.

4.3.9 Addition of Acetate to $\text{Pd}_2(\text{xylyl-bicyclam})](\text{OAc})_4$, **12**

The overall spectrum of **12** did not change when 4 molar equivalents of acetate were added (Figure 4.20). The only change in the spectrum was the increase in intensity of the acetate peak, the rest of the spectrum did not change. This shows that the configuration of the cyclam rings did not change upon addition of acetate.

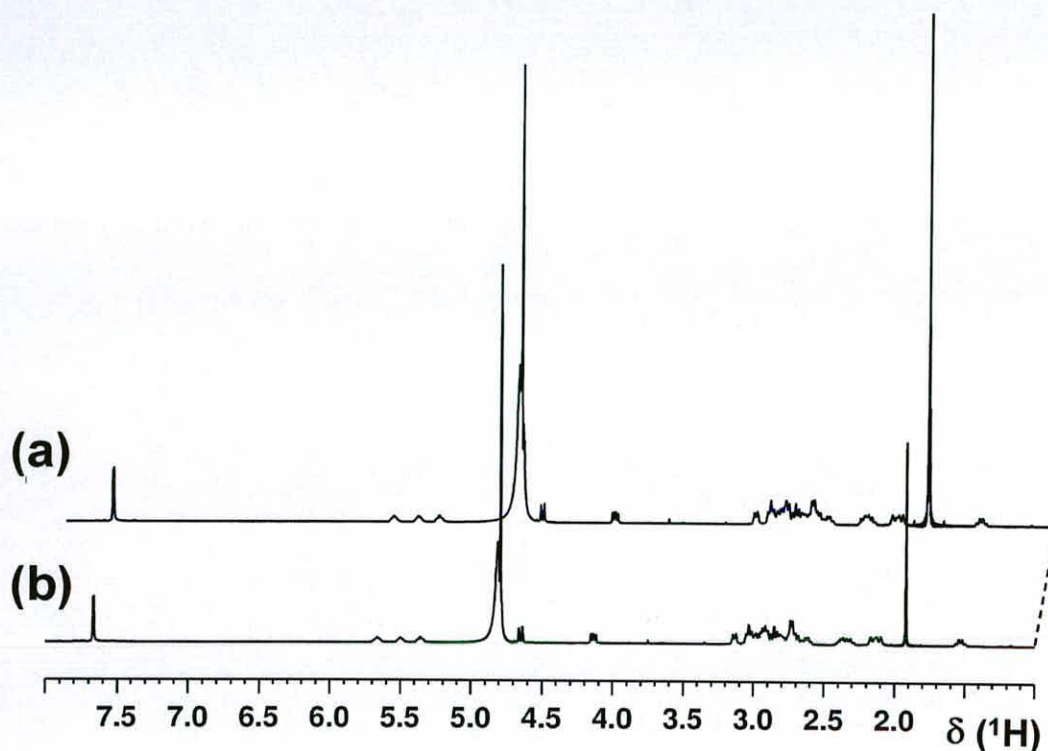


Figure 4.20 Staggered plot of (a) $[\text{Pd}_2(\text{xylyl-bicyclam})](\text{OAc})_4$ in 90 % H_2O / 10 % D_2O , dioxane ref, (b) with the addition of NaOAc (4 molar equiv). The only change observed in the spectrum is the increase in intensity of the acetate peak.

4.3.10 Addition of Acetate to $\text{Co}_2(\text{xylyl-bicyclam})\text{Cl}_4$, **13**

Addition of 6 molar equivalents of sodium acetate to this complex (**13**) resulted in an immediate shift in the spectrum. The 6 initial NH proton resonances

began to lose intensity, and several new peaks appeared. The reaction took 46 hours to reach completion. During this time several intermediate species were formed and disappeared, but these could not be identified due to the complicated nature of the NMR spectra. Once the reaction had reached completion, a 1D ^1H NMR spectrum (Figure 4.21) along with 2D [^1H , ^1H] COSY, TOCSY and NOESY NMR spectra were recorded, and 2D [^1H , ^{15}N] and [^1H , ^{13}C] HSQC spectra. ES-MS was then carried out on the product, and it showed the formation of $[\text{Co}_2(\text{xylyl-bicyclam})(\text{OAc})_4]^{2+}$. No chloride species were observed in the ES-MS, suggesting that all chloride ligands had been replaced with acetate.

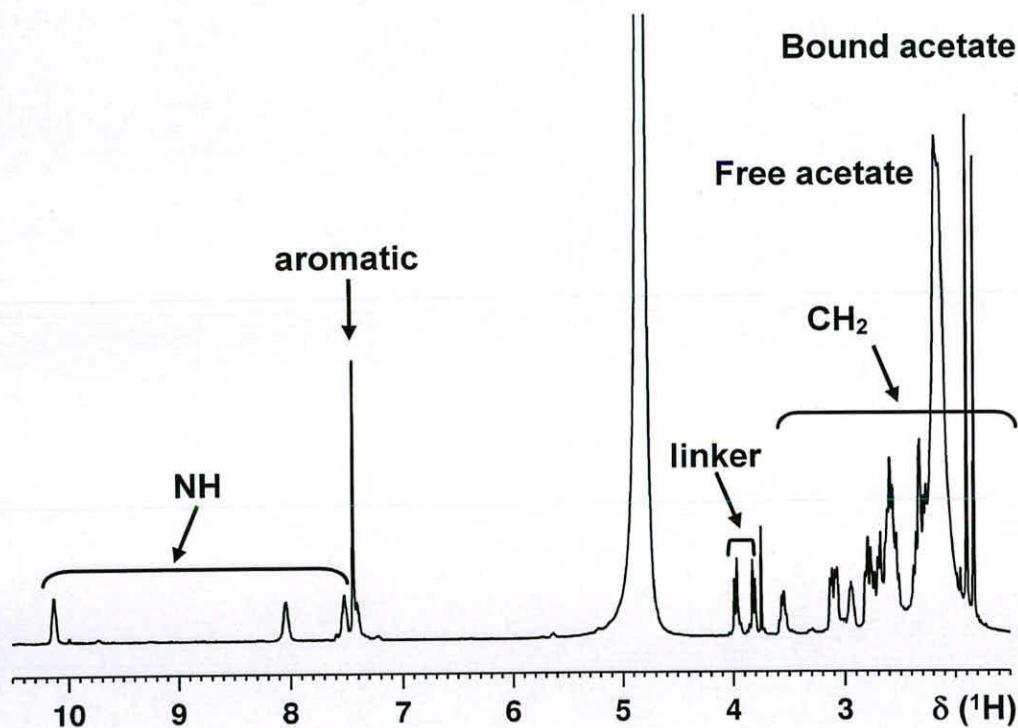


Figure 4.21 1D ^1H NMR spectrum of $\text{Co}_2(\text{xylyl-bicyclam})\text{Cl}_4]\text{Cl}_2 + 6$ molar equivalents of NaOAc, 46 hours after the addition was made. Key regions in the spectrum are highlighted.

NH Proton Resonances

There are 6 NH signals present in the initial chloride complex, but once the reaction had reached equilibrium, there were only 3 observable NH peaks in the [^1H , ^{15}N] HSQC (Figure 4.22). The NH resonances are all shifted downfield compared to the chloride version. One resonance has shifted to 10.2 ppm; this shift could arise because it is directly involved with hydrogen bonding, possibly from an acetate bound to the cobalt, as in the crystal structure of the $[\text{Co}(\text{cyclam})(\text{OAc})_2](\text{BPh}_4)$.

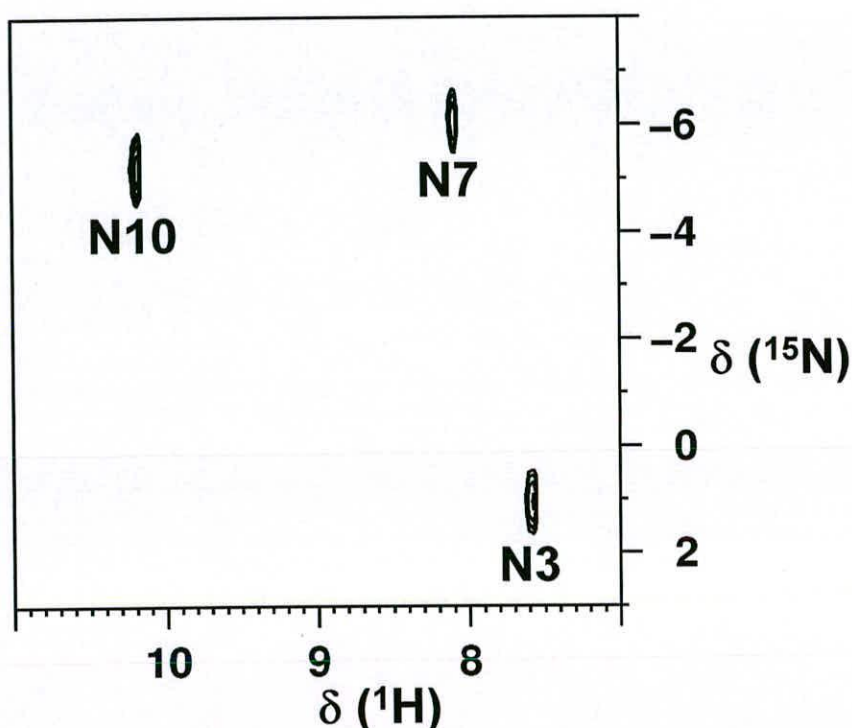


Figure 4.22 2D [^1H , ^{15}N] HSQC NMR spectrum of $\text{Co}_2(\text{xylyl-bicyclam})\text{Cl}_4\text{Cl}_2 + 6$ molar equivalents of NaOAc, recorded in 90 % H_2O / 10 % D_2O , at 25 °C. Three NH signals are observed, showing that both rings must be in the same configuration. For labelling scheme, see Figure 4.23.

Bridging Methylene Proton Resonances

Again, there is a shift from two sets of linker protons in the chloride complex to only one set showing that there is only one configuration present and the cyclam ring is in the same configuration in both rings.

Aromatic Resonances

There is only one resonance for the aromatic protons in the complex, indicating it is a symmetrical complex.

Proton Resonances from the Cyclam Rings

One set of NH peaks and one set of linking CH₂ groups shows that there is only one type of cyclam ring present in solution for the product of the reaction of [Co₂(xylyl-bicyclam)Cl₄]Cl₂ with 6 molar equivalents of sodium acetate. The [¹H, ¹³C] HSQC supports this, as there are 10 observable carbon signals in the region for the resonances from the cyclam rings, shown in Figure 4.23, along with the labelling scheme used. There are also three signals present from acetate, which could arise from two bound acetates, and one free acetate. One of the NH signals, proton 10, shows a NOESY cross peak in the 2D [¹H, ¹H] NOESY NMR spectrum to the signal for proton 12a, showing that these protons are both on the same side of the ring. The NH labelled proton 7 shows NOESY peaks to both proton 5a and proton 8a, showing that these are all on the same face of the cyclam ring. The linker proton 14a shows a NOESY peak to the proton 12a, which is one of the central methylene protons in one of the 3 carbon bridges, showing that proton 12a is axial and on the same face of the

ring as the linker group and the linker is on the same face as the NH labelled 10. The other linker proton, 14b, shows a NOESY cross peak to the signal from proton 2a. Since the linker protons only show interactions with one NH proton, and the UV-vis spectroscopy results show this to be *trans* configuration, it is likely that both the cyclam rings are in the *trans*-III configuration. A *trans*-I configuration would give NOESY signals between the linker and all three NH signals, but this does not happen in this case. The full assignment is listed in Table 4.8.

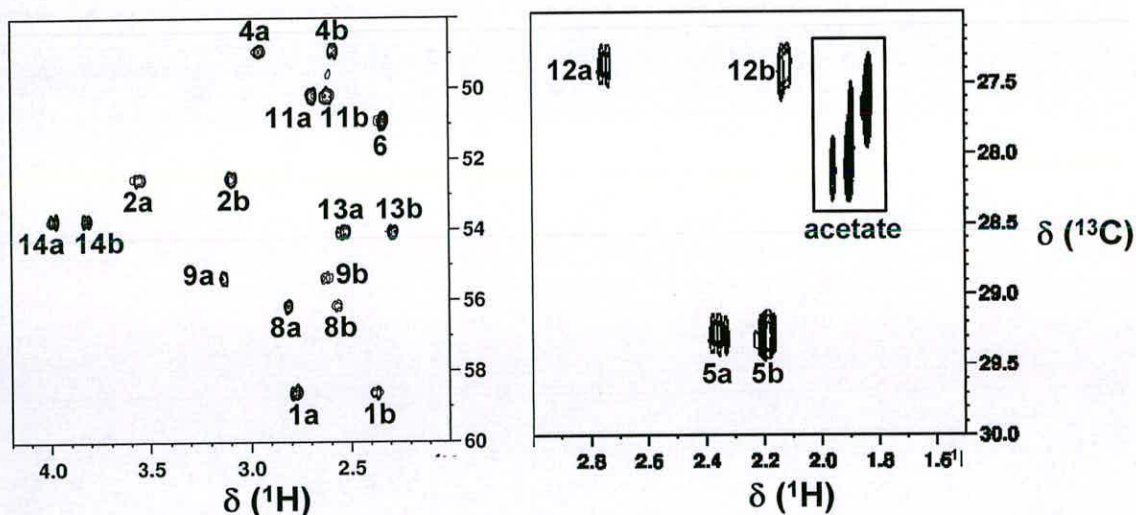
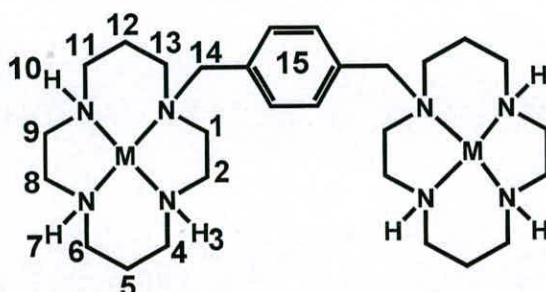


Figure 4.23 2D [^1H , ^{13}C] HSQC NMR spectrum of $\text{Co}_2(\text{xylyl-bicyclam})\text{Cl}_4\text{]Cl}_2 + 6$ molar equiv of NaOAc, recorded in 90 % H_2O / 10 % D_2O at 25 °C. Protons on the same carbon atom are differentiated by a and b. The labelling scheme is also shown.

Table 4.8 ^1H , ^{13}C and ^{15}N Chemical shifts of $\text{Co}_2(\text{xylyl-bicyclam})\text{Cl}_4\text{Cl}_2$, 13, reacted with 6 molar equiv of NaOAc, recorded in 90 % H_2O / 10 % D_2O at 25 °C.

Peak	^1H / ppm	^{13}C / ppm	^{15}N / ppm	Peak	^1H / ppm	^{13}C / ppm	^{15}N / ppm
1a	2.78	58.7		8b	2.56		
1b	2.37			9a	3.13		
2a	3.55	52.6		9b	2.61	55.4	
2b	3.09			10	10.19		
3	7.58		1.1	11a	2.68	50.2	
4a	2.94	48.9		11b	2.60		
4b	2.58			12a	2.74	27.4	
5a	2.33	29.3		12b	2.12		
5b	2.18			13a	2.52	54.1	
6a	2.33	50.9		13b	2.28		
6b				14a	3.98	53.7	
7	8.08		-5.99	14b	3.82		
8a	2.82	56.2		15	7.44	135.4	

4.4 Discussion

4.4.1 Reactions of Xylyl-bicyclam With Zinc Complexes

Zinc is found in the blood, especially on the surface of proteins. It is most commonly found bound to histidine and cysteine.⁹ The reactions in this work using zinc acetate and zinc histidine under physiological conditions were carried out to see if xylyl-bicyclam could bind zinc under such conditions. The results showed that xylyl-bicyclam could complex zinc from zinc acetate under these conditions, 45 % of

the xylyl-bicyclam remained uncomplexed. Three configurations were found, *trans*-I, *trans*-III and *cis*-V, with *trans*-I being the most abundant. When the reaction was repeated with zinc histidine, only the *trans*-I and *trans*-III configurations were observed. The bulky histidine ligand is likely to cause steric hindrance, preventing the formation of the *cis*-V configuration, found in the reaction of Zn(OAc)₂ with xylyl-bicyclam.

4.4.2 Configurations of Metal-Xylyl-Bicyclam Complexes in Solution

The palladium complex, **12**, was found to be in only one configuration, *trans*-III. Pd²⁺ is a d⁸ metal, and favours square-planar complexes, meaning that all its electrons are paired. All the published crystal structures for Pd-cyclam complexes are in the *trans*-III configuration, and NMR studies on various Pd(cyclam)²⁺ complexes in Chapter 3 showed the only configuration present to be *trans*-III. The addition of excess acetate to this complex (**12**) did not result in any change in configuration. This is in contrast to the Zn₂(xylyl-bicyclam)(ClO₄)₄ complex, which has been shown to change configuration in the presence of excess acetate, favouring the *cis*-V configuration.¹⁵ The lack of axial ligands in the case of [Pd₂(xylyl-bicyclam)](OAc)₄, and palladium's strong preference for square-planar coordination seem to prevent any change in configuration. This could be a main factor in its lack of anti-HIV activity.

Configurations of the nickel xylyl-bicyclam complex, **10**, could not be identified, due to the very complicated NMR spectrum. This is due to the presence of both paramagnetic and diamagnetic species in solution. This was also found in the NMR spectra of the [Ni(cyclam)]²⁺ complexes, **4-6**, in Chapter 3, and in

$[\text{Ni}(\text{cyclam})](\text{ClO}_4)_2$.¹⁶ However, the UV-vis spectroscopy showed the presence of one peak, at 456 nm, a d-d transition. Tetrahedral Ni(II) complexes have a strong absorption band of the order $\varepsilon = 10^2 \text{ M}^{-1} \text{ cm}^{-1}$, at approximately 670 nm, absent in these complexes.¹⁷ Furthermore, octahedral Ni(II) complexes show three absorptions bands, corresponding to the three spin-allowed transitions ${}^3\text{A}_{2g} \rightarrow {}^3\text{T}_{2g}$, ${}^3\text{A}_{2g} \rightarrow {}^3\text{T}_{1g}(\text{F})$ and ${}^3\text{A}_{2g} \rightarrow {}^3\text{T}_{1g}(\text{P})$.¹⁷ A *trans*- $[\text{Ni}(\text{cyclam})(\text{H}_2\text{O})_2]\text{Cl}_2 \cdot 4\text{H}_2\text{O}$ complex has been shown to have three absorption bands in the UV-vis spectra, at 333 nm, 507 nm and 667 nm, showing the Ni^{2+} to be octahedrally coordinated.¹⁸ Ni^{2+} is a d^8 metal, and generally shows a strong preference for square-planar coordination, as this results in all the electrons being paired. The UV-vis spectroscopy of **10** suggests that the majority of the complex is in the square planar configuration, however, the peaks for this are obviously masked in the NMR spectrum by the presence of other paramagnetic species. There are two weak shoulder peaks observable in the visible spectrum, at approximately 350 nm and 560 nm, which could be from a minor octahedral configuration.

It is possible for Ni-cyclam complexes to interconvert between *cis* and *trans* configurations, this has been followed by UV-vis spectroscopy, as reported by Billo.¹⁹ He reported the *cis*- $[\text{Ni}(\text{cyclam})(\text{H}_2\text{O})]^{2+}$ could convert to the *trans* form by changing the pH. He also noted that the *trans* isomer was in rapid equilibrium with the planar $[\text{Ni}(\text{cyclam})]^{2+}$, which had a UV-vis absorption peak at 450 nm. This agrees with the value found here for the UV-vis absorption of $\text{Ni}_2(\text{xylyl-bicyclam})(\text{OAc})_4$, **10**, which has a strong absorption band at 456 nm, showing it is a planar configuration. The *cis-trans* isomerism of Ni-cyclam complexes has been shown to be highly pH dependent. At pH = 3, the isomerism is very slow (half-life =

250 days), whereas at pH = 10, the isomerism is very rapid (half-life = 7 s).²⁰ Future work could involve investigating the ¹H NMR spectra of Ni₂(xylyl-bicyclam)(OAc)₄, **10**, at different pH values to see if isomerisation between the paramagnetic or the diamagnetic species can occur and under what conditions this is favoured.

Again, configurations of the copper xylyl-bicyclam complex, **11**, could not be identified due to the presence of a paramagnetic species broadening the NMR spectra. Cu²⁺ is a d⁹ metal, which means it always produces paramagnetic complexes, as there is always an unpaired electron. The acetate peak in the ¹H NMR spectrum was not broadened, which could mean the acetate is not bound to the paramagnetic Cu²⁺ centre, and water is in the axial positions, as in the copper-cyclam complex in Chapter 3. The absorption peak in the UV-vis spectrum is at 513 nm and gives an extinction coefficient of 84 M⁻¹, which is similar to the values found for [Cu(cyclam)(H₂O)₂](OAc)₂, **8**, in Chapter 3, and to Cu(cyclam)(ClO₄)₂.²¹ Both of these Cu-cyclam complexes were shown to be *trans*-III in the solid state, showing that this Cu₂-xylyl-bicyclam is also likely to be in this configuration.

Co³⁺ is a d⁶ metal, and in this case, a low spin complex was synthesised. A high spin complex would have produced broad peaks in the NMR spectrum, due to paramagnetic broadening effects. Co³⁺ is generally found to be low-spin, due to the extra stability for the filled *t*_{2g} orbital, but high-spin Co³⁺ complexes are known, for example in CoF₆³⁻. The chloride complex, **13**, was found to have two cyclam configurations present in solution. Both of these are *trans* configurations, as the UV-vis spectroscopy showed the presence of three absorption bands, which is characteristic of *trans* Co(III) complexes.^{17, 22} It is likely that these configurations are *trans*-III and *trans*-I, as these are the most stable configurations. The solid-state

structure of the analogous cyclam complex, $[\text{Co}(\text{cyclam})\text{Cl}_2]\text{Cl}$, is found to be in the *trans*-III configuration.²³ However, it could be that both chloride and water occupy the axial positions in solution, which would give the appearance of two species in solution. However, the ES-MS data showed no evidence of water being part of the coordination sphere.

4.4.3 Addition of Acetate to $[\text{Co}_2(\text{Xylyl-bicyclamCl}_4)]\text{Cl}_2$

There are many possible reactions that could occur upon the addition of acetate to $[\text{Co}_2(\text{xylyl-bicyclam})\text{Cl}_4]\text{Cl}_2$. It is possible that the chloride could dissociate first and be replaced with water. This could occur up to four times, then the water could be replaced by acetate ions, again up to four times. Or the reaction could involve direct substitution of chloride with acetate, up to four times. Furthermore, the order in which the acetate replaces the chloride could vary, the second acetate to go on could be on the same Co^{3+} as the first acetate, or the other Co^{3+} ion. Additionally, the configurations of the cyclam rings could be influenced by these changes, and could themselves be changing at the same time. Also, one or both of the cyclam rings could adopt a *cis* configuration instead of *trans*, resulting in only one acetate being bound to each Co^{3+} centre. The reaction reached completion after 46 hours. UV-vis spectroscopy on the final product indicates the configuration to be *trans*, as there are 3 absorption bands present in the UV-vis spectrum. Also, there are three NH signals observed in the 2D [^1H , ^{15}N] HSQC NMR spectrum, and only one set of linker protons in the 2D [^1H , ^{13}C] HSQC NMR spectrum, which further supports that the complex is all in the same configuration. The results here indicate a *trans* complex, which is in contrast to the zinc-xylyl-bicyclam complex, which upon

addition of excess acetate, drives the formation of the *cis-V* configuration, which is not apparent in this case.¹⁵

4.5 Conclusions

Xylyl-bicyclam was successfully synthesised. This was reacted with zinc acetate, with the reaction followed by ¹H NMR spectroscopy. The reaction occurred within 5 minutes and reached equilibrium in this time. Three configurations of cyclam were identified from this reaction; *trans-I*, *trans-III* and *cis-V*, with *trans-I* being the most abundant.

Xylyl-bicyclam was also reacted with zinc histidine. This reaction produced two configurations, *trans-I* and *trans-III*. The bulky histidine appears to prevent the folding of the cyclam ring into the *cis-V* configuration.

Pd²⁺, Cu²⁺, Co³⁺ and Ni²⁺ were reacted successfully with xylyl-bicyclam and the products were identified with mass spectrometry, NMR spectroscopy and UV-vis spectroscopy.

Pd₂(xylyl-bicyclam)(OAc)₄ was found to exist in only one configuration, and this was identified as *trans-III*. This was reacted with sodium acetate, but no change in the ¹H NMR spectrum occurred, showing that [Pd₂(xylyl-bicyclam)]⁴⁺ does not readily undergo a configurational change.

[Co₂(xylyl-bicyclam)Cl₄]Cl₂ was found to exist in two *trans* cyclam configurations in aqueous solution. This complex was reacted with sodium acetate, and it was found that there was a significant change in the NMR spectra. The spectrum changed immediately upon addition, with the final product was obtained after 46 hours. Intermediate species formed and disappeared within this time. These were not identified due to their rapid appearance and disappearance. The final

product consisted of only one isomer, shown by only 3 NH peaks in the [^1H , ^{15}N] HSQC. One of the NH peaks is shifted towards a high frequency (10.19 ppm), indicative of it being involved in hydrogen bonding with an acetate ion. The final configuration was identified as *trans*-III using UV-vis and NMR spectroscopy.

$\text{Ni}_2(\text{xylyl-bicyclam})(\text{OAc})_4$ was found to have a mixture of paramagnetic and diamagnetic peaks present in the 1D ^1H NMR spectra. The presence of the two cyclam rings allows a mixture of paramagnetic-paramagnetic, paramagnetic-diamagnetic and diamagnetic-diamagnetic species to be present, as well as different configurations of these combinations to be present.

$\text{Cu}_2(\text{xylyl-bicyclam})(\text{OAc})_4$ was paramagnetic, due to Cu^{2+} being d^9 , therefore always having an unpaired electron. In the 1D ^1H NMR spectrum, there was one unbroadened peak, from the acetate, at 1.93 ppm (23.5 ppm in the ^{13}C dimension). There were five broad peaks observed in the ^1H NMR spectrum. It is possible that acetate is not bound to the Cu^{2+} , and that water is bound in the axial positions, as in the Cu^{2+} -cyclam structure shown in Chapter 3. This would explain why the acetate peak appears to be unbroadened.

None of the metal-xylyl-bicyclam complexes made here were found to be in the *cis*-V configuration in solution, which has been shown to be important in the binding of metal-xylyl-bicyclams to the CXCR4 coreceptor.¹⁵ The inability to form this configuration could explain the reduced activity level of nickel-, copper-, cobalt- and palladium-xylyl-bicyclams against HIV.

4.6 References

- 1 W. Rozenbaum, D. Dormont, B. Spire, E. Vilmer, M. Gentilini, C. Griscelli, L. Montagnier, F. Barre-Sinoussi, and J. C. Chermann, *Lancet*, 1985, **1**, 450-451.
- 2 C. L. Hill, M. S. Weeks, and R. F. Schinazi, *J. Med. Chem.*, 1990, **33**, 2767-2772.
- 3 E. De Clercq, *Nature Rev. Drug Disc.*, 2003, **2**, 581-587.
- 4 E. De Clercq, N. Yamamoto, R. Pauwels, M. Baba, D. Schols, H. Nakashima, J. Balzarini, Z. Debyser, B. A. Murrer, D. Schwartz, D. Thornton, G. Bridger, S. Fricker, G. Henson, M. Abrams, and D. Picker, *Proc. Natl. Acad. Sci. USA*, 1992, **89**, 5286-5290.
- 5 G. J. Bridger, R. T. Skerlj, D. Thornton, S. Padmanabhan, S. A. Martellucci, G. W. Henson, M. J. Abrams, N. Yamamoto, K. De Vreese, R. Pauwels, and E. De Clercq, *J. Med. Chem.*, 1995, **38**, 366-378.
- 6 E. De Clercq, *Mole. Pharm.*, 2000, **57**, 833-839.
- 7 J. A. Este, C. Cabrera, E. De Clercq, S. Struyf, J. Van Damme, G. Bridger, R. T. Skerlj, M. J. Abrams, G. Henson, A. Gutierrez, B. Clotet, and D. Schols, *Mole. Pharm.*, 1999, **55**, 67-73.
- 8 X. Liang, M. Weishäupl, J. A. Parkinson, S. Parsons, P. A. McGregor, and P. J. Sadler, *Chem. Eur. J.*, 2003, **9**, 4709-4717.
- 9 D. W. Christianson and R. S. Alexander, *J. Am. Chem. Soc.*, 1989, **111**, 6412-6419.
- 10 L. D. Couves, D. N. Hague, and A. D. Moreton, *J. Chem. Soc. Dalton Trans.*, 1992, 217-223.

- 11 M. M. Harding and S. J. Cole, *Acta Cryst.*, 1963, **16**, 643-650.
- 12 R. H. Kretsinger, F. A. Cotton, and R. F. Bryan, *Acta Cryst.*, 1963, **16**, 651-657.
- 13 A. Filali, J. J. Yaouanc, and H. Handel, *Angew. Chem. Int. Ed.*, 1991, **30**, 560-561.
- 14 W. Yang, C. M. Giandomenico, M. Sartori, and D. A. Moore, *Tetrahedron Lett.*, 2003, **44**, 2481-2483.
- 15 X. Liang, J. A. Parkinson, M. Weishäupl, R. O. Gould, S. J. Paisey, H.-S. Park, T. M. Hunter, C. A. Blindauer, S. Parsons, and P. J. Sadler, *J. Am. Chem. Soc.*, 2002, **124**, 9105-9112.
- 16 P. J. Connolly and E. J. Billo, *Inorg. Chem.*, 1987, **26**, 3224-3226.
- 17 F. A. Cotton and G. Wilkinson, 'Advanced Inorganic Chemistry', John Wiley and Sons, New York, 1988.
- 18 K. Mochizuki and T. Kondo, *Inorg. Chem.*, 1995, **34**, 6241-6243.
- 19 E. J. Billo, *Inorg. Chem.*, 1981, **20**, 4019-4021.
- 20 E. K. Barefield, A. Bianchi, E. J. Billo, P. J. Connolly, P. Paoletti, J. S. Summers, and D. G. Van Derveer, *Inorg. Chem.*, 1986, **25**, 4197-4202.
- 21 A. W. Addison and E. Sinn, *Inorg. Chem.*, 1983, **22**, 1225-1228.
- 22 Y. Hung, L. Y. Martin, S. C. Jackels, A. M. Tait, and D. H. Busch, *J. Am. Chem. Soc.*, 1977, **99**, 4029-4039.
- 23 M. E. Sosa-Torres and R. A. Toscano, *Acta Cryst.*, 1997, **C53**, 1585-1588.

Chapter 5 Synthesis and Solution Studies of Pyridyl Isocyclam and its Metal Complexes

5.1 Introduction

5.1.1 Anti-HIV Macrocycles

In 1999, Bridger *et al.* reported the results of a study that involved varying the size and substituents of bis-tetraazamacrocycles, such as xylyl-bicyclam (AMD3100) with the aim of improving the anti-HIV activity of these bis macrocycles.¹ Many analogues were tested, with neutral heteroatoms, such as oxygen and sulphur, and heteroaromatic groups being introduced into the macrocycle as a replacement for the amino groups in AMD 3100. It was found that the introduction of one or more heteroatoms into the macrocyclic ring resulted in substantially reduced activity.

However, it was found that introducing a pyridine ring to the macrocycle gave activity comparable with that of the saturated macrocycle. The ring size of the macrocycle with the newly incorporated pyridine ring was also varied between 12-16 members per ring. The optimum structure with a pyridine ring incorporated was a new ligand, called AMD3329, which had better activity than AMD3100. The cyclam ring has been replaced with the pyridyl isocyclam, **14**, shown in Figure 5.1. The active form is the bis-macrocycle, **15**. The anti-HIV activity levels of AMD 3100 (xylyl-bicyclam) and AMD 3329 are shown in Table 5.1. AMD3329 inhibited HIV-1 and HIV-2 replication at a 3-5 fold lower concentration than that of AMD3100 required to inhibit viral replication by 50%.

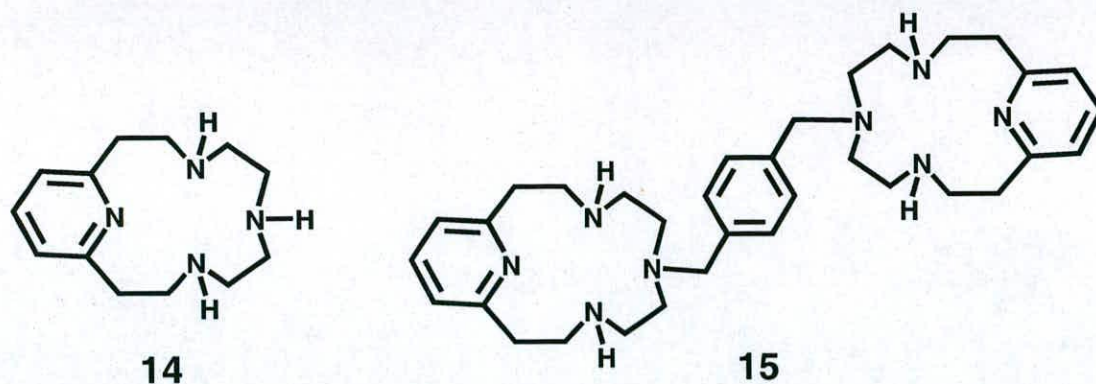
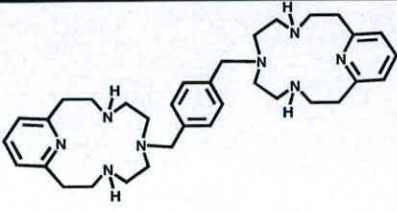
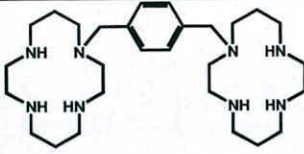


Figure 5.1 Structure of **14**, referred to as pyridyl isocyclam, and the structure of AMD 3329, referred to as **15**.

The macrocycle is still a 14-membered ring, with 4 nitrogen groups incorporated into the ring as for a cyclam. However, in the case of AMD 3329, the order of the carbon bridges between the nitrogen groups is not the same as it is in cyclam. In AMD 3329, the sequence is 2, 3, 3, 2 whereas in cyclam it is 2, 3, 2, 3. The pyridine ring in AMD 3329 adds rigidity compared to the more flexible cyclam.

In this thesis, studies were carried out on one of the constituent macrocycles of AMD 3329, 4,7,10,17-tetraaza-bicyclo[11.3.1]heptadeca-1(16),13(17),14-triene, **14**, and the bis-macrocycle **15**, including the binding of metal ions and its properties once complexed with metals, the configurations of metal adducts using ^1H , ^{13}C , and ^{15}N NMR spectroscopy. ^{111}Cd NMR studies aided the characterisation of the novel metallomacrocycles.

Table 5.1 Comparison of the Anti-HIV Activities of AMD 3100 and AMD 3329¹

Compound	Structure	EC ₅₀ (μM)		CC ₅₀ (μM)
		HIV-1 (III)	HIV-2 (ROD)	
AMD3329 (15)		0.0008	0.0016	194
Xylyl-bicyclam (AMD3100)		0.0042	0.0059	> 421 ^a

^a highest concentrations tested.

5.1.2 Cadmium Chemistry

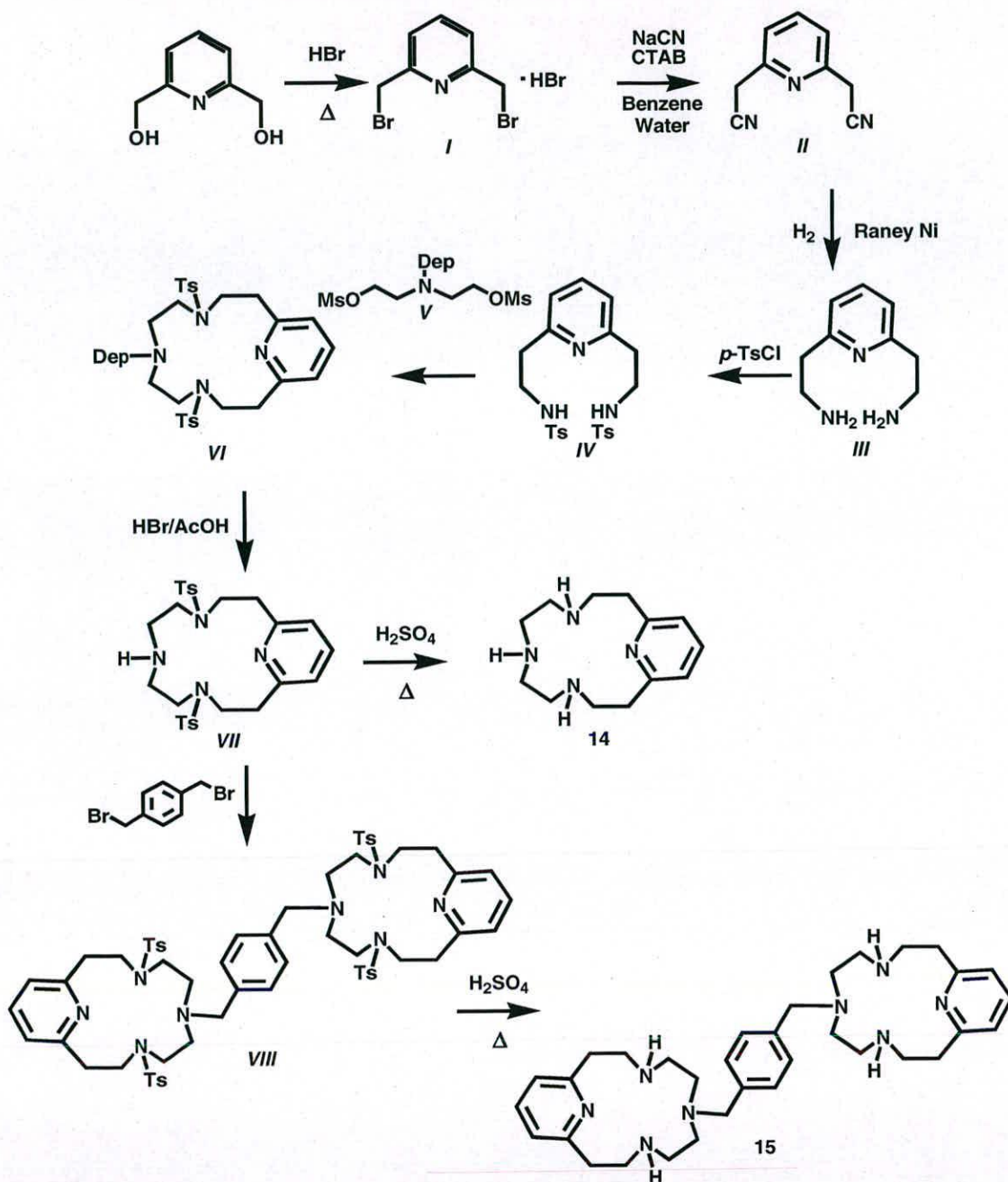
Cadmium, along with zinc and mercury, makes up group 12 of the periodic table. Its usual oxidation state is +2. Cadmium chemistry closely resembles that of zinc, and it can be used as an isomorphous replacement for zinc.² ⁶⁷Zn has a nuclear spin of 5/2, and as such produces very broad NMR lines, making it hard to study using NMR. Zn(II) is readily available in the body and it may play a key role in the activity of antiviral macrocycles. It is possible that the xylyl-bicyclam picks up zinc from the blood. The biological activity of metallomacrocycle complexes appears to depend on recognition of the membrane receptor protein CXCR4 via interactions with amino acid side chains. Cadmium NMR spectroscopy has been used in many cases to study interesting structural and dynamic problems in inorganic and bioinorganic chemistry.² Cadmium has many favourable chemical and magnetic properties which make it ideal for use as a replacement for several metal ions such as

the coordination of Cd^{2+} is similar to that of Zn^{2+} and Ca^{2+} . Also, Cd^{2+} and Ca^{2+} have very similar ionic radii, therefore Cd^{2+} can also be used as a replacement for Ca^{2+} .³ Cadmium is often used as a starting point to elucidate the structure of biomolecules that contain zinc, although there have been significant differences reported between the analogous Zn and Cd complexes. Furthermore, Cd^{2+} chemical shifts are extremely sensitive to the nature, number and geometric arrangement of the ligands within the coordination sphere. Both naturally occurring isotopes of cadmium (^{111}Cd and ^{113}Cd) have spin = $\frac{1}{2}$ isotopes, which are present in 12.7 % and 12.3 % natural abundance, respectively. The absolute sensitivity of ^{111}Cd is 7.6 times that of ^{13}C . ^{111}Cd with 96 % enrichment is commercially available, and the enrichment results in an 8 fold enhancement in sensitivity. Cadmium NMR can therefore be used to study complexes and examine their binding sites in proteins. Work has previously been carried out in our laboratory on ^{111}Cd cyclam complexes, proving that this is an effective and useful technique.⁴

5.2 Experimental

5.2.1 Synthesis of **14**

Macrocycle **14** was synthesised using a method based on a previously published synthetic route to AMD 3329, as shown in Scheme 5.1, using the compounds *I* - *VII*.¹



Scheme 5.1 Synthetic route to 14

Synthesis of 2,6-Bis(bromomethyl)pyridine Hydrobromide, I

2,6-Bis(bromomethyl)pyridine hydrobromide was made using a published method, as shown in Scheme 5.1.⁵

2,6-Pyridinedimethanol (2.3g, 16.5 mmol) was dissolved in hydrobromic acid (48 %, 30 mL) and acetic anhydride (150 mL) was added and the reaction was heated at 100 °C overnight. Upon cooling, a powder formed, which was separated and washed with ethyl acetate to give 2,6-bis(bromomethyl)pyridine hydrobromide (**I**) as a colourless solid (4.9 g, 14.1 mmol, 87 % yield).

¹H NMR (250 MHz, DMSO-*d*₆) 7.87 (1H, t, J = 7.7 Hz), 7.51 (2 H, d, J = 7.7 Hz), 4.70(4H, s).

Synthesis of (6-cyanomethyl-pyridin-2-yl)-acetonitrile, **II**

2,6-Bis(bromomethyl)pyridine hydrobromide (**I**, 12.0 g, 34 mmol) was dissolved in a mixture of benzene (100 mL) and water (50 mL) whilst under N₂. Cetyltrimethylammonium bromide (1.2 g, 3.4 mmol) was added, and sodium cyanide (10.2 g, 208 mmol) was then added with stirring. The reaction was heated under reflux (90 °C) for 4 hours and then allowed to cool to room temperature. The aqueous layer was then separated and washed with benzene (2 x 100 mL) and dichloromethane (2 x 75 mL). The combined organic layers were then dried using sodium sulfate. This was removed by filtration and the solvent removed under high vacuum. This produced a brown crystalline solid. A solution of this in CH₂Cl₂ was passed through a short plug of basic alumina gave a white solid (**II**, 4.6 g, 29.3 mmol, 86 % yield).

¹H NMR (CDCl₃, 500 MHz) : 7.79 (t, 1H, J = 7.78 Hz), 7.40 (d, 2H, J = 7.78 Hz), 3.94 (s, 4H).

ES-MS : m/z = 157.8 [M+H]⁺.

Synthesis of 2,6-Bis(2-aminoethyl)pyridine, *III*

The dinitrile *II* (2.0 g, 12.7 mmol) was dissolved in methanol saturated with ammonia (50 mL). Raney nickel (5 g) was added and the mixture was hydrogenated at 45 psi and room temperature for 48 hours. The catalyst was removed by filtration through Celite and the solvent was removed under high vacuum. This resulted in a brown oil (*III*, 1.5 g, 9.09 mmol, 71 % yield).

^1H NMR (CDCl_3 , 250 MHz) : 7.53 (t, 1H, $J = 7.6$ Hz), 7.01 (d, 2H, $J = 7.6$ Hz), 3.08 (t, 4H, $J = 6.4$ Hz), 2.95-2.83 (m, 4H).

ES-MS : $m/z = 165.8$ $[\text{M}+\text{H}]^+$.

Synthesis of 2,6-Bis(*N,N'*-*p*-toluenesulfonyl-2-aminoethyl)pyridine, *IV*

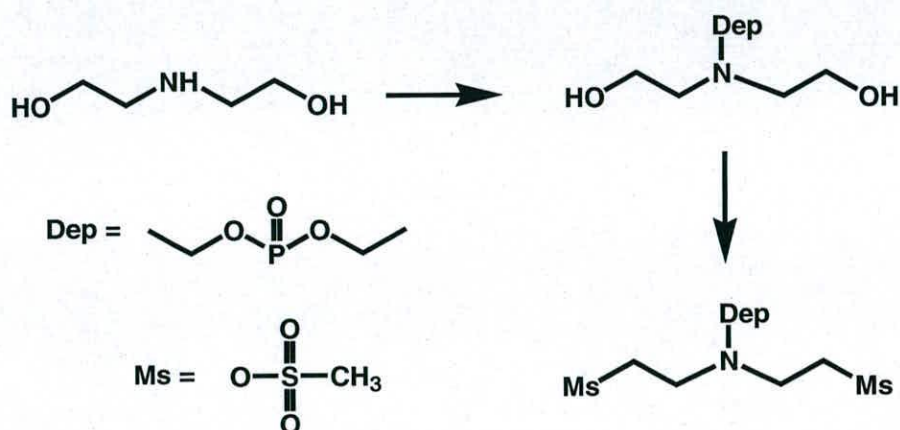
A solution of *p*-toluene-sulfonyl chloride (2.34 g, 13.33 mmol, 2.2 molar equiv) in DCM (50 mL) was added dropwise over one hour to a solution of the diamine *III* (1.0 g, 6.06 mmol) in DCM (100 mL) and triethylamine (2 mL). The mixture was then allowed to stir at room temperature under N_2 overnight. The solution was washed with saturated aqueous sodium bicarbonate and brine, and the organic layer was dried with Na_2SO_4 . This was removed by filtration and the solvent removed under high vacuum to give a brown oil. This was then purified using column chromatography on silica gel ($\text{CH}_2\text{Cl}_2/\text{MeOH}$ 98:2) to give a white solid (*IV*, 1.48 g, 3.13 mmol, 51 % yield.)

^1H NMR (CDCl_3 , 250 MHz) : 7.71 (d, 4H, 8.3 Hz), 7.43 (t, 1H, $J = 7.7$ Hz), 7.25 (d, 4H, 8.3 Hz), 6.90 (d, 2H, $J = 7.7$ Hz), 5.81 (t, 3H), 3.35-3.25 (m, 4H), 2.86 (t, 4H, 6.3 Hz), 2.39 (s, 6H).

ES-MS : $m/z = 474.0$ $[\text{M}+\text{H}]^+$.

Synthesis of N-(diethoxyphosphoryl)diethanolamine, V

N-(Diethoxyphosphoryl)-O,O'-bis(2-methylsulfonyl)diethanolamine was made using a published method, shown in Scheme 5.2.⁶



Scheme 5.2 Synthetic route to N-(diethoxyphosphoryl)-O,O'-bis(2-methylsulfonyl)diethanolamine, V, for use in Scheme 5.1

A solution of diethyl chlorophosphate (16.4 g, 96 mmol) in DCM (50 mL) was added dropwise to a solution of diethanolamine (10.0 g, 96 mmol) in DCM and triethylamine (16 mL) dropwise over one hour. The mixture was then left to stir at room temperature overnight. The solution was then washed with brine (100 mL) and the organic layer dried over Na_2SO_4 . This was removed by filtration and the solvent evaporated off to give a colourless oil. (12.2 g, 50.6 mmol, 52 %)

^1H NMR (250 MHz, CDCl_3) : 3.81-4.02 (m, 8H), 3.31-3.43 (m, 4H), 1.32 (td, 6H, $J = 7.2$ Hz, $J_{P-H} = 0.9$ Hz).

A solution of N-(diethoxyphosphoryl)diethanolamine (12 g, 49.7 mmol) in

DCM (200 mL) and triethylamine (20.4 mL) was cooled to 0 °C. A solution of methanesulfonyl chloride (12.0 g, 104 mmol, 2.1 molar equiv) in DCM (100 mL) was added dropwise to the chilled solution over a period of two hours. The reaction mixture was then left to stir overnight under N₂. The solution was then washed with saturated aqueous ammonium chloride (200 mL) and brine (200 mL). The organic layer was then dried using Na₂SO₄ for one hour and then this was removed by filtration. The solution was then dried under high vacuum to give an orange oil (**V**, 15.1 g, 38 mmol, 76 % yield).

¹H NMR (250 MHz, CDCl₃) : 4.29 (t, 4H, *J* = 5.6 Hz), 3.81-4.02 (m, 4H), 3.41 (dt, 4H, *J* = 5.6 Hz, ²*J*_{P-H} = 11.9 Hz), 3.02 (s, 6H), 1.32 (td, 6H, *J* = 7.1 Hz, *J*_{P-H} = 0.9 Hz).

ES-MS : *m/z* = 397.9 [M+H]⁺.

Macrocyclization, **VI**

A solution of the ditosylate (**IV**, 346 mg, 0.63 mmol) was prepared in anhydrous DMF (100 mL) with stirring under nitrogen. Cesium carbonate (619 mg, 1.9 mmol) was added and the yellow solution was heated to 65 °C. A solution of N-(diethoxyphosphoryl)-O,O'-bis(2-methylsulfonyl)diethanolamine (**V**, 167 mg, 0.63 mmol) was prepared in anhydrous DMF (100 mL) and added dropwise to the first solution over a period of 8 hours. The reaction was then stirred at 65 °C for 24 hours. The resulting yellow solution was concentrated to dryness to give an orange product. This was partitioned between CH₂Cl₂ (150 mL) and brine (90 mL). The aqueous layer was then further extracted with CH₂Cl₂ (2 x 50 mL) and the combined organic layers were dried over anhydrous magnesium sulfate. Once filtered, the

clear yellow solution was concentrated to dryness to give an orange oil. This was purified using column chromatography on silica gel (hexane : ethyl acetate, 9:1) to give a white powder (**VI**, 209 mg, 46 % yield).

^1H NMR (CDCl_3 , 250 MHz) : 7.66 (d, 4H, 8.4 Hz), 7.49 (t, 1H, $J = 7.8$ Hz), 7.25 (d, 4H, $J = 8.4$ Hz), 6.99 (d, 2H, 7.8 Hz), 3.93-3.83 (m, 4H), 3.63-3.56 (m, 4H), 3.02-2.95 (m, 4H), 2.80-2.73 (m, 4H), 2.50-2.39 (m, 4H), 2.24 (s, 6H), 1.22 (td, 6H, $J = 7.0$ Hz).

ES-MS : $m/z = 679.1$ $[\text{M}+\text{H}]^+$.

Removal of Dep Protecting Group, **VII**

A solution of the protected macrocycle (**VI**, 180 mg, 0.25 mmol) was dissolved in glacial acetic acid (4 mL) and 30 % HBr/acetic acid (2 mL) was added. The reaction mixture was then stirred at room temperature for 2 hours. Ether (250 mL) was added to precipitate a white solid. This was allowed to settle, and the ether was removed by decantation. The solid was washed with ether (3 x 100 mL), and the solid was dried under high vacuum. The solid was partitioned between sodium hydroxide (1 M, 5 ml) and dichloromethane (50 mL). The organic layer was separated and dried over sodium sulfate. This was removed by filtration and the solvent was removed under high vacuum to give a white solid (**VII**, 83 mg, 0.151 mmol, 61 % yield).

^1H NMR (360 MHz, CDCl_3) : 7.65 (d, 4H, $J = 8.2$ Hz), 7.45 (t, 1H, $J = 7.7$ Hz), 7.28 (d, 4H, $J = 8.2$ Hz), 7.01 (d, 2H, $J = 7.7$ Hz), 3.64-3.59 (m, 4H), 3.08-3.02 (m, 4H), 2.98 (t, 4H, $J = 6.3$ Hz), 2.51 (t, 4H, $J = 6.3$ Hz), 2.40 (s, 6H).

^{13}C NMR (360 MHz, CDCl_3) : 157.8, 143.2, 136.8, 135.6, 129.5, 127.1, 121.2, 49.7,

49.4, 47.9, 37.9, 21.3.

ES-MS : $m/z = 543.2 [M+H]^+$.

Removal of Tosyl Protecting Groups, **14**

A solution of the di-protected macrocycle (**VII**, 25 mg, 0.046 mmol) was dissolved in concentrated H_2SO_4 (1 mL) and stirred at 110 °C for two hours. The dark brown solution was allowed to cool to room temperature and the pH was adjusted to pH 14 with 10 M NaOH. The aqueous solution was extracted with $CHCl_3$ (3 x 20 mL) and the combined organic extracts were dried using $MgSO_4$. This was concentrated to give a pale yellow oil, **14** (8 mg, 0.034 mmol, 74 % yield).

1H NMR (360 MHz, $CDCl_3$) : 7.55 (t, 1H, $J = 7.6$ Hz), 7.04 (d, 2H, $J = 7.6$ Hz), 3.24-3.17 (m, 4H), 3.14-3.07 (m, 4H), 2.92-2.87 (m, 4H), 2.86-2.82 (m, 4H)

^{13}C NMR (69 MHz, $CDCl_3$) : 137.4, 121.8, 47.7, 46.4, 46.0, 35.7.

ES-MS : $m/z = 234.2 [M+H]^+$

5.2.2 Synthesis of **15**

Ligand **15** was synthesised using the synthetic route shown in Scheme 5.1, using compounds **I-VIII**.

Dimerisation, **VII**

To a solution of the di-protected tetraazamacrocyclic (**VII**, 40 mg, 0.073 mmol) in anhydrous CH_3CN (5 mL) was added α,α' -dibromo-*p*-xylene (9.8 mg, 0.037 mmol, 0.5 molar equiv) and potassium carbonate (31 mg, 0.22 mmol, 3.0 molar equiv), and the mixture was heated to reflux for 18 h with stirring whilst under

N₂. The reaction mixture was allowed to cool to room temperature and concentrated under high vacuum and the residue was partitioned between CH₂Cl₂ (30 mL) and H₂O (15 mL). The aqueous layer was separated and extracted with CH₂Cl₂ (2 x 15 mL). The combined organic phases were dried (MgSO₄) and concentrated, and the residue was purified by column chromatography on silica gel using ethyl acetate : hexane (1:1), giving the fully protected bis-tetraazamacrocyclic (**VIII**, 38 mg, 0.032 mmol, 86 % yield).

¹H NMR (360 MHz, CDCl₃) : 7.58 (d, 8H, J = 8.17 Hz), 7.49 (t, 2H, J = 7.5 Hz), 7.24 (d, 8H, J = 8.17 Hz), 7.08 (s, 4H), 6.97 (d, 4H, J = 7.5 Hz), 3.75-3.67 (m, 8H), 3.44 (s, 4H), 3.04-2.97 (m, 8H), 2.82-2.74 (m, 8H), 2.41 (s, 12H), 2.17-2.09 (m, 8H).

¹³C NMR (360 MHz, CDCl₃) : 160.3, 144.3, 138.5, 138.2, 137.8, 130.7, 129.7, 128.1, 123.5, 60.8, 54.1, 49.8, 49.1, 40.2, 22.5.

ES-MS : m/z = 1188.1 [M+H]⁺.

Removal of Ts Group, **15**

A solution of protected bis-tetraazamacrocyclic (**VIII**, 30 mg, 0.025 mmol) was dissolved in concentrated H₂SO₄ and stirred at 110 °C for two hours. The dark brown solution was allowed to cool to room temperature and the pH was adjusted to pH 14 with 10M NaOH. The aqueous solution was extracted with CHCl₃ (3 x 20 mL) and the combined organic extracts were dried using MgSO₄. This was concentrated to give a pale yellow oil, **15** (13 mg, 0.022 mmol, 88 % yield).

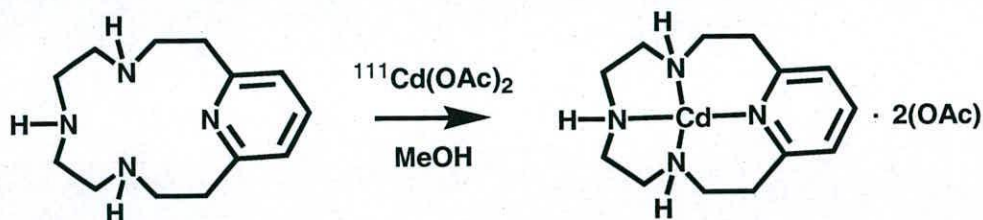
¹H NMR (500 MHz, CDCl₃) : 7.59 (t, 2H, J = 7.53 Hz), 7.03 (d, 4H, J = 7.53 Hz), 6.48 (s, 4H), 3.34 (s, 4H), 3.07-3.02 (m, 4H), 3.02-2.96 (m, 4H), 2.66-2.59 (m, 4H), 2.57-2.49 (m, 4H).

^{13}C NMR (125 MHz, CDCl_3) : 139.6, 124.0, 131.3, 61.8, 50.7, 39.8, 50.0, 56.4.

ES-MS : $m/z = 571.5$ $[\text{M}+\text{H}]^+$.

5.2.3 Preparation of ^{111}Cd Acetate Complex, **16**

The $^{111}\text{Cd}(\text{II})$ complex of macrocycle **14** was prepared using method based on $^{111}\text{Cd}(\text{cyclam})$ complexes.⁴



Scheme 5.3 Synthetic route to **16**

$^{111}\text{CdO}_2$ (1.64 mg, 0.0128 mM) was dissolved in acetic acid (2 molar equiv, 1 M, 25.4 μL) using a sonic bath until all the red $^{111}\text{CdO}_2$ had been converted to white $^{111}\text{Cd}(\text{OAc})_2$. The excess water was then removed using high vacuum to give $^{111}\text{Cd}(\text{OAc})_2$. (2.46 mg, 83 % yield).

The macrocycle **14** (2 mg, 0.0085 mmol) was dissolved in methanol (1 mL) and $^{111}\text{Cd}(\text{OAc})_2$ (2.0 mg, 1 molar equiv, 0.0085 mmol) was added. The solution was refluxed for two hours under N_2 with stirring. The clear solution was then filtered and concentrated under vacuum until a white precipitate had formed. The precipitate was filtered off and washed with ether and dried under high vacuum to give **16** (3.2 mg, 0.0069 mmol, 81 % yield). It was dissolved in 90 % H_2O / 10 % D_2O (600 μL , 12 mmol, pH = 6.8) and 2D [^1H , ^1H] COSY, NOESY and TOCSY,

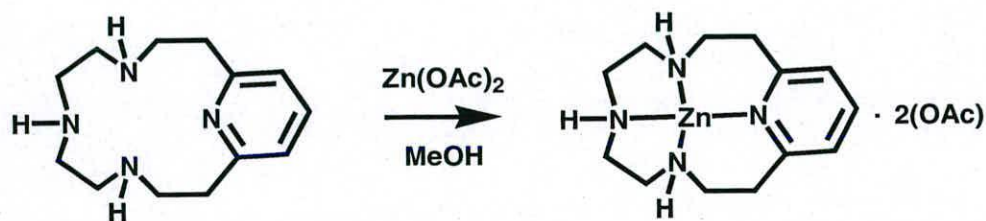
[^1H , ^{13}C] HSQC, [^1H , ^{15}N] HSQC and [^1H , ^{111}Cd] HSQC NMR spectra were recorded.

ES-MS : $m/z = 403.9$ [M-OAc] $^+$.

Selected IR (KBr, cm^{-1}): 3441 s (NH), 2925 m (CH), 2359 s (CH), 1573 m (CO), 1417 m (CO), 670 w (pyridine), 474 w (pyridine).

5.2.4 Preparation of Zn Acetate Complex, **17**

Complex **17** was prepared in the same way as the ^{111}Cd complex, as shown in Scheme 5.4.



Scheme 5.4 Synthetic route to **17**

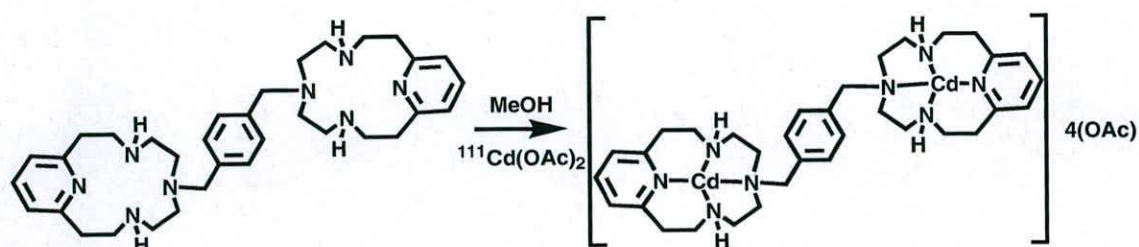
$\text{Zn}(\text{OAc})_2$ (0.0017 mmol, 3 mg) was dissolved in methanol (2 mL) and macrocycle **14** (1 molar equiv, 0.0017 mmol, 4 mg) was added. The reaction was then heated under reflux for 2 hours. The clear solution was then filtered and concentrated under vacuum until a white precipitate had formed. The precipitate was filtered off and washed with ether and dried under high vacuum to give **17** (5.3 mg, 0.0013 mmol, 76 % yield). It was dissolved in 90 % H_2O / 10 % D_2O (600 μL , 12 mmol, pH = 6.9) and 2D [^1H , ^1H] COSY, NOESY and TOCSY, [^1H , ^{13}C] HSQC and [^1H , ^{15}N] HSQC NMR spectra were recorded.

ES-MS : $m/z = 357.2$ $[M-OAc]^+$.

Selected IR (KBr, cm^{-1}): 3466 s (NH), 2359 s (CH), 1637 m (NH), 1572 m (CO), 1410 m (CO), 1384 (CO), 643 w (pyridine).

5.2.5 Preparation of ^{111}Cd Acetate Complex, **18**

The synthesis of **18** was based on the synthesis of similar zinc-xylyl-bicyclam complexes,⁷ and is shown in Scheme 5.5.



Scheme 5.5 Synthetic route to **18**

Ligand **15** (5 mg, 0.0087 mmol) was dissolved in methanol (1 mL) and $^{111}Cd(OAc)_2$ (4.0 mg, 2 molar equiv, 0.0175 mmol) was added. The solution was refluxed for two hours under N_2 with stirring. The clear solution was then filtered and concentrated under vacuum until a white precipitate had formed. The precipitate was filtered off and washed with ether and dried under high vacuum to give **18** (7.5 mg, 0.0073 mmol, 84 % yield). It was dissolved in 90 % H_2O / 10 % D_2O (600 μL , 12 mmol, pH = 6.8) and $[^1H, ^1H]$ COSY, NOESY and TOCSY, $[^1H, ^{13}C]$ HSQC, $[^1H, ^{15}N]$ HSQC and $[^1H, ^{111}Cd]$ HSQC spectra were recorded.

ES-MS : $m/z = 455.3$ $[M-2OAc]^{2+}$, 426.3 $[M-3OAc + H]^{2+}$.

Selected IR (KBr, cm^{-1}): 3420 s (NH), 2918 m (CH), 2870 s (CH), 1573 m (CO), 1412 m (CO), 620 w (pyridine).

5.2.6 Addition of Acetate to Zn Complex, 17

Complex **17** (1 mg, 0.0024 mmol) was dissolved in 90 % H₂O / 10 % D₂O (600 μL, pH = 6.6) and a 1D ¹H NMR spectrum was recorded. Then 1 molar equivalent of NaOAc (1 M, 2.4 μL) was added, and the pH was adjusted to pH = 6.8 with acetic acid and sodium hydroxide. Another 1D ¹H NMR spectrum was recorded. 1D spectra were recorded over 2 hours. This was repeated until 10 molar equivalents of acetate had been added, with the pH being adjusted to pH = 6.8 each time.

5.2.7 pH Titration of 14

Macrocycle **14** (2.3 mg, 0.0098 mmol) was dissolved in 90 % H₂O / 10 % D₂O (600 μL) to give a clear, colourless solution. Sodium perchlorate (7 mg, 0.1 M) was added. The pH of the solution was measured and a 1D NMR spectrum was recorded. The pH was adjusted using NaOH and HCl, and the pH was recorded over the range 0.5-13, with 1D NMR spectra being recorded at various intervals.

5.3 Results

5.3.1 Synthesis of 14

The macrocycle **14** was successfully synthesised using the synthetic route shown in Scheme 5.1. 1D and 2D NMR spectra ([¹H, ¹H] COSY, NOESY and TOCSY and [¹H, ¹³C] HSQC spectra (Figure 5.3)) were used to characterise the compound fully. The results are summarised in Table 5.2.

A NOESY cross-peak was observed between peak at 3.10 ppm and the peak at 7.04 ppm, and therefore it was concluded that the peak at 3.10 ppm must be due to the protons labelled 3 (for numbering scheme, see Figure 5.2). There was a further COSY cross-peak between 3 and the peak at 3.20 ppm, which was then assigned as 4. The peaks for 5 and 6 overlap in the ^1H NMR spectrum, but in the ^{13}C spectrum, there are two peaks at 46.0 ppm and 47.7 ppm. However, assignment of these two peaks proved impossible.

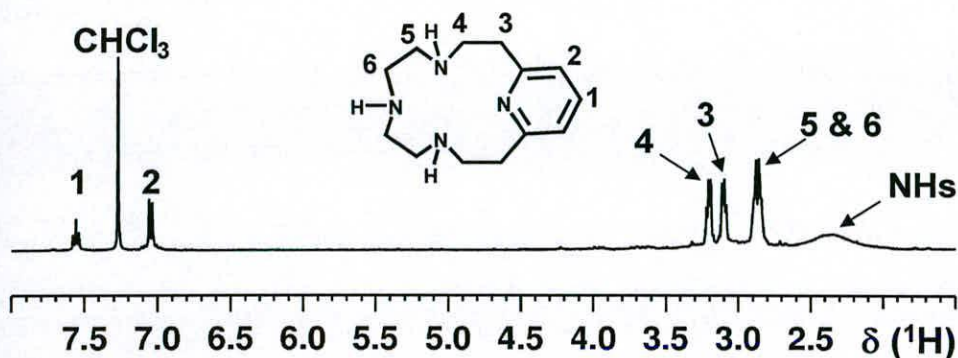


Figure 5.2 ^1H NMR spectrum of 14, recorded in CDCl_3 at 25 $^\circ\text{C}$, with the numbering scheme.

Table 5.2 ^1H and ^{13}C NMR shifts for 14, recorded in CDCl_3 at 25 $^\circ\text{C}$. For labelling scheme, see Figure 5.2.

Peak	^1H / ppm	^{13}C / ppm
1	7.55	137.6
2	7.04	121.8
3	3.14-3.07	35.7
4	3.24-3.17	46.4
5/6	2.92-2.87	46.0
5/6	2.86-2.82	47.7

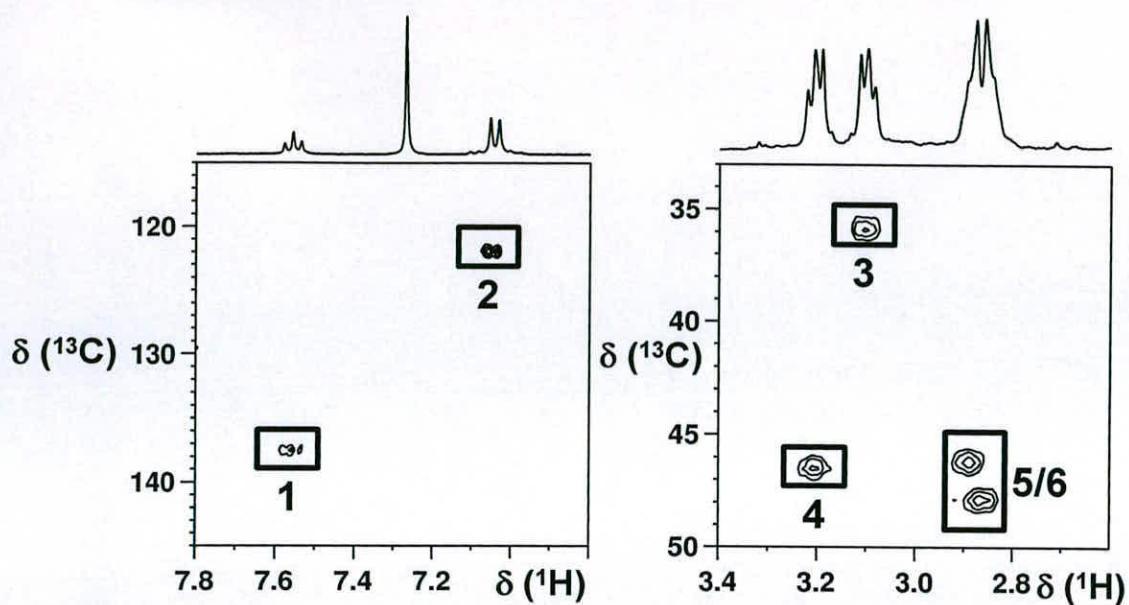


Figure 5.3 2D [^1H , ^{13}C] HSQC NMR spectrum of **14** recorded in CDCl_3 , at 25 $^\circ\text{C}$.

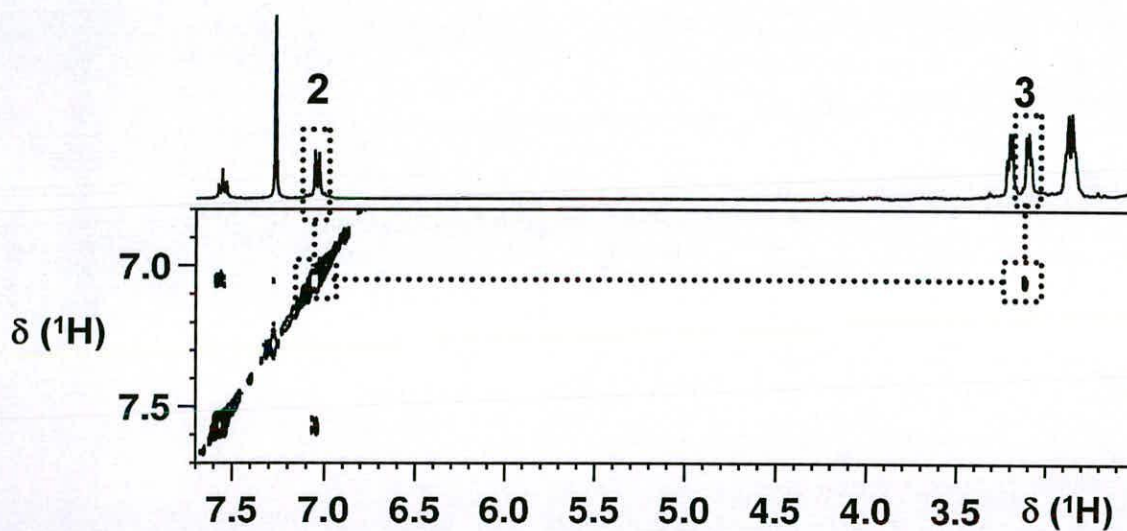


Figure 5.4 2D [^1H , ^1H] NOESY NMR spectrum of **14** recorded in CDCl_3 , at 25 $^\circ\text{C}$, showing the key NOESY interaction between CH (2) in the pyridine ring to the neighbouring CH_2 group (3). For labelling scheme see Figure 5.2.

5.3.2 Synthesis of 15

The bis-pyridyl isocyclam with a *p*-xylene linker **15** was successfully synthesised using the synthetic route shown in Scheme 5.1, and 1D and 2D NMR spectra ($[^1\text{H}, ^1\text{H}]$ COSY, NOESY and $[^1\text{H}, ^{13}\text{C}]$ HSQC) were used to fully characterise it (Figure 5.5 (a) - (c)). The data are summarised in Table 5.3.

The singlet from the methylene linker protons (labelled **7** in Figure 5.5) shows a NOESY peak to the singlet from the aromatic peaks from the phenyl linker (labelled **8**), and a further NOESY peak to the signals from the $\text{NCH}_2\text{CH}_2\text{N}$ region (labelled **5** and **6**). The *para* position in the pyridine ring (**1**) gives a triplet at 7.59 ppm. The *meta* protons in the pyridine ring (**2**) give a doublet at 7.03 ppm, which shows a NOESY peak to the CH_2 group next to the pyridine ring (labelled **3**, shown in Fig. 6.2). These protons (**3**) have a large shift of their associated carbon signal (39.8 ppm, shown in Figure 5.5 (c)), due to the close proximity to the pyridine ring.

Table 5.3 ^1H and ^{13}C NMR shifts of **15**, recorded in CDCl_3 at 25 °C.

Label	^1H shift / ppm	^{13}C shift / ppm
1	7.59	139.6
2	7.03	124.0
3	3.02-2.96	39.8
4	3.07-3.02	50.7
5/6	2.66-2.59	50.0
5/6	2.57-2.49	56.4
7	3.34	61.8
8	6.48	131.3

* 5 and 6 were indistinguishable.

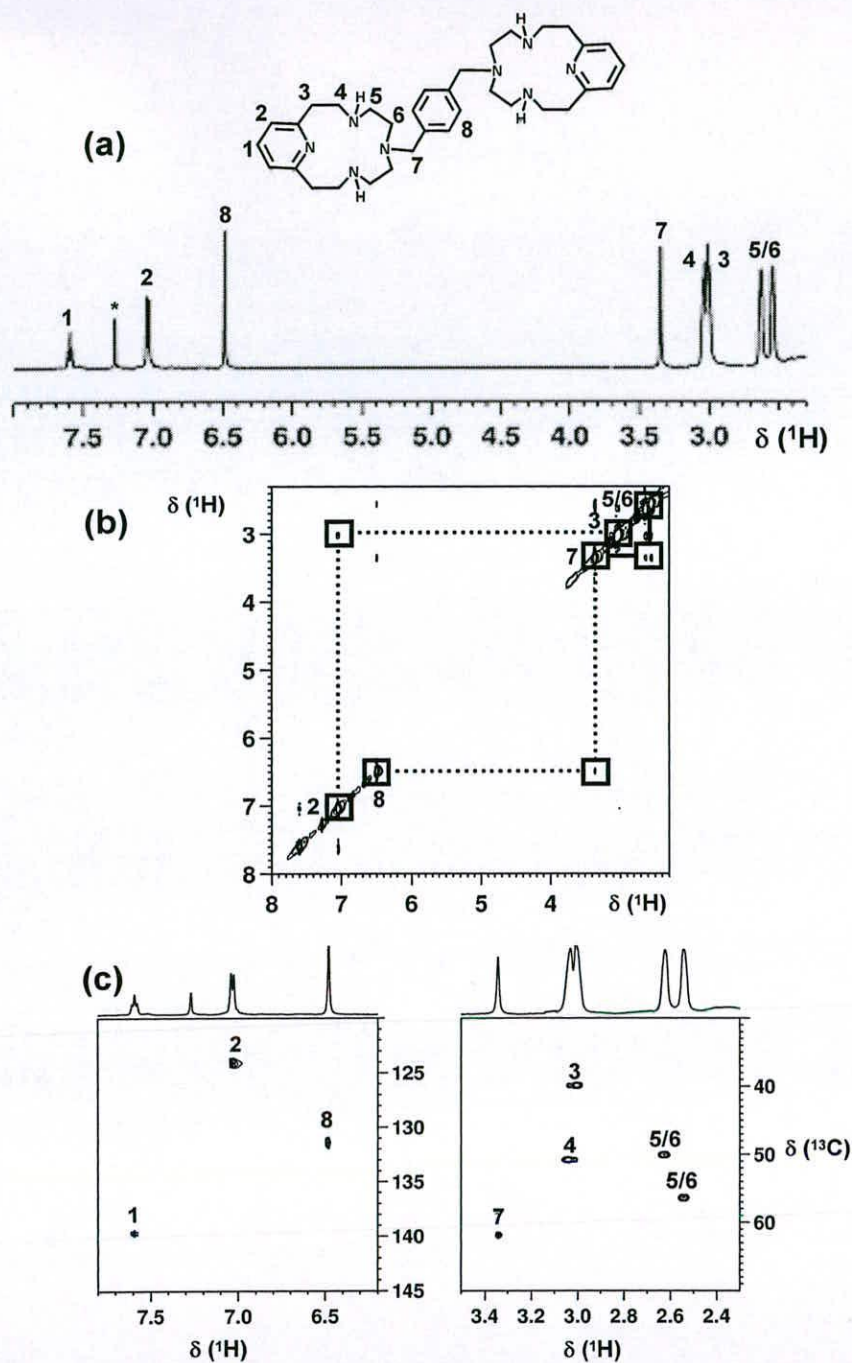


Figure 5.5 (a) Structure of **15** and its ^1H NMR spectrum, recorded in CDCl_3 , with corresponding labelling scheme. (b) $[\text{}^1\text{H}, \text{}^1\text{H}]$ 2D NOESY NMR spectrum, showing the key interactions (c) $[\text{}^1\text{H}, \text{}^{13}\text{C}]$ 2D HSQC NMR spectrum, showing the correlation between the proton and carbon peaks. * = CHCl_3 .

5.3.3 Synthesis and NMR Spectroscopy of $^{111}\text{Cd}(\text{II})$ Complex, 16

The $^{111}\text{Cd}(\text{II})$ complex **16** was synthesised successfully and characterised using mass spectrometry and NMR spectroscopy. The ^1H NMR spectrum of **16**, acquired immediately after dissolving the sample in 10% D_2O / 90% H_2O , is shown in Figure 5.6. No changes were observed over a period of 4 weeks at ambient temperature. There are three regions that can be studied for this complex, the aromatic region, the CH_2 groups from the macrocyclic framework, and the NH region. Few signals in the spectrum were cleanly resolved. In order to overcome this problem, and to assign fully the ^1H NMR spectrum, 2D NMR studies were used to identify and characterise the configurations present. The 2D [^1H , ^{111}Cd] HSQC NMR spectrum (Figure 5.7) showed that there were two ^{111}Cd peaks, at 212.7 ppm and 219.5 ppm. This spectrum was used in conjunction with the other 2D NMR spectra to identify which peaks belong to each species.

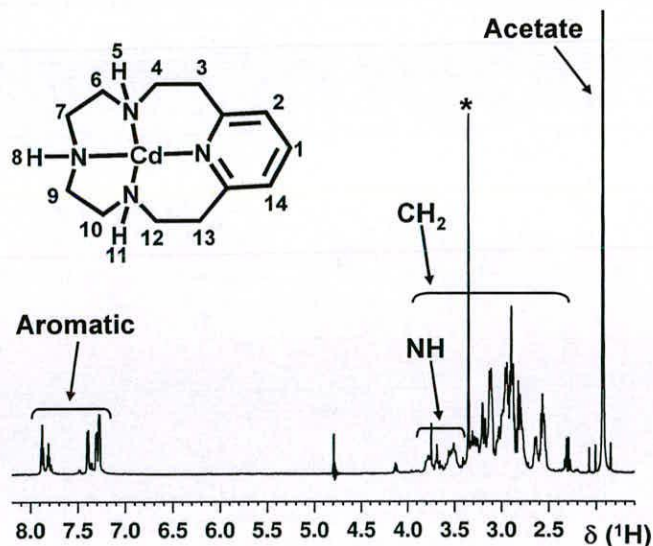


Figure 5.6 1D ^1H NMR spectrum of **16**, recorded in 90 % H_2O / 10 % D_2O at 25 $^\circ\text{C}$.

(* = residual solvent, MeOH). The labelling scheme is also shown.

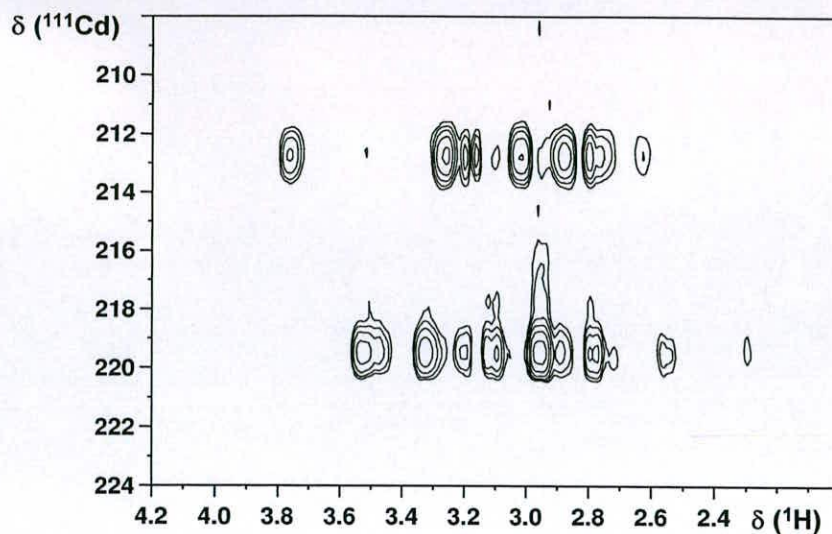


Figure 5.7 2D [^{111}Cd , ^1H] HSQC NMR spectrum of **16**, recorded in 90 % H_2O , 10 % D_2O at 25 °C, showing that two cadmium species are present.

Aromatic Region

There are two triplets from the *para* protons in the pyridine ring (Figure 5.8). This indicates that there are two configurations of the macrocycle present. One of these shows two cross-peaks to the *meta* protons in the pyridine ring in the 2 D [^1H , ^1H] COSY NMR spectrum. This indicates that this configuration (species A) is unsymmetrical, as in a symmetrical configuration these *meta* protons would be equivalent, and produce only one signal. This is the case in the second configuration (species B), where the triplet from the *para* proton only shows a COSY cross-peak to one doublet from the *meta* protons. Two possible structures for this complex are shown in Figure 5.9, with the chirality of the NH groups indicated. Only two of the NH groups are chiral, as opposed to the four chiral NH groups in cyclam.

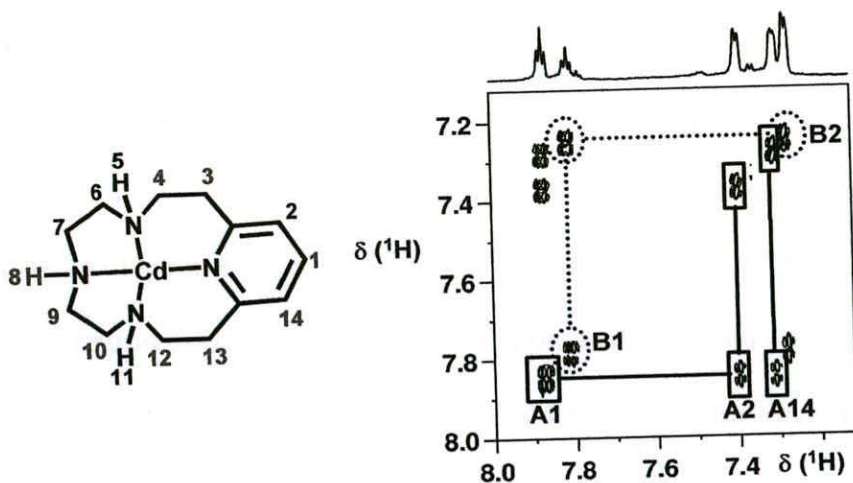


Figure 5.8 2D [^1H , ^1H] COSY NMR spectrum of **16**, recorded in 90 % H_2O / 10 % D_2O at 25 °C, showing connectivities between the *para* and *meta* protons of species A (solid lines) and species B (dashed lines). The labelling scheme is included.

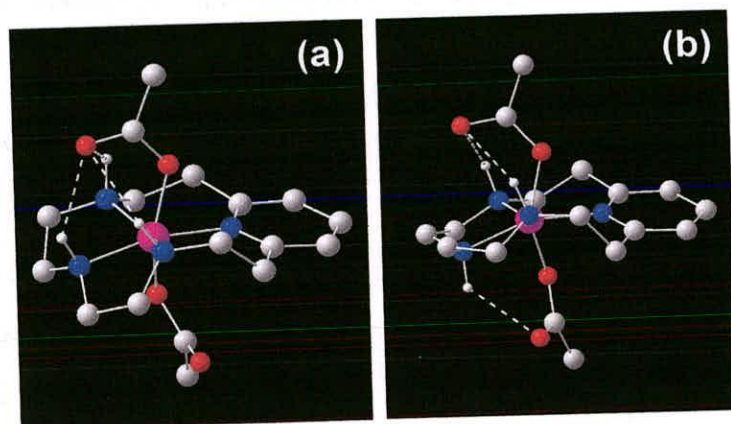


Figure 5.9 Possible structures for metal complexes of pyridyl isocyclam. Structures were drawn and optimised using HyperChem. Hydrogen atoms have been removed from all positions except the nitrogens for clarity. Possible hydrogen bond interactions between the acetate groups and the NH groups are indicated by dashed lines. (a) The NH groups are all on the same face of the macrocycle, (b) the two equivalent NH groups point in the same direction, while the third one points in the opposite direction.

CH₂ Groups From Ring

There were 12 pairs of signals in the 2D [¹H, ¹³C] H₂QC NMR spectrum. A symmetrical configuration would have 4 pairs of signals from the CH₂ groups in the ring, while an unsymmetrical configuration would have 8 pairs. The peaks split into two distinct regions, one ranging from 38-42 ppm and one from 45 to 52 ppm, shown in Figure 5.10-5.11. The peaks that are shifted towards higher field are those next to the pyridine ring, while the lower field peaks arise from CH₂ groups that are all next to NH groups. There are three pairs of peaks in the higher field region, two are from species A and one pair from species B. The peaks were integrated, and it was found that the ratio of species A : species was 60 % : 40 %.

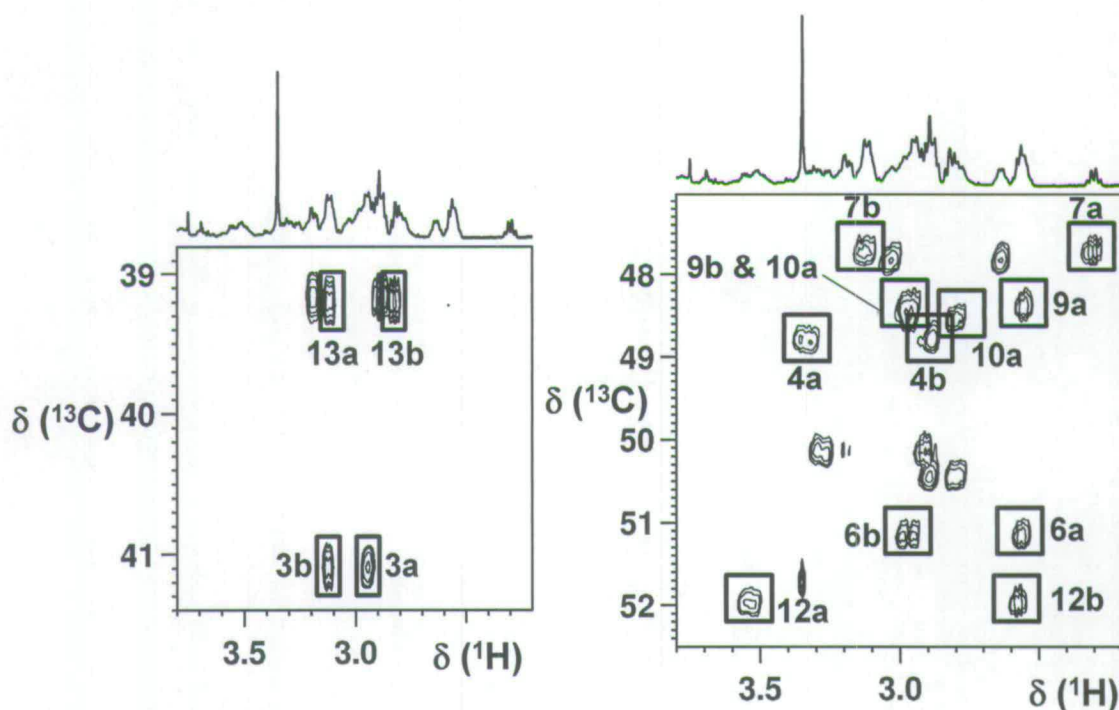


Figure 5.10 2D [¹H, ¹³C] NMR spectrum of the Cd(II) complex **16**, recorded in 90 % H₂O, 10 % D₂O at 25 °C. Peaks from species A are labelled. For labelling scheme, see Figure 5.8. Protons that are on the same carbon atom are referred to as a and b. Peaks for species B are labelled in Figure 5.11

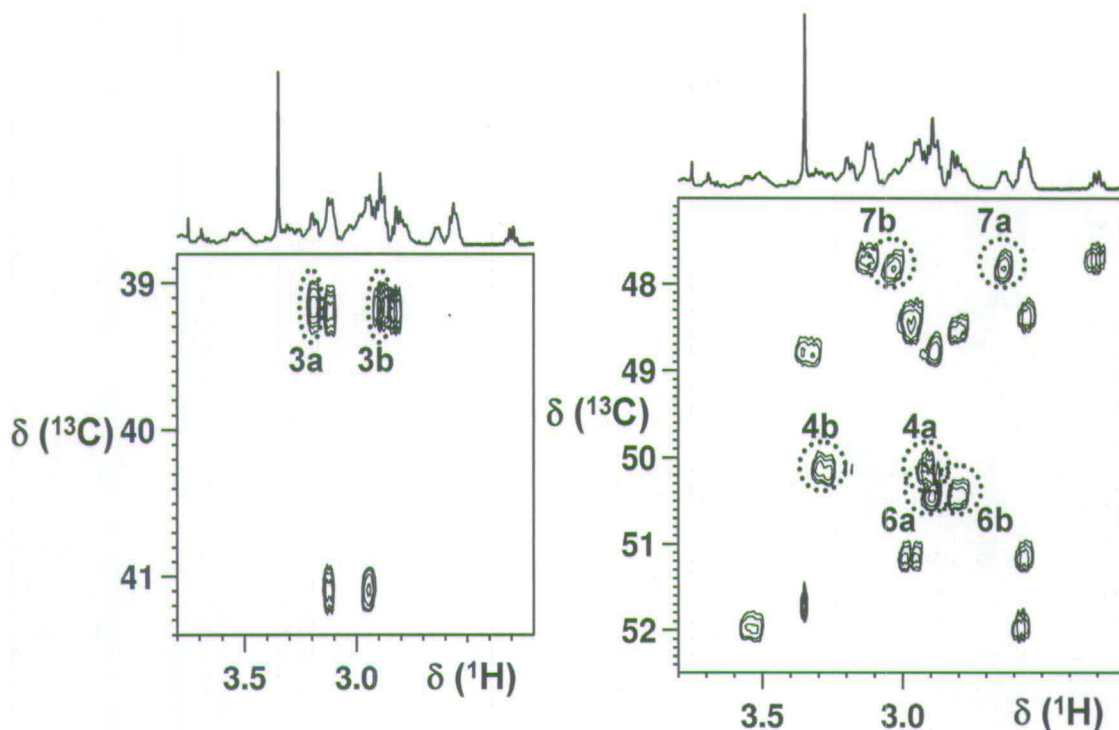


Figure 5.11 2D [^1H , ^{13}C] NMR spectrum of the Cd(II) complex **16**, recorded in 90 % H_2O , 10 % D_2O at 25 °C. Peaks from species B are labelled. For labelling scheme, see Figure 5.8. Protons that are on the same carbon atom are referred to as a and b. As it is a symmetrical configuration, only 4 pairs of protons are observed.

NH Region

Five signals are observed in the 2D [^1H , ^{15}N] HSQC NMR spectrum. These signals are all split into doublets, due to coupling to ^{111}Cd . Two coupling constants can be determined: 1J (^{15}N - ^{111}Cd) and 2J (^1H - ^{111}Cd). The values for these are listed in Table 5.4. The symmetrical configuration, species B, produces two NH signals, as N5 and N11 are equivalent, while species A shows three signals in the 2D [^1H , ^{15}N] HSQC NMR spectrum.

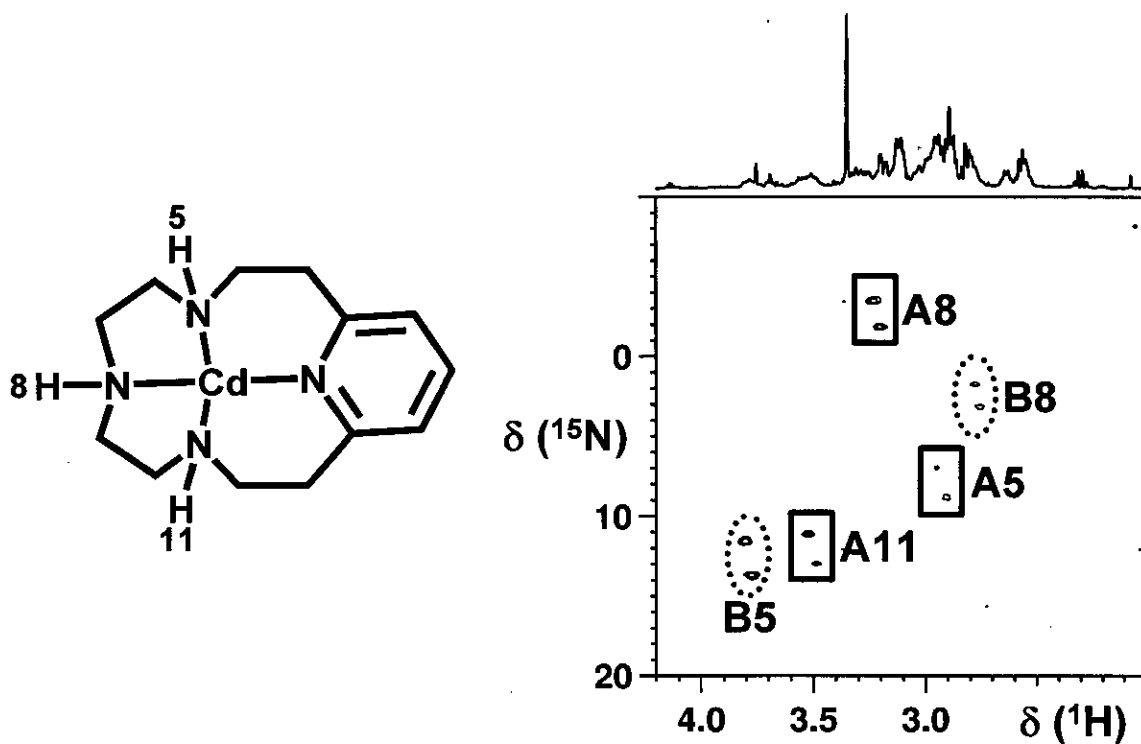


Figure 5.12 2D [^1H , ^{15}N] HSQC NMR spectrum of the Cd(II) complex 16, recorded in 90 % H_2O , 10 % D_2O , at 25 °C, showing peaks for the NH peaks of the two major species A and B. The splittings arise from ^{111}Cd coupling.

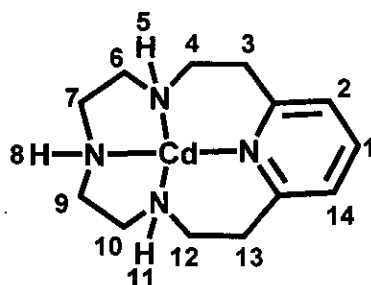
Table 5.4 Coupling constants involving ^1H , ^{15}N and ^{111}Cd for 16. For labelling scheme, see Figure 5.12

Peak label	^1H / ppm	^{15}N / ppm	$^1\text{J} (^{15}\text{N}-^{111}\text{Cd})$ / Hz	$^2\text{J} (^1\text{H}-^{111}\text{Cd})$ / Hz
A5	2.92	6.5	107	26
A8	3.21	-4.0	102	14
A11	3.48	10.6	111	24
B5	3.78	11.2	131	24
B8	1.11	2.8	179	15

The structure of species A was determined as follows. Protons on the same carbon atom are distinguished using a and b. From the 2D [^1H , ^1H] NOESY NMR spectrum, it can be seen that there are NOESY cross-peaks between the *meta* proton (2) on the pyridine ring, and a peak in the aliphatic region, labelled 3b. Then, in the 2D [^1H , ^{13}C] HSQC NMR spectrum, proton 3b is one the most upfield shifted peaks, further supporting that this proton is next to the pyridine ring. Proton 3b is likely to be equatorial, as this would be closest to the *meta* proton. From the 2D [^1H , ^{13}C] HSQC NMR spectrum, the pair can be found (3a). Then, in the 2D [^1H , ^1H] COSY NMR spectrum, a cross-peak is present between protons 3a and 4a, showing that proton 4a is an axial proton, as COSY interactions are strongest between axial-axial protons. There is also a cross-peak from proton 4a to proton 5, which is an NH proton, indicating that proton 5 is an axial proton. Proton 5 also has a COSY cross-peak to proton 6a, again suggesting that this is an axial proton on the same side of the ring as the NH. Proton 6a has a COSY cross-peak to proton 6b, confirmed by the 2D [^1H , ^{13}C] HSQC NMR spectrum, and also cross-peak to proton 7a. From the 2D [^1H , ^{13}C] HSQC NMR spectrum, proton 7b was found. Proton 7a was found to have COSY cross-peaks to protons 7b and 8. Proton 8 (an NH proton) then shows a COSY cross-peak to proton 9b. There is a COSY cross-peak from proton 9b to proton 10a, and proton 10b was found from the 2D [^1H , ^{13}C] HSQC NMR spectrum. Proton 10b has a COSY cross-peak to proton 11, which is an NH proton. Proton 11 shows a COSY cross-peak to proton 12b. From proton 12a, there is a COSY peak to proton 13a. Also proton 12b has a COSY peak to proton 13b. Proton 13a also shows a NOESY peak to proton 14, the proton in the *meta* position on the pyridine ring, suggesting that proton 13a is assignable to an equatorial proton. The data are

summarised in Table 5.5.

Table 5.5 Assignment of the major configuration of the Cd(II) macrocycle 16 in 90 % H₂O / 10 % D₂O at 25 °C, species A.

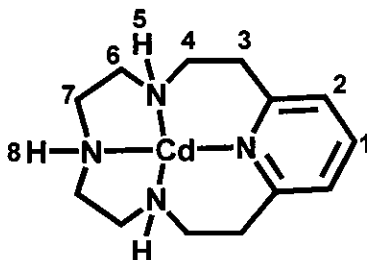


Assignment	¹ H / ppm	¹³ C / ppm	¹⁵ N / ppm	Assignment	¹ H / ppm	¹³ C / ppm	¹⁵ N / ppm	
1	7.87	143.6		8	3.21		-4.1	
2	7.39	126.2		9a	2.55	48.4		
3a	2.94	41.1		9b	2.96			
3b	3.12			10a	2.80	48.5		
4a	3.33	48.8		10b	2.97			
4b	2.88			11	3.48	10.6		
5	2.92			6.5	12a	3.53		52.0
6a	2.56	51.2		12b	2.57			
6b	2.97			13a	3.06	39.3		
7a	2.29	47.7		13b	2.82			
7b	3.12			14	7.30	125.8		

For species B, again there is a NOESY cross-peak between the signal from the *meta* proton from the pyridine ring and proton 3b, which is the most upfield shifted peak in the 2D [¹H, ¹³C] HSQC NMR spectrum. The proton that gives rise to this signal, labelled 3b, should be an equatorial proton. The pair to this proton was

found from the 2D [^1H , ^{13}C] HSQC NMR spectrum. The proton 3b was found to show a COSY cross-peak to proton 4b, which in turn showed a COSY cross-peak to the proton 4a. Proton 4a was also found to have a COSY cross-peak to proton 5, which is an NH proton. The signal from proton 5 also showed a COSY cross-peak to the signal from proton 6a. The 2D [^1H , ^{13}C] HSQC NMR spectrum was used to find proton 6b. From proton 6a, there is a COSY peak to proton 7a. The 2D [^1H , ^{13}C] HSQC NMR spectrum was used to locate the resonance for proton 7b. Proton 7a shows a COSY cross-peak to proton 8, an NH proton. This is the only COSY cross-peak observable from proton 8.

Table 5.6 Assignment of the minor configuration of the Cd(II) macrocycle 16 in 90 % H_2O / 10 % D_2O at 25 °C, species B.



Assignment	^1H / ppm	^{13}C / ppm	^{15}N / ppm	Assignment	^1H / ppm	^{13}C / ppm	^{15}N / ppm
1	7.81	143.0		5	3.78		11.2
2	126.5	7.27		6a	2.89	50.5	
3a	2.88	39.2		6b	2.80		
3b	3.19			7a	2.64	47.8	
4a	2.91	50.2		7b	3.03		
4b	3.28			8	2.76		

5.3.4 Synthesis and NMR Spectroscopy of Zn(II) Complex, 17

This complex was synthesised and its solution structure was investigated using 1D and 2D NMR studies. [^1H , ^1H] COSY, NOESY and TOCSY, [^1H , ^{13}C] HSQC and [^1H , ^{15}N] HSQC NMR spectra were recorded. The structure was solved in a similar manner to the ^{111}Cd complex, and two major configurations of the macrocycle were identified. The 1D ^1H NMR spectrum is shown in Figure 5.13. The full assignments of the two configurations are given in Table 5.7 and Table 5.8.

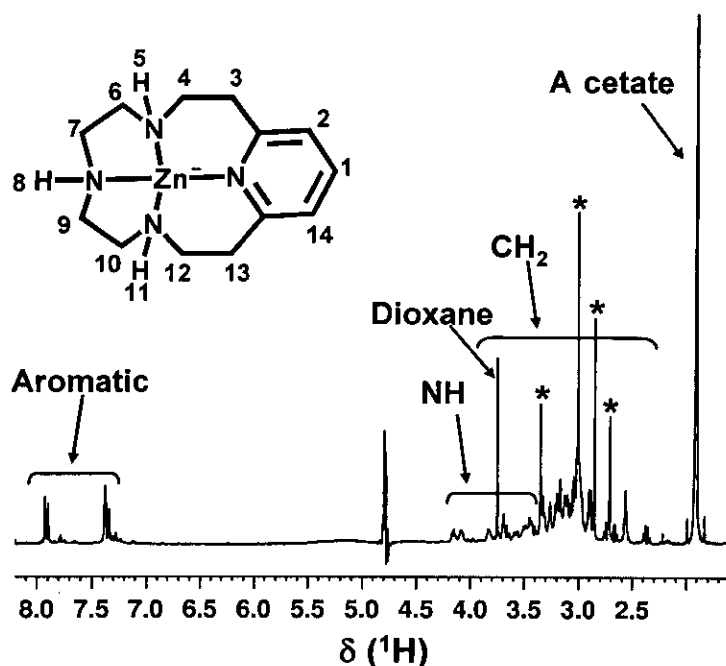


Figure 5.13 1D ^1H NMR spectrum of 17 in 90 % H_2O / 10 % D_2O at 25 $^\circ\text{C}$. (* = residual solvent peaks, methanol and DMF).

NH Region

Five signals were observed in the 2D [^1H , ^{15}N] HSQC NMR spectrum, as shown in Figure 5.14, which shows two configurations are present, an unsymmetrical one, species A, and a symmetrical one, species B. Integrating the NH peaks for

species A and B gives the ratio 67 % A : 33 % B.

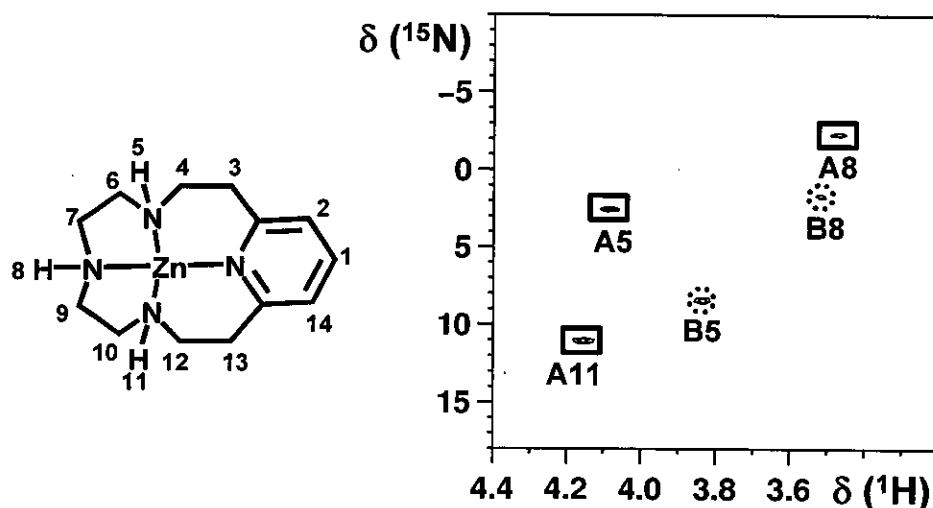


Figure 5.14 2D [^1H , ^{15}N] HSQC NMR spectrum of **17**, recorded in 90 % H_2O / 10 % D_2O at 25 °C. The peaks from species A are shown with a solid line, the peaks from species B are shown in a dotted line. Three peaks are present from species A because it is not symmetrical, whereas species B is symmetrical, and as such two of its NH protons are equivalent.

Aromatic Region

There are two triplets present from the *para* protons in the pyridine ring. This indicates that there are two configurations of the macrocycle present. A similar splitting pattern is observed to the ^{111}Cd complex, showing that there is one symmetrical and one unsymmetrical configuration present.

CH₂ Groups From Ring

There are 12 pairs of signals in the 2D [^1H , ^{13}C] HMQC NMR spectrum (shown in Figure 5.15). Species B has 4 pairs of signals from the CH_2 groups in the ring, while species A has 8 pairs. The signals closest to the pyridine ring (labelled 3

and 13) have the greatest upfield shift in the ^{13}C dimension of the 2D [^1H , ^{13}C] HSQC NMR spectrum. There are three pairs of signals in this region, two are from species A, with one pair from species B. These signals were integrated in the ratio 34:34:32, showing that the solution is made up of 68 % species A, 32 % species B.

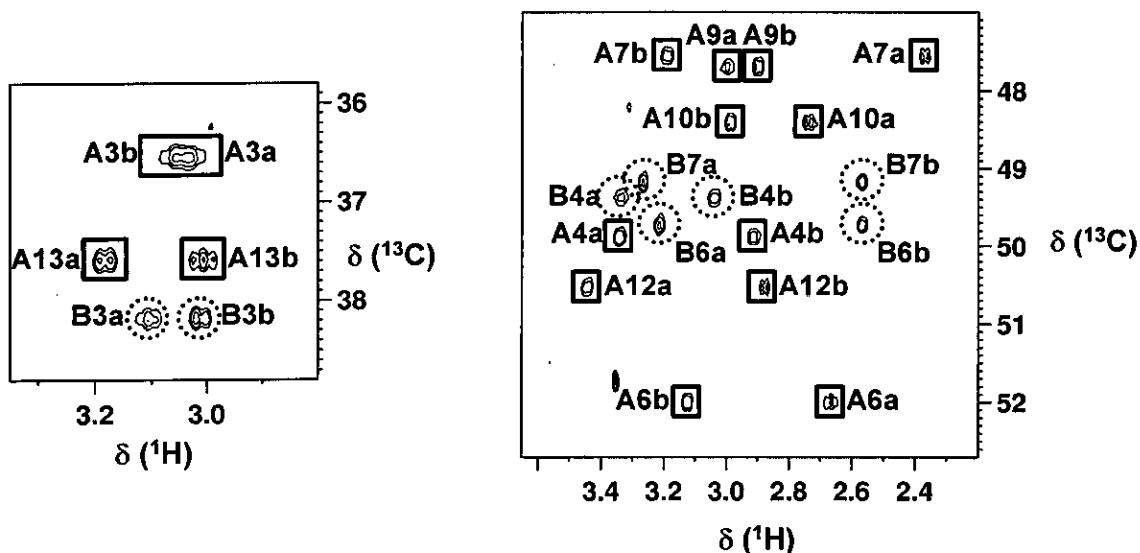
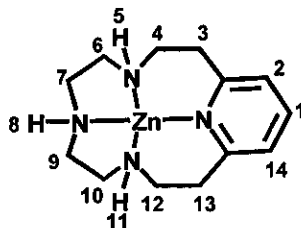


Figure 5.15 2D [^1H , ^{13}C] HSQC NMR spectrum of 17 in 90 % H_2O / 10 % D_2O at 25 °C. The peaks from species A are shown with solid boxes, the peaks from species B with dotted circles. Protons on the same carbon atom are referred to as a and b.

Table 5.7 Assignment of the NMR peaks for the major configuration of Zn(II) complex 17 in 90 % H₂O / 10 % D₂O at 25 °C, Species A. For labelling scheme see Figure 5.15.

Peak	¹ H / ppm	¹³ C / ppm	¹⁵ N / ppm	Peak	¹ H / ppm	¹³ C / ppm	¹⁵ N / ppm	
1	7.90	143.9		8	3.47		-2.3	
2	7.38	127.0		9a	2.99	47.7		
3a	3.03	36.5		9b	2.89			
3b	3.05			10a	2.74	48.4		
4a	3.34	49.9		10b	2.98			
4b	2.91			11	4.15	11.0		
5	4.09			2.6	12a	3.44		50.5
6a	2.68	52.0			12b	2.88		
6b	3.12			13a	3.18	37.6		
7a	2.37	47.6		13b	3.00			
7b	3.19		14	7.34	126.4			

Table 5.8 Assignment of the NMR peaks for the minor configuration of Zn(II) complex 17 in 90 % H₂O / 10 % D₂O at 25 °C, Species B. For labelling scheme see Figure 5.15.

Peak	¹ H / ppm	¹³ C / ppm	¹⁵ N / ppm	Peak	¹ H / ppm	¹³ C / ppm	¹⁵ N / ppm
1	7.92	144.0		5	3.83		8.5
2	7.39	126.5		6a	3.21	49.7	
3a	3.10	38.2		6b	2.56		
3b	3.01			7a	3.27	49.2	
4a	3.34	49.4		7b	2.57		
4b	3.04			8	3.51	1.7	

5.3.5 Synthesis and NMR Spectroscopy of 18

This Cd(II)₂-bis(pyridyl isocyclam) complex was characterised using 1D and 2D NMR studies. There are 4 regions of these spectra that can be studied, the aromatic region, the methylene linker proton region, the NH peaks and the peaks from the CH₂ groups in the ring (Figure 5.16). The [¹H, ¹¹¹Cd] HSQC spectrum showed that there were four ¹¹¹Cd peaks present (Figure 5.17). The major configuration has a ¹¹¹Cd peak at 215.8 ppm (species A), and there is another relatively intense peak at 201.8 ppm (species B). There are also very small signals for two other species present, at 208.5 ppm and 221.8 ppm, but these were not observed in any other spectra recorded ([¹H, ¹H] COSY, NOESY and TOCSY, [¹H, ¹³C] HSQC and [¹H, ¹⁵N] HSQC 2D NMR spectra, under the same conditions), and hence were not characterised any further.

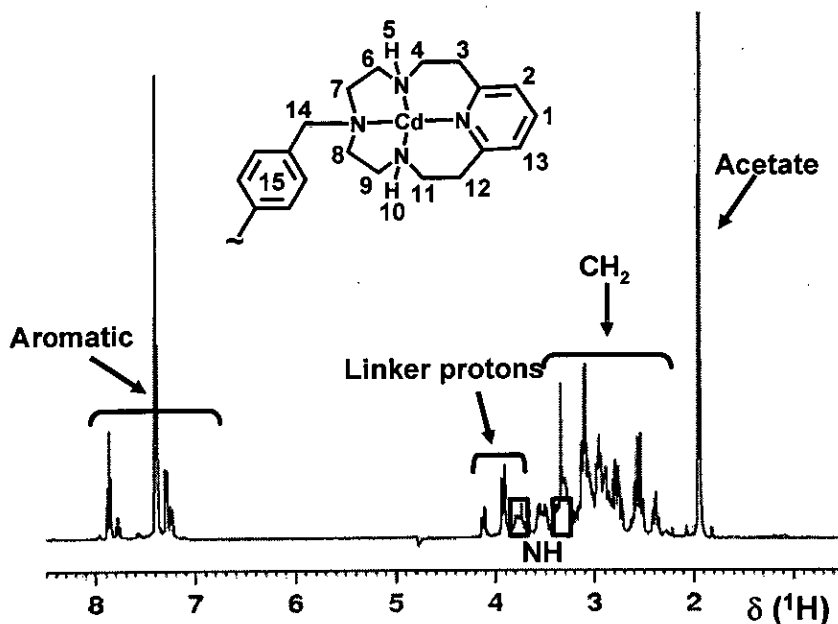


Figure 5.16 ¹H NMR spectrum of 18, recorded in 90 % H₂O / 10 % D₂O at 25 °C, with the numbering scheme for the complex shown.

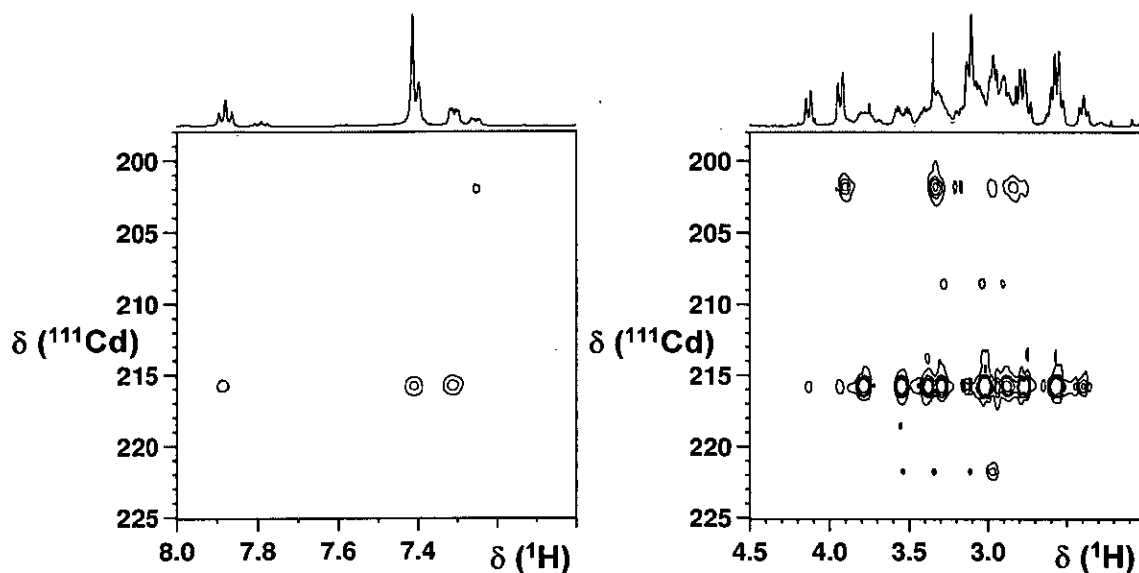


Figure 5.17 $[^1\text{H}, ^{111}\text{Cd}]$ HSQC spectra of **18**, showing 4 ^{111}Cd peaks. Only the major two peaks were found to correlate to peaks in the other 2D NMR spectra recorded.

Aromatic Region

In the 1D proton NMR spectrum, there are two triplets in the aromatic region (Figure 5.18). These arise from the proton in the *para* position in the pyridine ring. This can be used to identify the number of species present, as there should be one triplet for each species. There is one major one (82 %, species A) and one much smaller one (18 %, species B, calculated from the relative integrals).

The splitting pattern of the peaks for the protons in the *meta* position in the pyridine ring can be used to help identify the configuration of the macrocycle. In this case, this proved difficult, as the signal from the aromatic protons in the phenyl linker overlaps with peaks from the pyridine ring. However, this is resolved in the 2D NMR spectra. From the $[^1\text{H}, ^1\text{H}]$ COSY spectrum (Figure 5.19), there appear to

be two doublets present, as the triplet from species A shows two COSY peaks to the doublet region, which means that the ring is not in a symmetrical environment, and the NH groups have different orientations. The *para* proton (triplet at 7.89 ppm) should only show COSY cross-peaks to the *meta* protons in the pyridine ring, in this case the *para* proton shows two COSY peaks, which means that the molecule must be unsymmetrical to produce such splitting. This can also be observed in the [^1H , ^{13}C] HSQC, where three peaks are found in this region (Figure 5.20). These integrate to 41:41:18, indicating that two are from species A, and one is from species B.

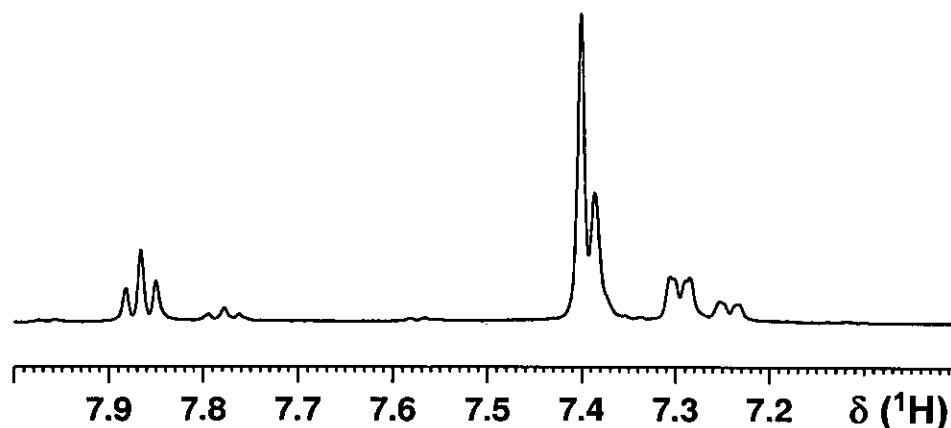


Figure 5.18 1D ^1H spectrum of **18** recorded in 90 % H_2O / 10 % D_2O , showing the aromatic region. A triplet is present from the *para* proton in the pyridine ring for each configuration of the macrocycle.

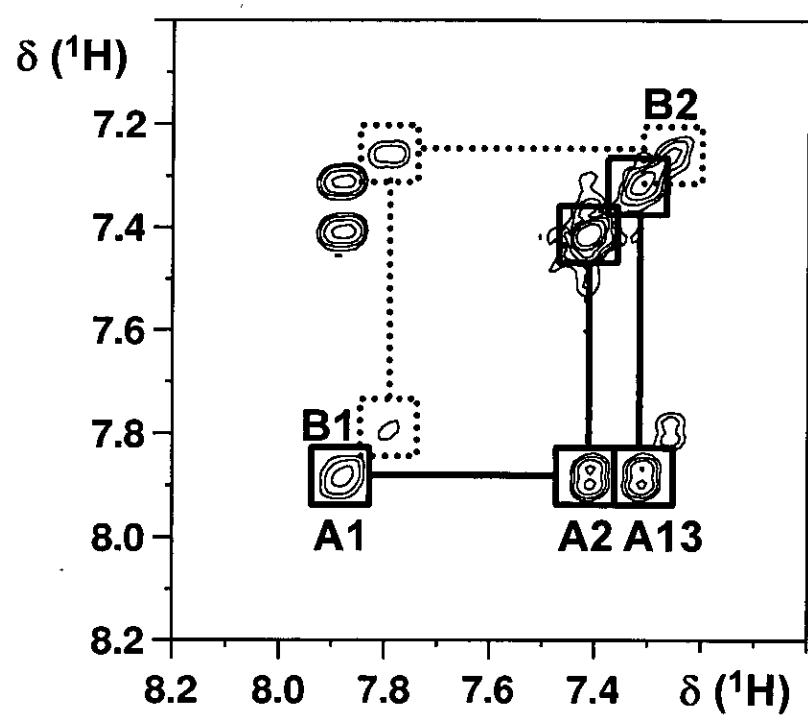
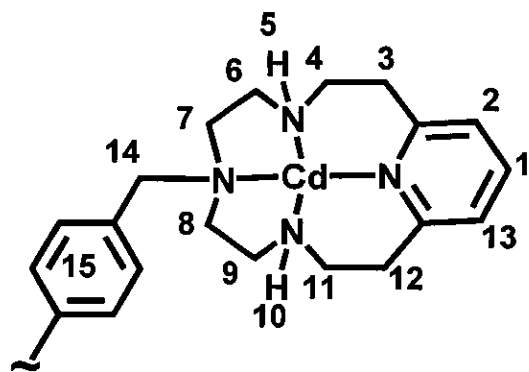


Figure 5.19 [^1H , ^1H] 2D COSY NMR spectrum of **18** recorded in 90 % H_2O / 10 % D_2O , showing the aromatic region. This shows that for species A (solid lines), there are two signals from the *meta* protons in the pyridine ring, implying that the molecule is not symmetrical. Furthermore, there is only one cross-peak from the *para* to the *meta* protons for species B (dotted lines), indicating it is in a symmetrical configuration.

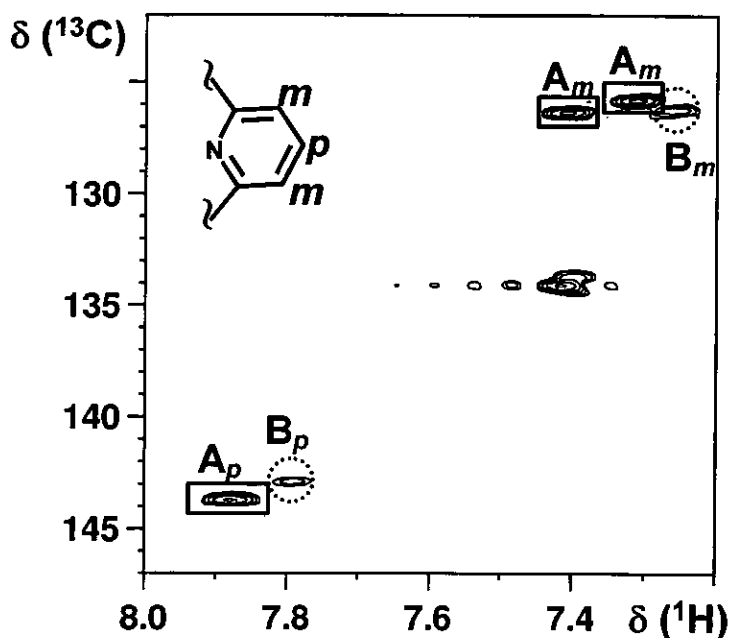


Figure 5.20 2D [^1H , ^{13}C] HSQC NMR spectrum showing the signals from the *meta* and *para* positions in the pyridine ring in **18**, shows there are three signals from the *meta* protons (shown by *m*). Only one peak is observed for the *meta* protons of species B, whereas two are observed for species A. The minor doublet shows a cross-peak in the [^1H , ^{111}Cd]-HSQC NMR spectrum to the ^{111}Cd peak at 201.8 ppm. There is one peak for each triplet (shown by *p*).

Methylene Linker Region

The signals from the phenyl linker protons overlap with one of the doublet peaks in the 1D and the 2D [^1H , ^1H] COSY NMR spectra. However, these can be distinguished from these peaks in the 2D [^1H , ^{13}C] HSQC NMR spectrum. The presence of a singlet for each species in this region indicates that both of the macrocycles for each species are in the same configuration, as if the macrocycles were in different configurations, AB quartets would be observed in this region. The

[^1H , ^{13}C] 2D HSQC NMR spectrum showed that there is one major set of linker protons, shown in Figure 5.21, labelled 14a and 14b, at 4.12 and 3.92 ppm. There is a small peak at 3.93 ppm, which is from species B, shown in Figure 5.23, labelled 14.

The NOESY spectrum shows cross-peaks from the *para* protons to peaks at 3.11 ppm and 3.18 ppm, which are assigned as the equatorial protons on the CH_2 groups closest to the pyridine ring (peaks 3a and 14a in Figure 5.21). These protons were found to correlate with the most low frequency shifted ^{13}C peaks in the 2D [^1H , ^{13}C] HSQC NMR spectrum (40.4 ppm and 39.2 ppm respectively). There is only one acetate signal present, (1.97 ppm, 25.15 ppm) indicating that all the acetate is in the same environment. There are three possibilities for this; either all the acetate is bound to the cadmium, all of the acetate is unbound, or finally, there could be free and bound acetate in fast exchange. If acetate was bound, this would allow hydrogen bonding to occur between the acetate and an NH group on each face of the macrocycle, stabilising the configuration.

NH Region

The 2D [^1H , ^{15}N] HSQC NMR spectrum showed that there are three NH signals (Figure 5.22). Both of these are split into two peaks due to coupling to ^{111}Cd . For the peak at 3.78 ppm, $^1J(^{15}\text{N}, ^{111}\text{Cd}) = 124 \text{ Hz}$; $^2J(^1\text{H}_\text{N}, ^{111}\text{Cd}) = 24 \text{ Hz}$. For the peak at 3.29 ppm, $^1J(^{15}\text{N}, ^{111}\text{Cd}) = 122 \text{ Hz}$; $^2J(^1\text{H}_\text{N}, ^{111}\text{Cd}) = 25 \text{ Hz}$. The two peaks were both attributed to species A. There is one weak peak observed for species B, at 3.92 ppm, with $^1J(^{15}\text{N}, ^{111}\text{Cd}) = 144 \text{ Hz}$; $^2J(^1\text{H}_\text{N}, ^{111}\text{Cd}) = 22 \text{ Hz}$.

The assignments of ^1H , ^{13}C and ^{15}N NMR peaks for the complex are given in

Table 6.2. The numbering scheme is shown in Figure 5.22, and a fully assigned ^1H , ^{13}C] HSQC spectrum is shown in Figure 5.21.

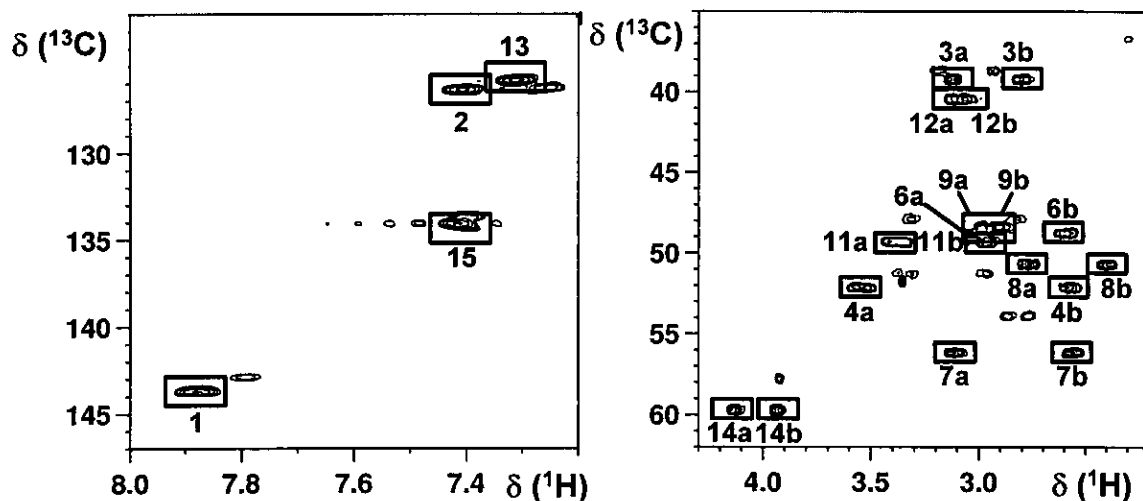


Figure 5.21 The assigned 2D ^1H , ^{13}C] HSQC NMR spectrum of the major configuration (species A) of **18** recorded in 90 % H_2O / 10 % D_2O . For the numbering scheme, see Figure 5.22. Protons on the same carbon atom are referred to as a and b.

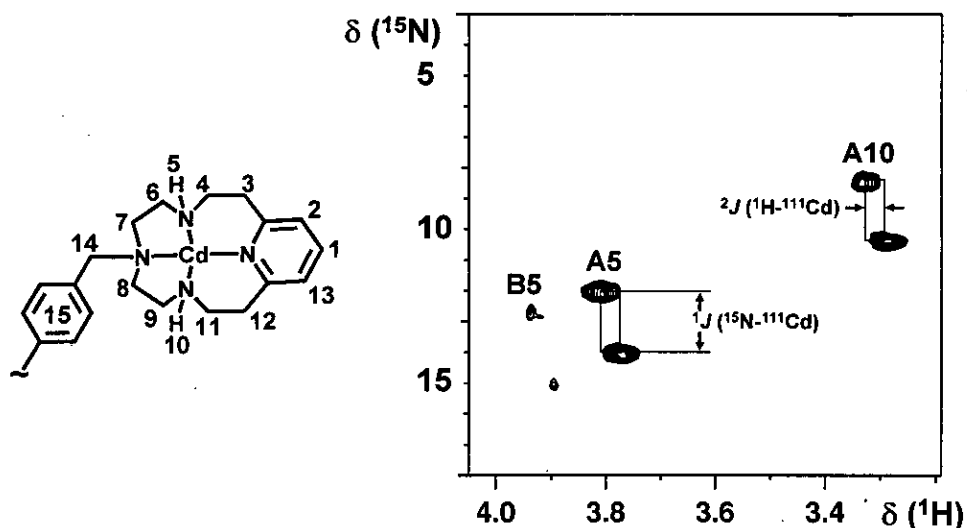
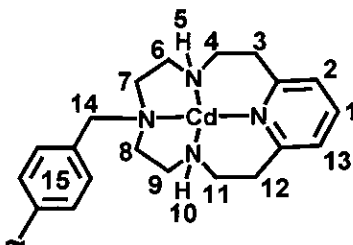


Figure 5.22 2D ^1H , ^{15}N] HSQC NMR spectrum of **18**, recorded in 90 % H_2O / 10 % D_2O . Three ^{15}NH peaks are observed, which are both split by coupling to ^{111}Cd , two from species A and one of weak intensity from species B.

Table 5.9 Assignment of the major configuration of 18 in 90 % H₂O / 10 % D₂O at 25 °C, corresponding to the ¹¹¹Cd peak at 215.8 ppm.



Peak	¹ H / ppm	¹³ C / ppm	¹⁵ N / ppm	Peak	¹ H / ppm	¹³ C / ppm	¹⁵ N / ppm	
1	7.89	143.7						
2	7.41	126.4		9a	2.96	48.4		
3a	3.13	39.2		9b	2.89			
3b	2.80			10	3.29		8.4	
4a	3.54			52.2	11a	3.37	49.3	
4b	2.57	11b			2.95			
5	3.78			12.1	12a	3.12	40.4	
6a	3.03	48.8			12b	3.07		
6b	2.57				13	7.41	126.4	
7a	3.10	56.2			14a	4.12	59.7	
7b	2.54				14b	3.92		
8a	2.76	50.7			15	7.32	125.9	
8b	2.38							

Species B

From the integrals, it can be calculated that species B makes up 18 % of the total **18** in solution. It appears to be a totally symmetrical form, as there are only 4 sets of ¹³C peaks present in the region from the ring CH₂ groups in the 2D [¹H, ¹³C] HSQC NMR spectrum (labelled 3-6 in Figure 5.23). These all show cross peaks in

the 2D [^1H , ^{111}Cd] HSQC NMR spectrum to the ^{111}Cd peak at 201.8 ppm. Only one peak was observed for the linker protons at 3.93 ppm (^{13}C shift = 57.8 ppm, labelled 7 in Figure 5.23). Based on the assignment of the major configurations, the peaks nearest the pyridine ring can be assigned (peaks 3 and 4). There is only one doublet present from the *meta* protons in the pyridine ring, supporting that the configuration is symmetrical. One peak was observed in the 2D [^1H , ^{15}N] HSQC NMR spectrum for this species. There is also only one signal for the aromatic protons in the phenyl linker. The assignment is given in Table 5.10, with the fully assigned 2D [^1H , ^{13}C] HSQC spectrum in Figure 5.23.

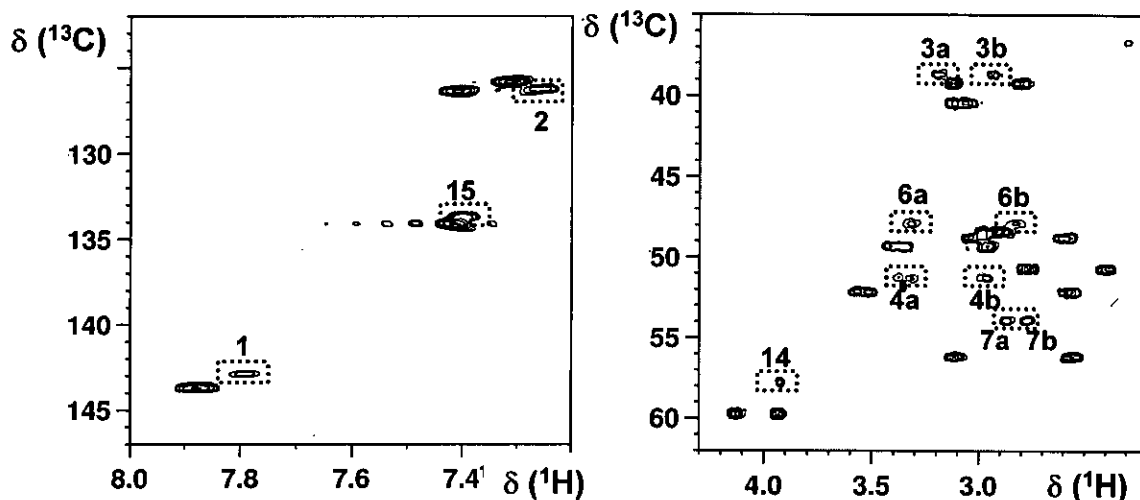
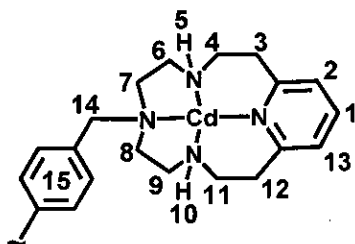


Figure 5.23 The assigned 2D [^1H , ^{13}C] HSQC NMR spectrum of the minor configuration (species B) of **18**. The numbering scheme used is shown in Table 5.10. Protons on the same carbon atom are referred to as a and b.

Table 5.10 ^1H and ^{13}C assignment for species B of 18



Peak	^1H / ppm	^{13}C / ppm	^{15}N / ppm	Peak	^1H / ppm	^{13}C / ppm
1	7.79	142.9		6 a	3.32	47.9
2	7.26	126.2		6 b	2.83	
3 a	3.20	38.7		7 a	2.87	53.9
3 b	2.94			7 b	2.77	
4 a	2.98	51.3		14	3.92	57.8
4 b	3.34			15	7.39	133.6
5	3.92			13.2		

5.3.6 Addition of Acetate to Zn(II) Complex, 17

Acetate was added to the Zn(II) complex, 17, from 1 to 10 molar equivalents, to investigate the effect of excess acetate on the configuration. The ^1H NMR spectra recorded showed that the peaks shifted slightly, but no configurational change occurred. The pH was kept constant throughout the reaction to ensure that any changes were not as a result of pH. The small change in peak positions could arise from non-specific interactions with the added acetate. The acetate peak increased in intensity, but no shift in the acetate peak was observed.

5.3.7 pH Titration of Ligand 14

The pH of a solution of ligand **14** was adjusted from pH = 0.5 to pH = 13.5, and ^1H NMR spectra were recorded with each adjustment. The peaks shifted greatly, and the change in each peak observed was plotted. The shift of peak 4 is shown in Figure 5.24. From this, $\text{p}K_{\text{a}}$ values can be determined using Henderson-Hasselbalch equation, giving the $\text{p}K_{\text{a}}$ values of 1.48 and 9.81. Similar values were obtained from plotting other peaks. There also appears to be at least one more $\text{p}K_{\text{a}}$ value, below 1, but this value could not be determined.

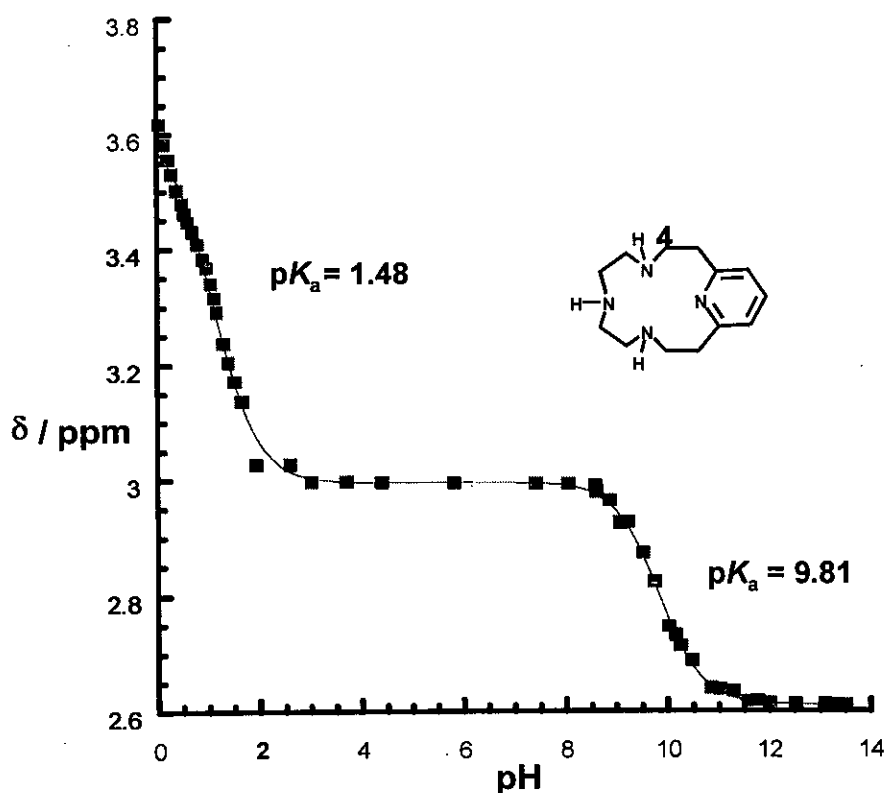


Figure 5.24 Chemical shift of peak 4 of ligand **14**, plotted against pH in order to determine $\text{p}K_{\text{a}}$ values of **14**. Two $\text{p}K_{\text{a}}$ values are determined, at 1.48 and 9.81. A further $\text{p}K_{\text{a}}$ is likely below pH = 1, shown by the steep slope below 1.

5.4 Discussion

5.4.1 Pyridyl Isocyclams

No work has been published on any metal complex of pyridyl isocyclam, **14**. Suggested structures for the metal complexes are shown in Figure 5.9. It is notable that once complexed to a metal, pyridyl isocyclam only has two chiral N centres, as opposed to cyclam, which has 4. Both the structures shown in Figure 5.9 have two NH groups on the same face of the macrocycle, and as such, could form the same double hydrogen bonds to aspartate and glutamate residues as seen in the model of Zn₂-xylyl-bicyclam bound to the CXCR4 receptor.⁷

There are reported crystal structures of the analogous 12 membered pyridyl complex, and of a 14-membered isomer of pyridyl isocyclam.^{8,9} They are shown in Figure 5.25. In the 12-membered complex, copper is five-coordinate, and the ligand is quite folded, whereas in the 14-membered complex, cobalt is six-coordinate, and the ligand is more planar. There are 4 crystal structures in the CSD of the 14-membered complex, two with octahedral Co(III),⁹ one with 5-coordinate Cu(II),¹⁰ and one with 4-coordinate Cu(II).¹¹ In all the complexes, the NH groups are all on the same face of the macrocycle, as shown in Figure 5.25. There is only one reported crystal structure of the 12-membered complex in the CSD.⁸ In this, the asymmetric unit contains 2 cations of the complex, with one containing copper in a distorted square pyramidal environment, and one copper in a distorted trigonal bipyramidal environment. It is notable that the NH groups are all on the same side of the macrocycle in each of the crystal structures shown. This leads to the conclusion that pyridyl isocyclam, **14**, would also adopt this configuration, and in solution, this would give rise to the main configuration shown in Figure 5.9(a). The minor

configuration could then be the structure shown in Figure 5.9(b).

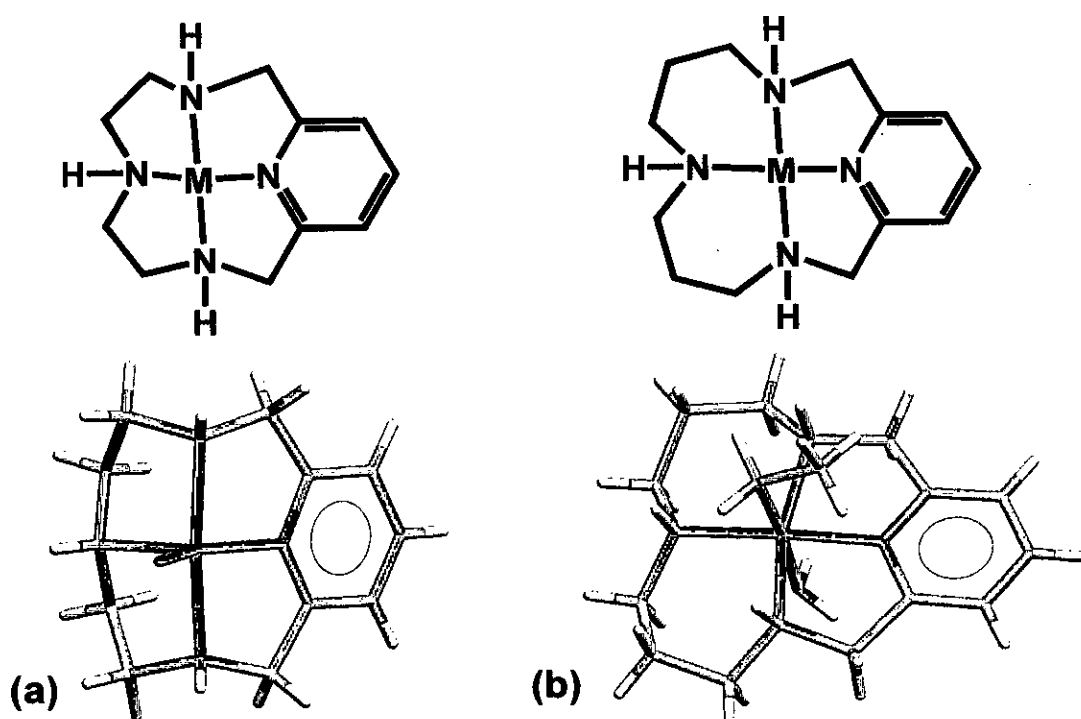
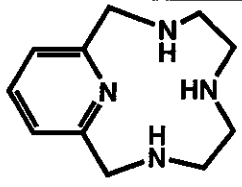
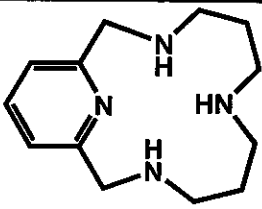


Figure 5.25 Line drawings and crystal structures of (a) a 12-membered pyridyl macrocycle⁸ and (b) a 14-membered isomer of pyridyl isocyclam.⁹

The pK_a values for these two macrocycles have also been published,^{12, 13} and are shown in Table 5.11. One of these is a 12-membered macrocycle, and one is a 14-membered one, an isomer of pyridyl-isocyclam, **14**. It was shown for these two macrocycles that they have lower pK_{a1} and pK_{a2} values than cyclam, which is to be expected, as the pyridine ring should impart lower basicity to the ring. Only 2 pK_a values for pyridyl isocyclam, **14**, could be determined: of 9.81 and 1.48. It appeared that there could also be another one of <1 .

Table 5.11 pK_a values for pyridyl macrocycles^{12, 13}

		
pK_{a1}	10.33	9.92
pK_{a2}	7.83	8.56
pK_{a3}	1.27	4.66
pK_{a4}	<1	<1

5.4.2 ^{111}Cd NMR Studies

^{111}Cd (or ^{113}Cd) is as sensitive to NMR detection as ^{13}C . Solid state $^{111/113}\text{Cd}$ NMR studies have been used to study both Cd coordinated compounds and Cd-substituted metalloproteins.^{14, 15} Solution state $^{111/113}\text{Cd}$ NMR spectroscopy has been used in many studies, for instance in the identification of Cd binding sites in bovine serum albumin,¹⁶ and in the study of pH dependence of metal-thiolate clusters in rabbit liver metallothionein.¹⁷ Generally, cadmium-substituted metalloproteins retain at least some of their biological activity.^{3, 18} Work has recently been done on the membrane-permeable metal chelator N,N,N',N'-tetrakis(2-pyridylmethyl)ethylenediamine (TPEN), using NMR studies to show there was a dynamic conformational flexibility in both the $[\text{Zn}(\text{TPEN})]^{2+}$ and the $[\text{Cd}(\text{TPEN})]^{2+}$ complexes in solution.¹⁹ A graph of chemical shifts of cadmium bound ligands is shown in Figure 5.26.

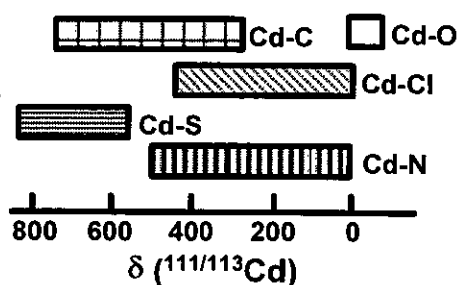


Figure 5.26 Typical ^{111}Cd NMR shifts. Cd-C refers to complexes such as $\text{Cd}(\text{CH}_3)_2$, $\text{Cd}(\text{CH}_3)(\text{OC}_6\text{H}_5)$ and $\text{Cd}(\text{C}_6\text{H}_5)_2$.²

It has been shown that there is a consistent correlation between ^{111}Cd (or ^{113}Cd) NMR chemical shift and the identity of the ligands bound to cadmium.² Cadmium has a large span of chemical shift, at over 900 ppm, which allows the characterisation of coordination number and type of ligands bound. Oxygen ligands have been shown to provide the greatest shielding, with shifts of -100 ppm to 0 ppm, nitrogen and halide ligands are relatively deshielding, with sulphur being the most deshielding. The shift of Cd-S compounds can be as high as 800 ppm. It has been shown that tetrahedral coordination appears to be deshielded relative to octahedral complexes by approximately 50-100 ppm. A similar relationship has been shown between octahedral and heptacoordinated complexes.

$^{111/113}\text{Cd}$ spectroscopy has been used in many studies, mainly of proteins to identify binding sites, in both solution and solid state NMR studies. Cd(II) is of similar size to both Zn(II) and Ca(II). The nuclear spin quantum number of $\frac{1}{2}$ and reasonably high detection frequency (similar to that of ^{13}C) makes ^{111}Cd easy to detect, although problems can arise from its negative gyromagnetic ratio and line-broadening due to relaxation via chemical shift isotropy mechanisms at high fields

and for large complexes (macromolecules). Unlike other probes, such as Co, Cd²⁺ has a filled d-shell and the coordination geometries are not influenced by ligand field effects.

The ¹¹¹Cd macrocycle **16** was found to be in two configurations, in 60:40 ratio, with the unsymmetrical configuration being the more abundant. The bis-macrocyclic ¹¹¹Cd complex **18** was again found to be in the same two configurations, with the ratio of unsymmetrical : symmetrical being 82:18. The ¹¹¹Cd chemical shifts are within the expected range for cadmium bound to nitrogen. Values for ¹J (¹¹¹Cd-¹⁵N) coupling constants, when pyridines and substituted pyridines are used as ligands, have been shown to be in the range 135 – 150 Hz.²⁰ Here, values were found to range from 100 – 180 Hz. Similarly, the ¹⁵N shifts are within the expected range for nitrogen bound to ¹¹¹Cd. There is only one acetate signal present, indicating that all the acetate is in the same environment, and if bound then is in fast exchange between bound and free. If the acetate binds to the Cd(II) in the macrocycle, this would allow hydrogen bonding to occur between the acetate and an NH group on the macrocycle, stabilising the configuration.

5.4.3 NMR Studies of Zn(II)-Pyridyl Isocyclam

Zn(II) has a full d shell, 3d¹⁰, and its coordination number can vary between 4, 5 and 6. There are 11 zinc-cyclam structures in the CSD. All of these are in the *trans*-III configuration. However, it has been shown that on dissolving the crystalline Zn-cyclam can equilibrate to a mixture of *trans*-III, *trans*-I and *cis*-V.²¹ In the present case, complex **17** was found to be in two configurations. There was only one acetate signal present, indicating that all the acetate is either bound or

unbound, or free and bound acetate could be in fast exchange. The two configurations were present in the ratio 68 % : 32 %, with the unsymmetrical configuration being more abundant. The isomer ratio is shifted slightly towards the unsymmetrical configuration compared to the equivalent cadmium complex (60:40). However, this difference could just arise from errors in calculating the integrals.

It was found that no significant changes occurred upon the addition of up to ten equivalents of acetate to the Zn(II) complex **17**. This could show that all the acetate is in fast exchange, or it could be that no acetate is bound to the metal, and water could be part of the inner coordination sphere. This is the case in $[\text{Zn}(\text{cyclam})(\text{H}_2\text{O})_2](\text{OAc})_2$.²¹ It has been shown previously that acetate can induce conformational changes in Zn-cyclam and Zn₂-xylyl-bicyclam complexes, however, no significant changes occurred in this case.^{7, 21} There is no evidence for interconversion between configurations in this pyridyl isocyclam under the investigated conditions.

5.5 Conclusions

The macrocycle **14** was successfully synthesised and two pK_a values were determined. The macrocycle was also successfully complexed with Cd(II) and Zn(II), complexes **16** and **17** respectively. The novel metallomacrocycles were identified using mass spectrometry and NMR spectroscopy. 2D NMR studies were used to identify the configurations of the metallomacrocycles in aqueous solution. There were two major configurations for both the cadmium and the zinc complexes, a symmetrical one and an unsymmetrical one. For both metal ions, the unsymmetrical configuration was the most abundant. It is possible that acetate bound to the metal forms hydrogen bonds to the NH groups on the ring. Addition of

excess acetate to the zinc complex **17** was found to have no effect on the configuration of the complex. These are the first reported metal complexes of this macrocycle.

The bis-macrocycle **15** was successfully synthesised and fully characterised by NMR. The ^{111}Cd complex was also synthesised as the acetate salt (complex **18**). The solution structure of this ^{111}Cd complex in aqueous solution was studied using 2D NMR. It was found to exist in two configurations, a symmetrical and an unsymmetrical one. The unsymmetrical one was found to be the most abundant, with the solution containing of 82 % of this configuration. There is a shift towards this unsymmetrical configuration compared to the monomer (complex **16**, in which the unsymmetrical configuration was 60 % of the solution). Detailed NMR studies showed both macrocycles to be the same configuration in the two species present.

This is the first reported metal complex of this potent anti-HIV agent, and this could be used in further studies with proteins to identify the binding sites, using ^{111}Cd NMR.

5.6 References

- 1 G. J. Bridger, R. T. Skerlj, S. Padmanabhan, S. A. Martellucci, G. W. Henson, S. Struyf, M. Witvrouw, D. Schols, and E. De Clercq, *J. Med. Chem.*, 1999, **42**, 3971-3981.
- 2 P. D. Ellis, in 'Cadmium-113 NMR Spectroscopy in Bioinorganic Chemistry. A Representative Spin 1/2 Metal Nuclide', D. Reidel Publishing Company, Holland, 1983.
- 3 I. M. Armitage and Y. Boulanger, in 'Cadmium-113 NMR', Academic Press, Inc., New York, 1983.
- 4 X. Liang, J. A. Parkinson, S. Parsons, M. Weishaupl, and P. J. Sadler, *Inorg. Chem.*, 2002, **41**, 4539-4547.
- 5 M. E. Haeg, B. J. Whitlock, and Whitlock, Jr. H. W., *J. Am. Chem. Soc.*, 1989, **111**, 692-696.
- 6 G. J. Bridger, R. T. Skerlj, D. Thornton, S. Padmanabhan, S. A. Martellucci, G. W. Henson, M. J. Abrams, N. Yamamoto, K. De Vreese, R. Pauwels, and E. De Clercq, *J. Med. Chem.*, 1995, **38**, 366-378.
- 7 X. Liang, J. A. Parkinson, M. Weishäupl, R. O. Gould, S. J. Paisey, H.-S. Park, T. M. Hunter, C. A. Blindauer, S. Parsons, and P. J. Sadler, *J. Am. Chem. Soc.*, 2002, **124**, 9105-9112.
- 8 V. Felix, J. Costa, R. Delgado, M. G. B. Drew, M. T. Duarte, and C. Resende, *J. Chem. Soc. Dalton Trans.*, 2001, 1462-1471.
- 9 H. A. A. Omar, P. Moore, and N. W. Alcock, *J. Chem. Soc. Dalton Trans.*, 1994, **18**, 2631-2635.

- 10 K. Panneerselvam, K. Hansongnern, N. Rattanawit, F. L. Liao, and T. H. Lu, *Anal. Sci.*, 2000, **16**, 1107-1108.
- 11 V. Felix, M. J. Calhorda, J. Costa, R. Delgado, C. Brito, M. T. Duarte, T. Arcos, and M. G. B. Drew, *J. Chem. Soc. Dalton Trans.*, 1996, 4543-4553.
- 12 J. Costa and R. Delgado, *Inorg. Chem.*, 1993, **32**, 5257-5265.
- 13 G. Bridger and R. T. Skerlj, *Ad. Anti. Drug Des.*, 1999, **3**, 161-229.
- 14 P. D. Ellis, R. R. Inners, and H. J. Jakobsen, *J. Phys. Chem.*, 1982, **86**, 1506-1508.
- 15 R. R. Inners, F. D. Doty, A. R. Garber, and P. D. Ellis, *J. Magn. Reson.*, 1981, **45**, 503-509.
- 16 E. O. Martins and T. Drakenberg, *Inorg. Chim. Acta*, 1982, **67**, 71-74.
- 17 M. Good, R. Hollenstein, P. J. Sadler, and M. Vasak, *Biochemistry*, 1988, **27**, 7163-7166.
- 18 M. F. Summers, *Coord. Chem. Rev.*, 1988, **86**, 43-134.
- 19 C. A. Blindauer, M. T. Razi, S. Parsons, and P. J. Sadler, *Polyhedron*, 2005, **In press**.
- 20 D. D. Dominguez, M. M. King, and H. J. Yeh, *J. Magn. Reson.*, 1978, **32**, 161-165.
- 21 X. Liang, M. Weishäupl, J. A. Parkinson, S. Parsons, P. A. McGregor, and P. J. Sadler, *Chem. Eur. J.*, 2003, **9**, 4709-4717.

Chapter 6 Interaction of Metal Cyclams with Lysozyme

6.1 Introduction

Lysozyme is a secretory enzyme, made up of 129 amino acid residues, with a molecular weight of 14 kD. It catalyses the hydrolysis of polysaccharides in cell walls, resulting in the breakdown of bacterial walls.¹ It is a widespread enzyme, found in both animals and plants. In humans, it is found in saliva, tears, leucocytes and the kidneys. It has been well studied, and its structure has been characterised in both the solid and solution states. The amino acid sequence was first determined in 1963.^{2, 3} Hen Egg White Lysozyme (HEWL) was the first enzyme to have its three-dimensional structure determined by X-ray diffraction techniques, in 1965,⁴ and has since been extensively studied. During this study, 4 disulfide bridges were clearly identified, along with a site where competitive inhibitor molecules can bind. It was found that the α -helical content was quite low, with only 6 lengths of helix identified, which included 55 of the 129 amino acid residues, resulting in only 42 % of the molecule being composed of α -helices. It was shown that the lysozyme molecule has a hydrophobic spine, containing several tryptophan residues.

In view of the targeting of anti-HIV cyclam derivatives to CXCR4, it is important to understand the nature of the interactions which determine their binding sites on proteins and in particular whether proteins can recognize different configurations of metal cyclams selectively. However, there appear to be no reported structures of protein adducts of metal cyclams. In particular it has been suggested⁵ that carboxylate groups in a protein positioned above the faces of a metallomacrocycle might stabilize the unusual *cis-V* configuration. Lysozyme was

chosen as a model protein to study protein-cyclam adducts, because it is readily crystallized⁶ and the active site contains carboxylates from Glu35 and Asp52 in close proximity which are known to bind to metal ions such as Gd³⁺.⁷

6.2 Experimental

Complexes **4**, **8** and **13** were prepared and characterised as described in Chapter 3 (**4** and **8**) and Chapter 4 (**13**).

6.2.1 Crystallization of Lysozyme with [Cu₂(xylyl-bicyclam)](OAc)₄

A 0.1 M sodium phosphate buffer solution at pH = 8.4 was prepared by mixing NaH₂PO₄ (5 mL, 0.5 M) and Na₂HPO₄ (95 mL, 0.5 M). A solution of Cu₂(xylyl-bicyclam)(OAc)₄ (**13**, 0.1 mM, 1 mL in buffer) was prepared to give a dark blue solution. A clear solution of HEWL (50 mg/ mL in buffer) and a saturated solution of NaCl in water were prepared. All solutions, and distilled water (20 mL), were filtered using a syringe filter to remove any particles. The reservoir solution for the crystallisation plate was prepared using buffer (100 µL), NaCl (200 µL) and water (700 µL) in each well (24 wells). On the cover slip, HEWL (2.5 µL), Cu₂(xylyl-bicyclam)(OAc)₄ (2.5 µL) and reservoir solution (5 µL) were added to form a drop. Six identical wells and coverslips were prepared and the cover slips were sealed to the wells using vacuum grease. Three further sets of six conditions were prepared using the following conditions: buffer (100 µL), NaCl (300 µL) and water (600 µL), buffer (100 µL), NaCl (500 µL) and water (400 µL) and finally buffer (100 µL), NaCl (400 µL) and water (500 µL). The hanging drop was prepared

in the same way each time. The crystallisation tray was stored in the refrigerator at 4 °C for 2 weeks.

6.2.2 Crystallization of Lysozyme at pH=4.5

Acetate buffer (0.05 M) was prepared from glacial acetic acid (0.003 moles) and NaOAc (0.0019 moles) made up to 100 mL with water. The pH was adjusted with NaOAc to obtain the desired pH. A solution of HEWL (50 mg/mL in buffer solution) and a saturated solution of NaCl were prepared. All solutions and water (20 mL) were filtered through a syringe filter. Six crystallisation wells were set up with the reservoir containing buffer (100 µL), NaCl (200 µL) and water (700 µL). A further six were set up with buffer (100 µL), NaCl (300 µL) and water (600 µL). Hanging drops were prepared on the cover slips using HEWL:reservoir solution in the following ratios : 2:3, 3:2, 4:1. Two of each were set up for each set of the reservoir solutions. The coverslips were sealed using vacuum grease and the crystallisation tray was stored in the fridge at 4 °C for 4 days. During this time hexagonal crystals had grown in all cells.

6.2.3 Soaking of Lysozyme Crystals With $[Cu(cyclam)(H_2O)_2](OAc)_2$, 8

The lysozyme crystals were soaked in a saturated solution of **8** in reservoir solution for 5 days at 288 K. The resulting purple crystal was then removed in a cryoloop and frozen in liquid nitrogen by using type B immersion oil as a cryoprotectant.

6.2.4 Soaking of Lysozyme Crystals With $\text{Cu}_2(\text{xylyl-bicyclam})(\text{OAc})_4$, 13

The lysozyme crystals were soaked in a saturated solution of **13** in reservoir solution for 27 hours. The resulting purple crystal was then removed in a cryoloop and frozen as above.

The handling of lysozyme crystals, collection of x-ray diffraction data and solution of the structure were carried out by Dr Lain McNae and Professor Malcolm Walkinshaw (School of Biological Sciences, University of Edinburgh)

6.2.5 NMR Studies of Lysozyme with $[\text{Cu}(\text{cyclam})(\text{H}_2\text{O})_2](\text{OAc})_2$, 8

All NMR experiments were performed in 90 % H_2O / 10 % D_2O . The water resonance was suppressed by presaturation. Standard pulse sequences were used for 2D TOCSY and COSY (mixing times of 60 and 80 ms, respectively). The pH of 5 mM solutions of HEWL in 90 % H_2O /10 % D_2O used for NMR titrations was adjusted to 4.6 using 0.1 M HCl. Titrations were carried out by adding microlitre aliquots of aqueous Cu-cyclam (**8**) (125 mM, pH 4.60), from 1 to 10 molar equivalents. The assignments for ^1H NMR resonances of HEWL are based on those given by Noda *et al.*⁸

6.2.6 NMR Studies of Lysozyme with $\text{Cu}_2(\text{xylyl-bicyclam})(\text{OAc})_4$, 13

All NMR experiments were performed in 90 % H_2O / 10 % D_2O . The water resonance was suppressed by presaturation. Standard pulse sequences were used for 2D TOCSY and COSY (mixing times of 60 and 80 ms, respectively). The pH of 5 mM solutions of HEWL in 90 % H_2O /10 % D_2O used for NMR titrations was adjusted to 4.6 using 0.1 M HCl. Titrations were carried out by adding microlitre

aliquots of aqueous $\text{Cu}_2(\text{xylyl-bicyclam})(\text{OAc})_4$ (**13**) (125 mM, pH 4.57), from 1 to 10 molar equivalents.

6.2.7 NMR Studies of Lysozyme with $[\text{Ni}(\text{cyclam})(\text{OAc})_2]\cdot\text{H}_2\text{O}$, **4**

All NMR experiments were performed in 90 % H_2O / 10 % D_2O . The water resonance was suppressed by presaturation. Standard pulse sequences were used for 2D TOCSY and COSY (mixing times of 60 and 80 ms, respectively). The pH of 5 mM solutions of HEWL in 90 % H_2O /10 % D_2O used for NMR titrations was adjusted to 4.6 using 0.1 M HCl. Titrations were carried out by adding microlitre aliquots of aqueous Ni-cyclam (**4**) (125 mM, pH 4.55), adding 1, 5 and 10 molar equivalents.

6.3 Results

6.3.1 NMR Studies with Lysozyme and Metal Cyclams

The main features of the 1D ^1H NMR spectrum of lysozyme were unchanged after the addition of up to 10 equivalents of complexes **8**, **13** and **4** (Figure 6.1-6.3). However, specific Trp resonances broadened, as seen in the 1D (Figure 6.4) and 2D (Figure 6.5-6.6) NMR spectra.

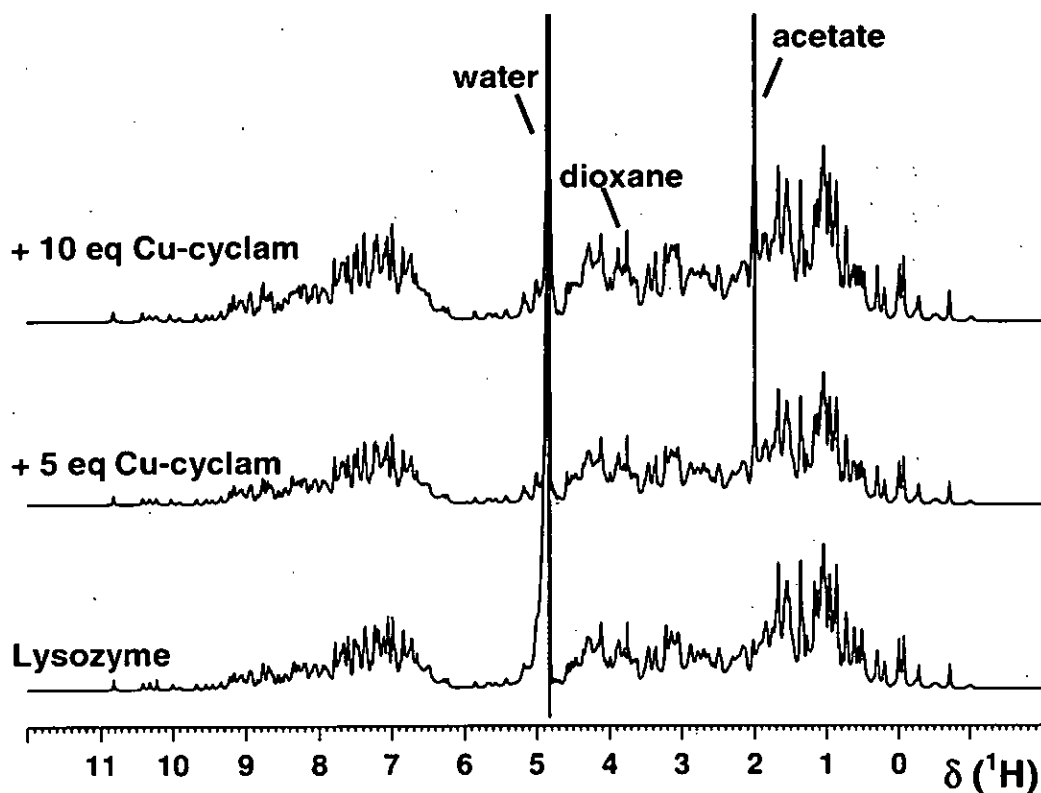


Figure 6.1 1D ^1H NMR spectra of lysozyme, lysozyme + 5 molar equiv Cu(cyclam), **8** and lysozyme + 10 molar equiv Cu(cyclam), **8**, recorded in 90 % H_2O / 10 % D_2O at 25 °C, pH = 4.60.

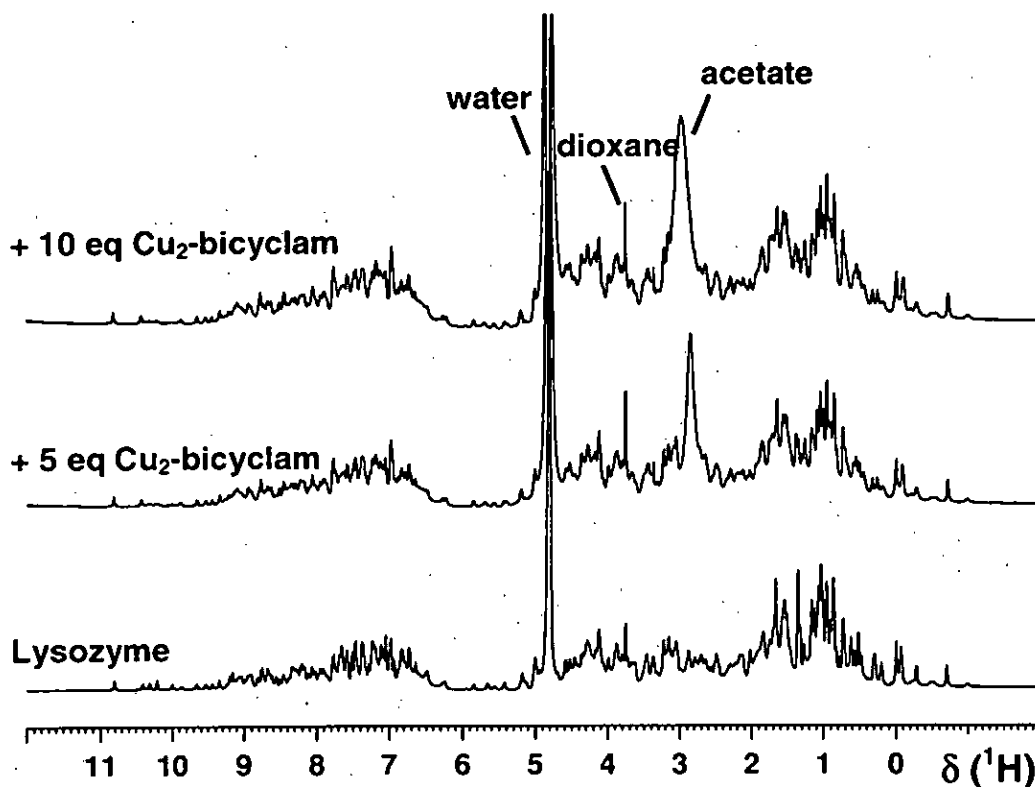


Figure 6.2 1D ^1H NMR spectra of lysozyme, lysozyme + 5 molar equiv Cu_2 -(xylyl-bicyclam), **13** and lysozyme + 10 molar equiv Cu_2 -(xylyl-bicyclam), **13**, recorded in 90 % H_2O / 10 % D_2O at 25 $^\circ\text{C}$, pH = 4.57.

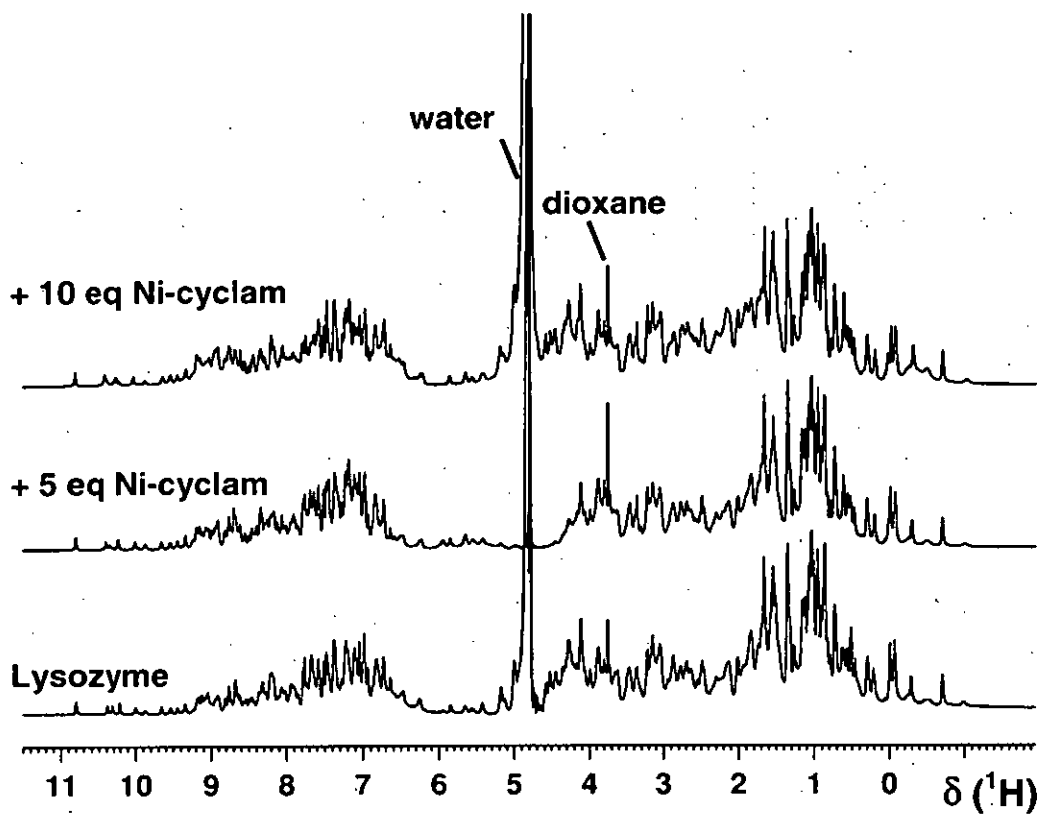


Figure 6.3 1D ¹H NMR spectra of lysozyme, lysozyme + 5 molar equiv Ni-(cyclam), **4** and lysozyme + 10 molar equiv Ni-(cyclam), **4**, recorded in 90 % H₂O / 10 % D₂O at 25 °C, pH = 4.50.

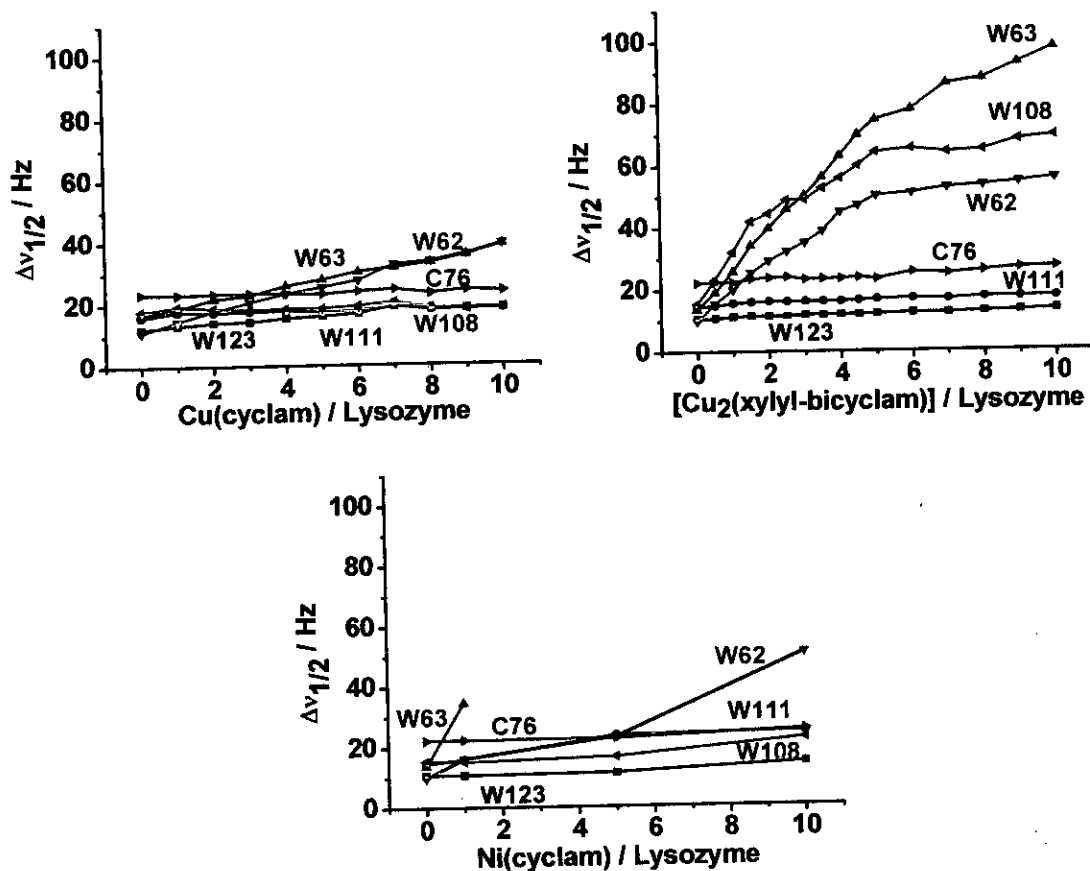


Figure 6.4 Effect of Cu(cyclam), $\text{Cu}_2(\text{xylyl-bicyclam})$ and Ni(cyclam) on tryptophan indole NH resonances of lysozyme. As is evident from the plot of linewidth versus Cu(cyclam) concentration, there are specific paramagnetic broadening effects on Trp-62, Trp-63, and slight broadening of Trp-123, implying that these residues are close to the bound Cu^{2+} . The linewidth of the backbone NH resonance of Cys-76 is also shown for comparison. However in the case of the $\text{Cu}_2(\text{xylyl-bicyclam})$, the broadening of Trp-62, Trp-63 and Trp-108 are the most significant, with Trp-123 only broadening slightly. Trp-111 broadens slightly in both cases. In the case of the Ni(cyclam), Trp 63 broadens to the point of not being observed in the 1D spectrum after the addition of 5 molar equiv.

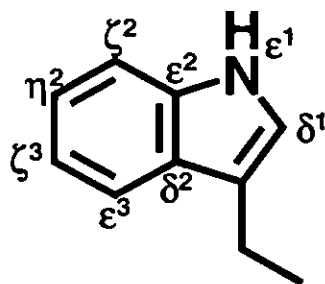
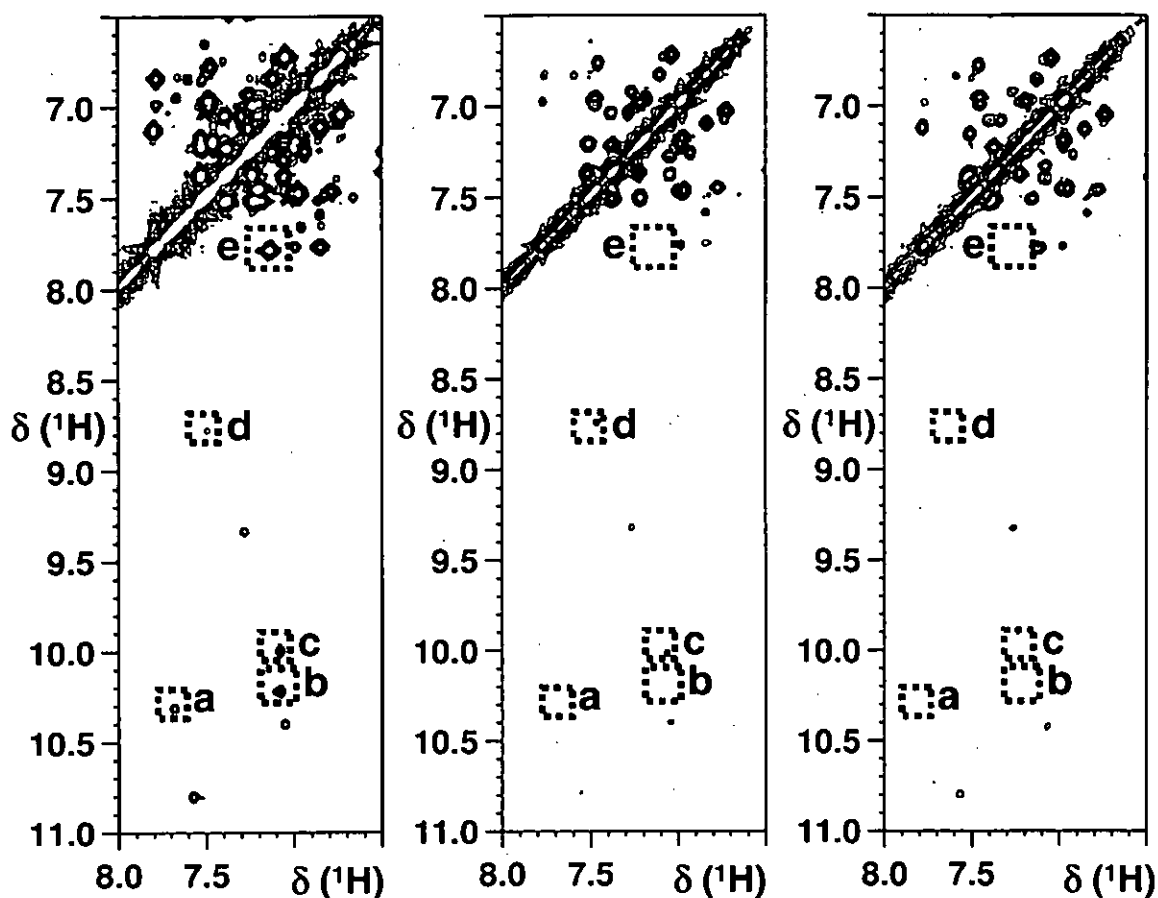


Figure 6.5 2D [^1H , ^1H] COSY NMR spectra of lysozyme in 90 % H_2O / 10 % D_2O , before (*left*), after (*middle*) addition of 10 molar equivalents of $[\text{Cu}(\text{cyclam})(\text{H}_2\text{O})_2](\text{OAc})_2$, and (*right*) addition of 10 molar equivalents of $[\text{Cu}_2(\text{xylyl-bicyclam})](\text{OAc})_4$. Assignments: a, Trp-63 $\text{H}\epsilon^1/\text{H}\delta^1$; b, Trp-62 $\text{H}\epsilon^1/\text{H}\delta^1$; c, Trp-108 $\text{H}\epsilon^1/\text{H}\delta^1$; d, His-15 $\text{H}\epsilon^1/\text{H}\delta^2$; e, Trp-123 $\text{H}\eta^2/\text{H}\zeta^3$. The labelling scheme for tryptophan is also shown.

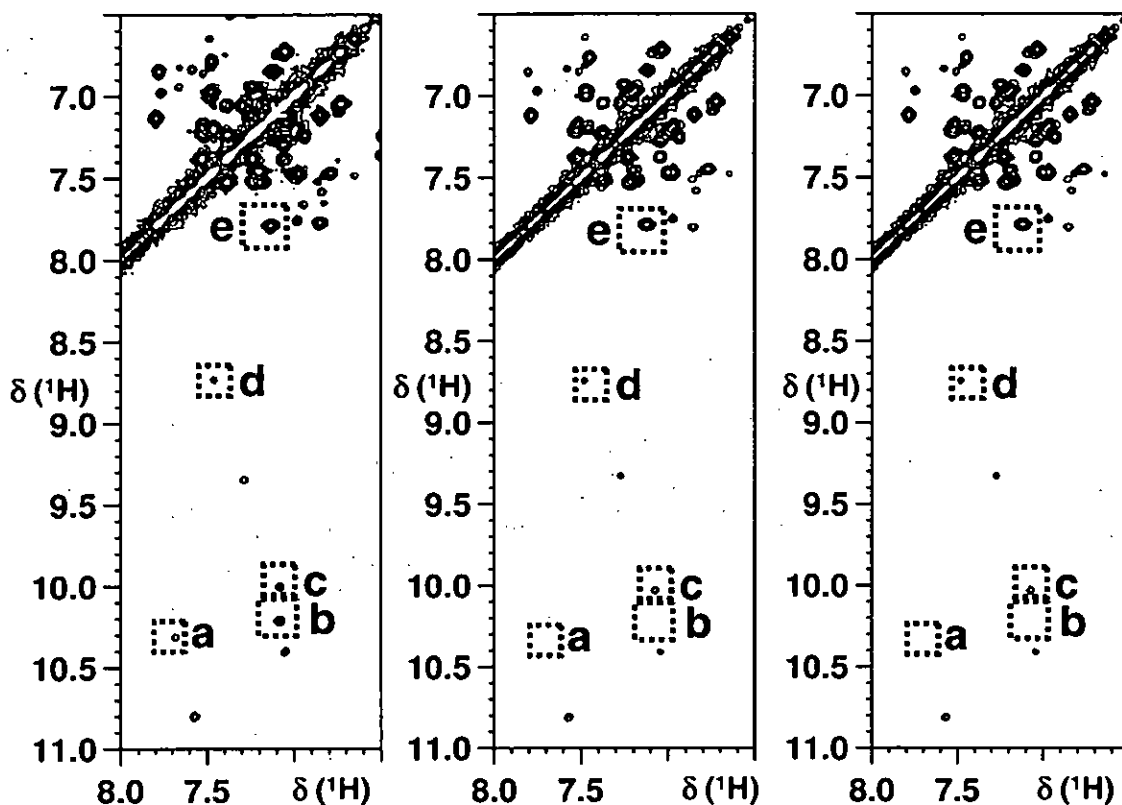


Figure 6.6 2D [^1H , ^1H] COSY NMR spectra of lysozyme in 90 % H_2O / 10 % D_2O , before (*left*), after (*middle*) addition of 1 molar equivalent of $[\text{Ni}(\text{cyclam})(\text{OAc})_2]$, and (*right*) addition of 5 molar equivalents of $[\text{Ni}(\text{cyclam})(\text{OAc})_2]$. There was little change in the 2D NMR spectrum after the addition of 10 molar equivalents of $[\text{Ni}(\text{cyclam})(\text{OAc})_2]$.

6.3.2 Crystallization of Lysozyme

The attempt to co-crystallize Cu_2 -xylyl-bicyclam, **13**, with lysozyme at pH = 8.4 resulted in only precipitate forming in each of the wells. The attempts to grow crystals of lysozyme alone at pH = 4.5 resulted in hexagonal crystals, which were then used in the soaking experiments with the copper complexes **8** and **13**, (Figure 6.7). The x-ray structures of these adducts were solved to a resolution of 1.75 and

1.6 Å, respectively, by Dr. Iain McNae. The overall structure of lysozyme is not changed by formation of adducts with either complex **8** or **13**. The positions of the copper atoms in both the monocyclam and bicyclam structures were unequivocally detected as strong peaks in an $|F_o|-|F_c|$ map. In each case, this revealed two binding sites per asymmetric unit. Site 1 is close to the side chain of Asp101, whilst site 2 is closest to the side-chain of Trp123 and the backbone carbonyl of Gly117 (Figure 6.8).

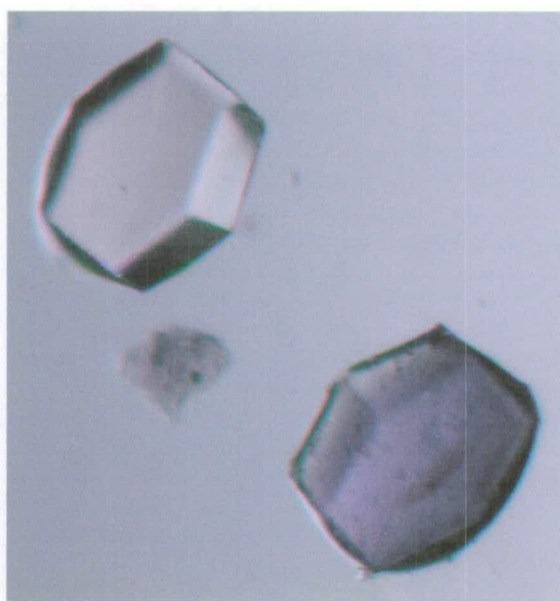


Figure 6.7 Hexagonal crystals of lysozyme in immersion oil before and after soaking in the presence of Cu_2 -xylyl-bicyclam. The colourless lysozyme crystals turned purple on soaking with **8** and **13**.

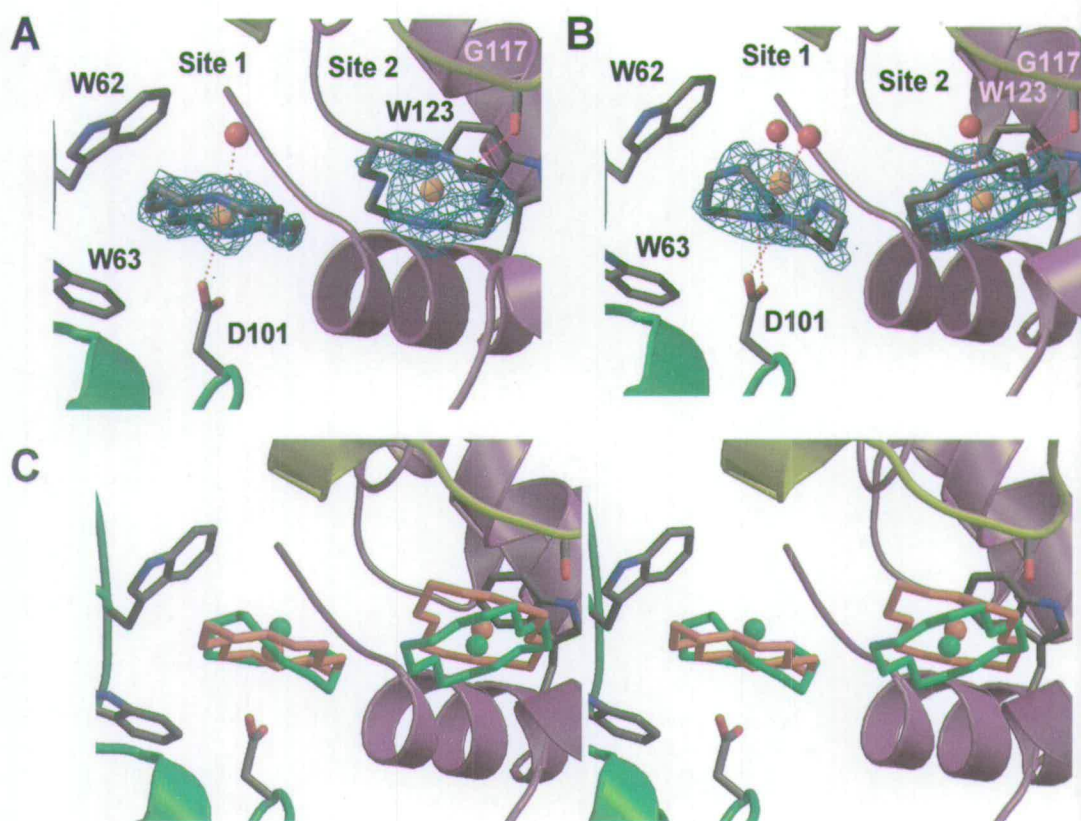


Figure 6.8 The two Cu-cyclam (8) and Cu₂-xylyl-bicyclam (13) binding sites in crystals of HEWL. (A) Cu-bicyclam-HEWL. $2|F_o| - |F_c|$ density is shown around the cyclams at 0.9σ . No electron density is seen for the *p*-phenylenebis(methylene) linker. (B) Cu-cyclam-HEWL. $2|F_o| - |F_c|$ density is shown around the cyclams at 0.9σ . (C) Stereoview of an overlay of the cyclam positions in lysozyme. Colour code: orange, Cu₂-bicyclam; green, Cu-cyclam. Molecule 1 (only just seen in bottom left of picture) is green and contains Asp-101, Trp-62, and Trp-63; molecule 2 is purple and contains Trp-123; and molecule 3 (only just seen at top of picture) is yellow and contains Gly-117. Amino acid code: D = Asp, W = Trp, G = Gly.

6.4 Discussion

6.4.1 Copper-Macrocycle-Lysozyme Interactions in Solution

Resonances from protons in the protein which are within a few Ångstroms of Cu^{2+} in a bound Cu-cyclam would be expected to broaden significantly on account of the paramagnetism of Cu^{2+} ($3d^9$; dipolar broadening $\propto r^{-6}$, where $r = \text{Cu} - \text{H}$ distance).⁹ The main effect of adding metal-cyclams to lysozyme was the broadening of specific Trp resonances, as seen in 1D (Figure 6.1-6.3) and 2D (Figure 6.5) NMR spectra. For Cu-cyclam, **8**, line-broadening of tryptophan indole NH resonances decreased in the order (Figure 6.4):

Trp62, Trp63 > Trp123 >> Trp108, Trp111,

with Trp108 and Trp111 being little affected by Cu-cyclam. Cu-cyclam also had little effect on the $\text{H}\delta$ and $\text{H}\epsilon$ resonances of the only His residue in lysozyme, His15. However, in the case of complex **13**, the Cu(II)-xylyl-bicyclam, (Figure 6.4-6.5) the effect is much more pronounced, with the most significant change being the effect on Trp108. The line broadening increases dramatically for Trp62 and Trp63 also. The order of line-broadening in this case is:

Trp63 > Trp108 > Trp62 >> Trp123, Trp111

The increased line broadening can be attributed to there being double the amount of paramagnetic copper present. Trp-108 is found in a region in the sequence in which a highly persistent hydrophobic cluster has been identified in lysozyme.^{10, 11} This could form key hydrophobic interactions with the cyclam ring. It is possible that the linker from xylyl-bicyclam brings the second cyclam ring into an orientation that allows it to interact with Trp-108 (Figure 6.9).

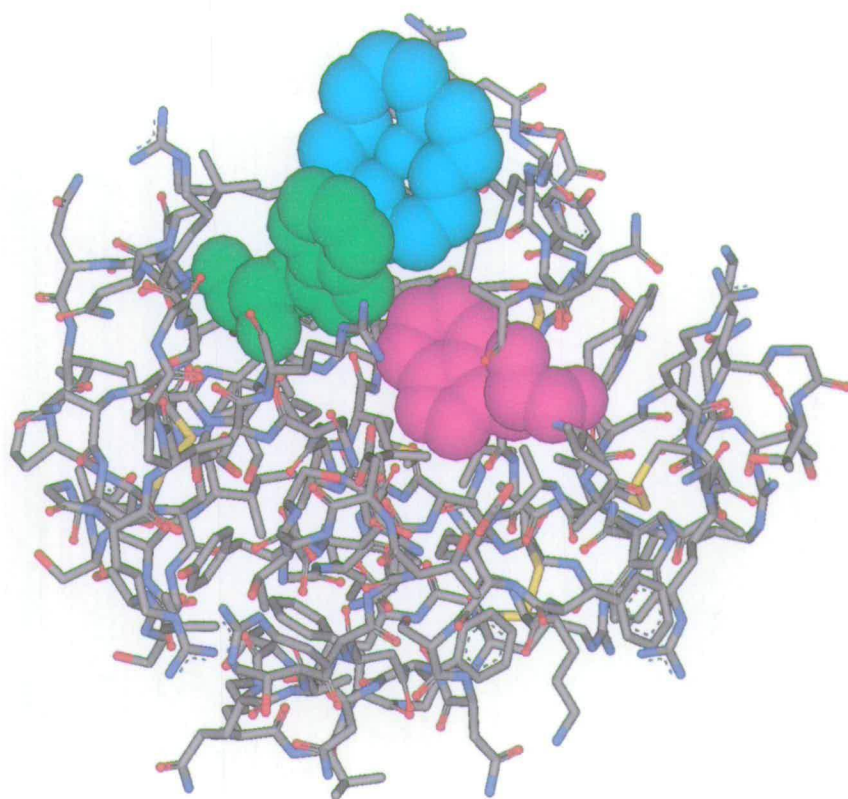


Figure 6.9 The location of Trp108 (purple) in relation to one the cyclam rings from $\text{Cu}_2(\text{xyllyl-bicyclam})$ (blue). Trp62 is also highlighted in green. In solution, the resonance for Trp108 broadens significantly, indicating that there is a copper atom close to it. It is possible that the orientation of the second cyclam ring (not found in the crystal structure) is such that the macrocycle is located close enough to bind to Trp108.

Several other residues change significantly upon reaction of complex **13** with lysozyme. The peak for Asn59H shifts from 5.64 ppm to 5.69 ppm. In the crystal structure, this can be seen to sit next to Trp62 and Trp63, which are both involved with bonding to the Cu-cyclam ring, and as such influence the chemical shift of amino acids in close proximity to themselves. Also, Asn59 sits on the surface of the

protein, close to the binding site for one of the cyclam rings, hence it could be directly involved with binding a second cyclam ring from Cu₂-bicyclam.

It can be seen clearly in the 1D NMR spectrum that the peak arising from Ala90 HB (1.34 ppm) is altered by the interaction with complex **13**. This residue is located on the surface of the protein, and it is not located near either of the two main binding sites found in the crystal structure. This could be a further binding site, and as a hydrophobic residue, could be involved in hydrophobic interactions with a cyclam ring.

6.4.2 Nickel-Macrocycle-Lysozyme Interactions in Solution

Again, the main features of the 1D ¹H NMR spectrum of HEWL were unchanged after addition of up to 10 molar equivalents of the Ni^{II} complex **3** (Figure 6.3) which indicated that the interaction had little effect on the overall protein fold. In this case, the solution contains a mixture of paramagnetic and diamagnetic Ni-cyclam, as shown by the presence of narrow and broadened peaks in the 1D spectrum (Figure 6.3). Upon binding to lysozyme, broadened peaks from paramagnetic Ni-cyclam can still be observed in the 1D spectrum, at 40.3, 19.0, -8.4 and -18.1 ppm. However, the fact that resonances from the lysozyme broadened, indicates that there is a paramagnetic species interacting with the lysozyme, as little broadening would be expected if the diamagnetic species was the only one to bind. In the case of this nickel complex, the residues from lysozyme that are broadened are Trp 62 and Trp 63 (Figure 6.4). Trp63 is the most affected peak in the spectrum, its NH signal is too broad to observe in the 1D NMR spectrum after the addition of 5 and 10 molar equivalents of the nickel complex. In the 2D NMR spectrum, the cross peak from

Trp63 disappears upon the addition of 1 molar equivalent (Figure 6.6). This is the only significant change to the 2D NMR spectra after the addition of 1 molar equivalent of Ni-cyclam. However, following the addition of 5 molar equivalents, the signal from Trp 62 also disappears. There is little change in the 2D spectra between the addition of 5 and 10 molar equivalents. This shows that initially, Trp63 is the favoured binding site, but with the addition of more complex Trp62 becomes important in binding Ni-cyclam.

6.4.3 Copper-Macrocyclic Binding Sites in Crystalline Lysozyme

Colourless lysozyme crystals turned purple on soaking in solutions containing either Cu-cyclam **8** or Cu₂-bicyclam **13** (Figure 6.7). The metal binding positions are similar in both the monocyclam and the bicyclam structures. Site 1 is close to the side chain of Asp101, whilst site 2 is closest to the side-chain of Trp123 and the backbone carbonyl of Gly117, Figure 6.8. These residues are on different regions on the protein surface. The packing of the protein molecules in the crystal brings the binding sites close to each other, Figure 6.10. The crystal packing and the interaction between the cyclam rings therefore appear to play a crucial role in the formation of the binding site.

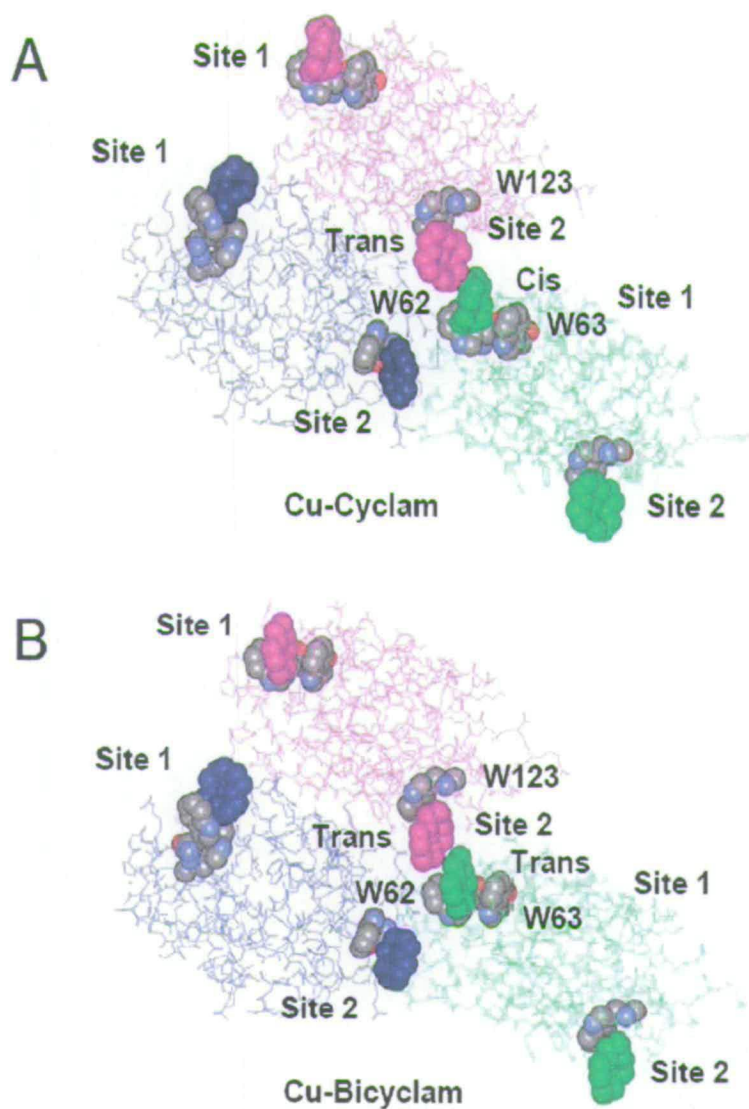


Figure 6.10 The location of Cu-cyclam (*A*) and Cu-bicyclam (*B*) sites at the interfaces between lysozyme molecules in crystals. No density is resolved for the linker or the second cyclam ring for the xylyl-bicyclam complex. Cu-cyclam rings and tryptophan residues in the binding sites are space-filling, and the former are coloured according to the lysozyme molecule to which they belong. (W = Trp).

In the structure of Cu_2 -bicyclam-HEWL, two cyclam rings were readily

identified. Both adopt the *trans* configuration (Figure 6.8). No electron density was present for the *p*-phenylenebis(methylene) group which links the two cyclam rings. Although the rings in the two sites are close (Cu - Cu distance 8.45 Å), it was not possible to model the two cyclam rings as part of a single bicyclam unit (therefore only monocyclam rings were built and refined). The next closest cyclam ring in the crystal is too distant (Cu - Cu distance 14.87 Å) to be modelled as part of a single bicyclam. Hence it appears that the cyclam rings in sites 1 and 2 belong to two different Cu₂-xylyl-bicyclam molecules.

In Cu-cyclam-HEWL, the Cu in site 1 is in a slightly different position to that in the bicyclam structure and the cyclam ring in this structure has strong density consistent with a *cis* configuration. Copper in site 2 is in a similar position to that found in the bicyclam structure and the planarity of the cyclam ring is indicative of the presence of a *trans* configuration (Figure 6.8).

6.4.4 Metal Coordination, H-bonding and Hydrophobic Interactions

In site 2, the cyclams in both the monocyclam and bicyclam structures adopt *trans* configurations. The *trans*-III configuration is common for octahedral metal cyclam complexes and *trans*-I for square-planar metal cyclam complexes¹². The cyclam ring stacks on Trp123 and a (cyclam)CH...OC(Gly117) hydrogen bond is formed (Figure 6.8). Cu²⁺ in the monocyclam structure is also very weakly coordinated to a water molecule (Cu-O 3.05 Å). Comparison of the positions of the cyclam in the monocyclam and xylyl-bicyclam structures reveals that although there is very little movement in the Cu position (0.8 Å) there is a distinct change in the orientation of the cyclam plane (Figure 6.8C). This appears to be a consequence of

the difference in binding mode for the cyclam in site 1.

In site 1, the cyclam ring of Cu₂-xylyl-bicyclam has a *trans* configuration. The Cu²⁺ in this cyclam coordinates directly to oxygen OD1 of the side-chain of Asp101 (Cu-OD1 2.7 Å) and also very weakly to a water molecule (Cu-O 3.07 Å) on the opposite side of the ring (Figure 6.11). In the monocyclam structure, the cyclam ring adopts a *cis* configuration. The Cu in this ring does not coordinate directly to Asp101 and is in a significantly different position to that found in the bicyclam structure (Cu movement 1.61 Å; Figure 6.8C). In this folded conformation, two NH...O hydrogen bonds are formed between the carboxylate oxygens of Asp101 and two NH groups on opposite sides of the cyclam ring (OD2 - N1 2.70 Å, OD1 - N10 2.93 Å, Figure 6.11).

The Cu in this ring coordinates weakly to two 2 water molecules (Cu - O = 2.76, 2.88 Å). In both the cyclam and xylyl-bicyclam structures, the cyclam in site 1 is sandwiched between the indole rings of Trp62 and Trp63 and stacks directly with Trp 62. This hydrophobic interaction with tryptophan would therefore appear to be important for the binding of these cyclams in both *cis* and *trans* configurations. Girard *et al.*¹³, in their search for heavy atom derivatives useful in anomalous dispersion methods of solving protein structures, have studied adducts of HEWL with Gd-HPDO3A, the Gd³⁺ complex of a derivative of the smaller [12]aneN₄ macrocycle cyclen (1,4,7,10-tetraazacyclododecane). They were unable to produce Gd-HPDO3A-lysozyme by soaking, only by co-crystallization. Intriguingly Gd-HPDO3A binds in same sites 1 and 2 as Cu-(bi)cyclam (Figure 6.12); the main protein interaction is between Trp62 and the cyclen with no direct metal coordination or involvement of H-bonds with Asp101 (which is turned away from the site).

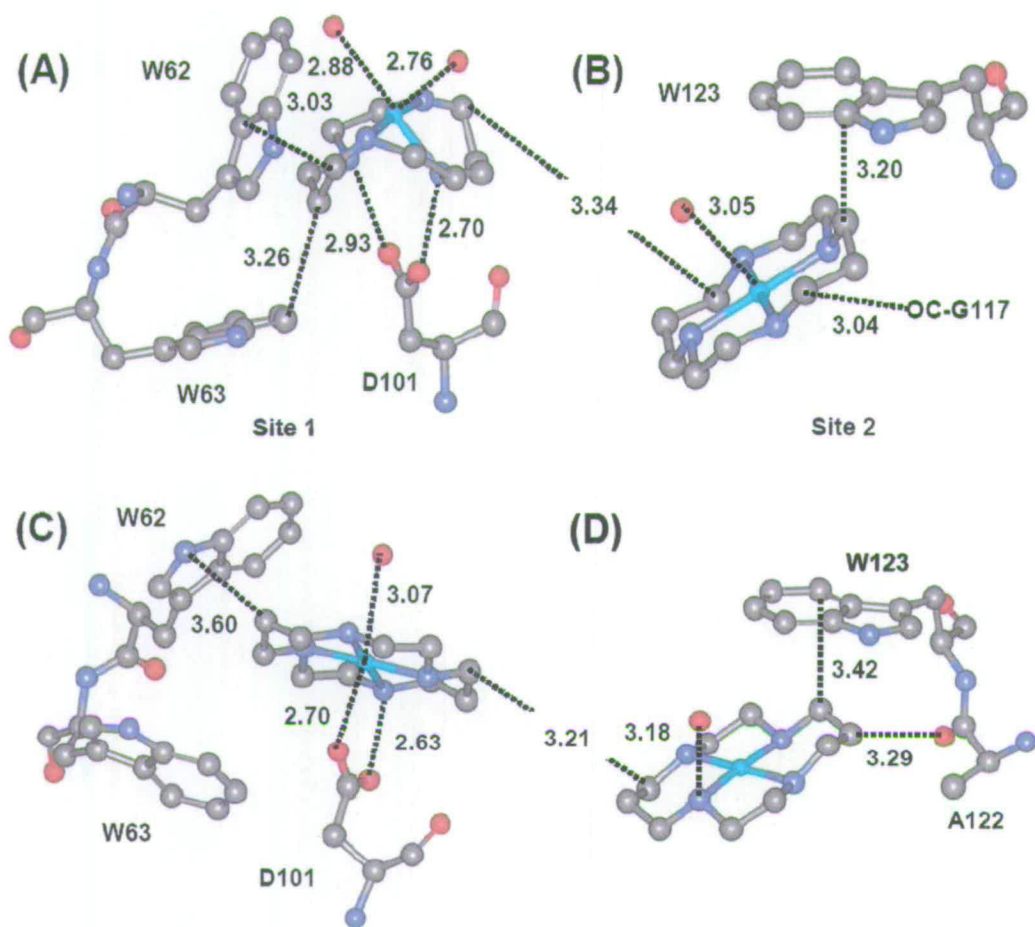


Figure 6.11 Close contacts in the binding sites. (A) Site 1 for Cu-cyclam. (B) Site 2 for Cu-cyclam. (C) Site 1 for Cu₂-bicyclam. (D) Site 2 for Cu₂-bicyclam. The shortest intersite contacts are indicated, but the relative orientations of the sites are arbitrary and do not relate to those in the crystal. Amino acid code: D = Asp, W = Trp, G = Gly.

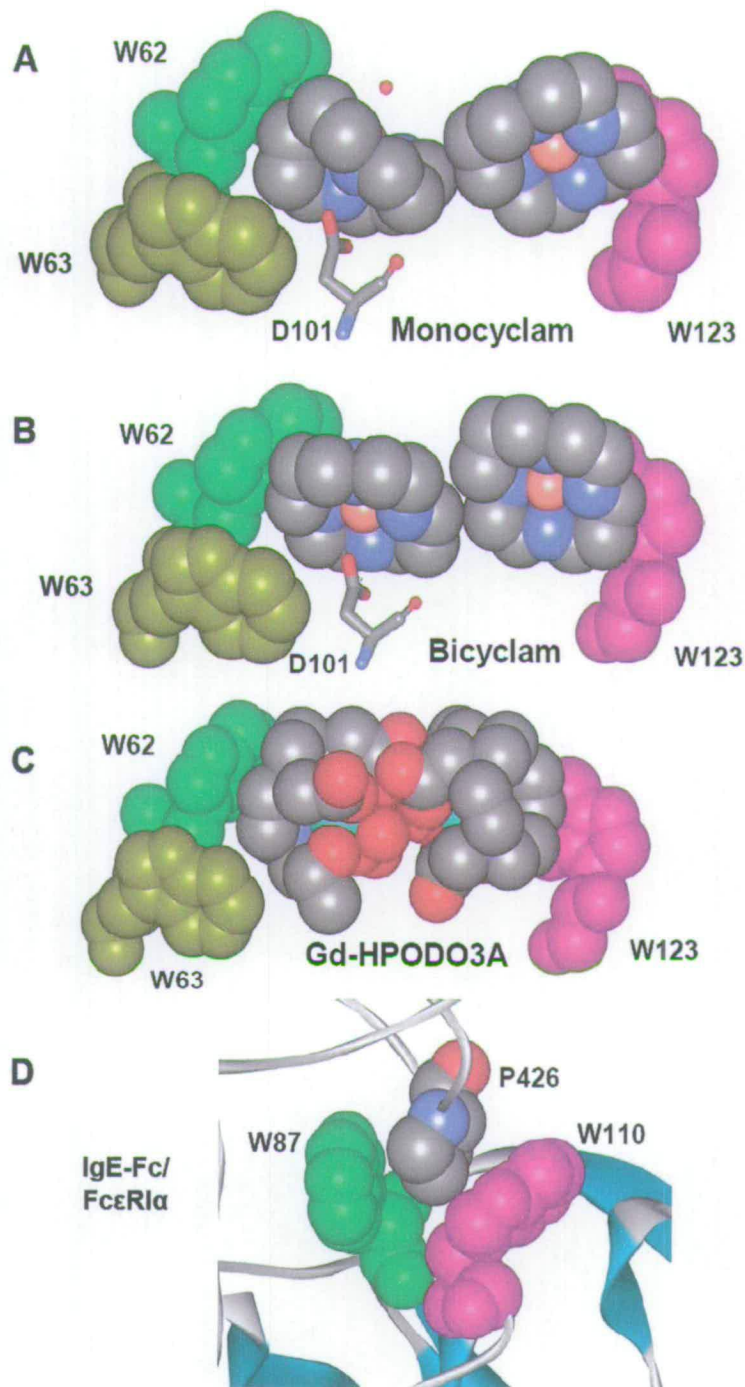


Figure 6.12 Tryptophan interactions with macrocycles and proline. (A) Lysozyme–Cu(cyclam). (B) Lysozyme–Cu₂(xylyl-bicyclam). (C) Lysozyme–Gd(HPDO3A) (PDB ID code 1H87). (D) Human IgE-Fc bound to high-affinity receptor FcεRIα (PDB ID code 1F6A). Amino acid code: D = Asp, W = Trp.

The difference in the orientation of the cyclam plane in site 2 of the monocyclam and xylyl-bicyclam structures is likely to be a consequence of the difference in conformation of the cyclam in site 1. In both structures, the cyclams interact weakly with each other (closest ring-ring distance 3.21 Å for xylyl-bicyclam, 3.34 Å for monocyclam, Figure 6.11-6.12). The overlay of the monocyclam and xylyl-bicyclam structures (Figure 6.8C) reveals that the different orientations of the plane conserve the tightness of the cyclam-cyclam interaction (which would otherwise increase to 3.62 Å). It is unclear why the cyclam in site 1 is in the *trans* configuration in the xylyl-bicyclam structure compared to the *cis* configuration for monocyclam. The lack of difference between the protein structures does not provide any clues. It would therefore seem likely that this difference is related to the presence of a linker between the cyclam rings for xylyl-bicyclam, although the linker is disordered.

The *cis* cyclam configuration in the solid state structure of the zinc complex of the drug xylyl-bicyclam, $[\text{Zn}_2(\text{xylyl-bicyclam})(\text{OAc}_2)_2](\text{OAc})_2 \cdot 2\text{MeOH}$, is stabilised by one bidentate acetate, the other acetate forms double H-bonds to the NH groups on the opposite face of the cyclam ring which adopts the folded *cis-V* configuration⁵. In the Cu-cyclam-HEWL structure, there is no direct coordination of Cu^{2+} to a carboxylate, only NH H-bonding, and the carboxylate oxygen coordination sites appear to be occupied by weakly-bound water molecules. *Cis* metallocyclams with two bound aqua ligands are unusual, although Barefield *et al.*¹⁴ prepared *cis*- $[\text{Ni}(\text{cyclam})(\text{H}_2\text{O})_2]\text{Cl}_2 \cdot 2\text{H}_2\text{O}$ via displacement of a chelated ethylenediamine by water under acidic conditions. In solution, the interaction of carboxylate groups with Zn^{2+} cyclams readily leads to the formation of the folded *cis-V* configuration,

equilibria being reached within an hour at millimolar concentrations, at 298 K^{5, 15}.

6.4.5 CXCR4 binding sites

Previously⁵ a model was built of human CXCR4 coreceptor based on the x-ray structure of rhodopsin¹⁶ and docked Zn₂-xylyl-bicyclam such that there is direct coordination of Zn²⁺ in one cyclam ring to the carboxylate of Asp171, and of Zn²⁺ in the other to Asp262. In the latter site, Glu288 on the opposite side of the ring can form double H-bonds to two ring NH groups, and the macrocycle folds into the *cis*-V configuration. In the first site a *trans*-I or *trans*-III configuration is more likely for the cyclam ring. Inspection of the same CXCR4 model reveals that there are Trp indole rings close to each of the docked cyclams, Figure 6.13.

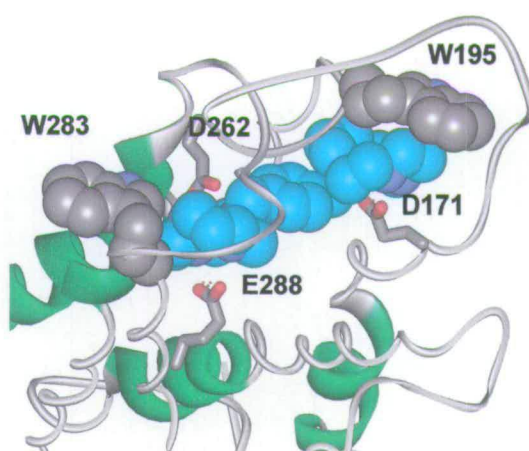


Figure 6.13 A model showing $[\text{Zn}_2(\text{xylyl-bicyclam})]^{4+}$ bound to the human coreceptor CXCR4. One of the cyclam rings in a *trans* configuration is stacked on Trp-195 and its Zn is bound to Asp-171. The other cyclam ring has a folded configuration (*cis*) and is close to Trp-283; its Zn is bound to Asp-262, and two ring NH groups are H bonded to the oxygens of Glu-288.

Notable is the stacking of Trp195 on the *trans*-cyclam ring which contains Zn^{2+} bound to Asp171. These are all features seen in the lysozyme-Cu-(bi)cyclam structures. The hydrophobic interaction of the $N(CH_2)_2N$ and $N(CH_2)_2N$ backbone of cyclam with tryptophan indole rings has a parallel in the hydrophobic contact of the $N(CH_2)_3CH$ cyclic side-chain of proline with tryptophan at some protein-protein interfaces, often as a Trp-Pro-Trp sandwich, e.g. the IgE receptor¹⁷, Fig. 6.12D. Such hydrophobic interactions may therefore play a key role in the binding of cyclam anti-HIV complexes to the CXCR4 co-receptor.

6.5 Conclusions

Antiviral bicyclams target the membrane co-receptor protein CXCR4¹⁸, and co-receptor binding is enhanced by the presence of Ni^{2+} , Cu^{2+} or Zn^{2+} in the cyclam ring¹⁹. Currently there are only structural models of CXCR4-cyclam adducts.^{5, 19, 20} These models have emphasized the importance of aspartate carboxylate side-chains of CXCR4 in forming the H-bonds to cyclam NH groups and in coordination to cyclam-bound metal ions. Cyclam rings in metallocyclam complexes have configurational flexibility and in one model a folded *cis* configuration is stabilized by interactions with carboxylate side-chains⁵.

The work reported in this chapter represents the first experimental characterisation of protein-metallocyclam interactions. The solution structures and x-ray crystal structures of Cu-cyclam and Cu_2 -xylyl-bicyclam complexes of lysozyme establish that protein recognition can involve a range of both polar and non-polar interactions. These include H-bonding between the cyclam ring and

protein carboxylate groups, which, for the Cu-cyclam structure, anchors the cyclam ring in the unusual folded *cis* configuration without direct coordination of Cu^{2+} to the protein. The key interactions in the solid state are with Trp123, Trp62, Trp63 and Asp101. However in solution the key residues that interact with Cu(cyclam) are Trp62, Trp63 and Trp123, and for Cu_2 (xylyl-bicyclam), they are Trp62, Trp63 and Trp108. The solution studies of the interaction of the Ni-cyclam complex with lysozyme showed the major interactions to be only with Trp 63 and Trp 62. The presence of an additional cyclam ring, as in a xylyl-bicyclam, can influence the configuration adopted by the bound macrocycle. Intriguingly hydrophobic interactions between the cyclam ring and the indole ring of tryptophan, reminiscent of tryptophan-proline sandwiches often found at protein-protein interfaces, occur not only in the crystals of HEWL but also in aqueous solution. Such tryptophan stacking interactions are possible in models of CXCR4 adducts of metallocyclams which contain at the same time other features important for metallocyclam docking, including metal coordination to Asp171 and Asp262. Tryptophan, an amphipathic amino acid, is often located towards the surface (interfacial regions) of membrane proteins²¹, and may play a crucial role in the recognition of antiviral metallocyclams by the protein co-receptor.

6.6 References

- 1 N. A. Campbell, 'Biology', Benjamin Cummings, California, 1996.
- 2 R. Canfield, *J. Biol. Chem.*, 1963, **238**, 2698-2707.
- 3 J. Jollés, J. Jauregui-Adell, I. Bernier, and P. Jollés, *Biochim. Biophys. Acta*, 1963, **78**, 668-689.
- 4 C. C. F. Blake, D. F. Koenig, G. A. Mair, A. C. T. North, D. C. Phillips, and V. R. Sarma, *Nature*, 1965, **206**, 757-761.
- 5 X. Liang, J. A. Parkinson, M. Weishäupl, R. O. Gould, S. J. Paisey, H.-S. Park, T. M. Hunter, C. A. Blindauer, S. Parsons, and P. J. Sadler, *J. Am. Chem. Soc.*, 2002, **124**, 9105-9112.
- 6 M. C. Vaney, S. Maignan, M. Ries-Kautt, and A. Ducruix, *Acta Cryst.*, 1996, **D52**, 505-517.
- 7 S. J. Perkins, L. N. Johnson, P. A. Machin, and D. C. Phillips, *Biochem. J.*, 1979, **181**, 21-36.
- 8 Y. Noda, A. Yokota, D. Horii, T. Tominaga, Y. Tanisaka, H. Tachibana, and S.-I. Segawa, *Biochemistry*, 2002, **41**, 2130-2139.
- 9 I. Bertini and C. Luchinat, *Coord. Chem. Rev.*, 1996, **150**, 1-292.
- 10 H. Schwalbe, K. M. Fiebig, M. Buck, J. A. Jones, S. B. Grimshaw, A. Spencer, S. J. Glaser, L. J. Smith, and C. M. Dobson, *Biochemistry*, 1997, **36**, 8977-8991.
- 11 J. Wirmer, C. Schlorb, J. Klein-Seetharaman, R. Hirano, T. Ueda, T. Imoto, and H. Schwalbe, *Angew. Chem. Int. Ed.*, 2004, **43**, 5780-5785.

- 12 X. Liang and P. J. Sadler, *Chem. Soc. Rev.*, 2004, **33**, 246-266.
- 13 E. Girard, L. Chantalat, J. Vicat, and R. Kahn, *Acta Cryst.*, 2002, **D58**, 1-9.
- 14 E. K. Barefield, A. Bianchi, E. J. Billo, P. J. Connolly, P. Paoletti, J. S. Summers, and D. G. Van Derveer, *Inorg. Chem.*, 1986, **25**, 4197-4202.
- 15 X. Liang, M. Weishäupl, J. A. Parkinson, S. Parsons, P. A. McGregor, and P. J. Sadler, *Chem. Eur. J.*, 2003, **9**, 4709-4717.
- 16 K. Palczewski, T. Kumasaka, T. Hori, C. A. Behnke, H. Motoshima, B. A. Fox, I. Le Trong, D. C. Teller, T. Okada, and R. E. Stenkamp, et al., *Science*, 2000, **289**, 739-745.
- 17 S. C. Garman, S. Sechi, J.-P. Kinet, and T. S. Jardetzky, *J. Mol. Biol.*, 2001, **311**, 1049-1062.
- 18 D. Schols, J. Este, G. Henson, and E. De Clercq, *Antiviral Res.*, 1997, **35**, 147-156.
- 19 L. O. Gerlach, J. S. Jakobsen, K. P. Jensen, M. R. Rosenkilde, R. T. Skerlj, U. Ryde, G. Bridger, and T. W. Schwartz, *Biochemistry*, 2003, **42**, 710-717.
- 20 L. O. Gerlach, R. T. Skerlj, G. J. Bridger, and T. W. Schwartz, *J. Biol. Chem.*, 2001, **276**, 14153-14160.
- 21 M. B. Ulmschneider and M. S. P. Sansom, *Biochim. Biophys. Acta*, 2001, **1512**, 1-14.

Chapter 7 Conclusions and Future Work

7.1 Conformations of Metallocyclams

Xylyl-bicyclam has been found to be a potent anti-HIV drug,^{1, 2} and is also currently in clinical trials as a stem cell mobilization drug.³ The zinc complex of xylyl-bicyclam has been shown to be more active than the ligand alone, whereas all other metals cause a decrease or a loss of activity.^{1, 4} Little is understood as to why this happens. Work in this thesis investigated the properties of metal cyclams, metal xylyl-bicyclams, and metal complexes of pyridyl isocyclam.

Antiviral bicyclams target the membrane co-receptor protein CXCR4,⁵ and co-receptor binding is enhanced by the presence of Ni²⁺, Cu²⁺ or Zn²⁺ in the cyclam ring.⁶ Currently there are only structural models of CXCR4-cyclam adducts.⁶⁻⁸ These models have emphasized the importance of aspartate carboxylate side-chains of CXCR4 in forming the H-bonds to cyclam NH groups and in coordination to cyclam-bound metal ions. Cyclam rings in metallocyclam complexes have configurational flexibility and in one model a folded *cis* configuration is stabilized by interactions with carboxylate side-chains.⁸

There are five possible *trans* configurations for metal-cyclam complexes in solution (Figure 1.12).^{9, 10} The configurations that are symmetrical about the diagonal can fold to form *cis* isomers, e.g., the *trans*-V isomer can fold to give the *cis*-V structure. Work done here on Pd(II)-cyclam and Pd(II)₂-xylyl-bicyclam showed the cyclam ring to be in the *trans*-III configuration in the solid and solution state. Varying the counterion had no effect on the configuration of the cyclam ring. Addition of acetate to the Pd(II)₂-xylyl-bicyclam did not induce any configurational

change in the cyclam framework. This is in contrast to Zn(II)-cyclam and Zn(II)₂-xylyl-bicyclam, which forms a higher proportion of the *cis*-V configuration in solution when excess acetate is added.

In the solid state, Ni(II)-cyclam was found to adopt the *trans*-III configuration, with axial counterions, whereas in solution, Ni(II) cyclam can also be found in the diamagnetic square-planar *trans*-I configuration. A paramagnetic configuration is also present in solution, as revealed by the NMR, likely to be the *trans*-III isomer, but this could not be fully characterised. Ni₂(xylyl-bicyclam)(OAc)₄ was found to have a mixture of paramagnetic and diamagnetic peaks present in the 1D ¹H NMR spectra. The presence of the two cyclam rings allows a mixture of paramagnetic-paramagnetic, paramagnetic-diamagnetic and diamagnetic-diamagnetic species to be present, as well as different configurations of these combinations.

Cu(II)-cyclam was found to be *trans*-III in the solid state, with water bound in the axial positions, and acetate as a counterion. The solution NMR supported this, with the acetate peak being the only non-broadened peak in the spectrum, showing that there is no configurational change between the solid and the solution state. The 1D ¹H NMR spectrum of Cu₂(xylyl-bicyclam)(OAc)₄ was significantly broadened because of paramagnetic broadening effects, due to Cu²⁺ being d⁹, therefore always having an unpaired electron. In the 1D ¹H NMR spectrum, there was one unbroadened peak, from the acetate, at 1.93 ppm, suggesting that the structure is the same as that for Cu-cyclam one, in that acetate is not bound to the copper, just a counterion.

Co(III)-cyclam adopts a *trans*-III configuration in the solid state, with acetate

in the axial positions. Three configurations were observed in solution, *trans*-III, *trans*-I and a further unidentified *trans* configuration. All the acetate was bound directly to the cobalt in solution, as no peaks were observed for free acetate. $[\text{Co}_2(\text{xylyl-bicyclam})\text{Cl}_4]\text{Cl}_2$ was found to have two *trans* cyclam configurations present. This complex was reacted with sodium acetate, and it was found that there was a significant change in the NMR spectra. The spectrum changed immediately upon addition, with the final product was obtained after 46 hours. Intermediate species formed and disappeared within this time. These were not identified due to their rapid appearance and disappearance. The final product consisted of only one *trans*-III isomer, shown by only 3 NH peaks in the [^1H , ^{15}N] HSQC. One of the NH peaks is shifted towards a high frequency (10.19 ppm), indicative of it being involved in hydrogen bonding with an acetate ion.

All the solution structures for the metal-xylyl-bicyclams made here were found to be in *trans* configurations, which could explain the loss of activity compared to the zinc complex. The zinc complex has been shown to exist in three configurations in solution, *trans*-I, *trans*-II and *cis*-V.⁸ In addition to this, addition of excess acetate has been shown to drive the formation of the *cis*-V configuration.⁸ However, in this case, no *cis* isomers were observed, either with or without the addition of excess acetate.

It is possible that xylyl-bicyclam forms complexes with zinc in the blood, and that this is actually the active form in the body. As such, it could be considered a pro-drug. In order to see if xylyl-bicyclam could complex zinc under physiological conditions, it was reacted with zinc acetate and zinc histidine, with the reaction followed by ^1H NMR. Both reactions occurred within 5 minutes and reached

equilibrium in this time. In the reaction with zinc acetate, *trans*-I, *trans*-III and *cis*-V were identified, with *trans*-I being the most abundant. However, the reaction with zinc histidine only produced two configurations, *trans*-I and *trans*-III. The bulky histidine appears to prevent the folding of the cyclam ring into the *cis*-V configuration.

The macrocycle pyridyl isocyclam was successfully synthesised and two pK_a values were determined, of 9.81 and 1.48. The macrocycle was also successfully complexed with Cd(II) and Zn(II). The novel metallomacrocycles were characterised using mass spectrometry and NMR spectroscopy. Both the zinc and the cadmium complexes were found to be in two configurations, an unsymmetrical one and a symmetrical one. The unsymmetrical configuration was the most abundant in both cases. Addition of excess acetate to the zinc complex was found to have no effect on the configuration of the complex. These are the first reported metal complexes of this macrocycle.

The bis-macrocycle of pyridyl isocyclam with a phenyl linker (AMD 3329) was synthesised and complexed with Cd(II), and the structure fully characterised using 2D NMR studies, including [^1H , ^{111}Cd] HSQC NMR spectra. It was again found to exist in two configurations; however the unsymmetrical configuration was more abundant in this bis-macrocycle compared to the monomer complexes. This bis-macrocycle (AMD 3329) is the most potent anti-HIV bis-macrocycle reported to date.¹¹

The first experimental characterisation of protein-metallocyclam interactions was carried out in this work. The solution structures and x-ray crystal structures of Cu-cyclam and Cu₂-xylyl-bicyclam complexes of lysozyme were studied, and the

key interactions in the solid state are with Trp123, Trp62, Trp63 and Asp101. Both polar and non-polar interactions between the protein and the metallomacrocycles were found. These include H-bonding between the cyclam ring and protein carboxylate groups, which, for the Cu-cyclam structure, anchors the cyclam ring in the unusual folded *cis* configuration without direct coordination of Cu^{2+} to the protein. In solution, the Cu-cyclam was found to interact with Trp62, Trp63 and Trp123, and for Cu_2 -xylyl-bicyclam, Trp62, Trp63 and Trp108. The solution studies of the interaction of the Ni-cyclam complex with lysozyme showed the major interactions to be only with Trp 63 and Trp 62. Tryptophan is often located towards the surface (interfacial regions) of membrane proteins¹², and may play a crucial role in the recognition of antiviral metallocyclams by the protein co-receptor.

7.2 Future Work

Future work that could be carried out on this project includes the following.

1. Studying the binding of metal complexes of AMD 3329 and its component monomer with lysozyme; the ^{111}Cd complexes made here could be used for this.
2. Analysis of the coordination number of the metal in the Cd (and other) complexes using EXAFS. This could be significant in identifying how many amino acids the metal complexes of AMD 3329 would interact with.
3. EPR studies on the paramagnetic copper and nickel cyclam and xylyl-bicyclam complexes.
4. pH studies on Ni(II)_2 -xylyl-bicyclam to investigate if either the paramagnetic or diamagnetic form is favoured at various pH values. This would identify which configuration is significant in the body at physiological pH.

5. Temperature-dependence studies on the metal-xylyl-bicyclam complexes, using NMR spectroscopy, to study any configurational changes that might occur at higher temperatures.
6. Synthesis of other metal complexes of AMD 3329, such as zinc and nickel, to investigate the configurations of the macrocycle when complexed to different metals and testing of these metal complexes for their anti-HIV activity.
7. Study the interaction in solution of metallomacrocycles and bovine rhodopsin using NMR spectroscopy and x-ray crystallography.
8. Preparation of xylyl-bicyclam with different metals in each cyclam ring, and investigating the solution and solid state structures of these heterometal bicyclams. This type of study could also be carried out on AMD 3329. This would be useful in trying to control the configuration of each component macrocycle, as it seems to be the *cis-V* configuration that is important in the anti-HIV activity of xylyl-bicyclam.

7.3 References

- 1 G. J. Bridger, R. T. Skerlj, D. Thornton, S. Padmanabhan, S. A. Martellucci, G. W. Henson, M. J. Abrams, N. Yamamoto, K. De Vreese, R. Pauwels, and E. De Clercq, *J. Med. Chem.*, 1995, **38**, 366-378.
- 2 G. J. Bridger, R. T. Skerlj, S. Padmanabhan, S. A. Martellucci, G. W. Henson, M. J. Abrams, H. C. Joao, M. Witvrouw, K. De Vreese, R. Pauwels, and E. De Clercq, *J. Med. Chem.*, 1996, **39**, 109-119.
- 3 E. De Clercq, *Nature Rev. Drug Dis.*, 2003, **2**, 581-587.
- 4 J. A. Este, C. Cabrera, E. De Clercq, S. Struyf, J. Van Damme, G. Bridger, R. T. Skerlj, M. J. Abrams, G. Henson, A. Gutierrez, B. Clotet, and D. Schols, *Mole. Pharm.*, 1999, **55**, 67-73.
- 5 D. Schols, J. Este, G. Henson, and E. De Clercq, *Antiviral Res.*, 1997, **35**, 147-156.
- 6 L. O. Gerlach, J. S. Jakobsen, K. P. Jensen, M. R. Rosenkilde, R. T. Skerlj, U. Ryde, G. Bridger, and T. W. Schwartz, *Biochemistry*, 2003, **42**, 710-717.
- 7 L. O. Gerlach, R. T. Skerlj, G. J. Bridger, and T. W. Schwartz, *J. Biol. Chem.*, 2001, **276**, 14153-14160.
- 8 X. Liang, J. A. Parkinson, M. Weishäupl, R. O. Gould, S. J. Paisey, H.-S. Park, T. M. Hunter, C. A. Blindauer, S. Parsons, and P. J. Sadler, *J. Am. Chem. Soc.*, 2002, **124**, 9105-9112.
- 9 B. Bosnich, C. K. Poon, and M. L. Tobe, *Inorg. Chem.*, 1965, **4**, 1102-1108.
- 10 P. J. Connolly and E. J. Billo, *Inorg. Chem.*, 1987, **26**, 3224-3226.
- 11 G. J. Bridger, R. T. Skerlj, S. Padmanabhan, S. A. Martellucci, G. W.

Henson, S. Struyf, M. Witvrouw, D. Schols, and E. De Clercq, *J. Med.*

Chem., 1999, **42**, 3971-3981.

- 12 M. B. Ulmschneider and M. S. P. Sansom, *Biochim. Biophys. Acta*, 2001, **1512**, 1-14.

Courses Attended

1. Transferable skills courses: UNIX 1, poster making, writing skills, introduction to HTML, more HTML, introduction to Excel.
2. Undergraduate Biophysical Chemistry lecture course, Professor Walkinshaw and Dr Barran.
3. Postgraduate NMR Spectroscopy lecture course, 2003.
4. Postgraduate Synthesis lecture course, 2002.
5. Weekly Inorganic section seminars during term times, 2001-2004.

Conferences Attended

1. 36th USIC conference, University of Edinburgh, UK, September 2002 (poster presentation).
2. 37th USIC conference, University of Strathclyde, UK, September 2003 (poster presentation).
3. SCIpharm conference, Edinburgh, UK, March 2004 (poster presentation).
4. International Symposium on Macrocyclic Chemistry, Cairns, Australia, July 2004 (poster presentation).
4. Biophysical Chemistry, Ligand-Protein Interactions conference, University of Edinburgh, UK, Sept 2004 (poster presentation).

Publications

Protein recognition of macrocycles: binding of anti-HIV metallocyclams to

Lysozyme.

Hunter, Tina M., McNae, Iain W., Liang, Xiangyang, Bella, Juraj, Parsons, Simon, Walkinshaw, Malcolm D., Sadler, Peter J., *Proceedings of the National Academy of Sciences of the United States of America*, 2005, **102**, 2288-2292

Half-sandwich arene ruthenium(II)-enzyme complex.

McNae, Iain W., Fishburne, Katy, Habtemariam, Abraha, Hunter, Tina M., Melchart, Michael, Wang, Fuyi, Walkinshaw, Malcolm D., Sadler, Peter J., *Chemical Communications*, 2004, **16**, 1786-1787.

Configurations of metallocyclams and relevance to anti-HIV activity.

Hunter, Tina M., Paisey, Stephen J., Park, Hye-Seo, Cleghorn, Laura, Parkin, Andrew, Parsons, Simon, Sadler, Peter J., *Journal of Inorganic Biochemistry*, 2004, **98**, 713-719.

Structure and Dynamics of Metallomacrocycles: Recognition of Zinc Xylyl-

Bicyclam by an HIV Coreceptor.

Liang, Xiangyang, Parkinson, John A., Weishaupl, Michael, Gould, Robert O., Paisey, Stephen J., Park, Hye-seo, Hunter, Tina M., Blindauer, Claudia A., Parsons, Simon, Sadler, Peter J., *Journal of the American Chemical Society*, 2002, **124**, 9105-9112.